Effet tunnel chaotique - Méthode différentielle

Amaury Mouchet

Université François Rabelais de Tours

Mémoire
d'habilitation à diriger des recherches

Spécialité : Physique théorique

présenté et soutenu publiquement par

Amaury MOUCHET
Laboratoire de Mathématiques et de Physique Théorique
Fédération Denis Poisson

le 7 décembre 2006

Effet tunnel chaotique — Méthode différentielle

devant le jury composé de

Eugène BOGOMOLNYI	Directeur de recherche	CNRS, Orsay
Andreas BUCHLEITNER	Chef d'équipe (HDR) *rapporteur*	Inst. M. Planck, Dresden
Stephen CREAGH	Associate professor *rapporteur*	Univ. of Nottingham
Dominique DELANDE	Directeur de recherche	CNRS, Paris
Hector GIACOMINI	Professeur	Univ. de Tours
Denis ULLMO	Chargé de recherche (HDR) *rapporteur*	CNRS, Orsay

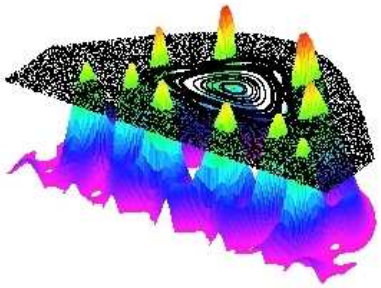

Il savait qu'il n'existe aucun accommodement durable entre ceux qui cherchent, pèsent, dissèquent, et s'honorent d'être capables de penser demain autrement qu'aujourd'hui, et ceux qui croient ou affirment croire, et obligent sous peine de mort leurs semblables à en faire autant.

Marguerite YOURCENAR — L'Œuvre au Noir (1968)

Remerciements

C'est fou c'qu'y faut comme monde pour faire un truc tout seul !
Philippe Avron — Comédien, créateur de magnifiques *one-man shows*.

Il en va de la recherche en science comme de la vie elle-même : la manufacture d'une étoffe dont les fibres, inextricablement enchevêtrées, proviennent d'origines diverses rarement identifiables. Somme toute, assez peu de créations humaines s'appuient avec autant d'équilibre à la fois sur un ouvrage collectif et sur ce qu'il faut bien appeler un travail individuel. On ne trouve pas un tel va-et-vient entre autrui et soi-même en littérature ou en peinture, du moins telles qu'elles sont conçues en Occident à partir de la Renaissance ; ni bien sûr dans les productions de masse. Tel celui d'un sculpteur de gargouilles de Notre-Dame, d'un figurant de théâtre ou d'un matelot de *La Boudeuse*, l'un des plaisirs, irremplaçable et privilégié, que me procure la recherche consiste précisément à pouvoir côtoyer et même travailler avec des maîtres d'exception.

Au premier rang de ceux-ci, je tiens à citer Dominique Delande, puisqu'il est le principal ourdisseur du travail sur l'effet tunnel que je présente dans ce mémoire. Inutile d'insister sur les prodigieux dons scientifiques de Dominique ; ses contributions vivaces et son influence durable parlent d'elles-mêmes et nourrissent évidemment les articles reproduits ci-après. Je préfère le remercier ici pour ses qualités humaines, la confiance qu'il m'a accordée à l'issue de ma thèse et la sollicitude qu'il manifeste en m'accueillant régulièrement au Laboratoire Kastler-Brossel. Sa générosité, sa bienveillance mais également son aiguillon salutaire, son soutien dans les moments de faiblesse et de doute me sont très précieux et il est notoire que tous ceux qui ont eu la chance d'être formés par lui ou de collaborer avec lui partagent mes sentiments. Il est donc peu surprenant que Dominique, bien que n'étant pas d'une nature expansive et ayant heureusement une aversion certaine à se mettre en avant, soit parvenu à tisser un réseau d'amitiés et de compétences scientifiques nationales, de Nice à Lille, et internationales, notamment en Allemagne, en Pologne et en Italie, réseau par lequel se diffusent l'originalité, la pertinence de ses idées et se transmettent la rigueur, l'exigence de ses méthodes.

À la suite de Patricio Lebœuf, mon autre mentor, j'ai eu la bonne fortune de croiser la route d'un deuxième physicien originaire d'Argentine, Hector Giacomini. Son enthousiasme contagieux à force d'être intense, sa vaste culture et sa curiosité universelle mêlés à un talent qui relève de la magie fusionnent en un alliage de grande valeur. Il est la preuve affable que « physique mathématique » n'est pas un oxymoron. Je suis enchanté que nos discussions animées qui s'étendent sur bientôt une décennie se cristallisent en une collaboration sur les problèmes spectraux dont il sera question dans la seconde partie de ce mémoire.

Même si les travaux entamés avec Renaud Parentani en théorie des champs dans une métrique fluctuante, ne se sont pas — temporairement, j'espère — concrétisés, je tiens à lui exprimer ma gratitude pour tout le temps qu'il a consacré sans compter pendant ses années tourangelles à m'initier, avec le sens physique aigu qu'on lui connaît, aux arcanes de la cosmologie quantique et des trous noirs ; ces sujets deviennent encore plus séduisants s'ils permettent de fertiliser ou d'être fécondés en retour par la physique des fluides quantiques, quant à elle beaucoup plus facilement reliée aux expériences.

À coup sûr, le travail présenté ici ne serait pas ce qu'il est sans la collaboration efficace, patiente et surtout amicale de Benoît Grémaud.

Je suis très reconnaissant envers Christian Miniatura et Robin Kaiser pour m'avoir proposé de travailler sur leur projet expérimental. Je garde aussi un souvenir très riche des échanges avec Winfried Hensinger. Plus récemment, j'ai beaucoup appris de Peter Schlagheck, et pas uniquement du fait de sa maîtrise experte de l'effet tunnel assisté par résonance.

Eugène Bogomolnyi ainsi que mes trois rapporteurs Andreas Buchleitner, Stephen Creagh et Denis Ullmo m'ont non seulement fait l'honneur d'accepter immédiatement de participer au jury et de donner de leur temps pour me lire, venir m'écouter et juger mon travail, mais surtout me font regretter de ne pas avoir plus souvent l'occasion de partager avec eux un moment autour d'une bonne bouteille de physique.

Les conditions de travail au laboratoire de mathématiques et de physique théorique de Tours ainsi qu'au département de physique sont exceptionnellement agréables et faciles. Il faut y voir, bien entendu, l'influence et l'énergie de ceux qui ont accepté au fil des ans de prendre plus que leur part de responsabilités : Laurent Véron, Guy Barles, Emmanuel Lesigne pour le laboratoire, Péter Forgács, Claude Barrabès, Hector Giacomini pour notre groupe de physiciens et, enfin, Jean-Claude Soret et Gisèle Gruener pour le département.

Un grand merci également à toutes celles et ceux qui ont soutenu mon travail par leurs compétences administratives et techniques, tout particulièrement Micheline Barbey, Sébastien Barranger, Solange Chauveau, Anne-Marie Chenais, Denis Couratin, Nathalie Doris, Liliane Hénault, Pierrette Mémin, Walter Saulquin, Bernadette Vallée.

Dès que l'on aborde des problèmes physiques où le chaos joue un rôle, les expériences numériques deviennent vite indispensables. Il est donc crucial dans ces domaines, même pour un théoricien, de pouvoir disposer d'un outil informatique fiable et efficace, ce qui ne va pas de soi. En la matière, on remarque plus aisément les dysfonctionnements que le travail quotidien réclamé par le maintien en bonne santé d'un parc toujours plus exigeant (je parle évidemment des ordinateurs). Je salue donc ici le travail remarquable d'Olivier Boebion et d'Olivier Thibault au lmpt et je remercie à nouveau — pour cela aussi — Dominique et Benoît au lkb. Serge Begon m'a sorti plus d'une fois des ornières informatiques dans lesquelles j'ai, c'est bizarre, la propension à me glisser.

Sans Patrick Drevet qui se donne sans compter — et, ce qui ne gâche rien, dans la bonne humeur — à l'enseignement de la physique et à l'administration de la préparation au Capes (entre autres), le déséquilibre permanent entre mon temps accordé à la recherche et celui dévoré par les cours aurait atteint un régime quasi-mortel pour le premier. C'est un vrai bonheur de travailler en équipe avec lui mais il ne faut pas le lui répéter, il deviendrait encore plus « insupportable »...

Parmi tous les autres collègues et néanmoins amis que je n'ai pas cités, et ils sont nombreux, je suis heureux de compter Noureddine Mohammedi et Karim Noui avec qui j'ai la chance de partager bien plus qu'un bureau.

Pour le meilleur et pour le pire, dit-on, je dédie ce travail à Thi Tu Anh et, bien sûr, à mes parents, Anne-Marie et Bernard.

Table des matières

Présentation générale

Ce mémoire d'habilitation à diriger des recherches tend à cerner, de la façon la plus synthétique possible, mon activité professionnelle s'étalant sur une période qui remonte, principalement, à mon recrutement au Laboratoire de Mathématiques et de Physique Théorique au printemps 1997, en tant que maître de conférences de l'université François Rabelais.

La fiche signalétique ci-après décrit surtout mon enseignement ainsi que ma participation à l'administration et à l'animation du département de physique et du laboratoire. Mon travail de chercheur n'y apparaît qu'à travers la liste exhaustive de mes publications et communications diverses.

C'est, bien entendu, à la recherche qu'est consacrée la suite de ce mémoire. Je reviens longuement sur mes contributions en tentant une composition cohérente et ramassée ; mais parce que celle-ci ne saurait être que provisoire, je me risquerai aussi à proposer des perspectives et des nouveaux projets à court et moyen terme, lignes de fuites sans lesquelles aucune activité de recherche n'est évidemment concevable.

La mise au net, pour ainsi dire, de dix années de recherche professionnelle en physique théorique suppose de gommer bien des fausses pistes, de garder pour soi les tentatives avortées et de passer sous silence les projets restés dans les tiroirs faute de temps, de lucidité sans doute, mais aussi de courage. Je n'ai retenu ici que deux veines, celles qui me semblent les plus abouties et auxquelles j'ai consacré la majeure partie de l'énergie que n'absorbait pas l'enseignement. La première, qui a pour thème l'*effet tunnel dans des systèmes non-intégrables*, remonte à ma thèse elle-même et a pu ainsi bénéficier de la mystérieuse opération de décantation qui accompagne inévitablement un travail de si longue haleine. J'essaierai de montrer, au premier chapitre, que ce sujet de recherche mérite bien plus que des efforts intermittents. La seconde veine, présentée au chapitre suivant, prend également sa source en physique quantique — notamment dans les problèmes liés aux propriétés spectrales d'opérateurs — mais diffèrent profondément, tant par les méthodes que par les motivations, de l'esprit avec lequel j'ai abordé l'effet tunnel. Il s'agit ici, de mettre en

œuvre une technique que j'appelle, faute de mieux, *méthode différentielle*, qui vise à donner un encadrement de l'énergie fondamentale d'un système en s'appuyant sur une stratégie radicalement différente des méthodes éprouvées comme l'approche perturbative ou l'approche variationnelle.

D'une certaine façon, en prenant un peu de recul, je suis tenté de discerner à travers les deux chapitres de ce mémoire, un reflet des deux situations typiques dans lesquelles on peut classer grossièrement tout domaine de recherche. Pour schématiser, il est des contrées inconnues qui s'apparentent à des jungles. La progression y est lente, compliquée par la présence de nombreux détours, de fausses pistes et de bifurcations inextricables. Même si l'on devine être à proximité d'une clairière ou d'un layon, on se heurte souvent à des obstacles qu'il faut défricher ou contourner de façon alambiquée au prix d'efforts qui peuvent s'avérer ingrats. Il existe ailleurs des terres beaucoup plus dégagées ; l'exploration y est rapide mais c'est précisément l'abondance des routes aisément praticables qui est à l'origine des difficultés : tout l'art et le plaisir consistent alors à suivre les voies qui conduisent à des plaines fertiles plutôt qu'à des déserts stériles. La recherche sur l'effet tunnel chaotique appartient incontestablement à la première catégorie de ces *terræ incognitæ* et celle sur la méthode différentielle me semble relever de la seconde.

Pour les deux chapitres, j'ai rédigé une présentation du contexte dans lequel s'inscrit l'ensemble des publications reproduites. Je me suis surtout étendu sur les projets de recherche qui les prolongent. En revanche, il m'a paru peu utile de faire une trop longue présentation individuelle de chaque article. Je renvoie pour cela aux articles eux-mêmes. En effet, j'ai toujours eu a cœur, avec plus ou moins de réussite d'ailleurs, de rédiger des textes en évitant de rebuter d'emblée le lecteur par des entrées en matière trop brusques ou trop allusives. J'ai toujours préféré, en tant que lecteur, auditeur ou auteur, des introductions en pente douce, quitte à risquer d'ennuyer le spécialiste averti par des considérations bien connues. On me pardonnera également, j'espère, que je m'écarte par instants de l'académisme de bon aloi.

Fiche signalétique

1 Coordonnées professionnelles

Laboratoire de Mathématiques et de Physique Théorique
UMR 6083

Université François Rabelais
Faculté des Sciences

Avenue Monge, Parc de Grandmont
37200 Tours - France

Tél. :(33).(0)2.47.36.73.70
Fax :(33).(0)2.47.36.69.56

2 Renseignements personnels

Né le : 3 décembre 1969 à Lyon, France.
Nationalité : française.
Situation familiale : marié sans enfants.
Langues parlées et écrites : Français (langue maternelle), anglais, italien.
Langages de programmation : Fortran, LaTeX, Maple, Mathematica, html.

3 Curriculum vitæ

1986 : Baccalauréat section C, math-physique (mention très bien).

1987-1989 : Classes préparatoires au lycée Louis-Le-Grand (Paris).

1989 : Admis aux Écoles Normales Supérieures de Paris, Lyon et Cachan ainsi qu'à l'École Polytechnique (option physique).

1989-1993 : Scolarité à l'École Normale Supérieure de Paris (45, rue d'Ulm) :

Magistère Interuniversitaire de Physique (MIP) de 1989 à 1992 (mention bien) { Licence de physique de l'université Paris-6/ENS (B) ; Maîtrise de physique de l'université Paris-6/ENS (B) ; DEA de physique théorique de l'univ. Paris-6/ENS (AB)

École doctorale en 1992/1993 et première année de thèse de doctorat de l'université Paris-6 effectuée sous la direction de P. LEBŒUF au Laboratoire de Physique Théorique et de Modèles Statistiques (LPTMS) d'Orsay : *Quelques applications des méthodes semiclassiques en chaos quantique.*

1993/1994 : seconde année de thèse et formation monitorale au CIES de Paris-Sud.

1994/1995 : interruption de 12 mois pour service national en tant que scientifique du contingent.

1995/1996 : troisième année de thèse ; soutenance le 29 novembre 1996 à Orsay. Deuxième année de formation monitorale au CIES de Versailles.

1997 : collaboration avec P. LEBŒUF à la Division de Physique Théorique de l'IPN (Paris-Sud) et avec D. DELANDE au laboratoire KASTLER-BROSSEL (Paris-6). Troisième et dernière année de formation monitorale au CIES de Versailles.

Recrutement en 1997 par l'université François Rabelais au Laboratoire de Mathématiques et de Physique Théorique (LMPT).

4 Liste des publications

a) Publications de recherche

Les articles reproduits dans cette habilitation sont indiqués par le signe ☜

HENSINGER W.K., MOUCHET A., JULIENNE P.S., DELANDE D., HECKENBERG N.R. & RUBINSZTEIN-DUNLOP H. (2004): "Analysis of dynamical tunneling experiments with a Bose-Einstein condensate", *Phys. Rev. A*, **70**, p. 013408. ☜

LEBŒUF P. & MOUCHET A. (1994): "Tunneling and the Band Structure of Chaotic Systems", *Phys. Rev. Lett.*, **73**(10), pp. 1360–1363.

_____ (1999): "Normal forms and complex periodic orbits in semiclassical expansions of Hamiltonian systems", *Ann. Physics*, **275**, pp. 54–112.

_____ (2003): "Large geometric phases and non-elementary monopoles", *J. Phys. A*, **36**, pp. 2847–2856.

MOUCHET A. (2002): "Chaos assisted tunnelling with cold atoms", *Bull. Am. Phys. Soc.*, **47**(3), p. 52.[a]

_____ (2005): "A differential method for bounding the ground state energy", *J. Phys. A*, **38**, pp. 1039–1047. ☜

([a]) Il s'agit du résumé de quelques lignes de l'intervention orale au DAMOP, *cf.* ci-après.

MOUCHET A. (2006A): "Bounding the ground-state energy of a many-body system with the differential method", *Nuclear Phys. A*, **765**, pp. 319–341.

_____ (2006B): "Upper and lower bounds for an eigenvalue associated with a positive eigenvector", *J. Math. Phys.*, **47**, p. 022109.

MOUCHET A. & DELANDE D. (2003): "Signatures of chaotic tunneling", *Phys. Rev. E*, **67**, p. 046216.

MOUCHET A., ELTSCHKA C. & SCHLAGHECK P. (2006): "Influence of classical resonances on chaotic tunnelling", *Phys. Rev. E*, **74**, p. 026211.

MOUCHET A., MINIATURA C., KAISER R., GRÉMAUD B. & DELANDE D. (2001): "Chaos assisted tunneling with cold atoms", *Phys. Rev. E*, **64**, p. 016221.

MOUCHET A. & ULLMO D. (2001): "Chaos gives quantum tunnelling a hand", *Physics World*, **14**(9), pp. 24–25.

b) Ouvrages d'enseignement

MOUCHET A. : *Apprendre la mécanique : cours et exercices corrigés* CAPES de physique et chimie - Dunod, 2000 (302 pages).

MOUCHET A. : *Apprendre les ondes : cours et exercices corrigés* CAPES de physique et chimie - Dunod, 2000 (354 pages).

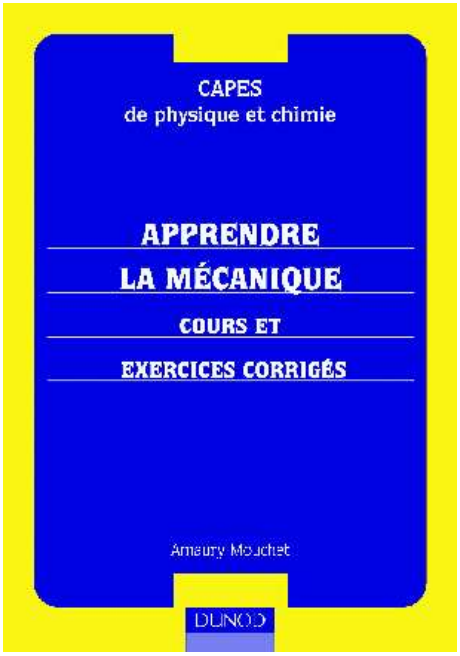

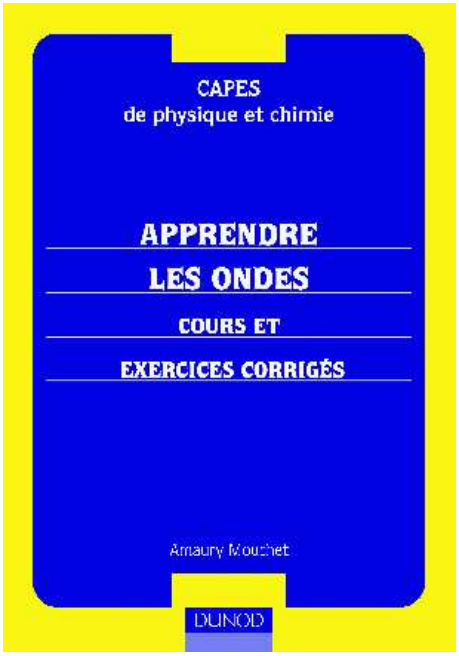

c) Non-publications

Lebœuf P. & Mouchet A. (1996): "Semiclassical study of Berry's two-form and Chern indices for chaotic maps on a torus", (chapitre III de ma thèse : (Mouchet, 1996)).

Mouchet A. (1998): « Introduction aux méthodes semiclassiques en chaos quantique», http://hal.ccsd.cnrs.fr/ccsd-00003591.

5 Communications et participations diverses

Février 1995 : Participation aux journées grenobloises de formation en physique non-linéaire (Quatrième session, Aix-les-Bains). Communication orale "Tunneling effect and semiclassical approach to chaotic systems".

Avril 1997 : Workshop *Tunneling in complex systems* de L'Institute for Nuclear Theory (Seattle, Washington) organisé par O. Bohigas, A. Leggett et S. Tomsovic. Communication orale "Semiclassical tunneling and complex orbits near hamiltonian bifurcations".

Juin 1998 : Invité à la session 1998 de l'école d'été de l'Institut Non-Linéaire de Nice "1998 - Summer School on Nonlinear Phenomena" (Peyresq) organisée par R. Kaiser et J. Montaldi.

Décembre 1999 : Séminaire de physique théorique du lmpt « Une expérience de chaos quantique avec des atomes froids ».

Juin 2000 : Invitation à l'université Libre de Bruxelles par N. Cerf et S. Massard (ainsi que le groupe chaos quantique de P. Gaspard) pour y donner un séminaire « Introduction aux méthodes semiclassiques en chaos quantique ».

Printemps 2001 : Cinq cours dans le cadre d'un groupe de travail du lmpt sur la « Condensation de Bose-Einstein avec des atomes froids ».

Juillet 2001 : Participation aux rencontres du coslab (Imperial College, London, United Kingdom) organisées par la *European Science Foundation*.

Printemps 2002 : Conférence internationale de la *Division of Atomic, Molecular and Optical Physics* organisée en 2002 à Williamsburg (États-Unis) par l'*American Physical Society*. Communication orale "Chaos assisted tunnelling with cold atoms".

Mai 2002 : Organisation locale et participation aux rencontres du coslab. (Tours)

Mars 2003 : Chaos and Quantum Transport (296. WE-Heraeus Seminar) Workshop (Bad Honnef, Allemagne) organisé par A. Buchleitner. Poster "Signatures of Chaotic Tunnelling".

Juin 2004 : Séminaire de physique théorique du lmpt « Une méthode différentielle pour encadrer le niveau d'énergie fondamental ».

Août 2005 : Invitation à l'*International Symposium of Complexified Dynamics, Tunnelling and Chaos* organisé à l'université Ritsumeikan (Kusatsu, Japon) par K. Ikeda. Communication orale "Chaotic tunnelling with cold atoms".

Novembre 2005 : Invitation par le Groupe de Travail Semi-Classique de l'aci Jeunes Chercheurs « Analyse Semi-Classique avec Applications Moléculaires » (Institut Fourier, Grenoble). Séminaire « Effet tunnel chaotique avec des atomes froids : liens entre structures classiques et quantiques dans l'espace des phases ».

6 Enseignement

a) Avant d'être recruté maître de conférences

➵ Colles de physique en mathématiques spéciales P'(PC*) au lycée Louis Le Grand [2h/semaine] (1992/1993, 1993/1994).

➵ Travaux dirigés de physique en première année de premier cycle d'études médicales de l'université d'Orsay et du centre hospitalier universitaire de Kremlin-Bicêtre, donnés dans le cadre d'un cours sous la direction d'Olivier Martin et de Jean-Claude Bizot. Rédaction des sujets de concours, des textes des td et corrections des copies [84h] (contrat d'allocataire moniteur normalien de l'université d'Orsay, 1992/1993, 1993/1994).

➵ Encadrement d'élèves de l'École Polytechnique pour des travaux expérimentaux d'optique, mise en place de montages, correction de rapports et auditions (service national scientifique du contingent, 1994/1995) :

— Astrophysique solaire et spectroscopie [5 séances de 4 heures] ;

— Transmission d'information par faisceau laser modulé au moyen de l'effet Pockels ou de l'effet Faraday (éléments d'optique anisotrope et d'électroptique) [7 séances de 4 heures] ;

— Effet laser et applications [10 séances de 4 heures].

➵ Initiation d'élèves en classe de première S à la polarisation de la lumière et aux transitions de phases (service national scientifique du contingent, 1994/1995).

➵ Encadrement de capitaines de l'armée de terre préparant le brevet technique de l'enseignement supérieur scientifique option « sciences de l'ingénieur » [2h par semaine] (service national scientifique du contingent, 1994/1995).

➵ Travaux dirigés et travaux pratiques de physique en deuxième semestre de deug sciences de la vie (université Paris-Sud) sous la responsabilité de Jean-Claude Roynette [64h] (contrat d'allocataire moniteur normalien de l'université d'Orsay, 1995/1996).

➵ Co-encadrement avec P. Lebœuf de deux étudiants (iut et licence de physique) pour un stage expérimental de trois mois ayant pour but de mesurer la quantification de la conductance lors de la rupture de nano-contacts (1996).

b) En temps que maître de conférences au département de physique de Tours (depuis 1997)

Depuis mon recrutement, j'ai effectué mon service complet chaque année sans bénéficier d'aucune sorte de décharge.

➵ Travaux dirigés de relativité et d'électromagnétisme sous la responsabilité de Claude Barrabès (mias seconde année).

➵ Cours magistraux de relativité et d'électromagnétisme (MIAS seconde année).

➵ Cours magistraux sur les ondes (licence, L3 de physique).

➵ Cours magistraux et travaux dirigés de physique microscopique (licence, L3 de sciences physiques).

➵ Cours magistraux de mécanique (licence de sciences physiques).

➵ Préparation aux épreuves écrites et orales du CAPES de physique-chimie (cours magistraux, travaux dirigés et travaux pratiques). Ce cours a donné lieu à la publication de deux ouvrages (*cf.* ci-dessus).

➵ Encadrement de travaux d'études et de recherche en maîtrise (Caroline DEURVEILHER, Mickaël DE MEULENEIRE, Guillaume THIÉBAULT) *Théorie des groupes et symétries en physique : quelques exemples* ; *Le théorème de NŒTHER* ; *Le groupe de LORENTZ*.

➵ Tuteur pédagogique de Nathaniel OBADIA et de David CAMPO dans le cadre de leur monitorat pendant leur thèse au LMPT.

➵ Cours magistraux et travaux dirigés de théorie quantique des champs et problèmes à N corps (master recherche « Phénomènes non-linéaires » 2e année).

c) Enseignement prédoctoral

Bien que n'ayant pas encore (co-)encadré de thèse, je me suis particulièrement investi dans la mise en place de la seconde année du master recherche *Phénomènes non-linéaires* ouvert à la rentrée de septembre 2005 par le département de physique de l'université FRANÇOIS RABELAIS. J'ai créé pour cela un nouvel enseignement de *Théorie quantique des champs et problèmes à N corps*, où il fallait présenter de la manière la plus simple possible (cours magistraux/travaux dirigés, 36 h au total), le plus souvent inédite même à un niveau plus avancé, des concepts et des techniques très élaborés, indispensables aux étudiants se destinant ou bien à une thèse de physique des hautes énergies ou bien à une thèse de matière condensée. Ces deux directions étant les plus naturelles si l'on se rapporte aux thèmes de recherche dominants dans les deux laboratoires de physique de notre département (groupe de Physique Théorique et Laboratoire d'Électrodynamique des Matériaux Avancés). Avant 2005, la formation du département de physique de l'université FRANÇOIS RABELAIS s'arrêtait à la maîtrise (M1) et ne reprenait qu'en thèse. J'ai cependant pu, plusieurs années durant, encadrer des étudiants de maîtrise, à l'occasion des travaux d'études et de recherche (TER), sur des thèmes toujours choisis dans l'optique d'une formation prédoctorale en physique fondamentale (*Symétries*, *Applications de la théorie des groupes à la physique*, etc.). Dès cette deuxième année de M2, je compte proposer à nos étudiants d'encadrer leur stage à plein temps prévu au second semestre (à partir de janvier 2007) sur *L'effet tunnel chaotique* qui peut donner lieu à une prolongation par une thèse à la rentrée 2007 (*cf.* aussi § 7c) p. 99).

d) Projets concernant l'enseignement et la politique du département de physique

J'ai bien évidemment la ferme intention de poursuivre ma forte implication dans la vie du département de physique tant en interne que — chose essentielle — vis-à-vis des autres départements, de l'administration de l'université et de l'extérieur (collèges et lycées, grand public,), *cf.* § 7 ci-après.

Mais ce qui me taraude surtout, et pour l'avenir du département et pour celui du laboratoire, c'est la fragilité de notre master recherche *Phénomènes non-linéaires* eu égard à la volatilité de nos étudiants. Si la qualité et la cohérence de la formation — s'appuyant sur les trois laboratoires de physique locaux (LMPT, LEMA, LUSSI) et une kyrielle de laboratoires européens, tous, eux aussi, de renommée internationale — ne fait aucun doute, le nombre d'inscriptions actuel est faible (la première année de création en 2005 fut pourtant très encourageante) et pour la rentrée 2007, les perspectives sont préoccupantes. Je crois absolument indispensable, pour la survie de notre M2, donc de notre formation en physique fondamentale dans son ensemble, d'essayer d'apporter du sang neuf venu de l'extérieur. En outre, il s'agit aussi d'ouvrir encore plus notre formation vers le national et l'international pour maintenir une école doctorale dynamique et de qualité. À cette fin, je me suis beaucoup impliqué en 2006, avec l'aide de notre directeur de département, Jean-Claude SORET et de Sébastien BARRANGER, dans la rédaction d'une plaquette attractive destinés aux autres étudiants universitaires français mais aussi européens([b]). S'ouvre aussi la possibilité de « débaucher » des élèves d'écoles d'ingénieurs (certaines offrant la possibilité de s'associer à des masters de haut niveau ; juste retour à l'envoyeur, en somme, puisque beaucoup de nos étudiants de M1 se dirigent vers elles) et de former également des agrégés en herbe désireux de finir leur master par une initiation à la recherche telle qu'elle se pratique en laboratoire (nous proposons un stage d'un semestre à plein temps) et à la physique développée depuis moins de cinquante ans. Étoffer les effectifs de nos étudiants requiert, on le devine, beaucoup de temps pour aller dans les forums étudiants, diffuser l'information par plaquette et pages web([c]), contacter les responsables d'autres formations et peut-être mettre en place des conventions avec certaines écoles d'ingénieurs. J'espère avoir l'énergie et le pouvoir de conviction nécessaire pour participer à ces tâches.

([b]) Après tout, l'un des arguments en faveur de la réforme LMD était l'uniformisation des formations européennes et l'assouplissement des passerelles entre-elles. L'un des effets secondaires de cette réforme, fût la création, dans des universités de province n'ayant pas jusqu'alors de troisième cycle, d'un très grand nombre de M2. L'augmentation des offres conjuguée à la tendance universelle à la baisse des étudiants en sciences fondamentales, est l'explication de nos difficultés, partagée par bon nombre d'autres masters.

([c]) `http://www.dept.phys.univ-tours.fr/html/enseignements.php?id=1`

7 Autres activités

a) Animation scientifique

(i) Membre titulaire élu depuis 2002 de la commission de spécialistes 29e section de l'université François Rabelais.

(ii) Membre élu depuis 2005 du bureau du département de physique de l'université François Rabelais.

(iii) Organisateur d'un groupe de travail interne au laboratoire en 2002 et, à cette occasion, j'ai donné un cours de niveau recherche d'une vingtaine d'heures sur la condensation de Bose-Einstein.

b) Diffusion dans le monde socio-économique et scolaire

(i) Organisateur pour le laboratoire de la *Fête de la science* depuis 2002 ainsi que d'autres manifestations qui visent à décloisonner la recherche en la présentant au grand public : *Journées Portes Ouvertes, Café des sciences* sur le chaos à l'occasion de l'année mondiale de la physique en 2005.

(ii) Conférences diverses adressées aux lycées ou à leurs professeurs qui présentent à la fois le métier de chercheur, les formations offertes par l'université et certains thèmes reliés à mes activités de recherche personnelle ; par exemple la conférence *La physique quantique, une étrange efficacité* donnée à Tours au lycée Grandmont en 2005 à l'occasion d'une invitation à la journée académique de l'Union des Professeurs de Physique et de Chimie.

c) Rayonnement

(i) Membre du comité éditorial de *European Journal of Physics* depuis 2003. L'ambition de cette revue bimestrielle de rayonnement largement international est d'établir des connections entre la recherche au plus haut niveau et sa transmission au niveau universitaire. Une fois par mois en moyenne, chaque membre du comité éditorial lit, critique et juge un manuscrit soumis à la revue. Seuls sont retenus les travaux qui allient à la fois une grande maturité, un souci profond de refonte ou de reformulation des résultats de pointe et de réelles qualités pédagogiques.

(ii) Organisateur depuis 2003 du *Colloquium* mensuel du lmpt. Il s'agit ici d'inviter des chercheurs prestigieux de renommée internationale à parler de thèmes qui ne sont pas forcément liés directement à ceux développés au laboratoire. De nombreux sujets traités ont un caractère nettement interdisciplinaire (mathématiques/biologie, physique appliquée/informatique, histoire des sciences, aspects sociologiques et, plus généralement, sciences humaines).

(iii) Co-organisateur local avec Renaud Parentani, professeur au Laboratoire de Physique Théorique d'Orsay, de la rencontre internationale du coslab (*Cosmology in the Laboratory*) intitulée *Quantum vacuum properties in condensed matter physics and cosmology* qui s'est déroulée à Tours en 2002.

L'effet tunnel chaotique

I.1 Le contexte

a) L'effet tunnel intégrable : les prémices et les concepts de base

L'effet tunnel désigne à l'origine le fait qu'une particule quantique, puisse, en vertu de son caractère ondulatoire (1), franchir des barrières énergétiques qui seraient insurmontables pour une particule classique. Si l'on attribue à Schottky le premier emploi de l'expression « Wellenmechanische Tunneleffekt » (effet tunnel en mécanique ondulatoire) au cours d'une conférence de 1931 publiée ensuite dans *Physikalische Zeitschrift* (2), l'importance de cet effet et ses multiples conséquences physiques avaient été déjà clairement établies dès 1927–1928. Ainsi, dans toute une série d'articles écrits en l'espace des deux ans qui suivent l'achèvement des premiers fondements de la physique quantique, on voit se dessiner avec une rapidité stupéfiante un corpus de concepts-clefs sur l'effet tunnel qui s'étendent même au-delà des systèmes intégrables (essentiellement unidimensionnels).

Hund ouvre ce bal destiné à un si beau succès avec la publication de deux articles, (1927a) et (1927b), dans lesquels il relie l'effet tunnel à l'existence de fins doublets $\Delta\varepsilon$ dans le spectre énergétique d'un système dont le potentiel (statique) possède deux puits symétriques (*cf.* figure I.1–1) (le travail de Hund était motivé par les spectres moléculaires ; on sait le rôle crucial de ces questions pour comprendre l'origine de la liaison chimique).

(1) Pour les ondes électromagnétiques, on peut déjà parler d'effet tunnel dans un sens qui dépasse donc le cadre quantique. La transmission de la lumière par une fine couche métallique peut s'expliquer en terme d'indice complexe. L'optique géométrique est incapable de rendre compte de la présence d'une onde évanescente, c.-à-d. exponentiellement atténuée, lors d'une réflexion totale. En approchant un troisième milieu dans la région où l'onde évanescente n'est pas négligeable, une fraction du faisceau incident peut être transmise à travers les deux interfaces (réflexion totale frustrée). On dispose donc, comme souvent, d'un moyen de tester certaines idées quantiques à l'aide de « modèles expérimentaux » purement électromagnétiques. Je ne connais pas d'expériences, faisant appel à la réflexion frustrée, conçues pour mettre à l'épreuve l'effet tunnel chaotique mais on pourrait peut-être s'appuyer sur l'idée des expériences de Nöckel & Stone (1997) ou de Pance, Violaand & Sridhar (2000).

(2) Ne lisant pas, hélas, la langue de Goethe, je suis ici l'étude de Merzbacher (2002).

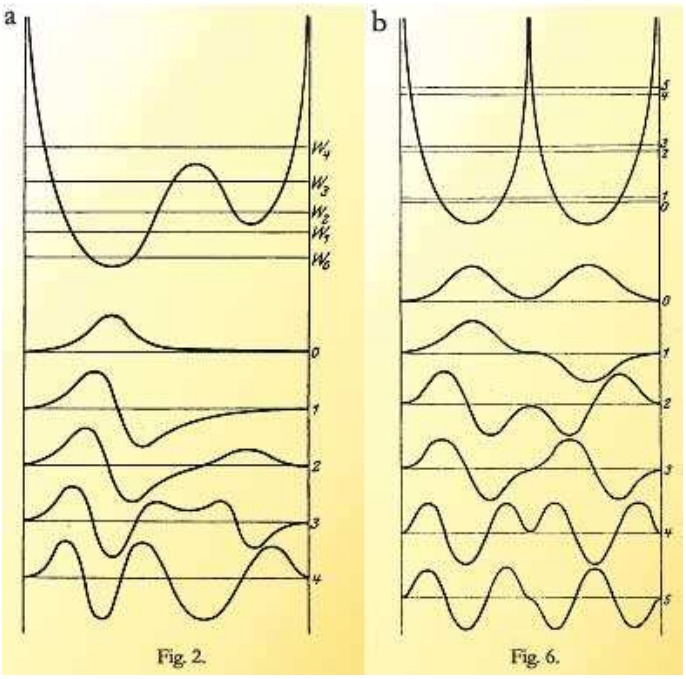

FIG. I.1–1 : *Deux potentiels à double puits considérés dans (*HUND, 1927A*). En (a) les fonctions propres des 5 premiers états excités correspondants aux énergies* W_n, $n = 0, \ldots 4$. *Les états* $n = 0$ *et* $n = 1$ *correspondent aux orbites périodiques dans le puits le plus profond. Les états* $n = 2$ *et* $n = 3$ *s'étalent sur les deux puits alors que leur énergie est plus faible que le maximum local du potentiel. L'effet tunnel se manifeste par la possibilité de franchir la barrière de potentiel. L'état* $n = 4$ *est construit semiclassiquement sur une orbite périodique réelle qui relie les deux puits. En (b), le potentiel est symétrique et la barrière, restant finie, introduit un couplage qui lève la dégénérescence des fréquences propres des puits si ces derniers étaient isolés. L'effet tunnel se manifeste par la présence de fins doublets dans le spectre entre les états symétriques et antisymétriques :* $n = (0, 1)$, $n = (2, 3)$, $n = (4, 5)$.

En outre, dans le second article, HUND illustre clairement la sensibilité exponentielle de la période d'oscillation d'un puits à l'autre, issue du battement des fréquences du doublet $\Delta\varepsilon$,

$$T_{\text{tunnel}} \stackrel{\text{def}}{=} \frac{h}{\Delta\varepsilon}\,, \tag{I.1–1}$$

vis-à-vis de la hauteur de la barrière énergétique à franchir (*cf.* figure I.1–2). Il est facile, en effet, pour un système à une dimension indépendant du temps, de montrer à l'aide de l'approximation JWKB due à JEFFREYS (1925), KRAMERS (1926), BRILLOUIN (1926) et WENTZEL (1926), que l'on a

$$\Delta\varepsilon \underset{\hbar\to 0}{\sim} \alpha\,\hbar\,\mathrm{e}^{-|A|/\hbar} \tag{I.1–2}$$

où A et le préfacteur α sont des fonctions du système classique associé au problème quantique, indépendantes de $\hbar$. En l'occurrence, pour un double puits symétrique, on obtient, pour le n^{e} doublet — voir par exemple (LANDAU & LIFSHITZ, 1977, § 50, problème 3)

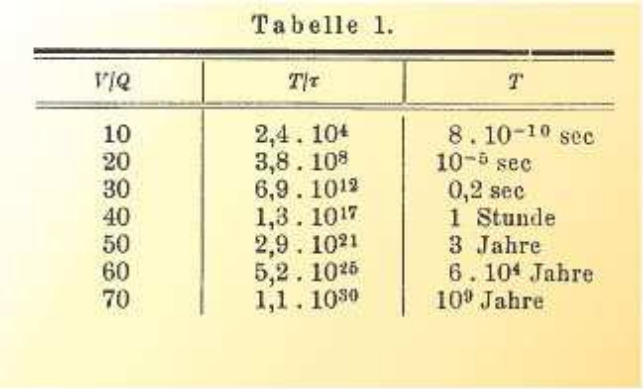

Tabelle 1.

V/Q	T/τ	T
10	$2{,}4 \cdot 10^{4}$	$8 \cdot 10^{-10}$ sec
20	$3{,}8 \cdot 10^{8}$	10^{-5} sec
30	$6{,}9 \cdot 10^{12}$	0,2 sec
40	$1{,}3 \cdot 10^{17}$	1 Stunde
50	$2{,}9 \cdot 10^{21}$	3 Jahre
60	$5{,}2 \cdot 10^{25}$	$6 \cdot 10^{4}$ Jahre
70	$1{,}1 \cdot 10^{30}$	10^{9} Jahre

FIG. I.1–2 : *Calcul de la période de battement* T_{tunnel} *du doublet* $(0,1)$ *effectué dans (*HUND, 1927B*) pour le potentiel symétrique (b) de la figure I.1–1. Les fréquences de fond de puits sont prises à* $1/\tau = \omega_0/2\pi = 3\ 10^{13}$ Hz *correspondant aux vibrations infrarouges de biomolécules entre deux isomères chiraux optiquement actifs (quelques décennies plus tard, en* 1954*, c'est ce genre de fréquence tunnel — mais cette fois-ci pour les molécules d'ammoniac — qui sera impliqué dans la réalisation du premier maser par Townes, Gordon et Zeiger).* V *représente la hauteur de la barrière et* $Q = \hbar\,\omega_0$*. La dépendance exponentielle vis-à-vis de* V/Q *apparaît très clairement.*

pour la méthode et (GARG, 2000) pour l'expression exacte du préfacteur[3] —,

$$a_n = \sqrt{\frac{2}{\pi}}\frac{\omega_0}{n!}\left(n+\frac{1}{2}\right)^{n+1/2} \mathrm{e}^{-(n+1/2)} \tag{I.1–3}$$

et

$$A_n = \int_{-a_n}^{a_n} p(q,E_n)\,\mathrm{d}q \tag{I.1–4}$$

où $\pm a_n$ sont les positions des points de rebroussement à énergie $E_n = (n+1/2)\hbar\,\omega_0$, ω_0 étant la pulsation harmonique au fond des puits. La fonction

$$p(q,E) \overset{\text{def}}{=} \sqrt{2m\left(E-V(q)\right)} \tag{I.1–5}$$

doit être considérée comme le prolongement analytique de l'impulsion classique lorsque, précisément, $E < V$.

[3] Comme le fait remarquer GARG avec une pointe de perfidie, le préfacteur donné par LANDAU et LIFSHITZ est faux d'un facteur deux pour le fondamental $(n=0)$: *Indeed, some of the confusion about the WKB results is perhaps due to the great authority of [*LANDAU *&* LIFSHITZ*]. For example, many workers in the field of macroscopic quantum tunneling, including the author, have often been puzzled and frustrated that the final formula in this book does not yield the same ground state splitting as the instanton approach for the quartic double well. An erudite colleague who studies chaos assisted tunneling once stated to the author that* "WKB is known to be wrong for the ground state splitting." (GARG, 2000, note 2).

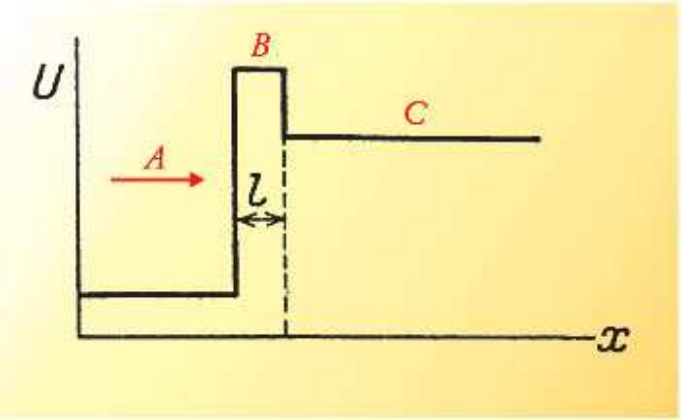

FIG. I.1–3 : *Potentiel U utilisé par Nordheim (1927) pour étudier le comportement d'électrons d'énergie A au voisinage d'une surface métallique. U est infini pour $x < 0$. La barrière de hauteur B confine les électrons dans le métal à gauche. L'effet tunnel s'observe lorsque A est suffisamment élevé pour dépasser l'énergie à l'infini C tout en restant inférieur à B. Pour $A > B$, le caractère ondulatoire des électrons quantiques autorise un phénomène également interdit en physique classique : la réflexion pour des énergies supérieures à la barrière.*

NORDHEIM (1927) fut le premier à considérer des transitions classiquement interdites vers un continuum d'états (*cf.* figure I.1–3). Il s'agissait de modéliser et de comprendre la présence simultanée d'émissions ou de réflexions d'électrons par un métal froid(4) pour une énergie voisine de l'énergie d'extraction B.

Quelques mois plus tard, sous l'influence d'un travail d'OPPENHEIMER (1928) portant sur l'ionisation de l'atome d'hydrogène dans un champ électrostatique intense, le même NORDHEIM en collaboration avec FOWLER (1928) fournit le résultat donnant, par un calcul exact, le taux d'émission d'électrons pour une barrière semi-triangulaire (*cf.* figure I.1–4), phénomène resté inexpliqué depuis son observation par LILIENFELD en 1922. Ici encore, c'est dans le recouvrement de fonctions d'onde qui s'étendent dans des régions interdites que réside la clef de l'effet tunnel.

Le premier grand succès de ce dernier est d'avoir levé (dès 1928, décidément une année faste : 2028 l'année mondiale de l'effet tunnel ?) le paradoxe de RUTHERFORD selon lequel l'uranium-238, ainsi que l'avaient montré des expériences de GEIGER en 1921, émettait des particules α d'énergies inférieures de plus de la moitié de la hauteur de la barrière de répulsion coulombienne. Faisant tomber dans l'oubli toutes les théories alambiquées tentant de rendre compte de ces faits, l'approche utilisant l'effet tunnel proposée indépendamment, et simultanément(5) par GAMOW (1928) (*cf.* fig. I.1–5 et I.1–6) et GURNEY & CONDON (1928) (*cf.* fig. I.1–7) s'appuie explicitement, à l'instar de FOWLER et NORDHEIM, sur la théorie JWKB.

(4) Expérimentalement, il s'agit d'isoler les processus tunnel de ceux qui sont activés thermiquement.

(5) Voir le compte-rendu historique de CONDON (1978) de ce qui est la première application quantitative de la physique quantique à la physique nucléaire, à une époque où le noyau n'était encore constitué que de protons et …d'électrons.

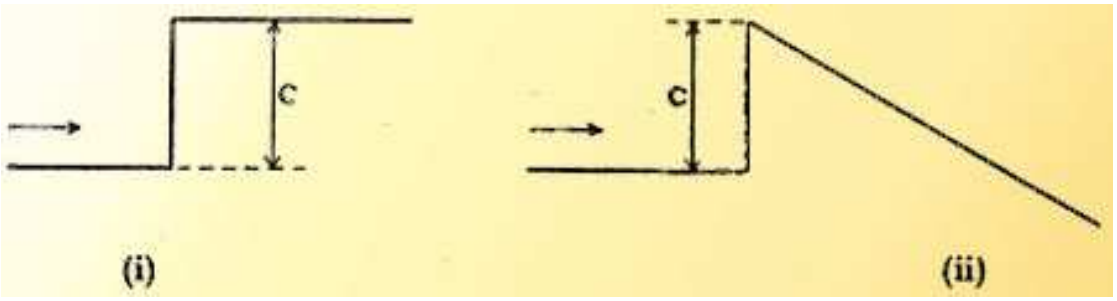

FIG. I.1–4 : *Modèle de Fowler & Nordheim (1928) pour décrire l'émission d'électrons par un métal froid. Il existe une énergie typique d'arrachement de surface C qui confine les électrons dans le métal (à gauche sur les deux schémas). En l'absence de champ électrique (i), si la température du métal est suffisamment basse, il n'y a pas d'émission. En revanche, un champ électrique statique permet d'abaisser l'énergie en dessous de celle des électrons à l'intérieur du métal et ce, à une distance proportionnelle à son intensité. Les électrons peuvent donc s'échapper par effet tunnel.*

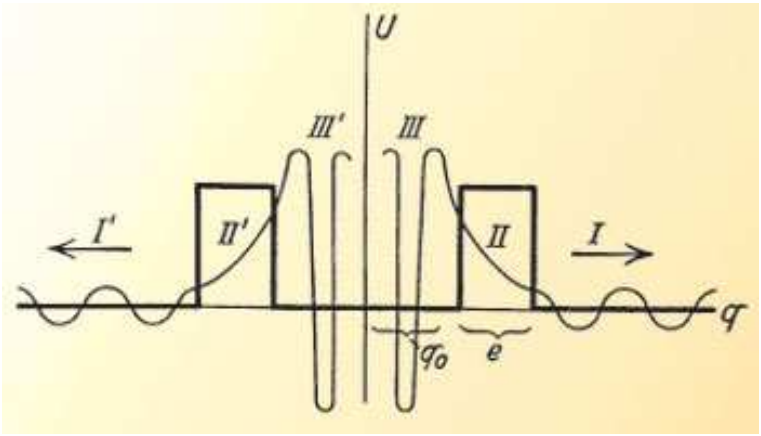

FIG. I.1–5 : *Modèle de Gamow (1928) pour rendre compte de la désintégration radioactive α par l'effet tunnel. Les particules α sont confinés dans un potentiel statique effectif à une dimension radiale q, résultant du champ moyen créé par les constituants du noyau lourd. Le rayon de la région de confinement est q_0 et ℓ désigne l'épaisseur de la barrière (du « sac » comme on dira bien plus tard). À l'extérieur du noyau (I et I′), la fonction d'onde d'une particule α d'énergie inférieure à la hauteur de la barrière est exponentiellement atténuée.*

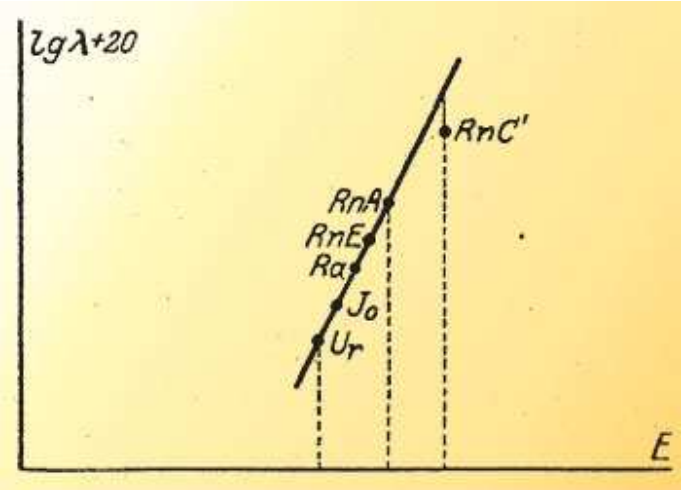

Fig. I.1–6 : *Tracé en échelle semi-logarithmique extrait de (Gamo, 1928) du taux de décroissance radioactive λ en fonction de l'énergie E. Les points correspondent aux données expérimentales de Geiger et Nuttall (1912) et la courbe est calculée par la formule approchée de Gamow. L'accord remarquable entre les deux est probablement le premier grand succès de l'effet tunnel.*

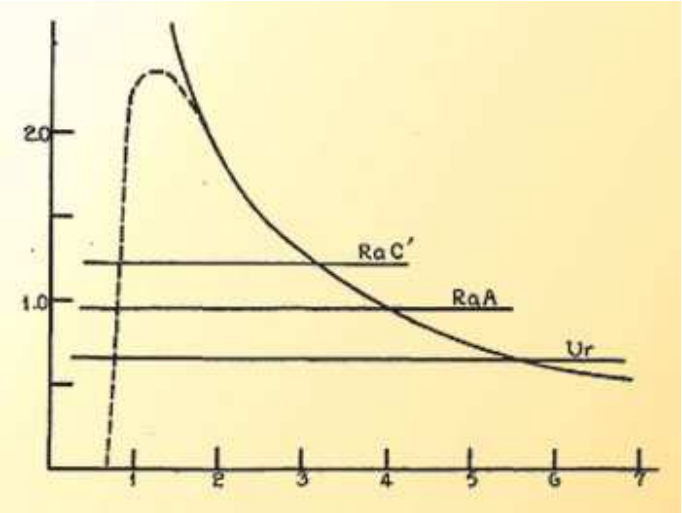

Fig. I.1–7 : *Le modèle de Gurney et Condon fut proposé simultanément à celui de Gamow (cf. fig. I.1–5). Le potentiel moyen (en pico-Joules) dans lequel évolue la particule α est représenté en fonction de la distance au centre du noyau (en dizaines de femtomètres) ; il est coulombien à grandes distances. Les lignes horizontales représentent les énergies de désintégration α de l'uranium 238 (*4.18 MeV *avec une demi-vie de 4.5 milliards d'années), le radium A (polonium 218 ;* 6 MeV, 3 mn*), le radium C' (polonium 214 ;* 7.7 MeV, 160 μs*). Le potentiel est calculé pour le radium A.*

Il serait intéressant, quoique très long (Esaki, 1974) de poursuivre l'histoire de l'effet tunnel tout au long du XX^e siècle. En revanche, la litanie exhaustive des domaines dans lesquels il joue un rôle pertinent serait, à elle seule, fastidieuse. Retenons tout de même, les réactions chimiques, les processus atomiques (ionisations, diffusions) ou nucléaires (désintégration, nucléosynthèse stellaire), la brisure de symétrie dans les transitions de phase, la cosmologie primordiale (déstabilisation du vide), les propriétés de transport (par exemple en nano-électronique). Pour recourir à un argument vendeur, un peu trop tape-à-l'œil sans doute, signalons que cinq prix Nobel ont couronné des travaux faisant explicitement référence à l'effet tunnel : Esaki et Giaever(6), Josephson(7), Binnig et Rohrer(8).

b) L'effet tunnel chaotique

Les résultats mentionnés à la section précédente concernent tous des modèles intégrables(9). Ce n'est que dans la dernière décennie du XX^e siècle qu'apparaissent les travaux précurseurs sur l'effet tunnel de systèmes chaotiques ou, pour être plus juste, dans les systèmes mixtes, c.-à-d. dont la dynamique possède des régions stables régulières, les *îlots*(10), entourées de régions chaotiques où les trajectoires ne sont pas contraintes par la présence de tores kam (*cf.* les exemples de sections de Poincaré reproduites pp. 34, 53, 64, 80 et 87).

b.1) Effet tunnel multidimensionnel intégrable et quasi-intégrable

Une étape préalable fut la généralisation de l'effet tunnel à tout *processus ondulatoire interdit aux solutions classiques réelles* (typiquement une sortie d'îlot), non seulement pour des raisons énergétiques mais, plus génériquement, à cause de la présence globale ou locale de constantes qui restreignent du mouvement. D'abord élaborée dans le cadre des réactions moléculaires (*cf.* Miller (1974, § 4.A) et les références données à la note 19 p. 21), elle fut ensuite étendue aux états liés par Heller & Davis (1981) — voir aussi (Davis & Heller, 1981). Cette notion, qualifiée d'effet tunnel dynamique (à titre d'illustration *cf.* la figure p. 52), prend évidemment tout son sens pour des systèmes à un degré de liberté dont le hamiltonien dépend du temps ou pour un système autonome à

(6) En 1973, *for their experimental discoveries regarding tunneling phenomena in semiconductors and superconductors, respectively.*

(7) En 1973, *for his theoretical predictions of the properties of a supercurrent through a tunnel barrier, in particular those phenomena which are generally known as the Josephson effects.*

(8) En 1986, *for their design of the scanning tunneling microscope.*

(9) Ou, du moins, se limitent aux régimes quasi-intégrables des systèmes mixtes comme l'atome d'hydrogène en champ électrique considéré dans (Oppenheimer, 1928). Il faut attendre la fin des années 1980 pour que soit démontrée et utilisée l'influence cruciale du chaos sur les propriétés dynamiques d'un tel système (Buchleitner, Delande & Zakrzewski, 2002, § 3.2).

(10) Pour un problème de diffusion, il faudrait parler de cap – que dis-je ? — de péninsule.

deux degrés de liberté[11]. Il a fallu attendre encore jusqu'au milieu des années 1980 pour que soit proposée une théorie satisfaisante (Wilkinson, 1986; Wilkinson & Hannay, 1987) de l'effet tunnel multidimensionnel non-séparable après plusieurs tâtonnements utiles (Uzer, Noid & Marcus, 1983; Ozorio de Almeida, 1984; Auerbach & Kivelson, 1985; Schmid, 1986; Farrelly & Uzer, 1986). Seuls les systèmes intégrables ou quasi-intégrables étaient concernés et le mérite de Wilkinson est d'avoir le premier attiré l'attention sur l'importance cruciale de la nature — régulière ou non — de la dynamique classique sous-jacente. En particulier, en dimension d, l'expression familière de type (I.1–2) se généralise en

$$\Delta\varepsilon \underset{\hbar\to 0}{\sim} \alpha\,\hbar^{\nu}\,\mathrm{e}^{-|A|/\hbar}\,, \tag{I.1–6}$$

mais la puissance ν dans le préfacteur est différente selon que le système est exactement intégrable (auquel cas $\nu = 1$) ou quasi-intégrable non-séparable ($\nu = (\mathrm{d}+1)/2$), ainsi que l'ont confirmé des études numériques ; (Creagh, 1994) dans le cas intégrable multidimensionnel et (Wilkinson, 1987; Takada & Nakamura, 1994; Takada, Walker & Wilkinson, 1995; Takada, 1996) dans le cas quasi-intégrable. L'analyse par Creagh & Finn (2001) des expériences micro-ondes de Pance, Violaand & Sridhar (2000) entre deux disques diélectriques confirme la validité de l'expression (I.1–6). Par ailleurs, Creagh (1997, § 3) a pu montrer que les ingrédients de cette dernière étaient indépendants du choix des coordonnées canoniques (simplectiques), notamment en interprétant le préfacteur en terme d'invariants géométriques.

Signalons aussi que des résultats mathématiques du type (I.1–6) avaient été obtenus quelques années avant Wilkinson également dans le cas multidimensionnel par deux écoles. La première s'appuyait sur l'idée des instantons[12] (appliquée en mathématiques pour la première fois par Harrell, 1978, pour le double puits quartique unidimensionnel) : Pour un potentiel multidimensionnel une majoration exponentielle est obtenue astucieusement par Davies (1982, Th. 4), puis Simon (1983, Th. 1) démontre le comportement exponentiel et le préfacteur est fourni par Helffer & Sjöstrand (1984; 1986; 1987)[13]. La seconde école, russe, joue elle-aussi sur les décroissances exponentielles des

(11) Pour un plus grand nombre de degrés de liberté le franchissement des tores kam peut être autorisé même classiquement et, en présence de diffusion d'Arnold, la définition de l'effet tunnel nécessite donc d'être nuancée par la prise en compte des différents temps caractéristiques.

(12) Les mathématiciens les définissent comme des géodésiques pour une mesure $\mathrm{d}s(q)$ de l'espace de configuration, dite mesure d'Agmon, et qui mesure la « quantité d'interdiction classique » d'une trajectoire : elle est identiquement nulle si $\mathrm{d}q$ est contenu dans les régions classiquement autorisées et est définie par $\mathrm{d}s(q) = |p(q)|\mathrm{d}q$ dans les régions interdites où p est imaginaire (*cf.* (I.1–5) p 13).

(13) Dans l'introduction de (Helffer & Sjöstrand, 1985), les auteurs écrivent : *Il s'agit de montrer comment des méthodes plus ou moins modernes en edp permettent d'obtenir des résultats rigoureux (bien que parfois « bien connus» par des physiciens) sur le comportement des valeurs propres quand $h \to 0$ de l'opérateur de Schrödinger $-h^2\Delta + V(x)$.*

fonctions propres hors des puits mais en complexifiant directement le temps dans l'équation de Schrödinger sur laquelle sont ensuite appliquées les méthodes semiclassiques à la façon de Maslov (1985) : (Dobrokhotov, Kolokoltsov & Maslov, 1991; Dobrokhotov & Kolokoltsov, 1993). Non seulement les deux écoles ne permettent d'obtenir le plus souvent que le doublet de plus basse énergie (*cf.* cependant Martinez, 1988), mais surtout l'hypothèse de la régularité de la dynamique classique associée est souvent voilée. Elle est implicite chez Simon (1983, 1984)(14) et n'apparaît dans les travaux d'Helffer & Sjöstrand qu'indirectement à travers l'hypothèse de non-dégénérescence des trajectoires instantons (*cf.* aussi Sordoni, 1997, § IV, hypothèse H_4). Je ne suis pas parvenu à la localiser clairement dans l'école russe(15).

b.2) Effet tunnel et chaos quantique

Les premiers résultats quantitatifs sur l'effet tunnel dans un système mixte furent obtenus quelques années plus tard par Lin & Ballentine (1990, 1992) et Grossmann, Dittrich, Jung & Hänggi (1991) qui exemplifièrent des écarts notables par rapport au comportement semiclassique (I.1–6) dans le cas d'un double puits quartique dépendant sinusoïdalement du temps(16). Ce bourgeonnement tardif tient essentiellement au fait qu'il réclame, avant tout, une profonde compréhension des rapports subtils qu'entretiennent les mondes classiques et quantiques lorsqu'il n'existe plus autant de constantes de mouvement que de degrés de liberté. Or, la pleine maturité de ce que l'on appelle chaos quantique n'a commencé que dans les années 1970 après un déploiement très lent depuis la toute première question posée dans ce domaine par Einstein (1917)(17).

C'est que l'effet tunnel est par essence un problème semiclassique, du fait de sa définition même, rappelée au début du § I.1 b.1), qui s'appuie explicitement sur une compa-

(14) Il faut pouvoir isoler les géodésiques d'Agmon (*cf.* la condition (1.1) du Th. (1.1) de Martinez, 1987), ce qui n'est pas une mince affaire dans le cas chaotique. Cette hypothèse essentielle est utilisée dans les démonstrations mais non pas mentionnée dans le théorème 1.5 de (Simon, 1984). Comme quoi la « rigueur » au sens de la note 13 précédente et la pertinence ne font pas toujours bon ménage même si Simon écrit avec un soupçon de condescendance p. 95 : *]…[our main theorem says that "tunneling is determined by the action of the instanton". This fact is a standard piece of wisdom from the physics literature; our result is a rigorous justification of these ideas from the physical literature.*

(15) La rotation de Wick qui transforme l'équation de Schrödinger dépendant du temps en équation de diffusion aurait-elle pour effet de gommer les effets du chaos dû au repliement des trajectoires classiques ? On retrouverait alors un phénomène analogue à celui décrit au § I.8 b.2) dans le cas d'une dynamique pulsée.

(16) Le mérite de ces travaux est effectivement d'avoir montré que le caractère chaotique ou régulier de la dynamique classique entre les îlots est déterminant ; plusieurs articles sur l'effet tunnel dans des systèmes non-intégrables les précèdent (notamment Büttiker & Landauer, 1982; Büttiker & Landauer, 1985; Fisher, 1988) ou leurs sont contemporains (Jauho, 1990; Azbel, 1991), mais sans mettre le doigt sur le rôle joué par l'irrégularité de la dynamique classique sous-jacente.

(17) Je me permets de renvoyer à l'étude historique des méthodes semiclassiques en chaos quantique, disponible sur la toile (Mouchet, 1998).

raison entre dynamiques quantique et classique. En dépit des nombreux succès des calculs semiclassiques en chaos quantique, la question de savoir quelles quantités classiques sont pertinentes pour rendre compte des traits majeurs de l'effet tunnel reste une question largement ouverte depuis plus de seize années. L'enjeu est d'importance étant donné, d'une part, la diversité des domaines où l'effet tunnel joue un rôle et, d'autre part, que la non-intégrabilité n'est pas une situation académique mais bien une propriété générique.

b.3) Caractérisation de l'effet tunnel chaotique

Tout comme dans le cas intégrable, en présence de symétries discrètes, l'effet tunnel se manifeste dans le spectre des (quasi-)énergies quantiques des états liés par la présence de doublets $\Delta\varepsilon$ (plus généralement de multiplets ou de bandes) exponentiellement fins. Mais ce qui constitue la grande différence entre le régime intégrable et le régime mixte, c'est que, dans le premier cas, $\Delta\varepsilon$ varie de façon lisse avec un paramètre classique ou quantique alors que, dans le second cas, les variations sont beaucoup plus marquées et se traduisent par des pics s'étendant sur plusieurs ordres de grandeur (*cf.* surtout (Tomsovic & Ullmo, 1994, fig. 6), (Buchleitner, Delande & Zakrzewski, 2002, fig. 42) et les deux figures reproduites p. 57 mais aussi celles pp. 38, 82, 83, 86 et 88). Ces pics restent cependant bien isolés dans un régime quasi-intégrable ; lorsque les mers chaotiques commencent à envahir notablement l'espace des phases entre les îlots, ils s'agglutinent alors en un écheveau qui devient vite très dense. L'expression *effet tunnel chaotique* embrasse l'ensemble de ce phénomène[18].

b.4) Contrôle et enjeux de l'effet tunnel chaotique

Une compréhension profonde de ces variations rapides ouvrirait la voie à un contrôle très fin et remarquablement sensible de l'effet tunnel et des propriétés de transport ou de réaction dans les systèmes complexes. Ainsi que l'ont montré Zakrzewski, Delande & Buchleitner (1998) dans une étude théorique soutenue par des expériences numériques, le chaos joue un rôle crucial pour amplifier l'ionisation d'un atome d'hydrogène plongé dans un champ micro-ondes. Le recours aux atomes froids, tant dans les premières

[18] À la suite des articles de Lin & Ballentine et de Grossman *et al.* déjà mentionnés ci-dessus, les années 1990 ont vu fleurir toute une série de travaux confirmant et raffinant ces premières observations (Peres, 1991; Plata & Gomez Llorente, 1992; Holthaus, 1992; Utermann, Dittrich & Hänggi, 1994; Hänggi, 1995; Korsch, Mirbach & Schellhaaß, 1997), le plus souvent pour d'autres systèmes que l'oscillateur quartique forcé ; pour un billard annulaire asymétrique (Bohigas, Boosé, Egydio de Carvalho & Marvulle, 1993), pour un système à deux doublets (Gomez Llorente & Plata, 1994; Utermann, Dittrich & Hänggi, 1994), pour le rotor pulsé (Casati, Graham, Guarneri & Izrailev, 1994), pour le modèle de Harper pulsé (Roncaglia, Bonci, Izrailev, West & Grigolini, 1994), pour un pendule forcé sinusoïdalement (Latka, Grigolini & West, 1994a; Latka, Grigolini & West, 1994b; Averbukh, Moiseyev, Mirbach & Korsh, 1995; Zanardi & Gomez Llorente, 1997; Bonci, Farusi, Grigolini & Roncaglia, 1998). A pu ainsi être récolté un précieux ensemble de données, indispensable pour espérer circonvenir l'effet tunnel chaotique.

études numériques (Mouchet *et al.*, 2001; Averbukh *et al.*, 2002) que dans les expériences prodigieusement délicates nécessitant une maîtrise parfaite des techniques de refroidissement et de manipulation des condensats de Bose-Einstein (Hensinger *et al.*, 2001, 2004 ; Steck *et al.*, 2001), s'inscrit aussi dans cette perspective. Une seconde stratégie fait appel aux cavités micro-ondes (Dembowski *et al.*, 2000 ; Hofferbert *et al.*, 2005) en s'appuyant sur l'analogie, déjà signalée à la note 1 p. 11, entre la correspondance quantique/classique d'une part et électromagnétisme/optique géométrique d'autre part. Il faut également ne pas oublier les diodes à effet tunnel résonnant (Monteiro, Delande, Fisher & Boebinger, 1997; Bogomolny & Rouben, 1998, 1999) constituées d'une double barrière et où les trajectoires des porteurs de charge, rendues chaotiques par un champ magnétique, affectent très fortement le facteur de transmission total de la diode.

Dès lors que l'on cherche à préserver la phase des ondes (électromagnétiques et surtout quantiques) pendant de longues durées (et c'est bien la tendance chez les périodes tunnel), on aborde les délicats problèmes de la décohérence. La façon dont l'effet tunnel est gommé par un couplage à un environnement — surtout si l'on cherche à obtenir un effet tunnel pour un degré de liberté macroscopique — est un problème persistent et crucial pour les expériences ; il suffit à lui seul à motiver bon nombre d'études théoriques (Caldeira & Leggett, 1983; Leggett, 1997; Stamp, 1997, et leurs références). Des ponts peuvent donc naturellement être établis avec les préoccupations de l'information quantique.

b.5) Complexification

Évidemment, pour reproduire semiclassiquement l'amplitude exponentiellement faible de l'effet tunnel, il faut s'attendre à devoir s'aventurer dans le domaine complexe des équations classiques. C'est déjà vrai dans le cas intégrable ; on l'a vu avec l'équation (I.1–5) (*cf.* surtout (Balian & Bloch, 1974, § 4); (Voros, 1983)). L'équation (I.1–6) s'obtient, elle aussi, en s'appuyant sur le prolongement analytique des tores dans le plan complexe et la loi de puissance en $\hbar$ du préfacteur dépend de la géométrie de l'intersection des tores prolongés dans le plan complexe (Creagh, 1994, 1997). Les premières utilisations fructueuses des solutions complexes des équations de Hamilton se rapportent à l'étude semiclassique de réactions moléculaires, conduite notamment par Miller dans les années 1970 [19].

Même dans les cas où la dynamique est quasi-intégrable, il est très difficile d'appliquer les méthodes utilisées par Wilkinson. L'une des raisons, invoquée par Creagh (1997, § 3.2) Brodier, Schlagheck & Ullmo (2002, § II.B) — à la suite de (Greene &

[19] Quelques articles originaux : (Miller, 1970), (Marcus, 1971), (Stine & Marcus, 1972) (George & Miller, 1972) et plus généralement (Miller, 1974, § IV). Pour des états liés voir aussi (Miller, 1979), (Lawton & Child, 1981).

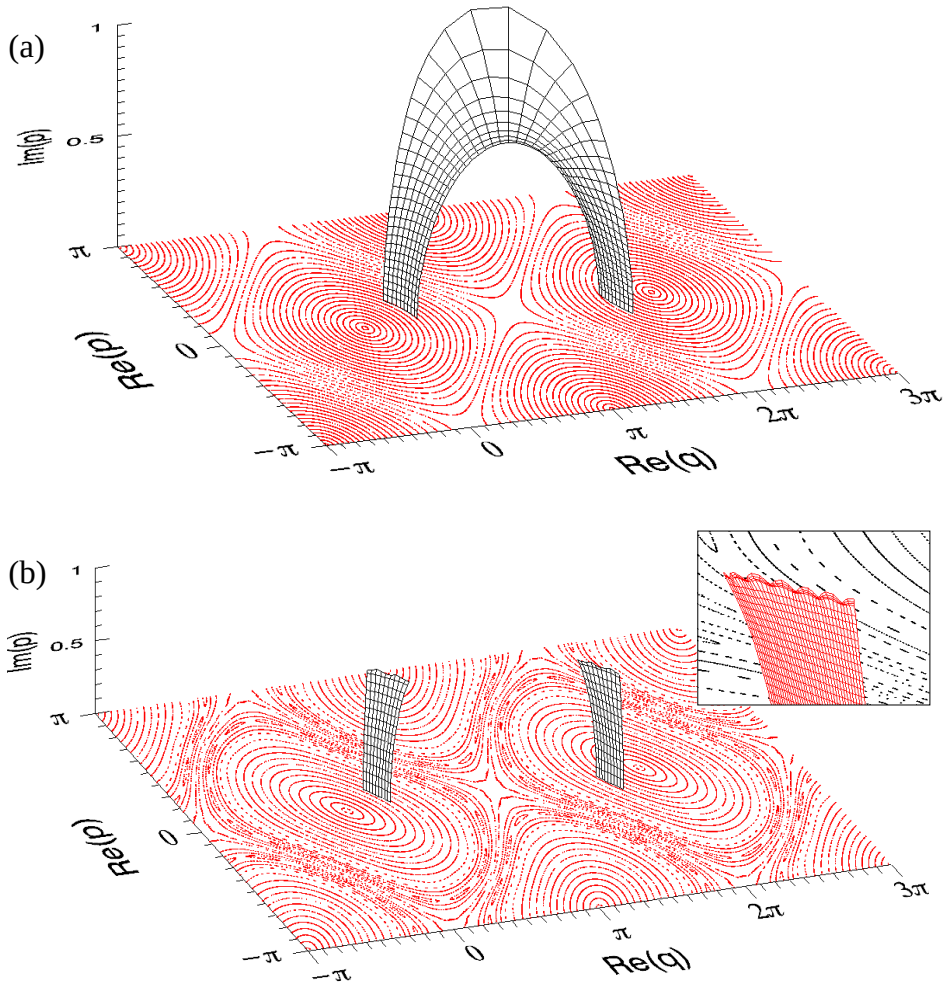

FIG. I.1–8 : *Figures 4 et 5 de* BRODIER et al. *(2002) reproduites avec la* ©*ourtoise autorisation des auteurs. Dans un cas intégrable (le modèle de* HARPER*) (a) les deux îlots tunnel que l'on peut voir dans l'espace des phases réel (plan horizontal* $\mathrm{Im}(p) = 0$*) peuvent être connectés par prolongation analytique des tores (ici en considérant une impulsion complexe* p*). Dans un cas quasi-intégrable (le modèle de* HARPER *pulsé) les tores réels* KAM *des îlots ne peuvent plus être considérés comme des sections d'un même tore complexe. Dès que l'on cherche à les prolonger on se heurte à une frontière naturelle qui se manifeste numériquement par les oscillations que l'on peut voir dans l'encart.*

PERCIVAL, 1981; PERCIVAL, 1982) (pour un travail plus récent, voir BILLI, TURCHETTI & XIE, 1993) — est que, contrairement à ce qui se passe dans le cas intégrable, on ne peut pas classiquement prolonger analytiquement les tores dans le plan complexe sans se heurter à une frontière naturelle (*cf.* figure I.1–8). Il faut donc au préalable approcher le modèle de départ par un modèle où la prolongation des tores pertinents dans l'effet tunnel est possible jusqu'à leur intersection (BRODIER, SCHLAGHECK & ULLMO, 2001, 2002). Très

récemment Smith & Creagh (2006) ont montré qu'une des clefs du problème pouvait être obtenue en construisant des tores approchés en généralisant la théorie des perturbations au cas complexe.

Au milieu des années 1990, les premières observations (Kuś, Haake & Delande, 1993; Scharf & Sundaram, 1994; Lebœuf & Mouchet, 1994; Creagh & Whelan, 1996) prouvant que les orbites périodiques complexes permettaient de reproduire quantitativement certains aspects de l'effet tunnel chaotique suggéraient que cette stratégie semiclassique était effectivement possible jusqu'au bout. Afin de ne pas se laisser déborder par la prolifération des solutions classiques (réelles et complexes) que l'on obtient en régime chaotique (formules à la Gutzwiller, divergentes si l'on n'opère pas avec soin et force d'astuces), il fallait absolument trouver un critère général pour ne retenir que les contributions les plus significatives. Or, dans le cas chaotique, la survie n'est jamais pérenne sur le champ de bataille des exponentielles : le phénomène de Stokes est omniprésent et rend ce critère hors de portée à l'heure actuelle.

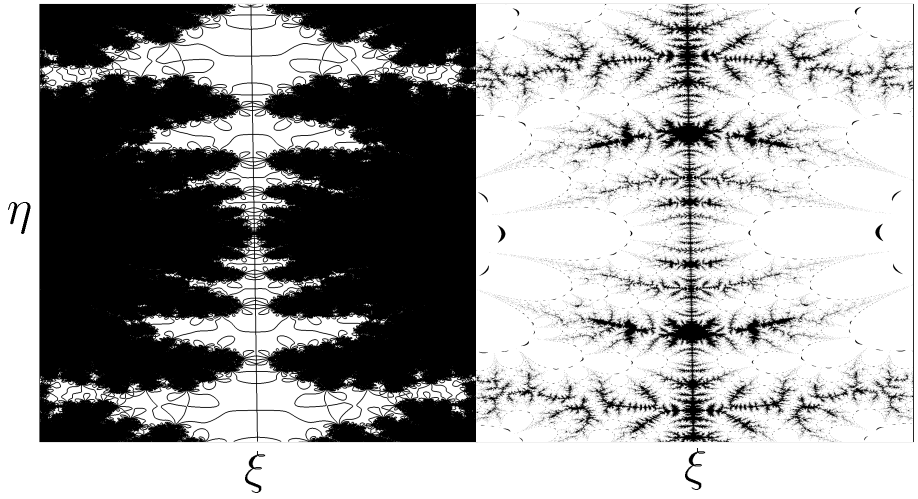

Fig. I.1–9 : *Figure 2 de* Shudo et al. *(2002) reproduite avec la* ©*ourtoise autorisation des auteurs. L'ensemble de Julia (à droite) rend bien compte de la structure des chaînes de Laputa observées à gauche dans l'espace des positions complexes* $q = \xi + \mathrm{i}\eta$ *pour l'application standard* (standard map). *Disons pour simplifier que ces dernières représentent les solutions des équations dynamiques (discrètes) pour lesquelles on impose une certains nombre de conditions, ici que les moments conjugués initial et final soient réels. La densité des courbes à gauche ne permet pas de les résoudre à l'intérieur des étendues sombres.*

Liée sans doute à ces difficultés, il faut signaler la découverte inattendue par l'école japonaise (Shudo & Ikeda, 1995, 1998) selon laquelle le chaos se trahit dans l'espace des phases complexe par la présence de structures fractales[20] dont les arcanes commencent à peine à être élucidées (Shudo, Ishii & Ikeda, 2002), *cf.* figure I.1–9.

[20] Appelées chaînes de Laputa, directement inspirées du nom coquin de l'île volante — reliée à la terre ferme par une chaîne — rencontrée par Gulliver lors de son troisième voyage. Mais est-il besoin de

b.6) Le jeu du chat et de la souris (*CAT and RAT game*)

Un second angle d'attaque pour tenter d'éclaircir l'effet tunnel chaotique consiste à renoncer à travailler avec un hamiltonien complètement déterminé. On évite de se scléroser sur une approche purement semiclassique en modélisant le chaos (ou le désordre) déterministe par un certain nombre de variables aléatoires. L'abandon d'une certaine information de détail au profit d'une plus grande universalité est remarquablement fécond pour des systèmes chaotiques, comme l'ont montré de façon éclatante BOHIGAS, GIANNONI et SCHMIT en (1983) dans un travail qui fait date. Remplacer les éléments de matrice du hamiltonien entre états chaotiques([21]) par un ensemble de variables aléatoires ne retenant qu'un petit nombre de propriétés pertinentes traduisant la présence de symétries globales est une stratégie qui a largement fait ses preuves ; pour une introduction sur l'application de la théorie des matrices aléatoires au chaos quantique, on pourra se reporter au cours de BOHIGAS (1989). Ces techniques hybrides, faisant intervenir à la fois des ingrédients semiclassiques et statistiques, sont à l'origine d'un progrès décisif dans notre compréhension quantitative de l'effet tunnel chaotique : plus précisément, elles ont sous-tendu la mise à jour de l'effet tunnel amplifié par chaos (*chaos-assisted tunnelling*, CAT pour les intimes) c.-à-d. l'observation (*cf.* note 18 p. 20) que l'effet tunnel est augmenté en moyenne de plusieurs ordres de grandeur lorsque le transport par les régions chaotiques de l'espace des phases s'accroît (BOHIGAS, TOMSOVIC & ULLMO, 1993; TOMSOVIC & ULLMO, 1994; LEYVRAZ & ULLMO, 1996). Néanmoins, l'extrême sensibilité de l'effet tunnel rend les prédictions très difficiles même si seul un ordre de grandeur est simplement requis. C'est déjà le cas dans les situations à priori plus simples des systèmes quasi-intégrables où il a été montré (sans l'aide de matrices aléatoires) que les résonances classiques internes peuvent amplifier les transitions tunnel de plusieurs ordres de grandeur. La première mise en évidence de ce rôle est due à BONCI *et al.* (1998) pour un pendule forcé et une étude systématique a été conduite dans (BRODIER, SCHLAGHECK & ULLMO, 2001, 2002) pour des applications discrètes (*quantum maps*)([22]). Cet effet tunnel amplifié par ré-

rappeler les sarcasmes anti-Lumières de SWIFT sur les insulaires, rompus à la physique, l'astronomie ou les mathématiques : *It seems the minds of these people are so taken up with intense speculations, that they neither can speak, nor attend to the discourses of others, without being roused by some external taction upon the organs of speech and hearing; for which reason those persons who are able to afford it always keep a flapper (the original is climenole) in their family, as one of their domestics, nor ever walk abroad or make visits without him.*

([21]) Les états chaotiques ont leur représentation de HUSIMI délocalisée dans la mer chaotique, par opposition, aux états réguliers qui vivent sur les îlots stables et peuvent se construire à partir des tores EBK. Les critères qui permettent une telle classification n'ont de sens que dans un régime semiclassique et sont bien évidemment valables à des termes exponentiellement petits près, ceux-là mêmes auxquels se rapporte l'effet tunnel.

([22]) Ces applications unitaires sont des opérateurs d'évolution $\hat{U}(\tau)$ introduits pour limiter les complications dues à l'intégration numérique de l'équation de SCHRÖDINGER sur de longues durées, *cf.* par exemple (BERRY, BALAZS, TABOR & VOROS, 1979), (TABOR, 1989, § 6.6) ou (HOLTHAUS, 1995). Semiclassiquement, l'application canonique classique associée Φ peut se déduire sans ambiguïté à partir de $\hat{U}(\tau)$. Une

sonance (*resonance-assisted tunnelling*, RAT pour les intimes) permet, par exemple, de mieux comprendre les temps caractéristiques de redistribution de l'énergie de vibration intermoléculaire (KESHAVAMURTHY, 2003; KESHAVAMURTHY, 2005). Il est aussi à l'œuvre lorsque le chaos est beaucoup plus développé (ELTSCHKA & SCHLAGHECK, 2005; SCHLAGHECK, ELTSCHKA & ULLMO, 2006).

seule itération est donnée explicitement en terme des variables canoniques et contient déjà en germe les non-linéarités qui, à plus long terme, peuvent engendrer une trajectoire chaotique. On peut déduire $\hat{U}(\tau)$ et Φ d'une dynamique hamiltonienne pulsée (en général considérée à une dimension toujours par souci de simplification) qui a pu, dans certains cas, être réalisée expérimentalement avec des atomes froids (MOORE, ROBINSON, BHARUCHA, WILLIAMS & RAIZEN, 1994). La limite $\tau \to 0$ fournit un système continu, donc forcément intégrable si l'on est à une dimension.

I.2 Bref survol de mes collaborations et de mes contributions

Voilà donc brossé à grands traits le contexte dans lequel se situe mon travail sur l'effet tunnel. Si pour faire (enfin ?) court je devais résumer en une phrase les questions qui nous passionnent, je proposerais : *Peut-on, à l'instar de la relation* (I.1–2)*, obtenir pour l'effet tunnel chaotique, des relations qui permettent de calculer, ne fût-ce qu'en moyenne et en n'étant pas trop exigeant, disons, un temps typique d'oscillation ou de désintégration en s'appuyant sur des quantités classiques ?* J'ai la prétention de croire que le mieux que l'on puisse faire, à l'heure actuelle, se trouve illustré sur la figure reproduite p. 88. Sans même rentrer dans les détails, on comprend que nous sommes encore loin d'avoir le dernier mot dans cette affaire.

ᔓ

De fait, les nombreuses avancées qui ont été effectuées sur l'effet tunnel chaotique depuis l'origine s'appuient autant sur le développement des bons outils conceptuels que des expériences à la fois numériques et physiques. C'est sur ce triple front que se place l'ensemble de mes contributions sur ce sujet. Elles n'ont été possibles uniquement que parce que j'ai pu bénéficier de collaborateurs chevronnés, tant sur le plan théorique, numérique qu'expérimental et toujours grâce à des environnements de travail exceptionnellement stimulants.

Tout d'abord, mes premiers travaux sur l'effet tunnel datent de ma thèse, dirigée par Patricio Lebœuf à la Division de Physique Théorique de l'Institut de Physique Nucléaire de l'université Paris-Sud (Orsay), devenue, depuis 1998, le Laboratoire de Physique Théorique et de Modèles Statistiques, cnrs umr 8626.

➳ Dans (Lebœuf & Mouchet, 1994), nous considérons un modèle d'électron dans un cristal bidimensionnel en présence d'un champ magnétique intense perpendiculaire au plan cristallin. Nous déterminons quelles sont les orbites classiques qui contribuent au courant électrique longitudinal et, dans le cas où ce dernier est gouvernée uniquement par l'effet tunnel, nous montrons comment l'inclusion de solutions complexes aux équations du mouvement classique permet de continuer à obtenir une description semiclassique fidèle. Nous montrons aussi que la prise en compte des orbites complexes permet d'étendre le domaine de validité du régime semiclassique à des valeurs de $\hbar$ non forcément petites.

➳ Dans (Lebœuf & Mouchet, 1999), nous présentons une étude systématique du poids des orbites complexes dans les développements asymptotiques semiclassiques génériques correspondant à des systèmes à deux degrés de liberté. On subodore que ces solutions complexes sont amenées à jouer un rôle dans une approche semiclassique de l'effet tunnel chaotique. De manière générale, une étude détaillée des bifurcations génériques apparaît nécessaire pour étendre les idées de Gutzwiller aux systèmes dont la dynamique est mixte. Partant de l'hypothèse que ces orbites complexes ne jouent un rôle notable que si elles sont peu éloignées du domaine réel et donc non loin d'une bifurcation, nous montrons que seules celles provenant d'un type bien précis de bifurcation donnent une contri-

bution exponentiellement décroissante. Les contributions de toutes les autres sont noyées dans « l'ombre » des termes oscillants habituels via des termes en puissances de $\hbar$ plus élevées.

Les autres travaux, effectués au Laboratoire de Mathématiques et de Physique Théorique de l'université François Rabelais (Tours) — cnrs umr 6083 — sont reproduits dans ce mémoire. Je les présenterai succinctement dans les sections correspondantes. Ils ont largement bénéficié de la généreuse hospitalité du Laboratoire Kastler-Brossel à l'université Pierre & Marie Curie (Paris) — cnrs umr 8552 — et, en particulier, du groupe Dynamique des Systèmes Coulombiens dirigé par Dominique Delande. Il convient ici de mentionner que toutes les diagonalisations numériques effectuées dans les articles ci-dessous ont bénéficié d'une routine basée sur l'algorithme de Lanczos écrite et fignolée au fil des ans par Dominique.

➵ Dans (Mouchet, Miniatura, Kaiser, Grémaud & Delande, 2001), écrit avec Dominique Delande et Benoît Grémaud (lkb) ainsi qu'avec Christian Miniatura et Robin Kaiser du groupe d'atomes froids de l'Institut Non-Linéaire de Nice — cnrs umr 6618 — nous proposons d'utiliser des systèmes d'atomes froids pour tester certaines idées de l'effet tunnel chaotique.

Des expériences très similaires dans les grandes lignes à celles que nous proposions ont été réalisées la même année par deux équipes aux États-Unis : le groupe *Laser Cooling and Trapping* dirigé par William Phillips au *National Institute of Standards and Technology* (Gaithersburg) et le groupe de Mark Raizen du *Center for Nonlinear Dynamics* à l'université du Texas (Austin).

➵ Dans (Mouchet & Ullmo, 2001), article de commande de *Physics World*, nous expliquons pour un large public la portée des expériences du nist et d'Austin.

➵ Dans l'article (Hensinger, Mouchet, Julienne, Delande, Heckenberg & Rubinsztein-Dunlop, 2004), écrit surtout en collaboration avec Dominique Delande et Winfried Hensinger, ce dernier étant post-doc dans le groupe de Phillips et directement en charge de l'expérience, nous analysons en détail leurs résultats et, en particulier, nous montrons qu'ils sont en excellent accord avec les prédictions du modèle numérique.

➵ Dans (Mouchet & Delande, 2003), nous proposons une mise au point nécessaire sur ce que l'on entend vraiment par effet tunnel chaotique. Le besoin s'en était fait sentir parce qu'il existait à l'époque une certaine confusion sur ce que les expériences du nist et d'Austin montraient et ne montraient pas. Nous discutons de questions encore largement ouvertes et proposons de futures expériences pour tenter d'y répondre en nous appuyant sur des simulations numériques.

➵ Dans (Mouchet, Eltschka & Schlagheck, 2006) écrit en collaboration avec Peter Schlagheck et Christopher Elstschka du groupe *Complex Quantum Systems* de l'université de Regensburg (Allemagne) dirigé par Klaus Richter, nous confirmons le rôle central joué par les résonances dans l'effet tunnel chaotique et nous apportons un nouvel éclairage sur la correspondance entre ces résonances, les fonctions d'onde impliquées dans l'effet tunnel chaotique et leur représentation dans l'espace des phases.

I.3 Effet tunnel amplifié par le chaos avec des atomes froids

Cet article a été écrit avec Dominique Delande et Benoît Grémaud (lkb) ainsi qu'avec Christian Miniatura et Robin Kaiser du groupe d'atomes froids de l'Institut Non-Linéaire de Nice — cnrs umr 6618. L'idée de départ (rédigée en 1996 dans une note interne non-publiée), à savoir proposer une configuration expérimentale précise utilisant des atomes froids pour tester certaines idées de l'effet tunnel chaotique, était la seconde des armatures du projet « chaos ondulatoire » de C. Miniatura et R. Kaiser, en collaboration avec D. Delande, visant à créer une nouvelle équipe de recherche, expérimentale, à l'inln. J'ai été invité à participer à ce projet en janvier 1997, juste après ma thèse tout en bénéficiant encore des derniers mois de mon allocation de moniteur normalien pour ce « mini-pseudo post-doc » et avant d'être recruté à Tours au printemps 1997.

Les raisons pour lesquelles les atomes froids sont des candidats de premier choix pour tester et utiliser certaines propriétés quantiques subtiles sont faciles à comprendre. La préférence se porte vers des atomes alcalins dont la structure interne est riche et bien connue, permettant ainsi de les manipuler aisément par le biais des forces dipolaires créées par des lasers. Les atomes choisis sont neutres pour éviter toute interaction coulombienne entre-eux, ce qui les rend dans une large mesure indépendants les uns des autres, du moins tant que l'on atteint pas la formation d'un condensat de Bose-Einstein([23]). Les températures envisagées à Nice ($T \gtrsim T_R \simeq 123$ nK pour les atomes de rubidium) devaient permettre d'obtenir des atomes suffisamment froids pour préserver la cohérence c.-à-d. limiter la dissipation sur des durées plus longues que les périodes tunnel recherchées mais il était hors de question, du moins dans les premières années, d'envisager de descendre à des températures inférieures à celle, T_R, correspondant à la vitesse de recul d'un atome sous l'effet d'une absorption ou de l'émission d'un photon et, à fortiori, d'atteindre la température requise pour un condensat ($T_{\text{BEC}} \simeq 75$ nK). Ayant tout à monter, il fallait que les projets expérimentaux niçois restent raisonnablement ambitieux. Or, la mise au point d'un piège atomique partant d'une table rase et les techniques de refroidissement des atomes jusqu'à la température de recul nécessitent déjà un investissement humain et matériel considérable([24]).

Malgré tout, encouragés par les résultats de récents de Moore, Robinson, Bharucha, Williams & Raizen (1994) tentant d'étudier la localisation dynamique grâce aux atomes froids, nous pouvions envisager une configuration expérimentale (*cf.* figure p. 32) qui permettait d'obtenir des atomes évoluant avec un hamiltonien effectif donné par l'équation (3) p. 33. Dans cet article, finalement publié en 2001, nous expliquons en détails les

([23]) Rappelons que les premiers condensats atomiques ont été obtenus en 1995 et que les deux équipes américaines de Wieman & Cornell et de Ketterle ont, pendant plus d'un an, été les seules à pouvoir le faire.

([24]) Pour donner une idée, « la plus basse température jamais atteinte sur la Côte d'Azur » (écrit Nice-Matin daté 21 octobre 1997 en marge du prix Nobel de physique remis cette même année à C. Cohen-tannoudji, W. Phillips et S. Chu) n'était encore que de l'ordre de 10^{-3} K courant octobre.

raisons pour lesquelles on obtient ainsi une configuration idéale pour étudier l'effet tunnel chaotique et nous dressons un tableau complet de la dynamique classique et quantique de ce modèle. Les principales difficultés qui se posaient alors avaient une double origine : d'une part, préparer expéri-mentalement un suffisamment grand nombre d'atomes dans l'un des îlots intégrables sans en avoir dans le second n'est pas une mince affaire ; d'autre part, il fallait analyser le plus soigneusement possible les conditions d'obtention d'un signal qui porteraient une signature quantitative de l'effet tunnel. Les expériences d'optique quantique et de physique atomique s'étalent sur plusieurs mois (au mieux) et il va de soi que l'on ne peut que rarement modifier sa stratégie en cours de route ou s'offrir le luxe de négliger des détails pouvant coûter quelques centaines de milliers d'euros. L'ambition de notre article était aussi de proposer des solutions réalistes dans ce contexte.

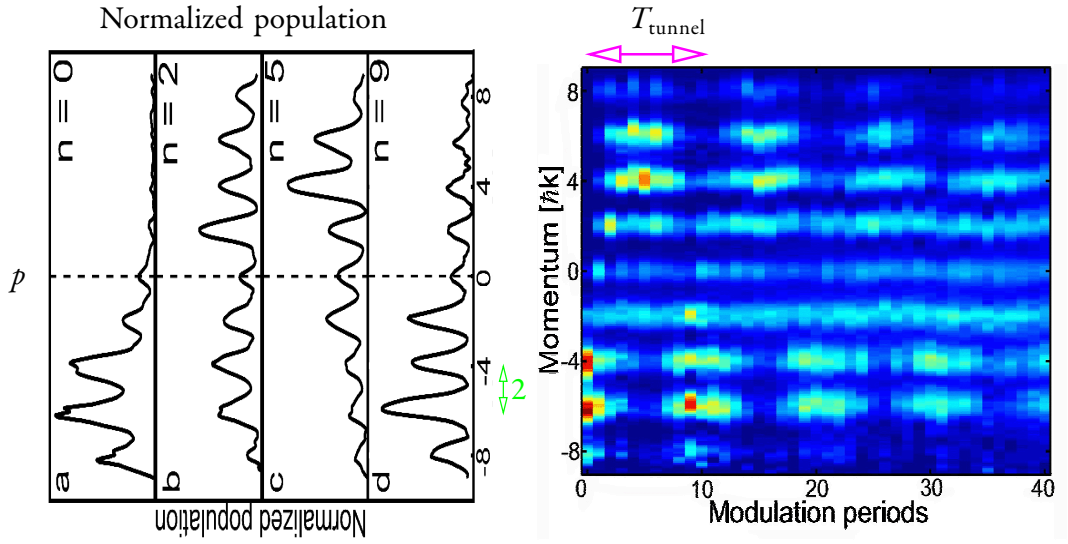

FIG. I.3–1 : *(couleur recommandée) Figures 3 et 5 de* HENSINGER et al. *(2001) reproduites avec la* ©*ourtoise autorisation de W.* HENSINGER. *La figure de droite est une image de la distribution en impulsions (axe vertical) des atomes de sodium évoluant sous le hamiltonien effectif (3) p. 33 avec* $\theta \simeq 1.72$ *et* $\gamma \simeq .96$. *La période de modulation du hamiltonien (2) est de* 20 μs. *La dynamique classique correspond à la section de* POINCARÉ *de la figure I.3–2 (les échelles en impulsion ne sont pas les mêmes) et interdit les transitions entre* $\mathcal{I}_\pm$ *que l'on observe ici. Pour un instant donné, les franges en impulsion de période* $2\hbar k$ *sont dues à la cohérence spatiale des ondes de matière sur quelques zones de* BRILLOUIN *(le hamiltonien est périodique aussi spatialement). cf. aussi la figure reproduite 48.*

Quelques mois après la publication de notre article, donc à trop brève échéance pour être véritablement influencé par lui, deux équipes aux États-Unis : le groupe *Laser Cooling and Trapping* dirigé par William PHILLIPS au *National Institute of Standards and Technology* (Gaithersburg) et le groupe de Mark RAIZEN du *Center for Nonlinear Dynamics* à l'université du Texas (Austin) obtiennent les premières manifestations d'une variation très

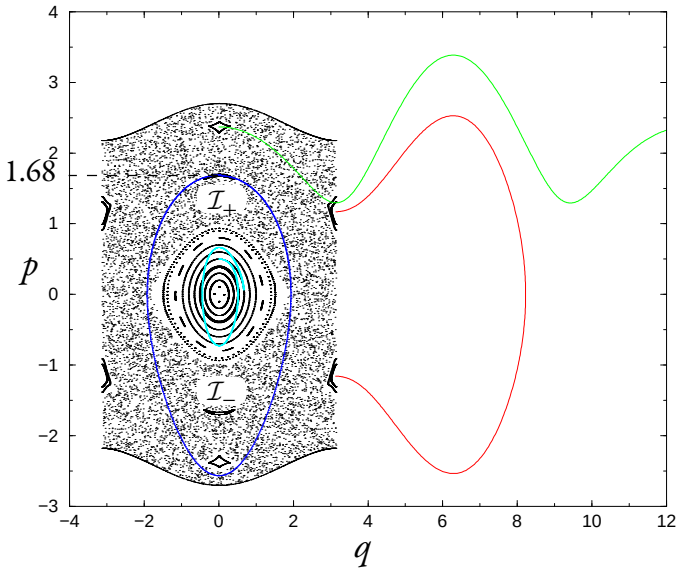

FIG. I.3–2 : *(couleur recommandée) Section de POINCARÉ correspondant au hamiltonien effectif (3) p. 33 avec les paramètres de la figure I.3–1. Comparée aux sections reproduites p. 53, ce choix ne semble pas optimal si l'on fait abstraction des contraintes expérimentales. Les deux îlots tunnel $\mathcal{I}_\pm$ en forme de croissants de Lune très fins — situés en $(p \simeq \pm 1.68, q = 0)$ — ont un faible volume dans l'espace des phases et sont à peine discernables. Les autres îlots ne sont pas pertinents pour l'effet tunnel. Les courbes continues représentent des trajectoires régulières non-stroboscopées, ni repliées sur $[-\pi, \pi[$. La bleue qui part de $\mathcal{I}_+$ permet de vérifier que $\mathcal{I}_\pm$ ne sont pas connectés entre eux.*

brutale d'une période tunnel. Leurs configurations expérimentales conduisent exactement au même hamiltonien effectif que celui que nous avions envisagé([25]). La différence (et de taille !) avec notre travail est que les équipes américaines pouvaient se permettre d'utiliser des condensats pour la préparation des atomes. Ce fut cependant un tour de force d'être capable de « voir » les oscillations tunnel (en impulsion) des atomes d'un îlot à l'autre et de pouvoir ainsi mesurer directement les périodes (I.1–1). On peut difficilement imaginer une signature plus claire (*cf.* figure I.3–1). On comprend alors que ces résultats et la disproportion de moyens entre les équipes aient fait avorter (provisoirement ?) le projet ambitieux des niçois. Ils se sont largement rattrapés depuis en devenant l'une des équipes les plus en pointe au niveau international sur la diffusion multiple, sujet qui constituait le premier volet de leurs propositions de 1996.

([25]) Sa forme est en fait très naturelle : dès lors que l'on cherche à obtenir un hamiltonien symétrique à une dimension dépendant du temps ou bien, de façon équivalente, un système autonome à deux degrés de liberté. Il s'agit d'un hamiltonien « minimal » où seules deux ou trois résonances sont retenues. En effet, exprimées avec des variables action/angle, les deux premières composantes de FOURIER du potentiel dépendantes du temps suffisent à engendrer une dynamique chaotique par recouvrement à la CHIRIKOV (1979) ; *cf.* aussi (LICHTENBERG & LIEBERMAN, 1983).

PHYSICAL REVIEW E, VOLUME 64, 016221

Chaos-assisted tunneling with cold atoms

A. Mouchet,[1,*] C. Miniatura, R. Kaiser,[2,†] B. Grémaud, and D. Delande[3,‡]
[1]*Laboratoire de Mathématiques et de Physique Théorique (CNRS UPRES-A 6083), Avenue Monge, Parc de Grandmont, 37200 Tours, France*
[2]*Laboratoire Ondes et Désordre (CNRS FRE 2302), 1361 route des Lucioles, Sophia Antipolis, F-06560 Valbonne, France*
[3]*Laboratoire Kastler-Brossel (CNRS UMR 8552), Université Pierre et Marie Curie, 4 place Jussieu, F-75005 Paris, France*
(Received 7 December 2000; published 26 June 2001)

In the context of quantum chaos, both theory and numerical analysis predict large fluctuations of the tunneling transition probabilities when irregular dynamics is present at the classical level. Here we consider the nondissipative quantum evolution of cold atoms trapped in a time-dependent modulated periodic potential generated by two laser beams. We give some precise guidelines for the observation of chaos-assisted tunneling between invariant phase space structures paired by time-reversal symmetry.

DOI: 10.1103/PhysRevE.64.016221 PACS number(s): 05.45.Mt, 05.60.Gg, 32.80.Qk, 05.45.Pq

I. INTRODUCTION

During the 1970's and 1980's it gradually became clear that classical Hamiltonian chaos profoundly affects the temporal evolution and spectral properties of the corresponding quantum system as compared to the integrable case [1]. Some of these features (dynamical localization, scars of periodic orbits [2], etc) share striking similarities with concepts originating from condensed matter physics such as weak and strong localization [3]. In fact these phenomena can be recast in terms of wave transport in disordered media, the (quasi) randomness being of statistical or dynamical origin. In this context, it is important to understand the mechanisms underlying a key feature of wave propagation which has no classical analog: tunneling.

Tunneling refers to any wave process which is classically forbidden to *real* solutions of the Hamilton equations. For one-dimensional (1D) autonomous systems, it is well known that the quantum tunneling probability through an energetic barrier can be evaluated semiclassically with the help of classical *complex* solutions of the Hamilton equations [4,5]. The direct generalization of this procedure to higher dimensional systems is straightforward for separable dynamics, but is already subtle for integrable, but no longer separable, dynamics [6,7]. In the generic case of chaotic dynamics, it even proves extremely hard to handle, and the situation, until recently, seemed hopeless. Indeed, in the presence of chaos, the analytical and topological properties of the classical *complexified* phase space are far from trivial. During the last ten years however, theoretical and numerical investigations on autonomous 2D and time-dependent 1D Hamiltonian systems have started to highlight some mechanisms [6–12], and much insight has been gained on the influence of such classical nonseparable dynamics. Experimental evidence of such mechanisms, which is still lacking, would be of great interest especially in the light of the subtle interplay between interferences and disorder.

In this paper, we consider 1D time-dependent dynamics, one of the simplest cases where irregular motion can appear, and we study chaos-assisted tunneling. Our effective Hamiltonian model, which is derived from an experimentally achievable situation, exhibits three main properties. First, its classical dynamics is invariant under time reversal. Second it is controlled by a single real external parameter γ (for $\gamma = 0$ the dynamics is integrable and chaos develops more and more in phase space as γ is increased). Third, there exists in phase space, for a whole continuous range of γ, a pair of stable islands $\mathcal{I}_+$ and $\mathcal{I}_-$ which are time-reversed images of each other. By stable islands we mean the set of regular classical trajectories in phase space which stay near a stable equilibrium point or near a stable periodic orbit of the system. In this case, no real classical orbit started in one of these islands can go into the other one. However, the quantum dynamics of a wave packet, initially prepared in one island, will display a periodic behavior. The wave packet oscillates from one island to its time-reversed image [13]. In the quantum spectrum this tunneling process appears via the existence of nondegenerate energy doublets whose splitting gives the inverse of the tunneling time between $\mathcal{I}_+$ and $\mathcal{I}_-$. Varying γ slowly modifies the geometry of the islands themselves. The crucial point is that it will drastically change the classical dynamics for some initial conditions lying between the islands. For small enough γ, the chaotic layers are too small to play a significant role at $\hbar$ scales, and hence cannot influence the quantum behavior of the system, which is essentially still regular. For larger values, but still before the stable islands are completely destroyed, there is a chaotic regime where varying γ or $\hbar$ ($\hbar$ being in this case Planck's constant divided by some typical classical action) alone induces large fluctuations, of several orders of magnitude, of the doublet splittings around their mean value. This in turn corresponds to large fluctuations of the tunneling periods. These large fluctuations, induced by small changes of any parameter, are a signature of the so-called ''chaos-assisted tunneling'' regime. This has been extensively studied both theoretically and numerically in the situation described above [8–11], but has not yet been observed in real experiments, the main reason being its extreme sensitivity to small changes in the classical dynamics. Any *uncontrolled* varia-

*Electronic address: mouchet@celfi.phys.univ-tours.fr
†Electronic address: miniat,kaiser@inln.cnrs.fr
‡Electronic address: gremaud,delande@spectro.jussieu.fr

tion of γ, be it noise or dissipation, will dramatically wash out or destroy the signal. The observation of this highly fluctuating tunneling regime thus requires both an accurate control of the dynamics of the preparation of the initial state and of the analysis of the final state. The observation of doublet splittings is rather common in molecular physics, when a discrete symmetry like parity is present. In most cases, the splitting is due to standard tunneling either through an energy barrier or a dynamical barrier (see, for example, Refs. [15–17]). It was suggested in some cases [18,19] that this splitting is influenced by the existence of chaos in the classical dynamics. Thus molecular physics provides us with systems where chaos-assisted tunneling could be experimentally observed. However, one usually lacks an external parameter which could allow for the observation of the fluctuations of the tunneling rate.

Atom cooling techniques [14] provide systems which fulfill all the desired requirements. They allow an accurate manipulation and control of internal and external degrees of freedom, and are a useful tool to produce situations where the wave character of the atomic motion is essential [20]. A great variety of interaction potentials can be produced to influence the atomic motion, be it by means of inhomogeneous magnetic fields, material gratings, or laser light. Optical lattices with crystalline or quasicrystalline order [21–23] can be easily produced where atoms mimic situations usually encountered in condensed matter [24,25]. Dissipation (spontaneous emission and atom-atom interaction) is easily controlled, and coherence times of the order of 10 ms can readily be achieved. This is why cold atoms are a unique tool to study transport properties of waves, be it quantum chaos [26] or weak localization [27,28].

This paper is organized as follows. In Sec. II we explain the origin of the effective Hamiltonian for the experimental situation under consideration. In Sec. III we study the corresponding classical dynamics, and show why this effective Hamiltonian is relevant for chaos assisted tunneling. In Sec. IV we quickly review some of the usual theoretical techniques when dealing with both space and time periodic quantum dynamics. We also illustrate how some quantum spectral properties have a natural classical interpretation. In Sec. V we show, with the help of numerical experiments, how chaos-assisted tunneling arises in our system, and then explain how to observe it in a real experiment. Section VII is devoted to some concluding remarks.

II. EFFECTIVE HAMILTONIAN

A. Light shifts

The very basic physical mechanism underlying our forthcoming discussion is the following: when an atom is exposed to monochromatic light, its energy levels are shifted by the interaction. These level shifts originate from the polarization energy of the atom in the incident light field, and are called light shifts [29]. In the dipolar approximation, they depend on the field intensity value at the center-of-mass position of the atom. If the field intensity is space-time dependent, then a moving atom will experience dipolar forces: inhomogeneous light shifts result in forces and alter the center-of-mass motion of the atom. By appropriately tailoring the space-time dependence of the light field, one can then produce a great variety of potentials for the external atomic motion, as proven by the atom cooling community. Note, however, that the atom-light interaction is also responsible for a dissipative phenomenon (real absorption of a photon followed by spontaneous emission) which shortens the temporal coherence of the atomic wave function. By using a laser light far detuned from any atomic resonance, it is possible to control this stray phenomenon and maintain it at a reasonably low rate. In the following, we shall describe a simple physical situation for atoms where chaos-assisted tunneling is expected to be present.

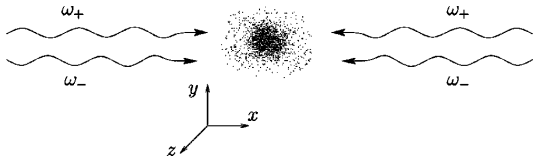

FIG. 1. Experimental configuration under consideration: a cloud of two-level atoms is illuminated by two monochromatic standing waves with frequencies $\omega_\pm = \omega_L \pm \delta\omega/2$ ($\delta\omega \ll \omega_L$). All fields are linearly polarized along the same direction, and are sufficiently far detuned from the atomic resonance so that dissipation effects can be ignored.

B. Experimental configuration

Although the internal structure (hyperfine Zeeman sublevels) are of major importance in atom cooling, here, for simplicity, we will model the atom by a two-level system (as only one optical transition usually governs the dynamics). We consider a dilute sample of identical (but independent) two-level atoms propagating in the light field configuration created by two monochromatic standing waves with frequencies $\omega_\pm = \omega_L \pm \delta\omega/2$ where $\delta\omega \ll \omega_L$. We denote the groundstate and excited state of each atom by $|g\rangle$ and $|e\rangle$, these levels being connected by an electric dipole transition of angular frequency $\omega_{\rm at}$ and width Γ. All atoms are supposed to be initially prepared in their ground state. Each standing wave is produced along the x axis by two counterpropagating laser beams, and we suppose all fields to be linearly polarized along the z axis (see Fig. 1). After a suitable choice of space-time origin, the total electrical field strength is

$$E(x,t) = [E_+ \cos(\omega_+ t) + E_- \cos(\omega_- t)]\cos(k_L x), \quad (1)$$

where $E_\pm$ are the field strengths of the two standing waves. At this point we have neglected the difference in wave vectors of the standing waves. For this to hold, it is sufficient to assume that the atomic sample size is small enough. Typically, the difference in the k vectors will be of the order of 10^{-9} or less (see below), so that this requires the atomic cloud to be smaller than typically a few kilometers, which is amply satisfied in a standard magneto-optical trap.

C. Dimensionless effective Hamiltonian

The effective Hamiltonian which describes the atomic motion is derived in Appendix A under some common and well-controlled approximations. It acts in the Hilbert space of a one-dimensional system which is simply the x component (position) of the center of mass of the atom (which means that the internal degree of freedom as well as the y and z coordinates can be eliminated; see Appendix A). This reads

$$H=\frac{p_x^2}{2M}-V_0\cos(2k_Lx)[\theta+\cos(\delta\omega\, t)], \tag{2}$$

where $V_0\overset{\text{def}}{=}-\hbar\Omega_+\Omega_-/8\delta_L$ and $\theta\overset{\text{def}}{=}(\Omega_+/2\Omega_-)+(\Omega_-/2\Omega_+)$, with $\delta_L=\omega_L-\omega_{at}$ the detuning with respect to the atomic frequency and $\Omega_\pm=dE_\pm/\hbar$ (d being the atomic dipole strength). Without loss of generality we will assume V_0 to be positive since, if V_0 is negative, it is sufficient to shift x by $\pi/2k_L$ to recover this case.

In the following, it will prove convenient to work with dimensionless quantities. Rescaling quantities through $\tau\overset{\text{def}}{=}\delta\omega\, t$, $q\overset{\text{def}}{=}2k_Lx$, $p\overset{\text{def}}{=}(2k_L/M\delta\omega)p_x$, $\gamma\overset{\text{def}}{=}(4k_L^2/M\delta\omega^2)V_0$, and $H_{\text{eff}}\overset{\text{def}}{=}(4k_L^2/M\delta\omega^2)H$ then yields the dimensionless effective Hamiltonian

$$H_{\text{eff}}=\frac{p^2}{2}-\gamma(\theta+\cos\tau)\cos q. \tag{3}$$

Such a Hamiltonian describes the dynamics of a periodically driven pendulum. The associated quantum canonical commutation relation is $[q,p]=i\hbar_{\text{eff}}$, and we obtain $\hbar_{\text{eff}}\hbar_{\text{eff}}=8\omega_R/\delta\omega$, where $\omega_R=\hbar k_L^2/2M$ is the atomic recoil frequency and $\delta\omega$ is the beating frequency between the laser waves.

Such an effective Hamiltonian clearly exhibits two of the three properties mentioned in Sec. I: the corresponding classical dynamics is governed by a single classical parameter, the dimensionless coupling strength γ, and is invariant under time-reversal symmetry $(p,q,\tau)\mapsto(-p,q,-\tau)$. It is worth mentioning that the semiclassical limit $\hbar_{\text{eff}}\to 0$ is realized here by increasing the beating frequency $\delta\omega$ between the two laser waves.

With our field configuration, only $\theta\geqslant 1$ can be achieved. As a slight generalization, we extend the range of θ to any positive value, since one can design other field configurations where $\theta\leqslant 1$ occurs. For example, $\theta=0$ yields the Hamiltonian studied in Ref. [13] in a different context.

D. Orders of magnitude

Let us give some typical experimental parameters. For rubidium atoms, the atomic parameters are $M=85$ amu, $\lambda_{\text{at}}=2\pi c/\omega_{\text{at}}=0.78$ μm, $\Gamma/2\pi=6$ MHz, $\omega_R/2\pi=3.8$ kHz, and the saturation intensity $I_{\text{sat}}=1.6$ mW/cm^2. Using far-detuned laser beams ($2\delta_L/\Gamma=10^4$) focused down to 500 μm (power 100 mW), with a frequency difference $\delta\omega/2\pi=60$ kHz, leads to $\gamma=0.4$ and $\hbar_{\text{eff}}=0.05$. With such values, spontaneous emission can be neglected up to times of the order of few ms. It is worth noting the tiny energies which come into play ($V_0\sim 5$ neV), by several orders of magnitude smaller than the typical ones for mesoscopic systems.

III. CLASSICAL DYNAMICS

A. Poincaré surface of section

A Poincaré surface of section provides the usual tool for visualizing the classical dynamics [30]. As H_{eff} is 2π periodic both in time and space, this surface of section simply consists in the whole phase space itself (which has the topology of a cylinder) where trajectories $(p(\tau),q(\tau))$ are seen stroboscopically at every time period 2π. In the following, without any substantial loss of generality, we will restrict our analysis to the case $\theta=1$ which is easily experimentally achieved when the standing waves have the same field strengths.

Figure 2 shows stroboscopic plots of phase space orbits for different values of γ. For $\gamma=0$, p is a constant of motion, so that the system is integrable and the surface of section is composed of horizontal lines. For a weak enough γ [Fig. 2(a)], the orbits remain confined to invariant curves. These invariant curves stratify the whole phase space, and the dynamics appears regular. One can clearly see well-separated stability islands, each being bordered by a separatrix. This is the situation encapsulated in the Kol'mogorov-Arnol'd-Moser (KAM) theorem for near-integrable motion: although no globally defined constants of motion exist, some invariant curves can still be constructed which order the dynamics. As γ is increased [Fig. 2(b)], more and more of the invariant curves are broken and chaotic layers start to spread around separatrices. These layers fill some portion of phase space, but the motion is still predominantly confined to invariant curves. Above some coupling threshold [Figs. 2(c)–2(e)], stochastic orbits invade the phase space, and the surviving stability islands are surrounded by a connected chaotic sea. This occurs for $\gamma\sim 0.1$. The phase space structure in this regime is typical of a mixed dynamics where regular orbits coexist with stochastic ones. If γ is increased further [Fig. 2(f)], the stability islands disappear (or are too small to be seen at this scale) and one obtains global chaos. However, we note that, even in this situation, the chaotic portion of phase space is still bounded by invariant curves, which means that chaos can only fully develop within some range of momentum p.

B. Resonances

At this stage, let us rewrite the effective Hamiltonian as follows:

$$H_{\text{eff}}=H_0+\gamma H_1=\frac{p^2}{2}-\gamma\cos q-\frac{\gamma}{2}\cos(q+\tau)$$
$$-\frac{\gamma}{2}\cos(q-\tau). \tag{4}$$

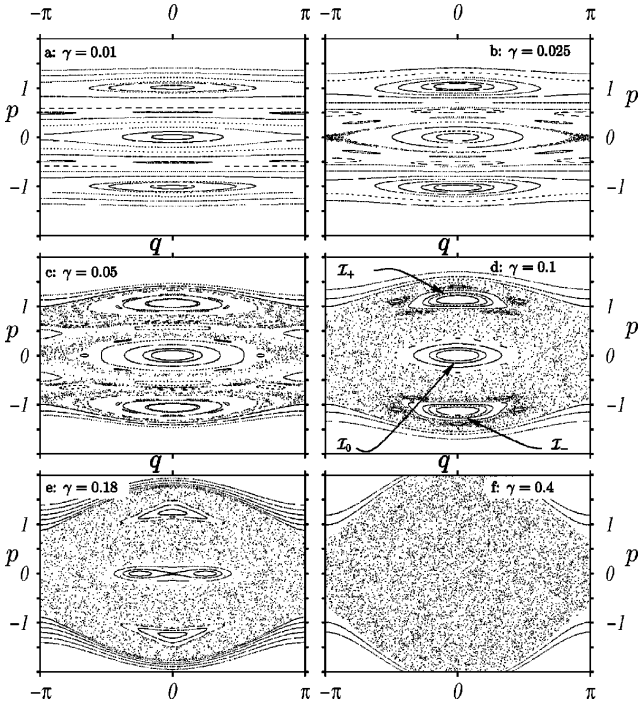

FIG. 2. Stroboscopic plots of trajectories in phase space for different initial conditions at $\tau=0$ and different γ's. The classical dynamics is governed by Hamiltonian 3 with $\theta=1$. At low γ values, resonance islands are visible separated by quasifree motion. As γ increases, the resonance islands grow and chaos appears close to the separatrices. The situation of interest for chaos-assisted tunneling is when two symmetric islands are separated by a chaotic sea, such as $\mathcal{I}_+$ and $\mathcal{I}_-$ in (d) and (e).

The physical interpretation of the various terms is rather simple: the two counterpropagating laser beams at frequency ω_+ create a stationary wave which, in turn, creates for the atom an effective optical potential proportional to the square of the modulus of the electric field in the standing wave; hence the $\cos q$ dependence (it is actually $1+\cos q$, but the constant term does not play any role in the dynamics). The same effective potential is due to the standing wave created by the two ω_- counterpropagating beams. A pair of counterpropagating beams at frequencies ω_+ and ω_- does not create a standing wave in the lab frame. However, in a frame moving at constant velocity $v_0=(\omega_+-\omega_-)c/2\omega_L$, ($v_0=1$ in rescaled units) the two laser beams are shifted in frequency by the Doppler effect and appear to have equal frequency, building another stationary wave and yet another effective optical potential. In the lab frame, this appears as a modulated optical potential moving at velocity v_0. By symmetry, there are two such effective potentials moving either to the right or to the left. These are the $\cos(q\pm\tau)$ terms in the Hamiltonian.

This form of the Hamiltonian allows us to point out the perturbative terms which may be resonant with the unperturbed frequencies. When $\gamma=0$, the system is integrable since we recover free motion: $H_{\rm eff}$ reduces to $H_0=p^2/2$, and (p,q) are exact action-angle variables. For $\gamma>0$, the absence of any constant of motion generates chaos. Stroboscopic plots of phase space trajectories are no longer constrained to follow lines of constant H_0, but generically fill densely a two dimensional volume in phase space. As long as γ is small enough, these volumes remain thin enough not to be distinguished from regular lines at the scale of finite precision of the measurements and/or the calculations [cf. Fig. 2(a)]. Nevertheless, for higher values of γ, some chaotic layers can be seen [cf. Fig. 2(b)] between regular regions. These consist of portions of phase space where trajectories are exponentially sensitive on initial conditions. From classical first-order perturbation theory (Ref. [30], Chap. 2), we can infer that a term of the form $A\cos(sq-r\tau)$, where (s,r) are integers, will create a resonance of width $\Delta p=4\sqrt{A}$ around the point $p=r/s$. In our case, $s=1$, and there exist only three such resonances. They are located at $p=0$ ($r=0$) and at $p=\pm1$($r=\pm1$). This can be seen in [Figs. 2(a)–2(e)]. For each resonance there exists one stable periodic orbit and one unstable periodic orbit with periods of approximately $2\pi|r|$. In the stroboscopic plot of the surface of section, they appear as stable and unstable fixed points, and give rise locally to the well-known phase space portrait of a pendulum. In the following, we will denote by $\mathcal{I}_0$,$\mathcal{I}_+$, and $\mathcal{I}_-$ the three stable islands associated with $r=0,+1$, and -1, respectively. The physical interpretation of these three resonances is simple: each resonance is associated with one of the modulated potentials (either static or moving) described above. For example, the fixed point at the center of the $\mathcal{I}_+$ resonance is associated with a periodic orbit where the atom moves at almost constant velocity v_0, being trapped in the minimum of the moving optical potential. The other two components of the potential appear along this orbit as rapidly varying potentials which are adiabatically averaged to constant values. As the atom can be trapped in any of the three modulated potentials, we obtain three stable periodic

orbits at the centers of the three resonance islands.

For a small enough γ, the resonances are well separated and the motion is quasi-integrable. Chaos will develop when the resonances start to overlap. This is the celebrated Chirikov's overlap criterion [31] and its evaluation gives $\gamma \simeq 0.1$ in our case. Thus chaos develops in phase space regions where the kinetic energy term and the perturbation are of the same order of magnitude. Taking into account higher perturbation orders in γ will shift the position in phase space of the previous resonances as well as the frequency around their stable points. For instance, it can be seen in Fig. 2(e) that the stable island $\mathcal{I}_+$ is centered on a point having a momentum slightly larger than $+1$. Perturbation terms of higher order will also introduce other resonances of smaller size. It is precisely the overlap of the infinite cascade of such resonances which gives rise to the chaotic layers. Nevertheless, Chirikov's criterion already gives a good order of magnitude for the onset of chaos. For higher γ, the previous three resonant islands of stability have shrunk inside a large chaotic sea, and will eventually disappear completely [cf. Fig. 2(f)]. Nevertheless a revival of some stable islands can still be observed for some narrow windows of high values of γ. In our situation, chaos cannot invade the whole phase space, but is bounded by regular coasts. This is so because chaos develops where resonances overlap. Sufficiently far away from the resonances, atoms move so fast that they experience an average time-independent potential. Then chaos is absent and one recovers (quasi) free motion when $|p| \gg 1$.

C. Typical classical phase space portrait in the chaos-assisted tunneling regime

The two resonant islands $\mathcal{I}_\pm$, when they exist, are related by a discrete symmetry: the time-reversal invariance. As can be seen in Fig. 3, the atoms trapped in one island cannot classically escape from it: the boundaries of the islands play the role of a dynamical barrier which atoms cannot cross. Hence jumping from one island to the other is a classically forbidden process, though it is expected to occur in quantum mechanics. This is precisely the tunneling situation we are interested in. In fact, we will study the tunneling between $\mathcal{I}_+$ and $\mathcal{I}_-$ for γ varying from 0.1 to 0.3 since, in that range, classical chaos may play a revealing role even though the two stable islands still occupy a significant volume in phase space.

Note that, in the physical situation described by $H_{\rm eff}$, tunneling occurs in momentum coordinates instead of space coordinates, as usually presented in standard textbooks. The denomination of ''dynamical tunneling'' [32], refers to this situation. The reason for investigating this situation is that manipulation of cold atoms allows for a better control (preparation and detection) of momentum rather than position.

IV. QUANTUM DYNAMICS

A. Floquet-Bloch theory

When an autonomous Hamiltonian is spatially periodic, it is well known [33] that its spectrum is organized in energy bands $E_n(k)$. These bands are labeled by a set of integers, the band index n, and depend continuously on a set of real numbers, the Bloch numbers k. As $E_n(k)$ and the associated eigenfunctions are periodic functions of the k's, all the physical information is contained in the first Brillouin zone. For 1D systems, it is simply the interval $[-\pi/Q, \pi/Q]$, where Q is the spatial period of the Hamiltonian.

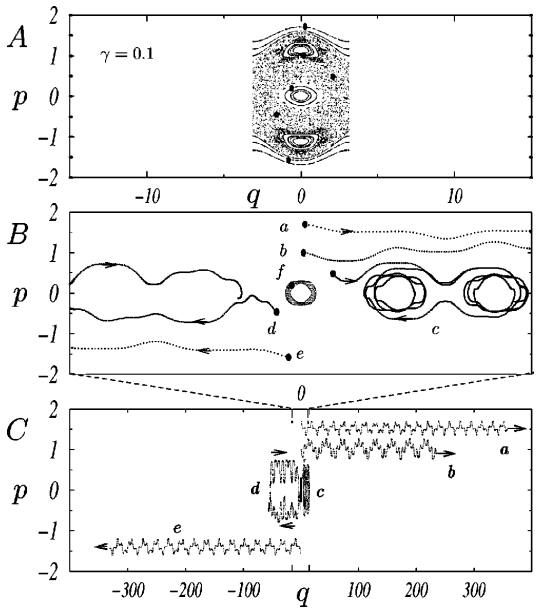

FIG. 3. Plots of some trajectories in phase space for different initial conditions ($\gamma = 0.1$). In *A*, we display a typical Poincaré surface of section as in Fig. 2, i.e., stroboscopic plots which are folded according to the spatial periodicity. The small black disks show some initial conditions. In *B* and *C*, trajectories are plotted every $2\pi/100$ and, unlike in *A*, we let $q(\tau)$ evolve continuously outside $[-\pi, \pi]$. Trajectories *b* and *f* are trapped in the $\mathcal{I}_+$ and $\mathcal{I}_0$ resonance islands, respectively. Trajectories *a* and *e* are two examples of regular quasifree motion. *c* and *d* correspond to chaotic motion; their initial conditions (at $\tau = 0$) lie in the chaotic sea of Fig. 2(d).

When the Hamiltonian is time periodic, with a period T, the analog of the Bloch theory is the Floquet theory [34–36]. The eigenvalues of the evolution operator $U(\tau + T, \tau)$ over one period take the form $e^{-i\epsilon T/\hbar_{\rm eff}}$. The ϵ's are τ-independent real quantities which are called the quasienergies of the system. Due to the time periodicity, the quasienergy spectrum as well as the associated eigenfunctions are now invariant under $\epsilon \mapsto \epsilon + 2\pi\hbar_{\rm eff}/T$.

For $H_{\rm eff}$, the application of Bloch and Floquet theorems with $Q = T = 2\pi$ yields a spectrum made out of quasienergy bands $\epsilon_n(k)$, where n goes over the whole set of integers (for a detailed derivation, see Appendix B). For brevity, we will define $|n,k,\tau\rangle$, the ket at time τ with Bloch angle k, with quasienergy $\epsilon_n(k)$, which is a solution of the Schrodinger equation [following the notations of Appendix B, we have set $|n,k,\tau\rangle \overset{\rm def}{=} |\psi_{\epsilon_n(k),k}(\tau)\rangle$]. We will also define $|n,k\rangle$

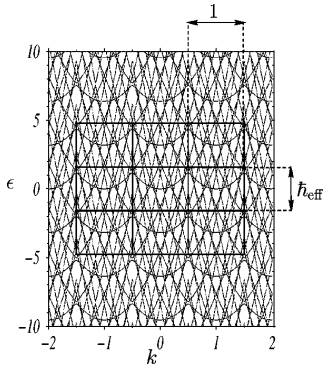

FIG. 4. For a Hamiltonian that is Q periodic in space and T periodic in time, the quasienergy spectrum is made of bands that are $2\pi/Q$ periodic in the Bloch numbers and $2\pi\hbar_{\rm eff}/T$ periodic in quasienergies. Such a spectrum is shown here for Hamiltonian 3 ($Q=2\pi$, $T=2\pi$), with $\gamma=0.18$ and $\hbar_{\rm eff}=3.1787$.

$\stackrel{\rm def}{=}|n,k,\tau=0\rangle$. As it can be seen in Fig. 4, the band spectrum has the topology of a torus since it is both periodic in quasienergy (with period $\hbar_{\rm eff}$) and Bloch number (with period 1).

B. Numerical calculation of the Floquet eigenstates

As derived in Appendix B, the Floquet eigenstates can be obtained by a diagonalization of the Floquet-Bloch operator $\widetilde{K}$,

$$\widetilde{K}(\hat{p},\hat{q},\tau,k)=\frac{(\hat{p}+\hbar_{\rm eff}k)^2}{2}-\gamma\cos\hat{q}(1+\cos\tau)-{\rm i}\hbar_{\rm eff}\frac{d}{d\tau}, \tag{5}$$

with periodic boundary conditions in both time and space. The eigenvalues, which depend on the Bloch vector k, are the quasienergies of the system. The band spectrum is symmetric with respect to the axis $k=0$, since operator 5 is invariant under the transformations $k\mapsto -k$ and $p\mapsto -p$. From the expression of the Floquet-Bloch operator and the boundary conditions, it is very natural to expand the eigenstates on a basis set composed of products of the type $\phi_{lm}(\tau,q)=\exp({\rm i}n\tau)\exp({\rm i}mq)$, which automatically obey the periodic boundary conditions. In such a basis, the operator $\widetilde{K}$ has very strong selection rules, namely,

$$|\Delta n|\leqslant 1 \quad \text{and} \quad |\Delta m|\leqslant 1 \tag{6}$$

All matrix elements violating one of these selection rules is zero. Hence the matrix representing the operator $\widetilde{K}$ in this basis is sparse and banded, and all matrix elements have simple analytical expressions. This is well suited for numerical diagonalization (powerful algorithms exist, for example the Lanczos algorithm). All the numerical results presented here use this method. We checked that the effect of the truncation of the basis is negligible: the size of the Floquet matrix is considered to be sufficiently large when increasing it modifies the value of the quasienergy on the scale of the numerical noise only, say 10^{-15} in double precision. Not only is this criterion a proof of the algorithmical convergence, but it also is a safeguard against numerical discrepancies, since we are looking for exponentially small quantities.

C. Husimi representation and classification of the quantum states

Classical dynamics is very illuminating when describing the states $|n,k,\tau\rangle$. In order to strengthen the correspondence between classical phase-space structures and quantum states, it is convenient to work with the Husimi representation of quantum states [37].

Such a representation associates, with each quantum state $|\psi\rangle$, a phase space function $\psi^{\rm H}(p,q)$ (where p and q are real numbers) defined by

$$\psi^{\rm H}(p,q)\stackrel{\rm def}{=}N_\psi|\langle z|\psi\rangle|^2, \tag{7}$$

where $|z\rangle$ is the normalized coherent state corresponding to the complex number $z=(q+{\rm i}p)/\sqrt{2\hbar_{\rm eff}}$. N_ψ is a (p,q)-independent normalization factor. Because $|z\rangle$ is a minimal Gaussian wave packet with average momentum p and average position q, the Husimi function $\psi^{\rm H}(p,q)$ contains some information about the degree of localization of $|\psi\rangle$ in phase space.

The minimal cell size in phase space, allowed by the Heisenberg inequalities, is $\hbar_{\rm eff}$. Let us see how classical phase space structures of a typical size larger than $\hbar_{\rm eff}$ are mirrored at the quantum level. In Figs. 5 and 6 we plot some values of $\epsilon_n(k)$ corresponding to Hamiltonian 3 for specified fixed values of γ and $\hbar_{\rm eff}$. von Neumann–Wigner arguments [38] claimed that, generically, no exact degeneracy can occur: rather one obtains avoided crossings. Of course, this is relevant provided the minimal energy splitting is greater than the resolution in energy. Some Husimi functions are plotted in Figs. 5 and 6 [(a)–(f)].[1]

In Appendix B, it is shown that we have

$$v_{n,k}\stackrel{\rm def}{=}\frac{1}{T}\int_0^T\langle n,k,\tau|\hat{p}|n,k,\tau\rangle d\tau=\frac{1}{\hbar_{\rm eff}}\frac{\partial\epsilon_n}{\partial k}, \tag{8}$$

$$|z,k\rangle\stackrel{\rm def}{=}\sum_{m\in\mathbf{Z}}{\rm e}^{{\rm i}mkQ}|z+mQ\rangle, \tag{9}$$

and define, for instance,

[1]A technicality should be mentioned here: $|u_{\epsilon,k}\rangle$ and $|\psi_{\epsilon,k}\rangle$ obey some spatial boundary conditions which are lost when working with their Husimi representations, essentially because the coherent states do not fulfill these properties themselves. To deal with spatially (quasi)periodic phase space functions, it is necessary to unfold the coherent states [39] into

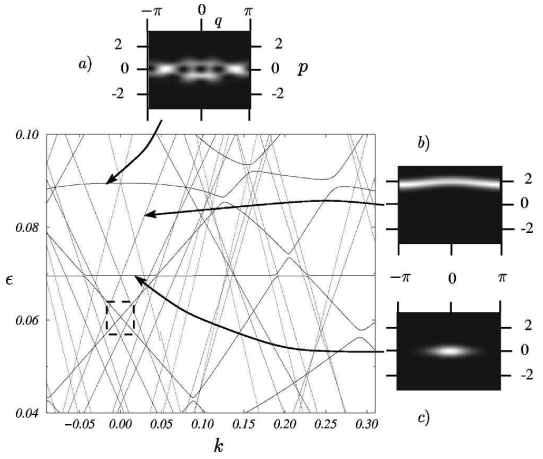

FIG. 5. Quasienergy bands for $\gamma=0.18$ and $\hbar_{\rm eff}=0.2037$ and some Husimi representations of typical states. In (b) we show a quasifree state with a well defined average velocity (the derivative of the energy level with respect to k) localized in phase space on regular trajectories [compare with Fig. 2(e)]. On this scale, the avoided crossings with other bands cannot be resolved. In (c) we show a state localized in the central stable island $\mathcal{I}_0$ (actually the ''ground state''). Far from quasidegeneracies the average velocity of this state is zero. In (a) we give an example of a chaotic state, whose Husimi function is localized in the chaotic sea [compare with Fig. 2(e)]. Unlike the former states, the average velocity fluctuates when the Bloch angle k is varied. The band spectrum is symmetric with respect to the axis $k=0$, since operator 5 is invariant under the transformations $k\mapsto -k$ and $\hat{p}\mapsto -\hat{p}$. The tunneling situation due to the time-reversal symmetry corresponds to the dashed squared zone (around $k=0$), which is enlarged in Fig. 6.

$$\psi^{\rm H}_{n,k}(p,q,\tau)\overset{\rm def}{=}N|\langle z,k|\psi_{n,k}(\tau)\rangle|^2. \tag{10}$$

which generalizes the velocity theorem (Ref. [33], Appendix E) to periodic time-dependent Hamiltonians.

Figure 5(b) shows an example of the Husimi representation of a state with sufficiently high average velocity to be like a free eigenstate of H_0. Far from quasidegeneracies it is localized in a narrow strip of width $\Delta p\sim 2\pi\hbar_{\rm eff}/\Delta q\sim\hbar_{\rm eff}$ (since Δq covers 2π), and which is centered on one of the two classical phase space trajectories of energy about $v^2_{n,k}/2$ [compare with Fig. 2(e)]. Its quasienergy band (Fig. 5) is an arc of the parabola of the free motion, but can hardly be distinguished from a straight line of slope $v_{n,k}$ if k is restricted to one Brillouin zone. We will naturally call these states quasifree states.

Some states have their Husimi functions localized in the resonant stable islands (in $\mathcal{I}_0$ but also in $\mathcal{I}_\pm$). The number of these states is semiclassically given by the volume of these islands divided by $2\pi\hbar_{\rm eff}$. Far away from quasidegeneracies, these states are at any time centered on the stable periodic orbit: this can be explained within a semiclassical approach, and can be observed in Fig. 5(c) for a state localized in $\mathcal{I}_0$, and in Figs. 6(d) and 6(e) for states in $\mathcal{I}_-$ and $\mathcal{I}_+$

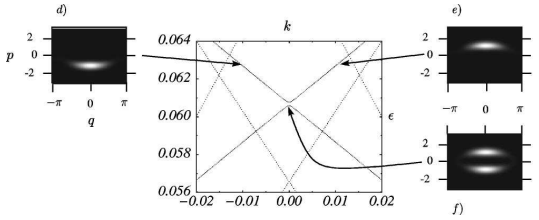

FIG. 6. Quasienergy bands for $\gamma=0.18$ and $\hbar_{\rm eff}=0.2037$ and some Husimi representations of typical states. This is a zoom of the dashed squared zone in Fig. 5. For $k\neq 0$, one can find states like those in (d) or (e), whose Husimi function is localized in one stable island $\mathcal{I}_-$ or $\mathcal{I}_+$ [compare with Fig. 2(e)]. In the frame, where the center of the island is fixed, these states correspond to the ''ground'' states (some excited states may of course exist if $\hbar_{\rm eff}$ is small enough, as can be seen in Figs. 12 and 13). For $k=0$, we recover time reversal symmetry through the existence of quasidegenerate doublets of symmetric or antisymmetric combinations. This is a typical tunneling situation: following the state in (e) (which has an average velocity about $+1$) adiabatically with k, by decreasing k we obtain a state in (d) that has a reversed velocity. This reversal of the velocity is a classically forbidden process (compare with orbit b in Fig. 3).

respectively. Their average velocity as well as their Husimi functions depend exponentially weakly on the Bloch parameter k.

The last class of states which can be encountered corresponds to chaotic ones, i.e., states whose Husimi functions are negligible on a typical distance of $\sqrt{\hbar_{\rm eff}}$ out of the chaotic seas [cf. Fig. 5(a)]. Unlike the previous ones, their Husimi functions are very sensitive to any variation of k since they are delocalized in the whole chaotic sea which spreads over all elementary cells. The large classical distribution of possible velocities is to be linked to the very fluctuating slopes of the quasienergies as k is varied.

D. Tunneling states

Although the system as a whole is of course time-reversal invariant, this is no longer true for its restriction at a fixed value k of the Bloch vector. Indeed, the operator $\tilde{K}$ is not time reversal invariant, because of the crossed term $k\hat{p}$. In other words, the time-reversed partner of a state with a Bloch vector k is a state with a Bloch vector $-k$. It is only at the special value $k=0$ (and also $k=1/2$ since k is defined modulo 1) that $\tilde{K}$ is invariant under time-reversal symmetry. Therefore, it corresponds to the typical situation of tunneling between $\mathcal{I}_+$ and $\mathcal{I}_-$. Every state localized in an island around $|p|=1$ is quasidegenerate with another one. These doublets represent a symmetric and antisymmetric combination of states localized in one island only [cf. Fig. 6(f)]. The energy splitting $\Delta\epsilon_n$ of these states for $k=0$ is precisely the signature of tunneling: it is $\pi\hbar_{\rm eff}$ divided by the typical time an atom takes to oscillate from one island to its time-reversed image, i.e., to reverse the sign of its velocity.

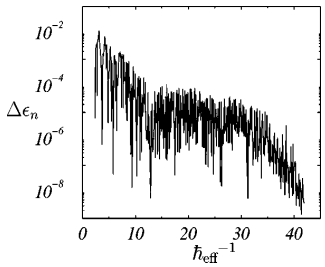

FIG. 7. Fluctuations of the energy splittings $\Delta\epsilon_n$ between pairs of symmetric or antisymmetric states localized in the $\mathcal{I}_\pm$ resonance islands (here shown for the ''ground state'' inside the island). The classical dynamics is fixed at $\gamma=0.18$ [compare with Fig. 2(e)]. The existence of large fluctuations over several orders of magnitude is a signature of chaos-assisted tunneling. On the average, $\ln|\Delta_{\epsilon_n}|$ appears to decrease more or less linearly with $\hbar_{\rm eff}^{-1}$ except for the plateau at $15\leqslant\hbar_{\rm eff}^{-1}\leqslant 30$.

V. CHAOS-ASSISTED TUNNELING

A. Large fluctuations

After having selected the two quasienergy bands corresponding to the two states which are localized most deeply inside the islands $\mathcal{I}_\pm$, we are able to plot the splitting as a function of $\hbar_{\rm eff}$. The great advantage of studying fluctuations when the effective Planck constant is varied is that it does not affect the classical dynamics. The behavior of the splitting is very different whether chaos is present at the $\hbar_{\rm eff}$ scale or not. In the chaotic regime (cf. Figs. 7 and 8), that is when $\hbar_{\rm eff}$ varies in a range where chaotic seas can be resolved, the splittings vary rapidly versus the change of any parameter, in our case $\hbar_{\rm eff}$. Moreover, the variations of the splittings, despite being perfectly deterministic, are apparently erratic—without any regular structure—and cover several orders of magnitude. They show that direct coupling to the chaotic sea is the key mechanism for their understanding, and are a signature of chaos-assisted tunneling [40,41]. In fact these huge fluctuations are reminiscent of the universal conductance fluctuations observed in mesoscopic systems [42,43] since tunneling is nothing other than wave transport from one stability island to the other. In contrast, in the regular regime where chaotic seas are smaller than $\hbar_{\rm eff}$, the splittings are expected to vary smoothly [6].

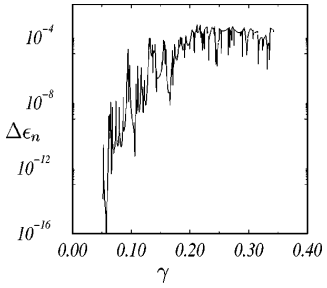

FIG. 8. Fluctuations of the energy splittings $\Delta\epsilon_n$ between the pair of symmetric or antisymmetric states ($\hbar_{\rm eff}^{-1}$ is fixed at 19.309) as a function of γ. Again, large fluctuations over several orders of magnitude are a signature of chaos-assisted tunneling. The global increase with γ is due to the growth of the chaotic sea as γ increases; see Fig. 2.

In Fig. 7, we show the splittings of the pair of states localized at the center of the resonances islands $\mathcal{I}_\pm$, as a function of $\hbar_{\rm eff}$. They display huge fluctuations over about four orders of magnitude while the general trend is a decrease as $\hbar_{\rm eff}\to 0$. Similarly, when plotted as a function of γ (see Fig. 8), they also display large fluctuations. The general trend here is a fast increase of the typical splitting with γ; this is associated with a shrinking of the regular island when γ increases, which results in an increasingly large tunneling probability. The overlap of the regular states (still supported by the islands) with the chaotic states increases. Therefore, the coupling between the two components of the tunneling doublets which involves the chaotic states increases as well. In order to understand both the general trend and the origin of the fluctuations, two points of view can be used: a quantum point of view and a semiclassical one.

B. Semiclassical interpretation

If the chaotic sea is large, it is rather intuitive that it can be easier first to tunnel from the center of the regular island to the chaotic sea, then propagate freely in the chaotic sea to the vicinity of the symmetric island, and finally tunnel to the center of the symmetric island than directly tunneling between the two islands. Actually, a rigorous quantitative treatment of this problem is highly nontrivial, and is beyond the scope of this paper. The crucial point is that because the chaotic sea is explored rapidly and densely, it does not cost anything to cross the chaotic sea. Tunneling trajectories can be viewed as complex trajectories (i.e., with complex position and momentum) connecting the symmetric islands. The tunneling amplitude associated with a single tunneling orbit is essentially $\exp[-\mathrm{Im}(S)/\hbar_{\rm eff}]$, where S is the complex action of the tunneling orbit. In a typical one-dimensional system (like a double well), there is only one such trajectory at each energy, and the tunneling rate thus displays the well-known exponential decrease. In a chaotic system, it may happen that there is a whole set of tunneling trajectories whose imaginary parts of the action are essentially identical. In such conditions, the actual tunneling amplitude is the sum of all individual amplitudes (each taken with its proper phase) which results in a very complicated quantity which fluctuates when parameters are changed. In some sense, this is analogous to the speckle pattern obtained when plenty of optical rays with various geometries are randomly interfering. This is the very origin of the (deterministic) fluctuations of the tunneling rates, and consequently of the energy splittings. The general trend (exponential decrease) is related to the typical imaginary part of the action of the tunneling trajectories.

C. Quantum point of view

A complementary quantum point of view is possible. One can divide the eigenstates of the system into two subsets:

''regular'' states localized in the resonance islands, and ''chaotic'' states localized in the chaotic sea. The two sets are only weakly coupled by tunneling. Because there are two symmetric islands, the regular states are essentially doubly degenerate (neglecting *direct* tunneling). The chaotic sea also has twofold symmetry, and states can be classified as even or odd. The two series of odd and even states ignore each other. Hence, when by accident, an even chaotic state is almost degenerate with an even regular state, they repel each other: at the same time, there is usually no odd chaotic state with the same energy. Thus the odd regular state is not significantly repelled. Hence the splitting appears due to different shifts of the even and odd regular states. Close to any avoided crossing between either the odd or even regular state and a corresponding chaotic state, a large splitting is obtained. Conversely, far from any avoided crossing, the splitting is small. Hence the fluctuations are associated with the existence of a large number of successive avoided crossings. The typical size of these fluctuations is related to the typical size of the avoided crossings, while the typical parameter range of these fluctuations is the distance (in parameter space) between two consecutive avoided crossings. A model implementing this idea (each regular state is independently and randomly coupled to the chaotic states of the same symmetry) was proposed in Ref. [44] and further used in Ref. [45]. In this model, the chaotic states are modeled by a Hamiltonian belonging to the Gaussian orthogonal ensemble of random matrices while the coupling between the regular state and the chaotic state is also taken as a random Gaussian variable. With these assumptions, the splitting distribution can be calculated. Let us denote the mean level spacing between chaotic states by Δ, and the typical strength of the coupling between the regular states and the chaotic sea by σ. Only if $\sigma \ll \Delta$ is a regular state weakly coupled to the continuum (if this inequality is violated, the regular state is completely diluted in the chaotic sea by the strength of the coupling). We thus assume the inequality to be valid. Then, the distribution of splittings $\Delta\epsilon$ is given by

$$P(\Delta\epsilon)=\frac{1}{\pi}\frac{s}{s^2+\Delta\epsilon^2} \quad \text{for } |\Delta\epsilon|<\sigma,$$

$$P(\Delta\epsilon)\simeq 0, \quad \text{for } |\Delta\epsilon|>\sigma, \tag{11}$$

where

$$s=\frac{\sqrt{2}\pi\sigma^2}{\Delta}. \tag{12}$$

The interpretation is rather simple. The maximum splitting is observed exactly at the avoided crossing where the levels are shifted by $\pm\sigma/2$ on both sides of their unpertubed positions. Hence the splitting cannot be larger than about σ. In fact, there is an exponentially decreasing tail in the distribution $P(\Delta\epsilon)$ (associated with the Gaussian fluctuations of σ) which we do not detail here because it is not relevant in our present case. s is the typical splitting one expects to observe: it corresponds to a shift typically due to the closest chaotic state. The full distribution is a (truncated) Cauchy distribution: it is obtained as the overall effect of all chaotic states lying above or below in energy. Note that, in the absence of a truncation of the Cauchy distribution, the average splitting is not defined because the corresponding integral diverges. Hence it is better to discuss the typical splitting s rather than the average splitting. It is the slow decrease of the Cauchy distribution for large splitting that is responsible for the huge fluctuations in the splittings, which can be as large as $\sigma \gg s$. This is reminiscent of random processes such as Lévy flights where rare events are dominant [46].

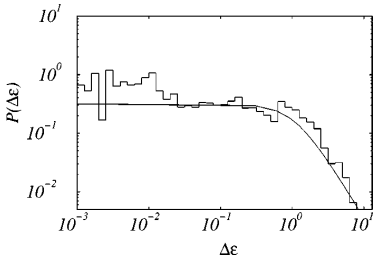

FIG. 9. Statistical distribution of the energy splittings $\Delta\epsilon$ (normalized to the typical splitting) between pairs of symmetric or antisymmetric states localized inside the $\mathcal{I}_\pm$ resonance islands ($\gamma=0.18$, $k=0$), represented on a double logarithmic scale. One can clearly distinguish two regimes: constant at small $\Delta\epsilon$ followed by a $1/\Delta\epsilon^2$ decrease, and finally a rapid cutoff (not shown in the figure). The solid line is the Cauchy distribution predicted by random matrix theory.

In Fig. 9, we show the statistical distribution of splittings that we obtain numerically in the chaotic regime (normalized to the typical splitting in order to work with $s=1$). The distribution is shown on a double logarithmic scale, and compared with the Cauchy distribution. One can clearly see two regimes: for small $|\Delta\epsilon|$, $P(|\Delta\epsilon|)$ is almost constant and decreases with a slope -2 for large $|\Delta\epsilon|$. The agreement with the Cauchy distribution is very good, which proves that the model catches the essential part of the physics in this system.

The typical splitting s is proportional to the square of the tunnelling matrix element from the initial state to the chaotic sea. Hence it is expected to decrease roughly as $\exp[-2\,\mathrm{Im}(S)/\hbar_{\mathrm{eff}}]$, where S is the complex action of tunneling orbits (the mean level spacing scales as a power of $\hbar_{\mathrm{eff}}$, and is thus a correction to the main exponential decrease). This is roughly what is observed in Fig. 7. Note, however, that there is a plateau in the range $15 \leqslant \hbar_{\mathrm{eff}}^{-1} \leqslant 30$. A similar observation was made in Ref. [47], Fig. 3. Although this is not a crucial problem (the statistics of the splitting distribution is not affected), a detailed explanation of this behavior is still lacking (however, see Ref. [47]). Finally, it should be interesting to calculate explicitly some of the complex tunneling orbits in our specific system in order to compare the imaginary part of their actions with the slope in Fig. 7. This work is currently in progress.

VI. EXPERIMENTAL SIGNAL

As can be seen in Fig. 5, the splittings we want to measure correspond to very tiny scales among the other struc-

tures in the band spectrum. For $\hbar_{\rm eff}\simeq 0.1$ e.g., the tunneling times are about $\hbar_{\rm eff}/\Delta\epsilon\sim 10^3$ times the typical period (T on the order of a few μs). The observation of atoms having reversed their velocity is therefore still possible since, for 1 ms, spontaneous emission has not begun to spoil our dynamical model. Nevertheless, measuring tiny splittings which are hidden so deeply in the spectrum is far from being straightforward. Several steps are needed: preparation of the initial state, the experiment itself (where chaos-assisted tunneling takes place), and an analysis of the final state. During the first step, one must prepare a state localized inside one resonance island, i.e., localized both in position and momentum spaces. The idea is to use an adiabatic transfer from an initial state extended in position space by slowly branching the effective potential. Although the second step looks trivial (one just has to wait), the dispersion in the vector angle k makes things much more difficult as only the $k=0$ states are related by time-reversal symmetry (see Sec. IV D), and thus tunnel relatively fast. However, it is possible to overcome this difficulty, as explained below. Finally, the detection should be rather easy, using velocity dependent Raman transitions. We now explain in detail how the various steps can be worked out.

A. Adiabatic preparation of the atoms in one lateral stable island

The first step consists of preparing an initial cloud of cold rubidium atoms in order to have it located in one of the stable island, e.g., $\mathcal{I}_+$, only. Using a standard magneto-optical trap, one can obtain a more or less thermal distribution of atoms with a velocity on the order of a few times the recoil velocity $v_{\rm rec}=\hbar k_L/M=6$ mm/s. However—as shown below—this is probably too much for a good measurement of the tunneling splitting. Additional techniques (side-band cooling [48], Raman cooling [49,50]) make it possible to obtain a subrecoil velocity distribution, i.e., atoms with an average momentum p_0 and a thermal dispersion $\Delta p_x=M\Delta v=M\alpha v_{\rm rec}$ with α significantly smaller than 1. We chose the initial momentum to be $M\delta\omega/2k_L$, so that, on average, the atoms exactly follow one of the sliding standing wave created by a pair $\omega_\pm$ of laser beams.

The next step is to slowly (i.e., adiabatically) switch on the standing waves. During this phase, the spatial periodicity is preserved, and the Bloch vector k is thus a conserved quantity. Initially, the momentum p_x is nothing but the Bloch vector (modulo a integer multiple of the recoil momentum). Thus, by preparing a subrecoil initial state, one populates only a small range of k values and, for each k value populated, a single state (momentum eigenstate). In other words, the initial momentum distribution becomes a statistical mixture of Bloch states with $\Delta k=\alpha/2$ in a single energy band. More generally, if the initial momentum distribution is not a subrecoil one, but has a width equal to α recoil momenta (with $\alpha>1$), about α bands will be populated.

Switching on the standing waves increases the optical potential V_0 and therefore γ from zero and enlarges the resonance islands. In the frame moving with velocity $p_0/M=\delta\omega/2k_L$, the atoms ''feel'' a pendulumlike potential

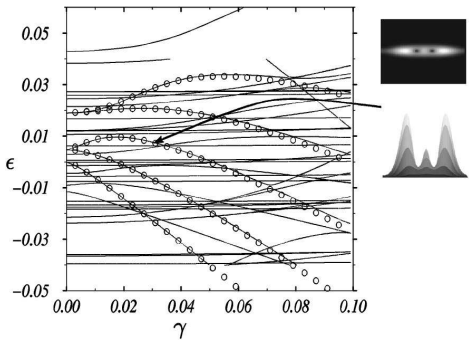

FIG. 10. Comparison between the quasienergies of Hamiltonian 3 (lines) and the energies (circles) obtained from the pendulum approximation in the stable island $\mathcal{I}_0$ ($\hbar=0.0976$, $k=0$). The avoided crossings that appear at $\gamma\sim 0.07$ illustrate the influence of classical narrow chaotic seas on the quantum properties. The Husimi distribution of the second excited state localized in $\mathcal{I}_0$ for $\gamma=0.03$ is shown.

$-\frac{1}{2}\gamma\cos q$ (in scaled coordinates) in addition to some rapidly time varying terms. Consequently, they will adiabatically localize in the potential minima, that is at the center of the resonance island. Increasing γ successively localizes an increasing number of states in $\mathcal{I}_+$. The switching time must be sufficiently long as compared to the beating period (in this case the discarded terms are still rapidly oscillating) but also to the inverse of the minimum energy gap (of the order of $\hbar_{\rm eff}^{-1}$ if Δk is sufficiently narrow). In order to trap all the initially populated states, γ has to be sufficiently large. For a given Bloch angle, we want to localize the α first states. The quantum energies of a pendulum are given by the eigenvalues of the Mathieu equation (Ref. [51], Chap. 20) (see Figs. 10 and 11). For a pendulum whose Hamiltonian is

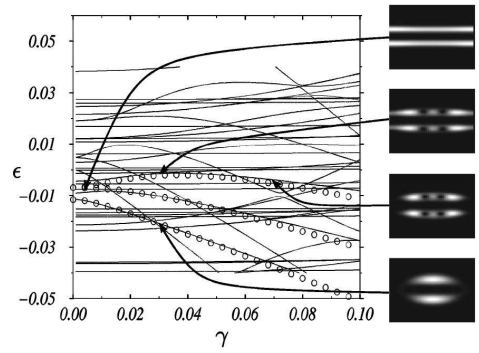

FIG. 11. Comparison between the quasienergies of Hamiltonian 3 (lines) and the energies (circles) obtained from the pendulum approximation in the stable islands $\mathcal{I}_\pm$ ($\hbar=0.0976$, $k=0$). The three upper Husimi plots show how a quasifree state doublet becomes progressively localized in a stable island when γ increases. The lower Husimi plot corresponds to the ''ground'' state of the pendulum approximation in the stable islands $\mathcal{I}_\pm$ for $\gamma=0.03$.

$$H_{\mathrm{pend}}=\frac{p^2}{2}-\frac{\gamma}{2}\cos q, \tag{13}$$

the phase space volume enclosed by the separatrix is $16\sqrt{\gamma/2}$. Semiclassically, this corresponds to $16\sqrt{\gamma/2}/(2\pi\hbar_{\mathrm{eff}})$ states. This number will be of the order of α when γ reaches the value

$$\gamma_{\mathrm{adiab}}\simeq\frac{(\alpha\pi\hbar_{\mathrm{eff}})^2}{128}. \tag{14}$$

Figures 10 and 11 show the exact energy levels of the system together with the ones using the pendulum approximation and the Mathieu equation, as well as plots of selected Husimi representations for few eigenstates. This allows us to check the following.

(i) The pendulum approximation works well in the regime of interest, up to about $\gamma=0.1$.

(ii) The semiclassical estimate of the number of trapped states is sufficiently accurate for our purpose.

(iii) The Husimi representations of the trapped states are well-localized: especially, the states in Fig. 11 have two well-separated components in the $\mathcal{I}_+$ and $\mathcal{I}_-$ islands, meaning that we are in a real case of tunneling.

(iv) During the initial increase of γ, the ''ground'' state is well isolated (in energy) from the other ones, which means that an adiabatic preparation is possible.

Nevertheless, for this adiabatic preparation to be valid, we must make sure that γ has not reached a range where chaos has non-negligible effects on quantum properties. Physically, we want chaotic layers at $\gamma=\gamma_{\mathrm{adiab}}$ to have a small volume compared to the Planck constant. From Fig. 10, we can obtain the upper bound limit of γ by estimating when the (small) avoided crossings become too large to be passed diabatically. For $1/50<\hbar_{\mathrm{eff}}<1/5$, we observe that chaos has no influence for $\gamma<\gamma_{\mathrm{chaos}}\simeq 0.04$.

The adiabatic preparation of all the atoms in one stable island will be achieved if $\gamma_{\mathrm{adiab}}<\gamma_{\mathrm{chaos}}$, that is, if the atoms are cold enough to have

$$\alpha<\frac{8\sqrt{2\,\gamma_{\mathrm{chaos}}}}{\pi\hbar_{\mathrm{eff}}}\simeq\frac{0.7}{\hbar_{\mathrm{eff}}}. \tag{15}$$

In every situation considered in the following, we will have to check that this condition is fulfilled. Next we have to reach the desired value for γ ($\simeq 0.18$) in the chaotic regime while preserving the state in the island. This will be achieved if γ is increased sufficiently fast so that all encountered avoided crossings with chaotic states are passed diabatically. Hence the whole preparation of the initial atomic state proceeds by two steps: a first adiabatic increase of γ at the very beginning to significantly populate regular states in one island, followed by a diabatic increase of γ to preserve them in the chaotic regime.

B. How to force tunneling?

As discussed in Sec. IV D, the tunneling splitting is small only for a Bloch vector $k=0$. As it is not presently possible to prepare only this value of k in a real experiment, it seems at first sight that only a small fraction of atoms (close to $k=0$) may effectively tunnel, hence considerably reducing the signal to noise ratio. A solution is to force all atoms to go through the $k\approx 0$ region. The simplest idea is to impose a slow increase of the k value, by adding a constant external force F from outside. Then the full Hamiltonian that governs the dynamics is

$$H'(p,q,\tau)=H(p,q,\tau)-qF. \tag{16}$$

The potential V induces a dynamical drift in the Bloch angle:

$$\frac{d}{d\tau}k(\tau)=\frac{1}{\hbar_{\mathrm{eff}}}F. \tag{17}$$

It is shown in Appendix C that this relation, which is well known in the time independent case (see, for instance, Ref. [52], Chap.6), remains valid when H is periodic in time.

A convenient way of realizing experimentally such a constant force is to chirp the laser frequencies, that is make all the frequencies drift linearly in time. In an accelerated frame, the laser frequencies appear as constants, and we are back to our model. However, in this noninertial frame, the constant acceleration is translated in a constant force; hence the system is governed by Eq. (16). This method has been used with cold atoms (see Ref. [24]).

The global result is a slow drift of the k distribution. This causes the various k classes to come successively closer to $k=0$, and thus become able to tunnel. Whether the atom will effectively tunnel or not depends on the time scale on which k changes. If k varies rapidly, the avoided crossing at $k=0$ is crossed diabatically, i.e., the velocity distribution will not be modified. If k varies slowly, it is crossed adiabatically (rapid adiabatic passage). The Landau-Zener formula [53] yields a typical time scale for the crossover between diabatic and adiabatic crossing.

Figures 12 and 13 illustrate, for $\hbar_{\mathrm{eff}}=0.2037$, the drift of atoms initially localized in $\mathcal{I}_+$ (one energy band) whose distribution in k covers 1/10 of the Brillouin zone from $k\simeq -1/10$ to $k\simeq 0$ (a subrecoil initial velocity distribution with a width on the order of $v_{\mathrm{rec}}/5$). We allow the atoms to evolve under the force F in order to obtain a global translation of 1/10 in k. After moving across the splitting at $k=0$, if the force F is weak to follow the energy level adiabatically, the average momentum of the atoms has reversed its sign, as can be seen in Fig. 13. Measuring the critical value of F for this Landau-Zener-like transition furnishes a means to measure the splitting. Another possibility would be to modulate the external force (and thus the k values) periodically in time in order to induce a resonant transfer between $\mathcal{I}_+$ and $\mathcal{I}_-$.

In any case, the method may work only if no other avoided crossing come into play. Numerical investigations show that there are mainly tiny avoided crossings along the energy curve of interest. However, as a general rule, there are usually a few avoided crossings with similar or larger sizes than the avoided crossing of interest. If such an avoided crossing is also passed adiabatically, it will of course spoil the momentum distribution. Hence it is crucial for the initial

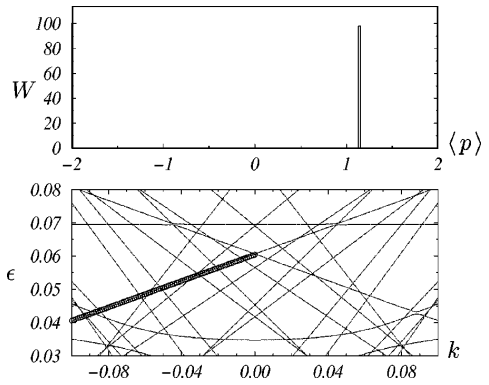

FIG. 12. In order to measure the tunneling splitting at $k=0$ (see Figs. 5 and 6), the atoms are prepared into states localized inside the $\mathcal{I}_+$ resonance island. The average momentum distribution (top graph) is peaked at a value slightly larger than $+1$ in agreement with Fig. 2. The initial states occupy one-tenth of the first Brillouin zone, and are represented by the circles in the lower graph. ($\hbar_{\rm eff}=0.2037$, $\gamma=0.18$.) After an adiabatic sliding of $\Delta k\simeq 0.1$, the states are populated, and the average momentum distribution is shown in Fig. 13.

k distribution to be sufficiently narrow to avoid this problem. Hence a subrecoil velocity distribution seems necessary.

C. Detection

After the atoms have interacted with the modulated waves, one can switch off the lasers either abruptly or adiabatically (in which case the atoms adiabatically leave the resonance island). In both cases, the atoms which have tunneled from $\mathcal{I}_+$ to $\mathcal{I}_-$ will end with a momentum close to $-p_0$. A standard time of flight technique should be enough to detect them. A more sophisticated technique, based for example, on velocity sensitive Raman transitions [54,48], could also be used with a subrecoil resolution if needed [24].

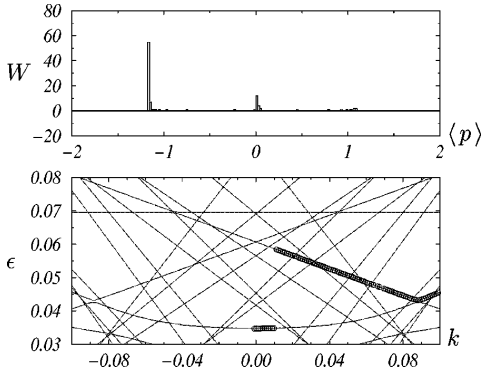

FIG. 13. The final states obtained after drift of the Bloch vector by $\Delta k\simeq 1/10$ (the initial state in Fig. 12). If the force governing the motion [Eq. (17)] is chosen such that the sliding is adiabatic through the avoided crossing at $k=0$, the momentum of the tunneling atoms just reverses its sign. If the initial states cover a small enough, well-centered, interval of the Brilloin zone, only the $k=0$ avoided crossing is important. Other avoided crossings can be seen at $k\simeq\pm 0.09$ and $\epsilon\simeq 0.43$. Those are responsible for the momentum dispersion of the atoms, and should be avoided as much as possible.

VII. CONCLUSION

In this paper we have proposed a simple and accessible experimental configuration in which the observation of chaos-assisted tunneling should be feasible. It consists of atoms propagating in the light field of two far-detuned monochromatic standing waves with slightly different frequencies. However, observing the tunneling effect requires subrecoil cooling techniques to conveniently prepare the atomic sample together with a well-controlled experimental procedure (adiabatic preparation of the atomic state in one stable island followed by a drift of the Bloch vector). As the tunneling period fluctuates over several decades when the potential strength varies (see Fig. 8), observing that these fluctuations requires a stabilization of the laser intensity at the level of a few percent.

ACKNOWLEDGMENTS

Ch.M., R.K., and A.M. would like to thank the Laboratoire Kastler Brossel for kind hospitality. CPU time on computers was provided by IDRIS. Laboratoire Kastler Brossel de l'Université Pierre et Marie Curie et de l'Ecole Normale Supérieure is UMR 8552 du CNRS.

APPENDIX A: DERIVATION OF THE EFFECTIVE HAMILTONIAN

To derive the effective Hamiltonian [Eq. 2], we basically proceed in three steps [55]. First we assume that any dissipation process can be safely ignored. Indeed for tunneling to be observable, the phase coherence of the atomic wave function must be preserved during all the process. In our case, this means that spontaneous emission must be negligible. It can be shown [56] that increasing the laser detuning considerably decreases the loss of phase coherence. Hence the evolution will be essentially Hamiltonian, provided that each laser beam is sufficiently far-detuned from the atomic resonance:

$$|\delta_\pm|=|\omega_\pm-\omega_{\rm at}|\gg\Gamma. \tag{A1}$$

When this holds, the total Hamiltonian operator for this two-level system is the sum of three terms: the kinetic energy operator describing the center-of-mass motion of atoms of mass M, the energy operator for the internal degrees of freedom, and the coupling between internal and external degrees of freedom. In the dipolar approximation, the interaction is just $dE(x,t)$, and it does not depend on y and z. The dynamics along y and z is just trivially described by free motion, and can be easily eliminated, since the total quantum state factorizes as a plane wave in y and z. One is then left with the dynamics along x which is described by the Hamiltonian

$$H_{\rm at}=\frac{p_x^2}{2M}(|e\rangle\langle e|+|g\rangle\langle g|)+\hbar\omega_{\rm at}|e\rangle\langle e| - dE(x,t)(|e\rangle\langle g|+|g\rangle\langle e|), \tag{A2}$$

where p_x is the atomic momentum along x. $|g\rangle$ and $|e\rangle$ are the ground and excited states, and d is the atomic dipole strength connecting them.

Second, we expand the total atomic state as

$$|\Psi\rangle=\psi_g(x,t)|g\rangle+\psi_e(x,t)\exp(-i\omega_L t)|e\rangle, \tag{A3}$$

and we neglect high frequency (optical) antiresonant terms and suppose that the amplitudes change slowly during an optical period. This is known as the rotating wave approximation [57], and features the averaging procedure to eliminate fast variables in classical perturbation theory [30]. This yields the coupled amplitude equations

$$i\hbar\,\partial_t\psi_g=-\frac{\hbar^2}{2M}\partial_{xx}^2\psi_g-\frac{\hbar\Omega(x,t)}{2}\psi_e, \tag{A4a}$$

$$i\hbar\,\partial_t\psi_e=-\frac{\hbar^2}{2M}\partial_{xx}^2\psi_e-\hbar\,\delta_L\psi_e-\frac{\hbar\Omega^*(x,t)}{2}\psi_g. \tag{A4b}$$

In these equations $\delta_L=\omega_L-\omega_{\rm at}$ is the mean laser detuning, the star denotes complex conjugation, and $\Omega(x,t)$ reads

$$\Omega(x,t)=[\Omega_+\exp(-i\,\delta\omega\,t/2)+\Omega_-\exp(i\,\delta\omega\,t/2)]\times\cos(k_L x), \tag{A5}$$

where $\Omega_\pm=d\,E_\pm/\hbar$ are the Rabi frequencies of each standing wave.

As a final step, we now assume that atoms initially prepared in their ground state mostly evolve in their ground state. This means that the whole atomic dynamics is solely determined by the ground-state amplitude ψ_g. For this to hold, an adiabatic elimination of the excited-state amplitude [56] must be justified. If the spatial partial derivatives were absent, Eqs. (A4) would just describe the Rabi oscillation phenomenon. It is then known that far off resonance, i.e., when the frequency separation of the states is much larger than any other frequencies, the Rabi oscillation is very small in amplitude. A sufficient condition is

$$|\delta_L|\gg\Omega_\pm,\delta\omega. \tag{A6}$$

If, in addition, we assume that the excited-state kinetic energy is very small (which will be easily achieved with cold atoms),

$$|\delta_L|\gg\left\langle\psi_e\left|\frac{p_x^2}{2M}\right|\psi_e\right\rangle, \tag{A7}$$

then an adiabatic elimination of the excited-state amplitude amounts to neglecting the spatial and temporal derivatives of ψ_e in Eq. A4b which is then solved as $\psi_e\simeq-(\Omega^*/2\delta_L)\psi_g$ $\ll\psi_g$. It is then easy to see that the ground-state amplitude ψ_g obeys an effective Schrödinger equation, with a Hamiltonian

$$H=\frac{p_x^2}{2M}+\frac{\hbar|\Omega(x,t)|^2}{4\,\delta_L}. \tag{A8}$$

Eventually, up to an irrelevant purely time-dependent term, we obtain

$$H=\frac{p_x^2}{2M}-V_0\cos(2k_L x)[\theta+\cos(\delta\omega\,t)], \tag{A9}$$

where $V_0\overset{\rm def}{=}-\hbar\Omega_+\Omega_-/8\delta_L$ and $\theta\overset{\rm def}{=}(\Omega_+/2\Omega_-)+(\Omega_-/2\Omega_+)$.

APPENDIX B: FLOQUET-BLOCH FORMALISM

In this appendix, we briefly recall the Floquet-Bloch formalism which is used for a quantum problem whose Hamiltonian H is periodic in both space and time. We will denote T and Q the temporal and spatial periods, respectively.

Let us first consider the time periodicity. We define [34,36,58]

$$K(\hat p,\hat q,\tau)\overset{\rm def}{=}-i\hbar\frac{d}{d\tau}+H(\hat p,\hat q,\tau), \tag{B1}$$

where $\hat p$ and $\hat q$ stand for canonical Hermitian operators whose commutator is $[\hat p,\hat q]=-i\hbar$.

If $U(\tau',\tau)$ denotes the unitary evolution operator from τ to τ' associated with Hamiltonian H, the periodicity of the dynamics implies that $U(\tau+T,T)=U(\tau,0)$ and

$$U(\tau+T,\tau)=U(\tau+T,T)U(T,0)U(0,\tau) =[U(0,\tau)]^{-1}U(T,0)U(0,\tau). \tag{B2}$$

This shows that $U(\tau+T,\tau)$ and $U(T,0)$ differ by a unitary transformation, and hence have the same spectrum (but of course different eigenvectors), independent of τ. The eigenvalues of $U(\tau+T,\tau)$ have a unit modulus, and can be written as $e^{-i\epsilon_n T/\hbar}$ where ϵ_n is the so-called quasi-energy defined modulo $2\pi\hbar/T$. If $|\psi_n(\tau)\rangle$ denotes the corresponding eigenvector, we can define the Floquet state

$$|\chi_n(\tau)\rangle\overset{\rm def}{=}e^{i\epsilon_n\tau/\hbar}|\psi_n(\tau)\rangle, \tag{B3}$$

which is by construction periodic with period T.

Inserting the definition of the Floquet state in the time-dependent Schrödinger equation, we immediately obtain

$$K(\hat p,\hat q,\tau)|\chi_n(\tau)\rangle=\epsilon_n|\chi_n(\tau)\rangle, \tag{B4}$$

which means that the quasienergy spectrum is obtained by diagonalizing the Floquet Hamiltonian in the space of time-periodic functions.

The second step consists of making use of the invariance of H under spatial translations with period Q. The unitary translation operator $\hat{T}_Q \overset{\text{def}}{=} e^{-i\hat{p}Q/\hbar}$ commutes with K. We can then use the spatial counterpart of the Floquet theorem, namely, the Bloch theorem [33], and label the eigenstates of K with the Bloch number $k \in [-\pi/Q, \pi/Q[$ (the first Brillouin zone), which means diagonalizing K in each subspace with fixed k. If one defines the Floquet-Bloch states as

$$|u_{n,k}(\tau)\rangle = e^{-ik\hat{q}}|\chi_{n,k}(\tau)\rangle = e^{i\epsilon_n(k)\tau/\hbar}e^{-ik\hat{q}}|\psi_{n,k}(\tau)\rangle, \tag{B5}$$

where $\{\psi_{n,k}(\tau)\rangle\}$ forms a complete orthogonal eigenbasis, it is easy to show that they can be obtained by diagonalizing the Floquet-Bloch Hamiltonian,

$$\tilde{K}(\hat{p},\hat{q},\tau,k) = K(\hat{p}+\hbar k,\hat{q},\tau), \tag{B6}$$

on the subspace of time and space periodic functions. In our specific case, the Floquet-Bloch Hamiltonian reads

$$\tilde{K}(\hat{p},\hat{q},\tau,k) = \frac{(\hat{p}+\hbar k)^2}{2} - \gamma(\theta+\cos\tau)\cos\hat{q} - i\hbar\frac{d}{d\tau}. \tag{B7}$$

The spatial periodicity of the Floquet-Bloch states leads to a discrete set of dispersion relations $\epsilon_n(k)$. For fixed n, the set of all quasienergies $\epsilon_n(k)$ for k in the first Brillouin zone $[-\pi/Q, \pi/Q[$ is called the nth band of the system.

Let us now obtain the velocity theorem [Eq. 10]. Using the above relations, we have

$$\begin{aligned}\langle\psi_{\epsilon,k}(\tau)|\hat{p}|\psi_{\epsilon,k}(\tau)\rangle &= \langle u_{\epsilon,k}(\tau)|(\hat{p}+\hbar k)|u_{\epsilon,k}(\tau)\rangle \\ &= \langle u_{\epsilon,k}(\tau)|(\hbar^{-1}\partial\tilde{K}/\partial k)|u_{\epsilon,k}(\tau)\rangle.\end{aligned}$$

The derivation with respect to k of the relation $\langle u_{\epsilon,k}(\tau)|\tilde{K}|u_{\epsilon,k}(\tau)\rangle = \epsilon(k)$ leads to

$$\begin{aligned}\langle\psi_{\epsilon,k}(\tau)|\hat{p}|\psi_{\epsilon,k}(\tau)\rangle = \frac{1}{\hbar}\frac{\partial\epsilon}{\partial k} &+ i\hbar\frac{d}{d\tau}\left(\langle u_{\epsilon,k}(\tau)|\frac{\partial}{\partial k}|u_{\epsilon,k}(\tau)\rangle\right) \\ &- \left(\frac{1}{\hbar}\frac{\partial}{\partial k}\langle u_{\epsilon,k}(\tau)|\right)\tilde{K}|u_{\epsilon,k}(\tau)\rangle \\ &- \left[\left(\frac{1}{\hbar}\frac{\partial}{\partial k}\langle u_{\epsilon,k}(\tau)|\right)\tilde{K}|u_{\epsilon,k}(\tau)\rangle\right]^*.\end{aligned} \tag{B8}$$

The two last terms on the the right hand side are opposite, since the normalization of the u's leads to $\partial\langle u_{\epsilon,k}|u_{\epsilon,k}\rangle/\partial k = 0$. Moreover, after time averaging Eq. B8 over T, the total τ derivative vanishes since the u's are precisely T periodic while the time-independent k derivative of the quasienergy remains unchanged. Eventually,

$$\frac{1}{T}\int_0^T \langle\psi_{\epsilon,k}(\tau)|\hat{p}|\psi_{\epsilon,k}(\tau)\rangle d\tau = \frac{1}{\hbar}\frac{\partial\epsilon}{\partial k}. \tag{B9}$$

APPENDIX C: BLOCH ANGLE DYNAMICS

In this appendix we derive Eq. (17), which is valid for an arbitrary strength of the constant force F provided that the potential $V = -Fq$ remains strictly linear in q. Let us choose a state $|\psi(\tau)\rangle$ evolving under $H' = H + V$, such that it coincides with a Floquet-Bloch state at $\tau = 0$:

$$i\hbar_{\text{eff}}\frac{d|\psi(\tau)\rangle}{d\tau} = H'(\hat{p},\hat{q},\tau)|\psi(\tau)\rangle \tag{C1}$$

and

$$|\psi(\tau=0)\rangle = |\psi_{n,k}(\tau=0)\rangle. \tag{C2}$$

In the interaction picture, we immediately have

$$i\hbar_{\text{eff}}\frac{d|\psi^I(\tau)\rangle}{d\tau} = -FU^\dagger(\tau,0)\hat{q}U(\tau,0)|\psi^I(\tau)\rangle, \tag{C3}$$

where $|\psi^I(\tau)\rangle \overset{\text{def}}{=} U^\dagger(\tau,0)|\psi(\tau)\rangle$, and where U denotes the evolution operator under H. Let $|\phi(\tau)\rangle$ be the ket defined by

$$|\phi(\tau)\rangle \overset{\text{def}}{=} e^{-iF\hat{q}\tau/\hbar_{\text{eff}}}|\psi^I(\tau)\rangle. \tag{C4}$$

It is straightforward to obtain its evolution,

$$i\hbar_{\text{eff}}\frac{d|\phi(\tau)\rangle}{d\tau} = G(\tau)|\phi(\tau)\rangle, \tag{C5}$$

where

$$G(\tau) \overset{\text{def}}{=} F(\hat{q} - e^{-i\tau F\hat{q}/\hbar_{\text{eff}}}U^\dagger(\tau,0)\hat{q}U(\tau,0)e^{i\tau F\hat{q}/\hbar_{\text{eff}}}). \tag{C6}$$

Since $U^\dagger(\tau,0)$ commutes with the translation operator $\hat{T}_Q$, it can be checked that $[G(\tau),\hat{T}_Q] = 0$. The evolution of $|\phi(\tau)\rangle$ under G will therefore preserve its initial quantum number k,

$$\hat{T}_Q|\phi(\tau)\rangle = e^{-ikQ}|\phi(\tau)\rangle, \tag{C7}$$

for all τ. Thus, making use of Eqs. (C3) and (C4), we have

$$\hat{T}_Q|\psi(\tau)\rangle = e^{-i(k+F\tau/\hbar_{\text{eff}})Q}|\psi(\tau)\rangle, \tag{C8}$$

which shows that $|\psi(\tau)\rangle$ is actually a Bloch wave with a Bloch angle given by $k(\tau) = k(0) + F\tau/\hbar_{\text{eff}}$, even if it spreads among the quasienergy bands [39,38].

[1] *Chaos et Physique Quantique—Chaos and Quantum Physics*, Les Houches, Ecole d'été de Physique Théorique 1989, Session LII, edited by M. Giannoni, A. Voros, and J. Zinn-Justin (North-Holland, Amsterdam, 1991).
[2] E.J. Heller, Phys. Rev. Lett. **53**, 1515 (1984).
[3] *Mesoscopic Quantum Physics*, Les Houches, École d'été de Physique Théorique 1994, Session LXI, edited by E. Akkermans, G. Montambaux, J. Pichard, and J. Zinn-Justin (North-Holland, Amsterdam, 1995), session LXI.
[4] A. Messiah, *Mécanique Quantique* (Dunod, Paris, 1964), Vol. 2.
[5] R. Balian and C. Bloch, Ann. Phys. (N.Y.) **84**, 559 (1974).
[6] M. Wilkinson, Physica D **21**, 341 (1986).
[7] M. Wilkinson and J.H. Hannay, Physica D **27**, 201 (1987).
[8] W.A. Lin and L.E. Ballentine, Phys. Rev. Lett. **65**, 2927 (1990).
[9] O. Bohigas, D. Boosé, R. Egydio de Carvalho, and V. Marvulle, Nucl. Phys. A **560**, 197 (1993).
[10] O. Bohigas, S. Tomsovic, and D. Ullmo, Phys. Rep. **223**, 43 (1993).
[11] S. Tomsovic and D. Ullmo, Phys. Rev. E **50**, 145 (1994).
[12] S.C. Creagh and N.D. Whelan, Phys. Rev. Lett. **77**, 4975 (1996).
[13] V. Averbukh, N. Moiseyev, B. Mirbach, and H.J. Korsh, Z. Phys. D: At., Mol. Clusters **35**, 247 (1995).
[14] *Laser and Manipulation of Atoms and Ions*, Enrico Fermi International Summer School, 1991, Course CXVIII, edited by E. Arimondo, W.D. Phillips, and F. Strumia (North-Holland, Amsterdam, 1992).
[15] R.T. Lawton and M.S. Child, Mol. Phys. **44**, 709 (1981).
[16] E.L. Sibert, W.P. Reinhardt, and J.T. Hynes, Chem. Phys. Lett. **92**, 455 (1982).
[17] M.E. Kellman and E.D. Lynch, Chem. Phys. **87**, 5386 (1987).
[18] J.P. Rose and M.E. Kellman, J. Chem. Phys. **105**, 7348 (1996).
[19] J.P. Rose and M.E. Kellman, J. Chem. Phys. **105**, 10743 (1996).
[20] *Atom Interferometry*, edited by P.R. Berman (Academic Press, New York, 1996).
[21] M. Weidemüller, A. Hemmerich, A. Görlitz, T. Esslinger, and T.W. Hänsch, Phys. Rev. Lett. **75**, 4583 (1995).
[22] L. Guidoni, C. Triché, P. Verkerk, and G. Grynberg, Phys. Rev. Lett. **79**, 3363 (1997).
[23] K. Drese and M. Holthaus, Phys. Rev. Lett. **78**, 2932 (1997).
[24] M. Ben Dahan, E. Peik, J. Reichel, Y. Castin, and C. Salomon, Phys. Rev. Lett. **76**, 4508 (1996).
[25] Q. Niu, X.-G. Zhao, G.A. Georgakis, and M.G. Raizen, Phys. Rev. Lett. **76**, 4504 (1996).
[26] F.L. Moore, J.C. Robinson, C. Bharucha, P.E. Williams, and M.G. Raizen, Phys. Rev. Lett. **73**, 2974 (1994).
[27] G. Labeyrie, F. de Tomasi, J.C. Bernard, C.A. Müller, C. Miniatura, and R. Kaiser, Phys. Rev. Lett. **83**, 5266 (1999).
[28] T. Jonckheere, C.A. Müller, R. Kaiser, C. Miniatura, and D. Delande, Phys. Rev. Lett. **85**, 4269 (2000).
[29] C. Cohen-Tannoudji, J. Dupont-Roc, and G. Grynberg, *Processus d'Interaction entre Photons et Atomes, Savoirs Actuels* (InterEditions/Editions du CNRS, Paris, 1988).
[30] A.J. Lichtenberg and M.A. Lieberman, *Regular and Stochastic Motion*, Applied Mathematical Sciences Vol. 38 (Springer-Verlag, New York, 1983).
[31] B. Chirikov, Phys. Rep. **52**, 263 (1979).
[32] M.J. Davis and E.J. Heller, J. Phys. Chem. **85**, 307 (1981).
[33] N.W. Ashcroft and N.D. Mermin, *Solid State Physics* (Saunders College, Philadelphia, 1976).
[34] G. Floquet, Ann. de l'Éc. Normale, 2e Sér. **12**, 47 (1883) (in French).
[35] T.M. Cherry, Proc. London Math. Soc. (2nd ser.) **26**, 211 (1927).
[36] J.H. Shirley, Phys. Rev. **138**, B979 (1965).
[37] W.H. Louisell, *Quantum Statistical Properties of Radiation* (Wiley, Chichester, 1973).
[38] J. von Neumann and E. Wigner, Phys. Z. **30**, 467 (1929). English translation in *Symmetry in the Solid State* (Ref. [60]), pp. 167–172.
[39] P. Leboeuf and A. Voros, in *Quantum Chaos—Between Order and Disorder*, edited by G. Casati and B. Chirikov (Cambridge University Press, Cambridge, 1992), pp. 507–533. See *Quantom Chaos—Between Order and Disorder* (Ref. [59]).
[40] E.M. Zanardi, J. Gutiérrez, and J.M. Gomez Llorente, Phys. Rev. E **52**, 4736 (1995).
[41] J. Zakrzewski, D. Delande, and A. Buchleitner, Phys. Rev. E **57**, 1458 (1998).
[42] S. Washburg and R. Webb, Adv. Phys. **35**, 375 (1986).
[43] S. Feng and P.A. Lee, Science **251**, 633 (1991).
[44] F. Leyvraz and D. Ullmo, J. Phys. A **29**, 2529 (1996).
[45] J. Zakrzewski and D. Delande, Phys. Rev. E **47**, 1650 (1993).
[46] J.-P. Bouchaud and A. Georges, Phys. Rep. **195**, 127 (1990).
[47] R. Roncaglia, L. Bonci, F.M. Izrailev, B.J. West, and P. Grigolini, Phys. Rev. Lett. **73**, 802 (1994).
[48] M. Morinaga, I. Bouchoule, J.-C. Karam, and C. Salomon, Phys. Rev. Lett. **83**, 4037 (1999).
[49] M. Kasevich and S. Chu, Phys. Rev. Lett. **69**, 1741 (1992).
[50] J. Reichel, F. Bardou, M. Ben Dahan, E. Peik, S. Rand, C. Salomon, and C. Cohen-Tannoudji, Phys. Rev. Lett. **75**, 4575 (1995).
[51] M. Abramowitz and I.A. Stegun, *Handbook of Mathematical Functions* (Dover, New York, 1965).
[52] J. Callaway, *Quantum Theory of the Solid State* (Academic Press, London, 1974), Vol. B.
[53] C. Zener, Proc. R. Soc. London, Ser. A **137**, 696 (1932).
[54] V. Vuletić, C. Chin, A.J. Kerman, and S. Chu, Phys. Rev. Lett. **81**, 5768 (1998).
[55] R. Graham, M. Schlautmann, and P. Zoller, Phys. Rev. A **45**, R19 (1992).
[56] C. Cohen-Tannoudji, in *Systèmes Fondamentaux en Optique Quantique — Fundamental Systems in Quantum Optics*, Les Houches, École d'été de Physique Théorique 1990, Session LIII, edited by J. Dalibard, J.-M. Raimond, and J. Zinn-Justin (North-Holland, Amsterdam, 1990), pp. 1–164.
[57] A.L.C. and J. Eberly, *Optical Resonance and Two Level Atoms* (Dover, New York, 1987).
[58] Y.B. Zeldovich, Zh. Éksp. Teor. Fiz. **51**, 1492 (1966) [Sov. Phys. JETP **24**, 1006 (1967)].
[59] *Quantum Chaos—Between Order and Disorder*, edited by G. Casati and B. Chirikov (Cambridge University Press, Cambridge, 1995).
[60] R.S. Knox and A. Gold, *Symmetry in the Solid State*, Lecture Notes and Supplements in Physics (Benjamin, New York, 1964).

I.4 Le chaos donne un coup de main à l'effet tunnel

Cet article écrit avec Denis Ullmo du Laboratoire de Physique Théorique et de Modèles Statistiques (lptms) d'Orsay est plus un article *sur* la recherche que *de* recherche proprement dit. Néanmoins, les raisons pour lesquelles j'ai trouvé important de l'inclure dans ce mémoire sont si indissociablement liées à ma conception du métier d'enseignant-chercheur que cela m'a paru indispensable.

Sur le fond d'abord : ce texte est à rapprocher de deux articles, (Heller, 2001, juillet) et (Goss Levi, 2001, août), qui présentent tous les trois un compte-rendu du contexte et des résultats des expériences américaines sur l'effet tunnel chaotique et dont j'ai déjà dit un mot dans la présentation de l'article précédent. Je n'y reviens donc pas. Le grand tirage des journaux en question et le fait que notre article soit un texte de commande (rémunéré) montre que le sujet de l'effet tunnel chaotique peut sortir d'un cercle d'initiés et toucher un large public de physiciens non-spécialistes pourvu que l'on veuille bien se donner la peine d'abandonner, provisoirement, le langage des spécialistes. Il faut reconnaître aussi que ce coup de projecteur est évidemment en partie motivé par le prestige de l'un des chefs d'équipe, l'excellent William Phillips, prix Nobel de physique en 1997.

L'important ici concerne aussi la forme : sans m'appesantir trop longuement sur les questions de la vulgarisation scientifique en particulier et sur les rapports délicats entre chercheurs, journalistes, politiques et grand public en général — questions certes passionnantes et incontournables mais qui nous entraîneraient trop loin ici —, il me semble utile de participer activement, à chaque fois que l'occasion se présente, (*cf.* aussi § 7b) p. 10) à la diffusion et surtout à la transmission[26] des connaissances.

Si je me permets d'adopter un ton moralisateur sans doute un peu déplacé, c'est que les enjeux sont tout de même de taille. Je n'en retiendrais que trois évidemment imbriqués :

(i) Un laboratoire ne peut pas être une tour d'ivoire ; que son financement soit public ou privé, il est normal de consacrer du temps à expliquer et rendre des comptes aux bailleurs de fonds, le plus souvent non-spécialistes, ne serait-ce que pour éviter de voir se tarir les sources, en mécontentant les contribuables ou en lassant les mécènes.

(ii) À une époque où le nombre d'étudiants en sciences fondamentales se raréfie et où les formations se spécialisent de plus en plus tôt, il faut être capable de séduire les jeunes élèves directement ou par le truchement de leurs parents et professeurs, et ce, non pas en les attirant par un miroir aux alouettes en mais surtout en encourageant leur curiosité naturelle au lieu de parfois l'étouffer[27].

(iii) Il y a aussi des risques à abandonner le terrain de la diffusion à des acteurs indirects de la recherche où, plus grave encore, à une minorité d'experts un peu trop aisément

[26] « Valorisation » ou « Communication » comme nous le rappellent les consignes des grands organismes avec une insistance qui fluctue au gré des modes.

[27] Il n'est pas besoin d'appartenir à l'université François Rabelais pour s'inspirer des méthodes de Ponocrates.

séduits par les sirènes d'une notoriété facile ou guidés par le sentiment fallacieux de supériorité que confère un peu d'érudition. Sans insister sur certains cas pathologiques extrêmes qui relèvent plus de l'escroquerie intellectuelle et de l'esbroufe que de la volonté véritable de transmettre un savoir et une passion, j'évoque ici le paradoxe, non pas du comédien, mais du savant qui cherche à partager un peu de son enthousiasme et de sa curiosité. Quoi qu'il fasse, il lui faut troquer la rigueur de son langage formalisé mais vernaculaire pour une langue moins précise donc moins correcte selon ses propres critères de valeur. Tout l'art de la vulgarisation consiste à savoir modérer ce hiatus et à résoudre une équation impossible dont l'origine remonte au moins aux querelles opposant Socrate aux sophistes : expliquer et séduire le plus grand nombre tout en escamotant le moins possible. On trouve parfois des déséquilibres abusifs, dans un sens ou dans l'autre ; par exemple le choix malheureux de « téléportation » en information quantique qui, tout en focalisant à coup sûr plus de crédits, trompe inévitablement le public en connaissance de cause (comment ne pas songer à ce qu'évoque véritablement ce mot aux personnes peu aguerries aux subtilités des raisonnements de type epr ?). Les « prodiges et vertiges de l'analogie », dénoncés ailleurs par Jacques Bouveresse, n'ensorcellent pas uniquement les « littéraires ».

Pour en revenir aux écueils qui se sont présentés lors de cette de cette commande, pour tenter de présenter les expériences américaines, l'image d'un surfeur nous a paru bien venue et pour expliquer l'effet tunnel, la référence à Houdini plus appropriée que l'évocation d'un tunnel([28]).

([28]) Malheureusement la note rappelant qui était Houdini, *the escape artist*, fût supprimée par l'éditeur. Signalons que des physiciens, Balibar & Lévy-leblond (1984, Chap. 6, § 5.B), soucieux de la « mise en culture » de la science ont proposé de parler d'effet « saute-mouton » à propos de l'effet tunnel car les propagateurs en temps ont des composantes de Fourier d'énergies supérieures à la barrière. Des arguments subtils sur les batailles d'exponentielles (Maitra & Heller, 1997) montrent que ce n'est pas la bonne interprétation.

Chaos gives quantum tunnelling a hand

From **Amaury Mouchet** in the Laboratoire de Mathématiques et de Physique Théorique, Université François Rabelais and **Denis Ullmo** in the Laboratoire de Physique Théorique et Modéles Statistiques, Orsay, France

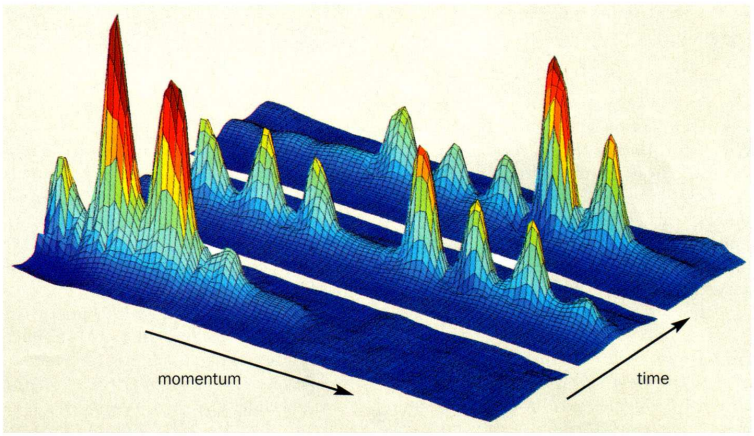

W Hensinger/University of Queensland

From the front. The evolution of the momentum distribution of a Bose–Einstein condensate as it oscillates within the wells of an optical lattice. The diffraction peaks at each stage are due to the interference between atoms in different wells. The atoms on the left have negative momentum, while those on the right have positive momentum. Classically we would expect most of the atoms to remain in a state with negative momentum (i.e. remain on the left). At some later time, however, most of the atoms have positive momentum (i.e. they have moved to the right), which is due to the occurrence of dynamical tunnelling.

Everyday macroscopic objects follow the laws of classical mechanics. For microscopic objects, such as atoms or nuclei, the wave character of their dynamics has to be taken into account within the framework of quantum mechanics. While wave-like behaviour can show up in various ways, one of the most striking is the tunnelling effect: some events that are classically forbidden for energetic reasons happen because the quantum particles can tunnel under a potential barrier. Similarly, events that are prohibited due to some other dynamical constraints can occur via a process known as dynamical tunnelling. Indeed, tunnelling plays a major role in a variety of physical phenomena, ranging from α-particle radioactivity to the current–voltage characteristics of transistors.

Being genuinely quantal in origin, one might think that the tunnelling of an atom is unrelated to the motion of a classical particle subject to the same forces. In particular, the classical phenomenon of chaos seems irrelevant, at first sight, in understanding tunnelling because it deals with the extreme sensitivity of classical trajectories to initial conditions. However, theoretical analyses and numerical studies of systems with a few degrees of freedom have shown that this is actually not the case, and that the nature of the underlying classical dynamics can alter drastically the way tunnelling takes place.

In the early 1990s Oriol Bohigas and one of the current authors (DU) at Orsay, together with Steven Tomsovic at Washington State University, demonstrated that the presence of chaotic trajectories in classical systems can increase the rate of quantum tunnelling by several orders of magnitude, and make the trajectories highly fluctuating functions of external parameters. Such effects were first studied experimentally in microwave and optical resonators that can

be described by wave equations similar to the Schrödinger equation, rather than with quantum-mechanical objects.

Now two independent teams at the University of Texas, and at the University of Queensland in Australia together with the National Institute of Standards and Technology in Gaithersburg, US, have studied the tunnelling of atoms in the presence of chaos. The work was made possible by the sophisticated tools that have been recently developed to study cold atoms and Bose–Einstein condensates (D Steck *et al.* 2001 *Science* **293** 274; W Hensinger *et al.* 2001 *Nature* **412** 52).

At the energy scale of visible light, an isolated motionless atom can be thought of as an object with a rather simple internal structure that obeys the laws of quantum physics. Of course, this is an oversimplified description because under ordinary physical conditions atoms are neither isolated nor motionless. At room temperature, the speed of atoms is so high (about 100 $m\,s^{-1}$ in a gas) that they usually interact many times with their environment.

To recover the richness of quantum dynamics, one must "domesticate" the atoms by cooling them down. At microkelvin temperatures, the atoms can be trapped and manipulated with lasers and electrostatic or magnetostatic fields. These atomic waves offer an alternative to light waves and become an extremely accurate and sensitive tool for applications in metrology, interferometry and lithography. Meanwhile, recent work on Bose–Einstein condensates has demonstrated the feasibility of a laser-like atomic beam (see *Physics World* August 1999 pp31–35).

Moreover, model systems can also be built from atoms and tuned to study phenomena in many other fields of physics. For example, neutral atoms exposed to monochromatic light feel a dipolar force that is proportional to the variations in the intensity of the light. Such systems have made it possible to mimic electronic waves in a crystalline potential, and thus provide a fuller understanding of electric conductivity at the quantum level. In this spirit, the Texas and NIST–Queensland teams placed atoms within two standing waves with slightly different frequencies. In this way they produced a time-dependent one-dimensional potential – the minimum condition for chaos to appear. Such a configuration for cold atoms was proposed in the mid-1990s and studied theoretically in great detail by Dominique Delande, one of the present authors (AM) and collaborators in Paris.

Imagine a surfer in the sea where the winds produce a superposition of counter-propagating waves of speed v and $-v$. In such circumstances, the surfer will usually feel the random effect of the waves, being shaken rather than pushed in any definite direction. On the other hand, if the surfer has an initial velocity close to v (or $-v$) just before a wave moving to the right (or left) reaches her, then she will be able to ride the wave.

The forces on the atoms in the above experiments produce a very similar situation. In general, the atoms essentially undergo chaotic motion, but if their initial speed and position are chosen carefully then the atoms will be pushed either to the right or to the left by the electromagnetic wave created by the lasers, while the classical laws of motion forbid any U-turn.

In principle, cold atoms can be prepared with sufficiently small uncertainty in their initial velocity, but this is rather difficult to achieve. Bill Phillips and co-workers at NIST and Queensland succeeded by first producing a Bose–Einstein condensate in which all the atoms are in the same quantum ground state. The condensate was released while the standing-wave potential was turned on in such a way that an atomic wavepacket with zero momentum was obtained. The researchers then shifted the position of the standing wave to give the atoms the proper initial momentum. The approach used by Mark Raizen and co-workers at Texas was similar, except that they used a cloud of cold atoms without actually forming a Bose–Einstein condensate. In both cases, the technology required to produce ultracold atoms was a prerequisite. Furthermore it was necessary to manipulate the resulting cold atoms in a very precise way.

It then became possible to follow the quantum-mechanical evolution of the wavepacket (see figure). At first the atoms followed a classical-like evolution, appearing to be trapped by a wave moving to the right, for example. But after some time, some atoms seemed to surf a wave moving in the *opposite* direction, although they were never observed to stop or change direction. After more time had elapsed, a coherent oscillation was found between the left and right motion. This classically forbidden back and forth "Houdinization" between two regular motions with different velocities was measured in both experiments and corresponds to the first observation of dynamical tunnelling for atoms with "non-integrable" dynamics.

In addition, Raizen and co-workers identified a significant increase in the tunnelling rate due to the presence of a third, presumably chaotic, delocalized state. This behaviour is typical of chaos-assisted tunnelling. Such experiments clearly offer the possibility of studying in depth the effect of chaos on quantum-mechanical tunnelling.

Some of the most exotic and fascinating concepts developed in the context of quantum chaos are now within range of experimental study, thanks to the remarkable progress that has been made in the production and manipulation of cold atoms. This should lead to better understanding and perhaps also to new applications in the context of quantum information.

I.5 Signatures de l'effet tunnel chaotique

Dans cet article, avec Dominique Delande nous revenons aux expériences américaines sur l'effet tunnel chaotique. J'ai présenté au § I.3 les raisons pour lesquelles, leurs méthodes employées et leurs résultats sont remarquables. Le travail que nous avions fourni pour (Mouchet *et al.* (2001)) nous a permis immédiatement de confirmer numériquement les observations quantitatives des deux équipes (*cf.* figures 3 p. 55 et 5 p. 56). En revanche, en ce qui concerne les premières interprétations, si l'équipe de Phillips est toujours restée très prudente, les conclusions de l'équipe de Raizen nous ont semblé d'emblée un peu trop optimistes, en particulier dans le choix du titre de leur article (comparer les titres de Hensinger *et al.* et de Steck *et al.*, 2001).

Le besoin d'une mise au point s'est donc fait ressentir très vite et nous a fourni l'occasion, en nous appuyant sur des expériences numériques, de clarifier de façon provisoirement définitive, à la fois pour nous-mêmes et, je l'espère, pour la communauté, ce que l'on entend par effet tunnel chaotique([29]).

Notre principale conclusion concernant les expériences est que celles-ci n'ont pas été assez loin pour pouvoir véritablement associer à une dynamique chaotique sous-jacente leur observation d'une grande fluctuation d'une période tunnel. En effet dans un système dépendant du temps, même quasi-intégrable lorsque le chaos n'est pas résolu du fait de la trop grande valeur de $\hbar$, il faut s'attendre à des dégénérescences quantiques (croisements de quasi-énergies) qui conduisent inévitablement à ce genre de fluctuations (*cf.* figure 4 p. 56). Le chaos, on l'a montré de façon nette dans ce travail, induit pour les doublets un brutal changement de régime (*cf.* figures p. 57) qui n'a jamais été observé à l'heure actuelle dans aucune expérience tant quantique qu'électromagnétique.

Il est vraiment dommage que ces expériences, une fois réalisées et leurs résultats publiés, n'aient pas été exploitées aux limites de leurs possibilités (les post-docs en charge des deux expériences, W. Hensinger et D. Steck, ont très vite changé d'équipe et les expériences reconverties). Comme nous l'écrivons dans cet article, il n'aurait peut-être pas fallu de si gros efforts pour apercevoir la transition représentée au graphe inférieur de la figure 8. Nous avons un temps caressé l'espoir de convaincre M. d'Arcy, alors post-doc fraîchement arrivé dans l'équipe de Phillips, de poursuivre dans cette direction, projet argumenté à l'appui. Je regrette que cela n'ait malheureusement pas abouti et que nous nous trouvions dans la situation décrite au § I.8a).

([29]) La transition nette de régime p. 57 avait déjà été observée par Buchleitner, Delande & Zakrzewski (2002, fig. 42) pour une particule rebondissant sur un sol oscillant (*gravitationnal bouncer*).

PHYSICAL REVIEW E **67**, 046216 (2003)

Signatures of chaotic tunneling

Amaury Mouchet*
Laboratoire de Mathématiques et de Physique Théorique, Université François Rabelais, Avenue Monge, Parc de Grandmont 37200 Tours, France†

Dominique Delande‡
Laboratoire Kastler-Brossel, Université Pierre et Marie Curie, 4, place Jussieu, F-75005 Paris, France
(Received 11 December 2002; published 25 April 2003)

Recent experiments with cold atoms provide a significant step toward a better understanding of tunneling when irregular dynamics is present at the classical level. In this paper, we lay out numerical studies that shed light on the previous experiments and help to clarify the underlying physics. This study also provides guidelines for future experiments.

DOI: 10.1103/PhysRevE.67.046216 PACS number(s): 05.45.Mt, 05.60.Gg, 32.80.Qk, 05.45.Pq

I. INTRODUCTION

When studying tunneling in nonseparable systems with more than one degree of freedom, one immediately encounters difficulties which generally can be traced back to the absence of sufficient constants of motion. Even in the very particular case of integrable systems, where continuous symmetries provide as many constants of motion as degrees of freedom, as soon as separability is lost, the analysis of tunneling is not a simple generalization of what occurs in one-dimensional (1D) autonomous systems. The latter case is detailed in textbooks on quantum physics (see, for instance, Ref. [1]) and it has even been possible to give a comprehensive analytical treatment in term of complex solutions of the Hamilton equations [2]. However, it was not until the mid-1980's that a satisfactory quantitative approach was proposed [3,4] for tunneling in nonseparable integrable systems involving a larger number of dimensions. Moreover, integrability is a property of higher-dimensional systems which is not generic. The coupling between several internal degrees of freedom as well as the coupling to an external source usually destroys some global constants of motion. With such a lack of constraints on the dynamics, the classical motion in phase space may become chaotic: it may explore volumes with higher dimensionality and therefore becomes exponentially sensitive to the initial conditions. It is not surprising that these deep qualitative differences between an integrable regime and a chaotic one appear at the quantum level, too. Some of the properties of a *quantum* system do change when constants of motion are broken. Indeed, it is the very object of quantum chaos to study the signatures of classical chaos at the quantum level (see for instance, Ref. [5] to realize how rich, vivid, and successful this domain is).

We define tunneling as a quantum process which is forbidden in *real* classical solutions of classical equations of motion. In this paper, we consider Hamiltonian systems only and study how the nondissipative breakdown of continuous symmetries affects tunneling. We do not consider how tunneling is modified by dissipation and decoherence of the quantum wave. Of course, this requires great care in real experiments, where making dissipation negligible is always a hard task. This is one of the main reasons why very few real experiments have been done on these questions. Such experiments would definitely help to understand tunneling in the presence of chaos (as far as we know, the only experiments explicitly made on chaotic tunneling in the 20th century are those presented in Ref. [6] with electromagnetic microwaves instead of quantum waves).

During the past 15 years, however, theoretical and numerical investigations on autonomous 2D and time-dependent 1D Hamiltonian systems have highlighted some mechanisms [3,4,7–12] and substantial information has been collected on the influence of nonseparable dynamics. Experimental evidence of such mechanisms would be of great interest, especially in light of the subtle interplay between interferences and disorder. These phenomena lie in the general context of wave transport in complex media where the role of disorder is played by the (deterministic) chaotic dynamics instead of having a statistical random origin. Of course, other important motivations can be found in the numerous domains where tunneling plays a crucial role as a fundamental quantum process: ionization [13], absorption, nuclear radioactivity, molecular collisions, mesoscopic physics etc. More speculatively, studies on tunneling in high-dimensional Hamiltonian systems should provide us with a natural extension of the instanton techniques. These techniques deal with quantum field theories which are reducible to effective 1D autonomous Lagrangian systems.

In 2001, it was shown both theoretically [14] and experimentally [15–18] that atom cooling techniques [19] (and possibly molecular physics as well, where formally similar systems have been extensively studied [20–23]) yield systems which fulfill all the severe requirements for studying tunneling in the presence of classical Hamiltonian chaos: accurate manipulation of internal and external degrees of freedom, precise control of dissipation and decoherence, and the preparation/detection setup. For a brief account intended for a large audience, see Refs. [24–26]. The aim of the present paper is to suggest challenging experiments that remain to be

*Electronic address: mouchet@celfi.phys.univ-tours.fr
†URL: http://www.phys.univ-tours.fr/~mouchet
‡Electronic address: delande@spectro.jussieu.fr

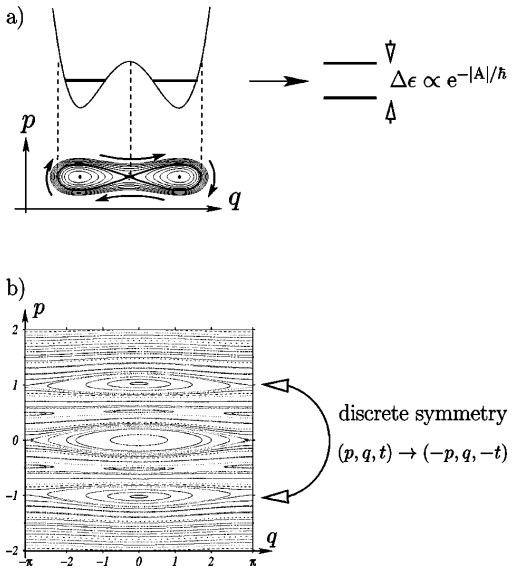

FIG. 1. A generalization of the paradigmatic double-well potential (a) is to consider tunneling between stable islands that are related by any discrete symmetry in phase space; (b) corresponds to Hamiltonian (2) with $\theta=1$ and $\gamma=0.018$. Here, the time reversal symmetry plays the role of parity in (a).

done for reasons which will hopefully become clear in the following.

This paper is organized as follows. In Sec. II we give a general and informal overview. In Sec. III, we briefly recall the main theoretical apparatus that is needed. We implicitly refer to Ref. [14] for details and demonstrations. In Sec. IV, we comment on the results of Refs. [15] and [16]. In Sec. V, we show in this context, with the help of numerical experiments, the very precise form taken by the phenomenon known as chaos-assisted tunneling. We explain why it has not been observed yet with real atoms and propose how to actually bring it to the fore. Before the concluding remarks in Sec. VII, we give in Sec. VI some more numerical results that illustrate how subtle the signatures of chaotic tunneling can be.

II. CHAOTIC TUNNELING

The simplest situation with which to illustrate tunneling is probably the case of a particle in a 1D time-independent symmetric double-well potential [see Fig. 1(a)]. Starting in one well, with an energy that is below the maximum of the potential, a quantum particle can jump into the other well with a nonzero probability, though it is a forbidden classical process. In addition to the classical time scale τ given by the oscillating period *inside* one well, we therefore have a longer time scale: the tunneling period $T \gg \tau$ of the oscillations *between* the wells. In the eigenenergy spectrum, tunneling appears as a quasidegeneracy of the odd- and even-symmetry states whose energies are both of the order of $\hbar/\tau$ but differ by an exponential energy splitting

$$\Delta\epsilon = \frac{2\pi\hbar}{T} \sim e^{-A/\hbar} \tag{1}$$

where A is an $\hbar$-independent typical action and can be interpreted in terms of a unique complex classical trajectory under the barrier [1,27].

In the following we generalize this elementary situation in two ways. First, unlike the parity in the previous example, we can deal with a symmetry which is not necessarily either a spatial one or a twofold one. In other words, we can have any discrete symmetry group acting on the whole phase space as well as any N-fold symmetry which leads to bunches of N-uplets in the energy spectrum (or bands if $N \gg 1$). In the following we keep $N=2$ since we have a twofold symmetry $\mathcal{T}$ actually playing the role of parity [see Fig. 1(b)] and being somehow decoupled from the other discrete symmetries. The classical structure in phase space is globally invariant under $\mathcal{T}$ and the quantum eigenstates can be classified according to their symmetric or antisymmetric character under the unitary transformation which represents $\mathcal{T}$ in the Hilbert space of states. Because $\mathcal{T}$ acts in phase space, it is usually more complicated than a pure spatial transformation. Thus, the two regions of phase space connected by *quantum* tunneling, but *classically* not connected, are in general not separated by a simple potential barrier, but by a more complicated dynamical barrier. In such a case, tunneling is called ''dynamical tunneling'' as suggested by Davis and Heller in Ref. [28]. It often happens that the classically unconnected region are associated with the same region of configuration space, with different momenta. A simple study of the density probability in configuration space is then insufficient to characterize dynamical tunneling; an analysis of the density probablility in momentum space is required.

The second kind of generalization leads to much more puzzling questions. When dealing with systems with several degrees of freedom or, equivalently, if an external time dependence exists, classical trajectories generally lose their regular behavior. They cannot analytically be computed and are organized in a fractal hierarchy that is described by the Kolmosorov-Arnold-Moser (KAM) perturbative scenario. Recently, important progress has been achieved in the understanding of the continuation of these intricate structures in complex phase space and their role at the quantum level (see Refs. [29,30] and especially Ref. [31]). We are therefore led to the following typical quantum chaos question: if one is able to create two symmetric stable islands separated in classical phase space by a chaotic sea whose volume is under control (see Fig. 2), what is the effect of this sea on the (dynamical) tunneling between the islands?

The ''dual'' situation where chaos is created *inside* the wells while the dynamical barrier is kept regular has been introduced and studied theoretically and numerically in Ref. [11]. For a better understanding of what occurs in the energy spectrum when regular wells are separated by a chaotic sea, it was proposed in Ref. [32] to slightly break the tunneling symmetry. Nevertheless, in the present paper, it must be kept in mind that a discrete symmetry will always be maintained

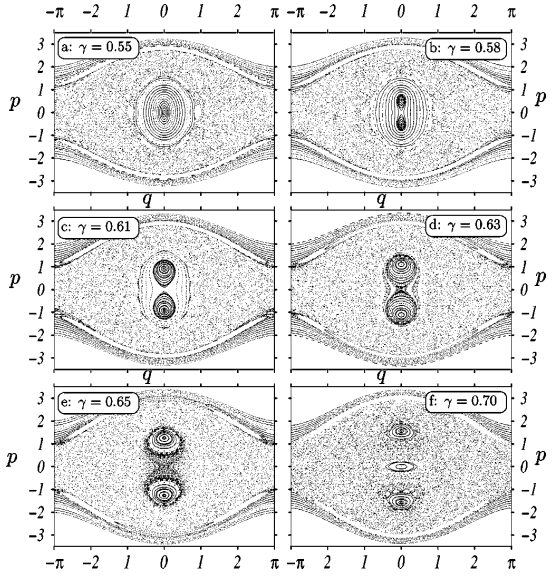

FIG. 2. Poincaré surfaces of section correspond to Hamiltonian 2 at $t=0$ with $\theta=1.724\,137$. Two stable islands in the vicinity of the origin are created by a pitchfork bifurcation at $\gamma\simeq 0.56$. Above this value, chaotic motion progressively invades phase space in between the two stable islands. At $\gamma>\gamma_c\simeq 0.625$, the latter are no longer connected by regular trajectories. The experimental configuration used in the NIST experiments corresponds to $\gamma=0.96$ just before the islands disappear in a bifurcation cascade at $\gamma\simeq 0.97$.

exactly. Finally, a third kind of generalization, where the Hamiltonian character is destroyed by introducing dissipation and/or coupling into a thermal bath, is beyond the scope of this work [33].

III. EFFECTIVE HAMILTONIAN SYSTEM

Following Refs. [14–16] (see also Ref. [34] in a different context) we deal with an effective 1D time-dependent system whose Hamiltonian is

$$H(p,q;t)=\frac{p^2}{2}-\gamma(\theta+\cos t)\cos q \qquad (2)$$

in dimensionless units. γ and θ are two classical real parameters that can be modified in real experiments. In addition, there is also one parameter, namely $\hbar_{\rm eff}$, which fixes the quantum scale and is defined by the usual relation between canonical operators: $[q,p]=i\hbar_{\rm eff}$. It turns out that $\hbar_{\rm eff}$ is not constant any longer (see Sec. IV below). It can be also experimentally varied via the rescaling factor that is needed in the canonical commutation relation in order to work in dimensionless units used to write Eq. 2.

The time dependence breaks the conservation of energy, and therefore may generate chaos. In order to deal with such a Hamiltonian, it is crucial to remark that it has both a spatial and a temporal periodicity. The latter implies that the Floquet theorem can be used, which states that the Hilbert space is spanned by an orthonormal eigenbasis of the evolution operator over one period. The corresponding eigenvalues of this unitary operator are distributed on the unit circle and are, therefore, labeled by their phase. This is conveniently written as $\exp(-i2\pi\epsilon/\hbar_{\rm eff})$, where 2π stands for the period of the modulation and ϵ can be interpreted as a quasienergy, a generalization of the notion of energy level for a time-periodic system.

The spatial periodicity of the Hamiltonian is also extremely important, as it makes it possible to split the Hilbert space into independant components, each component being characterized by the so-called Bloch vector k in the $]-0.5,0.5]$ range: under translation of 2π along q, the quasienergy eigenstates are just multiplied by the phase factor $\exp(i2\pi k)$. Thus one has to solve the Floquet-Schrödinger equation in an elementary spatial cell with boundary conditions depending on k. In this way, one generates—for a fixed value of k—a discrete quasienergy spectrum $\epsilon_i(k)$. When the full range of k values is considered, one obtains the familiar (quasi)energy bands [35].

There is an additional discrete symmetry which can be used. The Hamiltonian (2) is invariant under the time-reversal symmetry $(q,p,t)\rightarrow(q,-p,-t)$. In the classical surfaces of section, this implies a symmetry with respect to the q axis. In situations like the one in Fig. 1(b), this implies the existence of pairs of symmetric classically unconnected tori, i.e., a situation where tunneling could be observed. In the quantum world, the situation is slightly more complicated, because this symmetry connects the k subspace to the $-k$ subspace. In the particular case $k=0$ ($k=0.5$ could also be used), this implies that the Floquet eigenstates can be split into two subclasses of states which are either even or odd under the symmetry operation. The splitting between a doublet of even and odd states, $\Delta\epsilon_n=|\epsilon_n^+(0)-\epsilon_n^-(0)|$, will be a measure of tunneling.

We will extensively use the Husimi representation of a quantum state [36]. Such a representation associates with each quantum state $|\psi\rangle$ a phase space function $\psi^{\rm H}(p,q)$ (where p and q are real numbers) defined by

$$\psi^{\rm H}(p,q)=|\langle z|\psi\rangle|^2, \qquad (3)$$

where $|z\rangle$ is the coherent state corresponding to the complex number $z=(q+ip)/\sqrt{2\hbar_{\rm eff}}$. Since $|z\rangle$ is a minimal Gaussian wave packet with average momentum p and average position q, the Husimi function $\psi^{\rm H}(p,q)$ contains some information about the degree of localization of $|\psi\rangle$ in phase space. It is then possible to associate quantum states with classical phase space structures.

IV. EXPERIMENTS WITH COLD ATOMS

Under some severe conditions which constrain the experiments, Hamiltonian (2) can be obtained as an effective dimensionless Hamiltonian for cold neutral independent atoms of mass M interacting with two counterpropagating laser beams [14–16]. These two beams have two slightly different frequencies at $\omega_L+\delta\omega/2$ and $\omega_L-\delta\omega/2$. The longitudinal

coordinate x and the dimensionless q are related by $q=2k_Lx$, where $k_L=\omega_L/c$. The rescaling of the momentum is given by $p=(2k_L/M\delta\omega)p_x$. γ and θ are fixed by the intensity of the lasers and the detuning of the laser frequencies with respect to the atomic resonance. The dimensionless time t is taken in $\delta\omega^{-1}$ units and the expression of the effective Planck constant is $\hbar_{\rm eff}=8\omega_R/\delta\omega$, where $\omega_R=\hbar k_L^2/2M$. Since *in fine* we want to measure exponentially small tunneling splittings $\Delta\epsilon$, it is necessary to maintain these conditions for a time at least longer than $\hbar_{\rm eff}/\Delta\epsilon$. Moreover, a very accurate control of the preparation of the initial state and of the analysis of the final state is compulsory.

As shown above, due to the temporal and spatial periodicity of the Hamiltonian, observing the standard signature of tunneling—that is, an oscillation of a quantum state between two classically unconnected regions of phase space—requires that a single doublet of Floquet-Bloch eigenstates be initially populated, with well-defined values of the parameters $(\gamma,\theta,\hbar_{\rm eff})$, and a well-defined value of the Bloch angle k. If more than a single doublet is populated, additional frequencies (related to energy differences between the various populated Floquet states) will appear in the temporal evolution. If any parameter is not fixed, the experimental signal will be the superposition of tunneling oscillations (with different frequencies) for various sets of parameters. This will at best—if the dispersion of the parameter values is reasonably small—blur the oscillations at long times and at worst will completely destroy the signature of dynamical tunneling. It is experimentally rather simple to keep an accurate time periodicity of the driving signal, i.e., to fix $\hbar_{\rm eff}$. Similarly, the balance between the constant and the oscillatory term, hence the parameter θ in Eq. (2), is easily controlled. The γ parameter is proportional to the laser intensity and may thus slightly vary across the atomic cloud (because of the transverse structure of the laser beams). The most difficult part is to be sure that a single Bloch angle k is excited. Indeed, this requires a phase coherence of the initial wave function over a large number of laser wavelengths, which is extremely difficult to achieve experimentally [37], as will be shown in the following. In any case, the inhomogeneous broadening of the experimental signal because of the dispersion in k will be responsible for a decay of the tunneling oscillations.

A. NIST experiments [15]

In the NIST experiments, the two stable symmetric islands are chosen quite close in phase space in order to deal with not too small splittings. Another crucial point of this experiment is that the classical motion of the islands over one period, unlike those in Refs. [14] and [16], always remains trapped in one spatial elementary cell of length 2π. The quantum states localized in these islands are consequently only weakly sensitive to the boundary conditions which are governed by the Bloch angle. In other words, the tunneling period will be only weakly dependent on the Bloch angle k. This implies that the unavoidable broadening over k will not spoil too much the signature of tunneling. This is a major improvement over the tunneling described in Refs. [14,16], where a very narrow band of Bloch angle is required to observe clear tunneling oscillations. Moreover, the atoms involved in the tunneling process stay longer in the region where the laser intensities are uniform.

Indeed, as proposed in Ref. [38] and Chaps. 4 and 5 of Ref. [17], the two stable symmetric islands are created from a pitchfork bifurcation of the fixed point at $(p,q)=(0,0)$. To visualize it [see Figs. 2(a) and 2(b)], we extract a one-parameter sequence by varying γ while θ is fixed to the experimentally chosen value in Ref. [15], i.e., $\theta=1.724\,137$. When γ is increased, the pairs of symmetric tori appear at $\gamma\simeq0.56$. At the center of each set of tori, there is a periodic orbit. Over one period of the driving, the periodic orbit is essentially a rotation over the fixed point at $(p,q)=(0,0)$. This explains that the whole structure remains trapped in a single spatial cell. For $0.56\lesssim\gamma\lesssim\gamma_c$, the tori remain nested in one connected stable island. At $\gamma=\gamma_c\simeq0.625$, a chaotic sea separates the symmetric islands which shrink and move away from the central point before being dissolved through a cascade of bifurcations starting at $\gamma\simeq0.97$.

In one series of experiments, $\gamma\simeq0.96$ and $\hbar_{\rm eff}\simeq0.8$, the atoms are prepared in one island and their average momentum $\langle p\rangle$ is measured stroboscopically at every modulation period ($=2\pi$ in dimensionless units). Since in phase space the islands rotate about the origin with the same period, no variation in $\langle p\rangle$ would be noticeable if no tunneling occurred. In fact, starting the measurement sequence when $\langle p\rangle$ has its maximum value, oscillations are observed which illustrate the back and forth motion of the atoms between the islands due to dynamical tunneling. The tunneling period T is about 10 modulation periods in this case ($200\ \mu$s). This is in perfect agreement with the quasienergy splitting obtained numerically for the two Floquet eigenstates having the largest Husimi functions inside the islands.

It is worth noting that the NIST group uses a Bose-Einstein condensate as a preliminary step for preparing atoms in well-defined quantum states, especially for achieving a large coherence length for the wave function, i.e., a small spreading of the Bloch angle k. In order to prepare phase space localized states, an optical lattice is carefully turned on. When the tunneling experiment starts, the atomic density and the interaction between atoms is sufficiently small, and the experiment can be described by the interaction of individual independent atoms with the laser beams, i.e., using Hamiltonian (2). However, the cloud of atoms remains cold enough, at a subrecoil temperature, to prevent a large thermal broadening of momentum distribution that would destroy the signal. Because they start from very low temperature, these preparation techniques based on condensate manipulation seem to allow greater room to maneuver than those working with thermal clouds only. Adiabatic switching of the light potentials is not required and one can actually work with values of the classical parameters γ and θ which are far from the perturbative regime of an integrable system.

By diagonalizing the evolution operator corresponding to Eq. (2) over one period, we are not only able to reproduce the oscillatory behavior of $\langle p(t)\rangle$ [see Fig. 3(a)], but also can

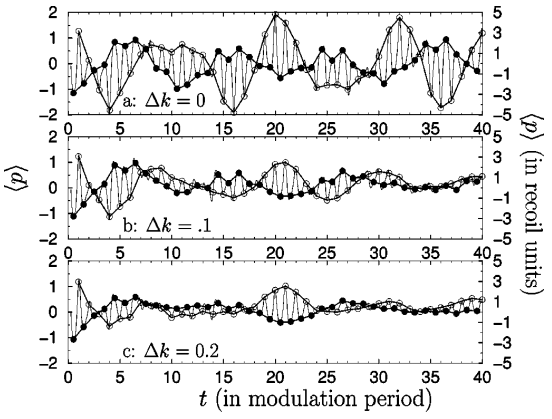

FIG. 3. Numerical simulation of the quantum evolution, in the conditions of the NIST experiment, i.e., $\theta = 1.72$, $\gamma = 0.96$ and, $\hbar_{\text{eff}} = 0.8$ (compare to Fig. 4(a) of Ref. [15]). Starting at $t = \pi/2$ with a Gaussian wave packet whose Husimi function is localized in one stable island (with a vanishing average momentum), we follow the average momentum $\langle p \rangle$ as time evolves. The stroboscopic measurements at times $2\pi + 2m\pi$ ($\pi + 2m\pi$) with $m \in \{0,1,\ldots,40\}$ are plotted with the white (black) circles. The tunneling oscillations are clearly visible; the tunneling period can be extracted from the typical time scale of the envelope: it is about 10 modulation periods. In the upper plot (a), we assume that a single Bloch angle $k = 0$ is initially prepared (which implies a perfect phase coherence of the wave function across the optical lattice). The (thermal) dispersion of the Bloch angle washes out the signal: in case (b), we take a momentum distribution with width $\Delta p = \alpha = 2\Delta k = 0.2$ and in case (c) $\Delta p = 0.4$. In the latter case, the amplitudes of the envelopes are so weak that this corresponds to an upper bound in temperature (about 1/5 of the recoil temperature) at which tunneling can be measured.

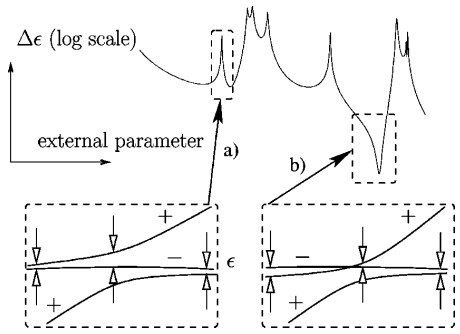

FIG. 4. When a third level is crossing a tunneling doublet when a parameter of the Hamiltonian is varied, there is an avoided crossing between the third level and the member of the doublet with the same symmetry, while the other member of the doublet (with opposite symmetry) ignores the third level. Two generic scenarii exist: in case (a), the tunneling splitting increases in the vicinity of the avoided crossing; in case (b), it decreases and vanishes at a specific value of the parameter.

study the spoiling effect of the thermal dispersion $\Delta p \propto \sqrt{\text{temperature}}$ and predict the maximum allowed temperature [see Figs. 3(b) and 3(c)] [48]. If α denotes the width of the momentum distribution in recoil momentum units, it can be shown ([14], Sec. 6 A) that it corresponds to a statistical mixture of Bloch states with $\Delta k = \alpha/2$. Figure 3](a) corresponds to the ideal situation where all atoms are prepared with $\alpha \ll 1$ about the $k = 0$. When a small but nonvanishing α is introduced, some states of the quasienergy bands with nonvanishing k get involved and blur the tunneling oscillations. For $\alpha = 0.2$, the oscillation amplitude is reduced by a factor of 2 and for $\alpha = 0.4$ the oscillations nearly disappear. Therefore, in this experiment, having a subrecoil atom cloud is essential.

In the following we want to focus on tunneling only and we will implicitly keep $k = 0$.

B. Austin experiments [16]

For a better understanding of the dynamics, one must go beyond the two-level model involving the symmetric and the antisymmetric states only. Other states must be taken into account and their influence can be felt when a classical parameter (γ or θ) or the quantum one ($\hbar_{\text{eff}}$) is continuously varied. Two (quasi)energies may exactly become degenerate if they belong to distinct symmetry classes. If not, they may follow a so-called avoided crossing whose size reflects both the direct coupling between the two states (more precisely, the off-diagonal matrix element of the coupling perturbation) and the indirect coupling to other states. One of the keys to the chaotic tunneling problems is to clearly identify the qualitative nature and the quantitative influence of indirect coupling. This is the background of the Austin experiments.

A third level is involved in a non-negligible indirect coupling when its quasienergy approaches the tunneling doublet energies. This can be understood from perturbation theory, since the leading term of the indirect coupling is proportional to the inverse of the energy difference. The two generic scenarios of the crossing of the doublet by a third state are shown in Fig. 4. Aside from the unavoidable ambiguous definition of the splitting, it appears clear that case (a) corresponds to an increase of the tunneling splitting during the crossing while, conversely, case (b) can lead to arbitrarily small splittings, since an exact degeneracy occurs. Thus, such a crossing by a third state produces a sharp variation of the tunneling period that can be measured experimentally. This is actually what is observed in the Austin experiments and can be confirmed by numerical experiments as shown in Fig. 5. When looking at the Husimi representation of the states, Fig. 6, one can immediately distinguish between the tunneling doublet and the third state sufficiently far from the crossing. As expected, the tunneling doublet has Husimi representations localized in the stable islands, though they also spread in the chaotic sea. On a classical Poincaré surface of section, it is easy to make the difference between chaotic and regular motion; how to transpose this distinction at the quantum level is not known with the large values of $\hbar_{\text{eff}}$ used in both the Austin and the NIST experiments. Some classical structures much smaller than the de Broglie wavelength are possibly present in some of the states [49], but just looking at

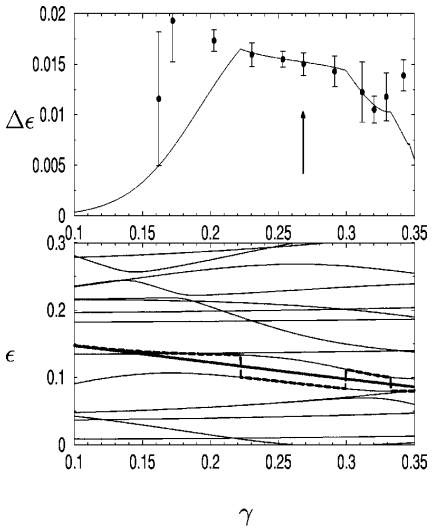

FIG. 5. Numerical results obtained with the parameters of the Austin experiment, that is Hamiltonian (2), with $\theta=1$ and $\hbar_{\rm eff}=0.33$. The lower plot shows a part of the quasienergy spectrum when γ is varied. Thick lines show the two quasienergies whose difference is the tunneling splitting plotted in the upper plot. The two states are selected to have the largest localization of the Husimi function at the center of the stable islands. When a third level couples to the state that belongs to the same symmetry class, an avoided crossing can be seen and the definition of the doublet becomes necessarily ambiguous. There, some discontinuity in the selected state (and in the slope of the tunneling frequency) cannot be avoided. The tunneling splitting is shown as a function of γ in the upper plot, and is compared with the experimental results from Ref. [16]. The agreement is very good, which validates the numerical approach. Around $\gamma=0.2$, a discrepancy is visible. This is precisely the ''ambiguous'' region where the dynamics cannot be reduced to a simple tunneling oscillation, but at least three levels must be taken into account, leading to several relevant energy splittings.

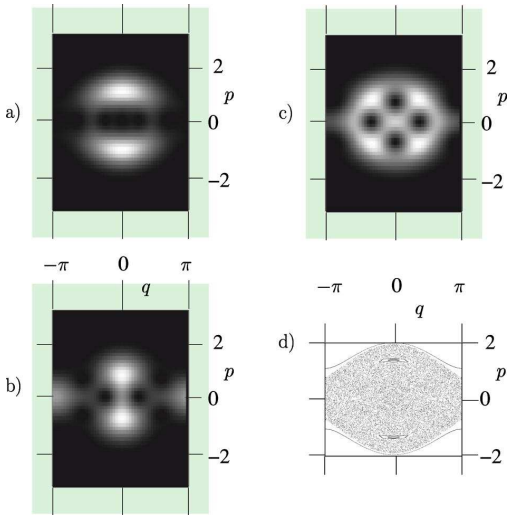

FIG. 6. (a), (b), and (c) show the density in gray scale of the Husimi functions associated with the three states which play an important role for tunneling at $\gamma=0.25$ (parameters of the Austin experiment, as in Fig. 5). As expected, the two members of the doublet, (a) and (b), have their Husimi function localized about the two symmetric islands visible in the classical Poincaré surface of section (d). (b) is strongly coupled to a third states shown in (c). $\hbar_{\rm eff}$ is too large to attribute any regular or chaotic character to the third state. (c) clearly plays a role in the enhancement of the tunneling splitting through an indirect coupling; this is thus an ''assisted tunneling'' mechanism, which cannot be unambiguously characterized as chaos assisted.

the Husimi representation of the third state for $\hbar_{\rm eff}\simeq 1$ does not make it possible to attribute any chaotic or regular character to it. It is only for much smaller $\hbar_{\rm eff}$ that chaotic or regular wave functions make sense. This is not surprising: the dichotomy between regular and irregular motion is a classical one and, at present, it can be extrapolated at the quantum level within the semiclassical regime only. Anyway, one must keep in mind that tunneling only makes sense in the semiclassical regime. One of the great merits of the Austin experiments is that they show a quantum tunneling effect where an indirect process is involved. However, it is an exageration to attribute any chaotic origin to it.

V. NUMERICAL EVIDENCE OF A CHAOTIC TUNNELING REGIME

It was one of the first successes of quantum chaos to have shown that the energy levels of an integrable system are independent of each other, because they are localized on different classical tori, while in chaotic systems level repulsion is the rule. Following the discussion in the preceding section, one may therefore expect that the average size of avoided crossings is increased when chaos is present. The fluctuations of a tunneling process which should be narrow and sparse in an integrable regime should be broader, more numerous, and possibly involving many states in a chaotic regime. We now illustrate this statement in the framework of the experimental atomic Hamiltonian (2).

There are two different ways of rendering chaos observable by quantum eyes: the first one consists of increasing the volume of the chaotic sea with the help of a classical parameter, the second one fixes the classical dynamics and decreases $\hbar_{\rm eff}$. We will present in both ways.

One may try to study the tunneling *fluctuations* separately from the *average behavior*. This average—in a somewhat vague sense—is increased, because chaos diminishes the classical dynamical barrier [50], and this is the reason why the phenomenon can be called chaos assisted tunneling. However, as far as only fluctuations are concerned (there can be an enhancement or a decrease as well), the words ''chaos assisted tunneling'' (CAT) [10] may lead to confusion and we simply use ''chaotic tunneling.'' At last, Brodier, Schlagheck, and Ullmo discovered what they called ''resonant assisted tunneling'' (RAT) [42] to describe an enhancement of tunneling due to an indirect process. It involves one or several quasimodes localized in the secondary resonances surround-

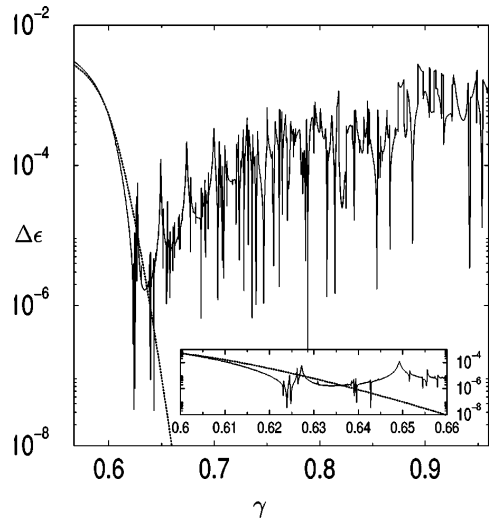

FIG. 7. The tunneling splitting as a function of γ, for $\theta = 1.724\,137$ and $\hbar_{\rm eff} = 0.079\,638$, that is ten times smaller than in the NIST experiments. Two regimes are clearly separated by the critical value $\gamma_c \simeq 0.625$; these two *quantum* regimes correspond to two different *classical* regimes in the Poincaré surfaces of section in Fig. 2. The smooth average decrease with sparse and narrow fluctuations ($\gamma < \gamma_c$) corresponds to the case where the symmetric classical tori belong to the same regular island. The Hamiltonian there can be approximated by a simple integrable Hamiltonian, using the normal form described in the Appendix. The dotted line corresponds to the splitting calculated with this normal form and is in good agreement with the numerical result. In the second regime ($\gamma > \gamma_c$), there are huge quantum fluctuations of the tunneling splitting (and a slightly increased average value). Classically, this corresponds to tunneling between unconnected symmetric islands, separated by a chaotic sea.

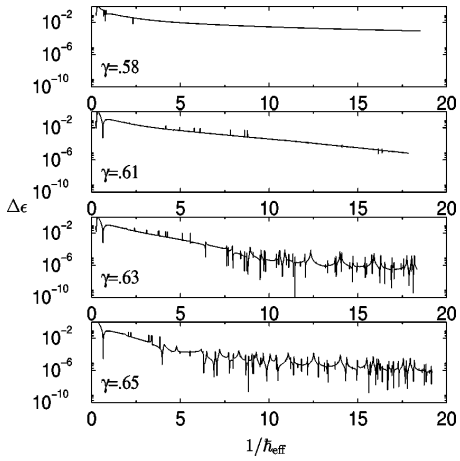

FIG. 8. The tunneling splitting as a function of $\hbar_{\rm eff}$ for fixed values of the classical parameters, i.e., fixed classical dynamics ($\theta = 1.724\,137$ and four values of γ). In the regular regime, an exponential decrease, as described by Eq. (1) is visible as a straight line with a negative slope in a logarithmic scale. The regime of fluctuations can be seen for $\gamma > \gamma_c$ when $\hbar_{\rm eff}$ is small enough for the de Broglie wavelength to be comparable to the size of the chaotic sea between the two islands.

ing the main symmetric islands. Up to now, RAT has been studied quantitatively in a purely quasi-integrable case but there are clues that it can be extended far beyond KAM theory.

A. γ change

Let us first take $\hbar_{\rm eff}$ ten times smaller than the values in the NIST and Austin experiments. It is much easier to do it numerically than experimentally, as it requires the increase of the modulation frequency of the laser beams by one order of magnitude. We then follow the quantum states through the classical bifurcation shown in Fig. 2 and discussed in Sec. IV A. Again, in order to calculate the tunneling splitting $\Delta\epsilon$, we select the states that have the largest Husimi functions inside the islands.

Figure 7 shows that, after a smooth decrease of $\Delta\epsilon$ up to $\gamma = \gamma_c \simeq 0.625$ there is an abrupt change of regime. First, the mean value of $\Delta\epsilon$ increases and second, many fluctuations appear which modify the splitting by several orders of magnitude. It is remarkable that this change of regime can be matched on the Poincaré surfaces of section. The smooth tunneling regime occurs when the resonant tori belong to one quasi-integrable island. For $\gamma < \gamma_c$, we are able to reproduce the main features of tunneling by using an integrable approximation (see Appendix). The decrease of tunneling can be explained in terms of the lengthening of the dynamical barrier. γ_c exactly corresponds to the point where the islands get disconnected. In addition, one can follow the bifurcation on the Husimi representations of the tunneling doublet.

One can hardly detect by eye any regularity in the chaotic regime, but four large spikes in the range $\gamma_c < \gamma < 0.7$ can be seen. This can be traced back to the crossing by the same third state whose quasienergy line is folded four times in the Floquet zone centered on the doublet.

B. $\hbar_{\rm eff}$ change

Figure 8 shows $\Delta\epsilon$ as a function of $1/\hbar_{\rm eff}$ for four values of γ. Here again, two types of regimes, a quasiregular and a chaotic one, can clearly be distinguished. For the values of γ where some substantial chaos is present in between the islands, by decreasing $\hbar_{\rm eff}$ one gets to the chaotic regime. For $\gamma < \gamma_c$, i.e., in the quasiregular regime, one may enter a chaotic regime but for much lower values of $\hbar_{\rm eff}$, since the chaotic layers between KAM tori are so thin that they are not even resolved in the Poincaré surface of section given in the figures.

In these plots, a purely exponential law given by Eq. (1) would produce a straight line with negative slope. For $\gamma < \gamma_c$ and small values of $\hbar_{\rm eff}$, this is also the prediction for the integrable approximation (see Appendix) of the Hamiltonian. Deviations from a pure exponential decrease are observed at low values of $\hbar_{\rm eff}$. This is not surprising, as the

integrable approximation is a local approximation of the Hamiltonian which must fail when large phase space structures are involved. This is, for example, the case for the NIST experiment at $1/\hbar_{\rm eff}\simeq 1.3$ where the model is only qualitative and predicts a splitting about ten times smaller than that numerically and experimentally observed. However, that the model correctly predicts the behavior at small $\hbar_{\rm eff}$ values is a strong indication that it is qualitatively correct.

On the other hand, in the chaotic regime, both the integrable model and the exponential law cannot reproduce the fluctuations in the splitting observed in Fig. 8. Whenever such a fluctuation is due to a crossing by a quasimode (and not to a state delocalized in the surrounding chaotic sea), it might be reproduced by the resonance assisted tunneling techniques.

VI. STATISTICAL SIGNATURE OF CHAOTIC TUNNELING?

In order to reproduce quantitatively the statistics of the tunneling splitting fluctuations in the chaotic regime, Leyvraz and Ullmo [43] have introduced a random matrix model. The Hamiltonian can be split into two uncoupled components associated with the even and odd symmetry subspaces. The corresponding matrices are written as

$$H^{\rm even}=\begin{pmatrix} \epsilon_0^+ & v_1^+ & v_2^+ & \cdots \\ v_1^+ & & & \\ v_2^+ & & H_\perp^+ & \\ \vdots & & & \end{pmatrix} \tag{4}$$

and

$$H^{\rm odd}=\begin{pmatrix} \epsilon_0^- & v_1^- & v_2^- & \cdots \\ v_1^- & & & \\ v_2^- & & H_\perp^- & \\ \vdots & & & \end{pmatrix}, \tag{5}$$

where $\epsilon_0^\pm$ represent the energies of the doublet, $H_\perp^\pm$ is the Hamiltonian in the chaotic sea (modeled by a random Gaussian matrix), and v is the indirect coupling.

Neglecting direct tunneling consists in taking $\epsilon_0^+=\epsilon_0^-$. The central hypothesis is to consider all the v's as independent variables with *the same* Gaussian distribution. This is quite natural in order to treat all the other states on the same footing, as they are assumed to be chaotic states randomly delocalized in the chaotic sea. With these assumptions, the splitting distribution can be calculated and is given by a (truncated) Cauchy distribution, see Ref. [43]. For Hamiltonian (2), in each chaotic case where it has been tested, the Leyvraz-Ullmo prediction is in agreement with the numerical results (see Ref. [14]). More surprisingly, we have found that the Leyvraz-Ullmo law gives correct predictions even when the classical dynamics is quasiintegrable (see Fig. 9 and the corresponding Poincaré surface of section in Fig. 1) and the de Broglie wavelength is much larger than the chaotic layers.

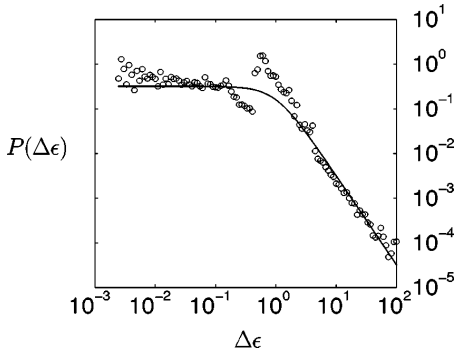

FIG. 9. Statistical distribution of the tunneling splittings as $\hbar_{\rm eff}$ is varied in the quasiintegrable case corresponding to Fig. 1(b) ($\theta=1,\gamma=0.018$). Surprisingly, the numerically observed distribution (small circles) is in good agreement with the Leyvraz-Ullmo law (solid line) which is supposed to be valid in the chaotic case, as it treats all the states coupled to the tunneling doublet on the same footing. This clearly indicates that a Leyvraz-Ullmo distribution is not sufficient to characterize chaotic tunneling.

When looking at the splitting, one observes numerous and large fluctuations (over several orders of magnitude) which were supposed to characterize the chaotic regime. Conversely, we have not been able to find a regular regime of fluctuations with classically chaotic dynamics. Therefore, one must conclude that even though two different regimes of tunneling fluctuations can be identified unambiguously, classical chaos appears to be a sufficient, but not a necessary, condition for having numerous and large fluctuations governed by the Leyvraz-Ullmo law.

These unexpected results are not explained at the present state of the theoretical approaches of chaotic tunneling. If it appears, within future numerical or real experiments, that these results are not due to the peculiar properties of our system, it would definitely mean that further theoretical studies are needed.

VII. CONCLUSION

In this paper we have studied in great detail the transition between a regular and a chaotic regime of tunneling within a classical configuration that can be achieved experimentally. We have shown why $\hbar_{\rm eff}$ has to be small enough if one wants to reach for the first time the chaotic regime in real systems. In recent experiments with cold atoms, it requires the increase of the modulation period up to one order of magnitude (that is, at least the MHz).

Theoretically, there is also a lot of work to be done if we want to understand and therefore predict the fluctuations quantitatively. The semiclassical regime requires careful study of the dynamics with complex coordinates. However, the present work has shown clearly that the abrupt transition between a regular and a chaotic regime of tunneling corresponds to a classical transition that can be identified very precisely. Tunneling being a relevant concept in a semiclassical regime only, it is therefore not surprising that future

investigations of chaotic tunneling will have to keep track of the classical dynamics in one way or another.

ACKNOWLEDGMENTS

We acknowledge A. Shudo, S. Tomsovic, D. Ullmo, and W. Hensinger for stimulating discussions. A.M. is grateful to N. Mohammedi for his kind reading of the original manuscript and to O. Boebion for computer assistance in the Laboratoire de Mathématiques et de Physique Théorique of Tours and thanks the Laboratoire Kastler Brossel of Paris for kind hospitality. Laboratoire Kastler Brossel de l'Université Pierre et Marie Curie et de l'Ecole Normale Supérieure is Unité Mixtè de Recherche No. 8552 du CNRS. Laboratoire de Mathématiques et de Physique Théorique de l'Université François Rabelais is Unité Mixtè de Recherche No. 6083 du CNRS.

APPENDIX A: INTEGRAL APPROXIMATION NEAR THE PITCHFORK BIFURCATION

When one classical parameter is smoothly varied in a nonintegrable Hamiltonian system, its periodic orbits follow an infinite fractal-like cascade of bifurcations through which they cannot be followed smoothly. However, all the bifurcations can be classified according to a simple set of scenarios: for a given bifurcation of a given periodic orbit, the phase-space dynamics of the original parameter-dependent Hamiltonian can be uniformly approximated by an integrable parameter-dependent Hamiltonian that retains the relevant features only. Of course, because one cannot get rid of the chaotic dynamics, this approximation makes sense only locally, that is, near the periodic orbit, in the neighborhood of the bifurcation. It is the object of the Hamiltonian normal form theory to classify the bifurcations and obtain the simplest form of the approximated integrable Hamiltonians (the so-called normal forms). Generally, i.e., when no constraint or symmetry is present, the one parameter Hamiltonian normal forms have been completely classified by Meyer [30,44,45]. However, the bifurcation shown in Fig. 2 is outside the scope of Meyer's classification precisely because the time reversal symmetry plays a key role. Even if the Poincaré surface of section near the origin [see Fig. 2(b)] cannot be distinguished from that corresponding to Meyer's transitional bifurcation (see, for instance, Fig. 9(b) in Ref. [30]), it is crucial to note that, in our case, two *distinct* 2π-periodic orbits have emerged from the origin. In a transitional bifurcation, the two stable islands would correspond to the *same* 4π-periodic orbit. Therefore, they would be classically connected to each other and would be irrelevant for tunneling. Let us sketch briefly how to obtain the Hamiltonian normal form in our case.

(1) The first step is to find the value γ_0 of γ at which the bifurcation occurs (θ is kept fixed). Such a bifurcation occurs when the trace of the monodromy matrix M_γ at the origin after one period is 2 and corresponds in the $(-2\gamma, 4\gamma\theta)$ plane to the border of the even Arnold tongues (see Fig. 20.1 in Ref. [46]) (the transitional case occurs when $\mathrm{tr}\, M_\gamma = -2$ at the border of the odd Arnold tongues). More precisely, the case shown in Fig. 2 corresponds to $\theta = 1.724\,137$ (the experimental value in the NIST experiment) and the bifurcation takes place at $\gamma_0 \simeq 0.564673$. In the following, we use $\varepsilon = \gamma - \gamma_0$.

Let us denote by $\mathcal{Y}_\varepsilon(z)$ [respectively, $\mathcal{Z}_\varepsilon(z)$] the solution of the Mathieu equation

$$y''(x) + [4\gamma\theta + 4\gamma\cos(2x)]y(x) = 0 \tag{A1}$$

such that $\mathcal{Y}_\varepsilon(0) = 0$ and $\mathcal{Y}'_\varepsilon(0) = 1$ [respectively, $\mathcal{Z}_\varepsilon(0) = 1$ and $\mathcal{Z}'_\varepsilon(0) = 0$]. The prime stands for the derivative with respect to x. For $\varepsilon = 0$, it is straightforward to show that

$$M_{\gamma_0} = \begin{pmatrix} 1 & \dfrac{1}{4\pi}\mathcal{Z}'_0(\pi) \\ 0 & 1 \end{pmatrix}, \tag{A2}$$

where $\mathcal{Z}'_0(\pi) \simeq 1.480\,919$ for $\theta = 1.724\,137$.

(2) The second step is to make a (linear) 2π-periodic canonical change of coordinate that eliminates the time dependence in the quadratic part of Hamiltonian (2), near the origin and uniformly in ε. We are then led to the Hamiltonian

$$\left(-\frac{1}{2}\frac{1}{4\pi}\mathcal{Z}'_0(\pi) + \alpha\varepsilon\right)q^2 + \frac{1}{2}\beta\varepsilon p^2 + \frac{1}{2}\delta\varepsilon p^2 + \text{higher order } 2\pi\text{-periodic terms}, \tag{A3}$$

where α, β, δ are ε-independent coefficients. Only $\beta = 1/\pi\partial_\varepsilon \mathcal{Y}_\varepsilon(\pi)$ evaluated at $\varepsilon = 0$ will be relevant, since α and δ can be eliminated by a suitable canonical change of coordinates following a method explained in Ref. [30], Sec. 4.2. In our case $\beta \simeq 2.008/\pi$. We are therefore led to the following normal form of the quadratic part of the Hamiltonian:

$$\left(-\frac{1}{2}\frac{1}{4\pi}\mathcal{Z}'_0(\pi)\right)q^2 + \frac{1}{2}\beta\varepsilon p^2 + \text{higher order } 2\pi\text{-periodic terms}. \tag{A4}$$

(3) Following the same reasoning that led to the transitional normal form ([30], Sec. 4.2), all higher order 2π-periodic terms except the resonant terms of the form $h_k(\varepsilon)p^k$ can be canceled by a suitable canonical change of coordinates. Because of the time-reversal symmetry, the coefficient h_3 vanishes identically, and therefore the leading order normal form is

$$\left(-\frac{1}{2}\frac{1}{4\pi}\mathcal{Z}'_0(\pi)\right)q^2 + \frac{1}{2}\beta\varepsilon p^2 - \frac{1}{4}h_4(0)p^4. \tag{A5}$$

The explicit calculation of $h_4(0)$ is tedious but it can be estimated numerically by fitting the coordinate $q=0$, $p=\pm\sqrt{\beta\varepsilon/h_4}$ of the satellite 2π-periodic orbits for $\varepsilon>0$. We obtain $h_4\simeq 0.0320$.

It is far from obvious that the quantization of the normal form (A5) will give a good approximation of the quasienergies of the tunneling doublet. Some discrepancies may arise from the fact that quantum physics is invariant under canonical transformations only at the leading order in $\hbar$. When we replace p with q and change the sign of the energies, the normal form (A5) leads to a standard 1D double-well problem whose quantum spectrum can be found by numerically diagonalizing the Hamiltonian written in a harmonic basis. The tunneling splitting of the ground doublet is given by the dotted line in Fig. 7 and it agrees reasonably well with the exact numerical result for γ near γ_0.

[1] A. Messiah, *Mécanique Quantique* (Dunod, Paris, 1964) (English translation published by North-Holland, Amsterdam, 1964).
[2] R. Balian and C. Bloch, Ann. Phys. (N.Y.) **84**, 559 (1974).
[3] M. Wilkinson, Physica D **21**, 341 (1986).
[4] M. Wilkinson and J.H. Hannay, Physica D **27**, 201 (1987).
[5] *Chaos et Physique Quantique—Chaos and Quantum Physics*, Les Houches, École d'Été de Physique Théorique 1989, Session LII, edited by M. Giannoni, A. Voros, and J. Zinn-Justin (North-Holland, Amsterdam, 1991).
[6] C. Dembowski, H.-D. Gräf, A. Heine, R. Hofferbert, H. Rehfeld, and A. Richter, Phys. Rev. Lett. **84**, 867 (2000).
[7] W.A. Lin and L.E. Ballentine, Phys. Rev. Lett. **65**, 2927 (1990).
[8] O. Bohigas, D. Boosé, R. Egydio de Carvalho, and V. Marvulle, Nucl. Phys. A **560**, 197 (1993).
[9] O. Bohigas, S. Tomsovic, and D. Ullmo, Phys. Rep. **223**, 43 (1993).
[10] S. Tomsovic and D. Ullmo, Phys. Rev. E **50**, 145 (1994).
[11] S.C. Creagh and N.D. Whelan, Phys. Rev. Lett. **77**, 4975 (1996).
[12] O. Brodier, P. Schlagheck, and D. Ullmo, Ann. Phys. (N.Y.) **300**, 88 (2002).
[13] J. Zakrzewski, D. Delande, and A. Buchleitner, Phys. Rev. E **57**, 1458 (1998).
[14] A. Mouchet, C. Miniatura, R. Kaiser, B. Grémaud, and D. Delande, Phys. Rev. E **64**, 016221 (2001).
[15] W.K. Hensinger, H. Häffner, A. Browaeys, N.R. Heckenberg, K. Helmerson, C. McKenzie, G.J. Milburn, W.D. Phillips, S.L. Rolston, H. Rubinsztein-Dunlop, and B. Upcroft, Nature (London) **412**, 52 (2001).
[16] D.A. Steck, H.O. Windell, and M.G. Raizen, Science **293**, 274 (2001).
[17] W.K. Hensinger, Ph.D thesis, The University of Queensland, Autralia, 2002.
[18] W.K. Hensinger, A. Mouchet, P.S. Julienne, D. Delande, N.R. Heckenberg, and H. Rubinsztein-Dunlop, Phys. Rev. A (to be published).
[19] *Laser and Manipulation of Atoms and Ions*, Enrico Fermi International Summer School, Course CXVIII, 9–19 July 1991, edited by E. Arimondo, W.D. Phillips, and F. Strumia (North-Holland, Amsterdam, 1992).
[20] R.T. Lawton and M.S. Child, Mol. Phys. **44**, 709 (1981).
[21] E.L. Sibert, W.P. Reinhardt, and J.T. Hynes, J. Chem. Phys. **77**, 3583 (1982).
[22] M.E. Kellman and E.D. Lynch, J. Chem. Phys. **87**, 5386 (1987).
[23] J.P. Rose and M.E. Kellman, J. Chem. Phys. **105**, 7348 (1996).
[24] E.J. Heller, Nature (London) **412**, 33 (2001).
[25] A. Mouchet and D. Ullmo, Phys. World **14**(9), 24 (2001).
[26] B. Goss Levi, Phys. Today **54**(8), 15 (2001).
[27] J. Heading, *An Introduction to Phase-Integral Methods* (Methuen, Wiley, London, 1962).
[28] M.J. Davis and E.J. Heller, J. Phys. Chem. **85**, 307 (1981).
[29] M. Kuś, F. Haake, and D. Delande, Phys. Rev. Lett. **71**, 2167 (1993).
[30] P. Lebœuf and A. Mouchet, Ann. Phys. (N.Y.) **275**, 54 (1999).
[31] A. Shudo and K.S. Ikeda, Physica D **115**, 234 (1998).
[32] S. Tomsovic, J. Phys. A **31**, 9469 (1998).
[33] *Tunneling in Complex Systems*, edited by S. Tomsovic, Proceedings of the Institute for Nuclear Theory Vol. 5 (World Scientific, Singapore, 1998).
[34] V. Averbukh, N. Moiseyev, B. Mirbach, and H.J. Korsh, Z. Phys. D: At., Mol. Clusters **35**, 247 (1995).
[35] N.W. Ashcroft and N.D. Mermin, *Solid State Physics* (Saunders College, Philadelphia, 1976).
[36] K. Husimi, Proc. Phys. Math. Soc. Jpn. **22**, 264 (1940).
[37] M. Greiner, O. Mandel, T. Esslinger, T.W. Hänsch, and I. Bloch, Nature (London) **415**, 39 (2002).
[38] W.K. Hensinger, B. Upcroft, N.R. Heckenberg, G.J. Milburn, and H. Rubinsztein-Dunlop, Phys. Rev. A **64**, 063408 (2001).
[39] R. Luter and L.E. Reichl, Phys. Rev. A **66**, 053615 (2002).
[40] W.H. Zurek, Nature (London) **412**, 712 (2001).
[41] N.L. Balazs and A. Voros, Ann. Phys. (N.Y.) **199**, 123 (1990).
[42] O. Brodier, P. Schlagheck, and D. Ullmo, Phys. Rev. Lett. **87**, 064101 (2001).
[43] F. Leyvraz and D. Ullmo, J. Phys. A **29**, 2529 (1996).
[44] K.R. Meyer, Trans. Am. Math. Soc. **149**, 95 (1970), reprinted in Ref. [47].
[45] K.R. Meyer and G.H. Hall, *Introduction to Hamiltonian Dynamical Systems and the N-Body Problem*, Applied Mathematical Sciences Vol. 90 (Springer-Verlag, New York, 1992).
[46] M. Abramowitz and I.A. Segun, *Handbook of Mathematical Functions* (Dover Publications, New York, 1965).
[47] R.S. Mackay and J.D. Meiss, *Hamiltonian Dynamical Systems* (Adam Hilger, Bristol, 1987).
[48] After the first version of the present paper was written, we learned that an independent numerical work [39] had obtained the same results as those in our Fig. 3(a). But Ref. [39] does not consider the thermal effects and does not always work within the Floquet theory at $k=0$ instead of the Floquet-Bloch theory. In the present work we clearly demonstrate that thermal effects cannot be neglected and must be studied carefully when experiments are discussed.
[49] From time to time, it is claimed [40] that a simple matching between classical structures and quantum wave sub-Planckian

structures was found but, as was understood a long time ago (Ref. [41]), the latter are generally washed out as soon as one tries to measure global averages.

[50] The question of defining an integrable system with which the chaotic one should be compared is extremely difficult because of the exponential sensitivity of tunneling to the classical parameters. It is a much more serious problem than defining an averaging procedure.

I.6 Analyse d'expériences sur l'effet tunnel dynamique réalisées avec un condensat de Bose-Einstein

Écrit avec Dominique Delande et en collaboration avec l'équipe de Phillips (groupe *Laser Cooling and Trapping* du nist, Gaithersburg), Winfried Hensinger en particulier, qui était en post-doc directement en chargé de l'expérience, nous analysons en détail les résultats en nous appuyant sur des simulations de l'équation de Gross-Pitaevskii, d'une part, et sur un analyse de la dynamique de Floquet d'autre part.

PHYSICAL REVIEW A **70**, 013408 (2004)

Analysis of dynamical tunneling experiments with a Bose-Einstein condensate

W. K. Hensinger,[1,2,*] A. Mouchet,[3,†] P. S. Julienne,[2] D. Delande,[4] N. R. Heckenberg,[1] and H. Rubinsztein-Dunlop[1]
[1]*Centre for Biophotonics and Laser Science, Department of Physics, The University of Queensland, Brisbane, Queensland 4072, Australia*
[2]*National Institute of Standards and Technology, Gaithersburg, Maryland 20899, USA*
[3]*Laboratoire de Mathématique et de Physique Théorique (CNRS UMR 6083), Avenue Monge, Parc de Grandmont, 37200 Tours, France*
[4]*Laboratoire Kastler-Brossel (CNRS UMR 8552), Université Pierre et Marie Curie, 4 place Jussieu, F-75005 Paris, France*
(Received 26 September 2003; revised manuscript received 5 April 2004; published 15 July 2004)

Dynamical tunneling is a quantum phenomenon where a classically forbidden process occurs that is prohibited not by energy but by another constant of motion. The phenomenon of dynamical tunneling has been recently observed in a sodium Bose-Einstein condensate. We present a detailed analysis of these experiments using numerical solutions of the three-dimensional Gross-Pitaevskii equation and the corresponding Floquet theory. We explore the parameter dependency of the tunneling oscillations and we move the quantum system towards the classical limit in the experimentally accessible regime.

DOI: 10.1103/PhysRevA.70.013408 PACS number(s): 42.50.Vk, 32.80.Pj, 05.45.Mt, 03.65.Xp

I. INTRODUCTION

Cold atoms provide a system which is particularly suited to study quantum nonlinear dynamics, quantum chaos, and the quantum-classical borderland. On relevant time scales the effects of decoherence and dissipation are negligible. This allows us to study a Hamiltonian quantum system. Only recently dynamical tunneling was observed in experiments with ultracold atoms [1,2]. "Conventional" quantum tunneling allows a particle to pass through a classical energy barrier. In contrast, in dynamical tunneling a constant of motion other than energy classically forbids one to access a different motional state. In our experiments atoms tunneled back and forth between their initial oscillatory motion and the motion 180° out of phase. A related experiment was carried out by Steck, Oskay, and Raizen [3,4] in which atoms tunneled from one unidirectional librational motion into another oppositely directed motion.

Luter and Reichl [5] analyzed both experiments calculating mean momentum expectations values and Floquet states for some of the parameter sets for which experiments were carried out and found good agreement with the observed tunneling frequencies. Averbukh, Osovski, and Moiseyev [6] pointed out that it is possible to effectively control the tunneling period by varying the effective Planck's constant by only 10%. They showed one can observe both suppression due to the degeneracy of two Floquet states and enhancement due to the interaction with a third state in such a small interval.

Here we present a detailed theoretical and numerical analysis of our experiments. We use numerical solutions of the Gross-Pitaevskii equation and Floquet theory to analyze the experiments and to investigate the relevant tunneling dynamics. In particular we show how dynamical tunneling can be understood in a two and three state framework using Floquet theory. We show that there is good agreement between experiments and both Gross-Pitaevskii evolution and Floquet theory. We examine the parameter sensitivity of the tunneling period to understand the underlying tunneling mechanisms. We also discuss such concepts as chaos-assisted and resonance-assisted tunneling in relation to our experimental results. Finally predictions are made concerning what can happen when the quantum system is moved towards the classical limit.

In our experiments a sodium Bose-Einstein condensate was adiabatically loaded into a far detuned optical standing wave. For a sufficient large detuning, spontaneous emission can be neglected on the time scales of the experiments (160 μs). This also allows us to consider the external degrees of freedom only. The dynamics perpendicular to the standing wave are not significant, therefore we are led to an effectively one-dimensional system. The one-dimensional system can be described in the corresponding two-dimensional phase space which is spanned by momentum and position coordinates along the standing wave. Single frequency modulation of the intensity of the standing wave leads to an effective Hamiltonian for the center-of-mass motion given by

$$H = \frac{p_x^2}{2m} + \frac{\hbar\Omega_{\mathrm{eff}}}{4}[1 - 2\varepsilon\,\sin(\omega t + \phi)]\sin^2(kx), \qquad (1)$$

where the effective Rabi frequency is $\Omega_{\mathrm{eff}} = \Omega^2/\delta$, $\Omega = \Gamma\sqrt{I/I_{\mathrm{sat}}}$ is the resonant Rabi frequency, ε is the modulation parameter, ω is the modulation angular frequency, Γ is the inverse spontaneous lifetime, δ is the detuning of the standing wave, t is the time, p_x is the momentum component of the atom along the standing wave, and k is the wave number. Here I is the spatial-mean of the intensity of the unmodulated standing wave (which is half of the peak intensity) so Ω

*Electronic address: hensinge@umich.edu; Present address: Department of Physics, University of Michigan, 2477 Randall Laboratory, 500 East University Ave., Ann Arbor, MI 48109-1120, USA.
†Electronic address: mouchet@celfi.phys.univ-tours.fr

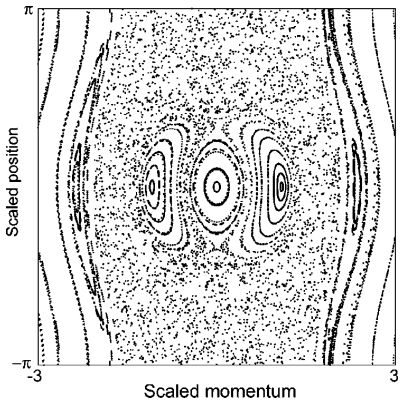

FIG. 1. Poincaré section for a classical particle in an amplitude-modulated optical standing wave. Momentum and position (one well of the standing wave) of the particle along the standing wave are plotted stroboscopically with the stroboscopic period being equal to the modulation period. The central region consists of small amplitude motion. Chaos (dotted region) separates this region from two period-1 regions of regular motion (represented in the Poincaré section as sets of closed curves) located left and right of the center along momentum $p=0$. Further out in momentum are two stable regions of motion known as librations. At the edges are bands of regular motion corresponding to above barrier motion. It is plotted for modulation parameter $\varepsilon=0.20$ and scaled well depth $\kappa=1.20$.

$=\Gamma\sqrt{I_{\mathrm{peak}}/2I_{\mathrm{sat}}}$ where $I_{\mathrm{sat}}=hc\Gamma/\lambda^3$ is the saturation intensity. λ is the wavelength of the standing wave. ϕ determines the start phase of the amplitude modulation. Using scaled variables [7] the Hamiltonian is given by

$$\mathcal{H} = p^2/2 + 2\kappa[1 - 2\varepsilon\ \sin(\tau+\phi)]\sin^2(q/2), \tag{2}$$

where $\mathcal{H}=(4k^2/m\omega^2)H$, $q=2kx$, and $p=(2k/m\omega)p_x$.

The driving amplitude is given by

$$\kappa = \omega_r\Omega_{\mathrm{eff}}/\omega^2 = \frac{\hbar k^2\Omega_{\mathrm{eff}}}{2\omega^2 m} = \frac{4U_0\omega_r}{\omega^2\hbar}, \tag{3}$$

where $\omega_r=\hbar k^2/2m$ is the recoil frequency, $\tau=t\omega$ is the scaled time variable, and U_0 is the well depth. The commutator of scaled position and momentum is given by

$$[p,q] = i\,\bar{\kappa}, \tag{4}$$

where the scaled Planck's constant is $\bar{\kappa}=8\omega_r/\omega$. For $\kappa=1.2$ and $\varepsilon=0.20$ the classical Poincaré surface of section is shown in Fig. 1. Two symmetric regular regions can be observed about $(q=0,p=1)$ and $(q=0,p=-1)$. These regions correspond to oscillatory motion in phase with the amplitude modulation in each well of the standing wave. In the experiment [1,2] atoms are loaded in a period-1 region of regular motion by controling their initial position and momentum and by choosing the starting phase of the amplitude modulation appropriately. Classically atoms should retain their momentum state when observed stroboscopically (time step is one modulation period). A distinct signature of dynamical tunneling is a coherent oscillation of the stroboscopically observed mean momentum as shown in Fig. 2 and reported in Ref. [1].

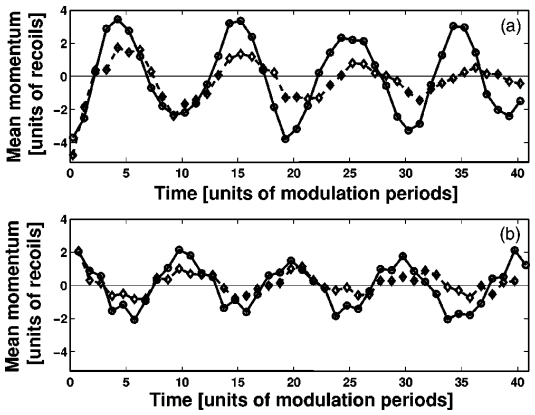

FIG. 2. Stroboscopic mean momentum as a function of the interaction time with the modulated standing wave measured in modulation periods, n, for modulation parameter $\varepsilon=0.29$, scaled well depth $\kappa=1.66$, modulation frequency $\omega/2\pi=250$ kHz, and a phase shift $\varphi=0.21\times2\pi$. (a) and (b) correspond to the two different interaction times $n+0.25$ and $n+0.75$ modulation periods, respectively. Results from the dynamic evolution of the Gross-Pitaevskii equation are plotted as a solid line (circles) and the experimental data are plotted as a dashed line (diamonds).

In Sec. II we introduce the theoretical tools to analyze dynamical tunneling by discussing Gross-Pitaevskii simulations and the appropriate Floquet theory. We present a thorough analysis of the experiments from Ref. [1] in Sec. III. After showing some theoretical results for the experimental parameters we give a small overview of what to expect when some of the system parameters in the experiments are varied in Sec. IV and give some initial analysis. In Sec. V we point to pathways to analyze the quantum-classical transition for our experimental system and give conclusions in Sec. VI.

II. THEORETICAL ANALYSIS OF THE DYNAMIC EVOLUTION OF A BOSE-EINSTEIN CONDENSATE

A. Dynamics using the Gross-Pitaevskii equation

The dynamics of a Bose-Einstein condensate in a time-dependent potential in the mean-field limit are described by the Gross-Pitaevskii equation [8,9]

$$i\hbar\frac{\partial\Psi(\mathbf{r},t)}{\partial t} = \left[-\frac{\hbar}{2m}\nabla^2 + V_{\mathrm{trap}}(\mathbf{r},t) + V(\mathbf{r},t) + N\frac{4\pi\hbar^2 a}{m}|\Psi(\mathbf{r},t)|^2\right]\Psi(\mathbf{r},t), \tag{5}$$

where N is the mean number of atoms in the condensate, and a is the scattering length with $a=2.8$ nm for sodium. $V_{\mathrm{trap}}(\mathbf{r})$ is the trapping potential which is turned off during the interaction with the standing wave and $V(\mathbf{r},t)$ is the time-

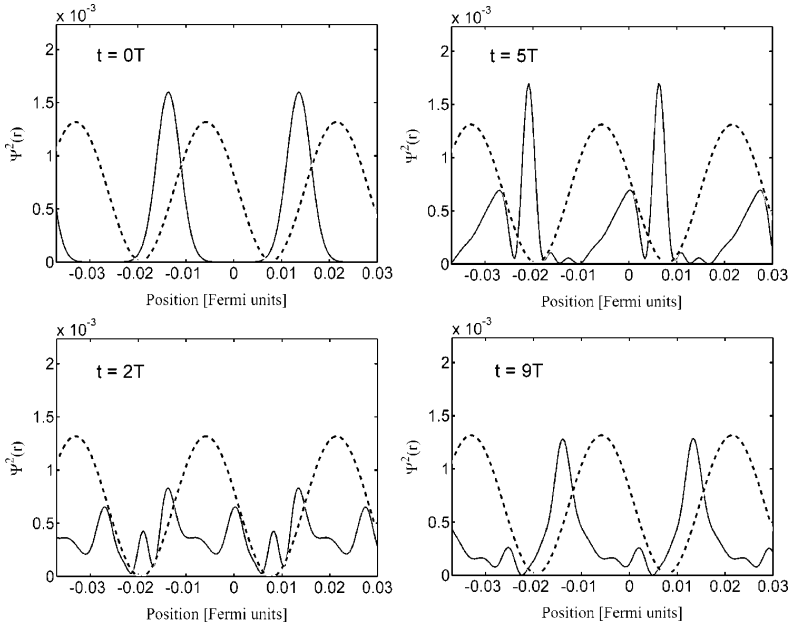

FIG. 3. Position representation of the atomic wave function as a function of the number of modulation periods calculated using the Gross-Pitaevskii equation. The wave packet is plotted stroboscopically at a phase so it is located classically approximately at its highest point in the potential well. The position of the standing wave wells is also shown (dotted line). Dynamical tunneling can be observed. At $t=5T$ most atoms have tunneled into the other period-1 region of regular motion. The position axis is given in Fermi units (scaled by the mean Thomas-Fermi diameter).

dependent optical potential induced by the optical standing wave. The Gross-Pitaevskii equation is propagated in time using a standard numerical split-operator, fast Fourier transform method. The size of the spatial grid of the numerical simulation is chosen to contain the full spatial extent of the initial condensate (therefore all the populated wells of the standing wave), and the grid has periodic boundary conditions at each side (a few unpopulated wells are also included on each side).

To obtain the initial wave function a Gaussian test function is evolved by imaginary time evolution to converge to the ground state of the stationary Gross-Pitaevskii equation. Then the standing wave is turned on adiabatically with $V(\mathbf{r},t)$ approximately having the form of a linear ramp. After the adiabatic turn-on, the condensate wave function is found to be localized at the bottom of each well of the standing wave. The standing wave is shifted and the time-dependent potential now has the form

$$V(\mathbf{r},t) = \frac{\hbar\Omega_{\text{eff}}}{4}[1 - 2\varepsilon\ \sin(\omega t + \phi)]\sin^2(kx + \varphi), \qquad (6)$$

where φ is the phase shift which is applied to selectively load one region of regular motion [1]. The position representation of the atomic wave function $|\Psi(\mathbf{r})|^2$ just before the modulation starts (and after the phase shift) is shown in Fig. 3 ($t=0T$).

The Gross-Pitaevskii equation is used to model the experimental details of a Bose-Einstein condensate in an optical one-dimensional lattice. The experiment effectively consists of many coherent single-atom experiments. The coherence is reflected in the occurrence of diffraction peaks in the atomic momentum distribution (see Fig. 4). Utilizing the Gross-Pitaevskii equation, the interaction between these single-atom experiments is modeled by a classical field. Although ignoring quantum phase fluctuations in the condensate, the wave nature of atoms is still contained in the Gross-Pitaevskii equation and dynamical tunneling is a quantum effect that results from the wave nature of the atoms. The assumption for a common phase for the whole condensate is well justified for the experimental conditions as the time scales of the experiment and the lattice well depth are sufficiently small. It will be shown in the following (see Fig. 8) that the kinetic energy is typically of the order of 10^5 Hz which is much larger than the nonlinear term in the Gross-Pitaevskii equation (5) which is on the order of 400 Hz. The experimental results, in particular dynamical tunneling, could therefore be modeled by a single particle Schrödinger equation in a one-dimensional single well with periodic boundary conditions. Nevertheless the Gross-Pitaevskii equation is used to model all the experimental details of a Bose-Einstein condensate in an optical lattice to guarantee maximum accuracy. We will discuss and compare the Gross-Pitaevskii and the Floquet approaches below (last paragraph of Sec. II).

Theoretical analysis of the dynamical tunneling experiments will be presented in this paper utilizing numerical solutions of the Gross-Pitaevskii equation. Furthermore we will analyze the system parameter space which is spanned by the scaled well depth κ, the modulation parameter ε, and the scaled Planck's constant $\bar{\hbar}$. In fact variation of the scaled Planck's constant in the simulations allows one to move the quantum system towards the classical limit.

B. Floquet analysis

The quantum dynamics of a periodically driven Hamiltonian system can be described in terms of the eigenstates of

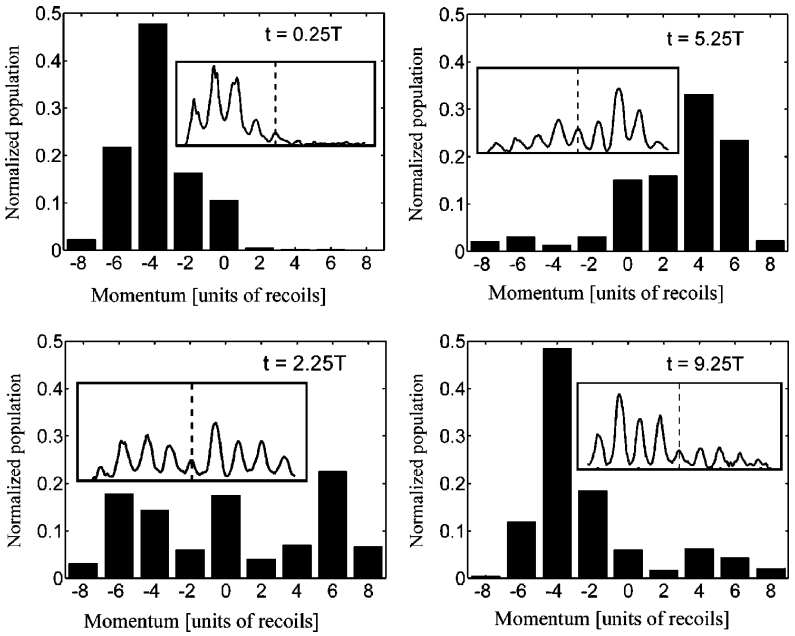

FIG. 4. Momentum distributions as a function of the interaction time with the modulated standing wave calculated using numerical solutions of the Gross-Pitaevskii equation for the same parameters as Fig. 3. Initially atoms have mostly negative momentum ($t=0.25T$). After approximately five modulation periods most atoms populate a state with positive momentum, therefore having undergone dynamical tunneling. Corresponding experimental data from Ref. [1] is also included as insets.

the Floquet operator F, which evolves the system in time by one modulation period. In the semiclassical regime, the Floquet eigenstates can be associated with regions of regular and irregular motion of the classical map. However, when $\hbar$ is not sufficiently small compared to a typical classical action the phase-space representation of the Floquet eigenstates do not necessarily match with some classical (regular or irregular) structures [10,11]. However, initial states localized at the stable region around a fixed point in the Poincaré section can be associated with superpositions of a small number of Floquet eigenstates. Using this state basis, one can reveal the analogy of the dynamical tunneling experiments and conventional tunneling in a double well system. Two states of opposite parity which can be responsible for the observed dynamical tunneling phenomenon are identified. Floquet states are stroboscopic eigenstates of the system. Their phase space representation therefore provides a quantum analog to the classical stroboscopic phase space representation, the Poincaré map.

Only very few states are needed to describe the evolution of a wave packet that is initially strongly localized on a region of regular motion. A strongly localized wave packet is used in the experiments (strongly localized in each well of the standing wave) making the Floquet basis very useful. In contrast, describing the dynamics in momentum or position representation requires a large number of states so that some of the intuitive understanding which one can obtain in the Floquet basis is impossible to gain. For example, the tunneling period can be derived from the quasi-eigenenergies of the relevant Floquet states, as will be shown below.

For an appropriate choice of parameters the phase space exhibits two period-1 fixed points, which for a suitable Poincaré section lie on the momentum axis at $\pm p_0$, as in Ref. [1]. For certain values of the scaled well depth κ and modulation parameter ε there are two dominant Floquet states $|\phi_\pm\rangle$ that are localized on both fixed points but are distinguished by being even or odd eigenstates of the parity operator that changes the sign of momentum. A state localized on just one fixed point is therefore likely to have dominant support on an even or odd superposition of these two Floquet states:

$$|\psi(\pm p_0)\rangle \approx (|\phi_+\rangle \pm |\phi_-\rangle)/\sqrt{2}. \tag{7}$$

The stroboscopic evolution is described by repeated application of the Floquet operator. As this is a unitary operator,

$$F|\phi_\pm\rangle = e^{(-i2\pi\phi_\pm/\bar{k})}|\phi_\pm\rangle. \tag{8}$$

$\phi_\pm$ are the Floquet quasienergies. Thus at a time which is n times the period of modulation, the state initially localized on $+p_0$ evolves to

$$|\psi(n)\rangle \approx (e^{(-i2\pi n\phi_+/\bar{k})}|\phi_+\rangle + e^{(-i2\pi n\phi_-/\bar{k})}|\phi_-\rangle)/\sqrt{2}. \tag{9}$$

Ignoring an overall phase and defining the separation between Floquet quasienergies as

$$\Delta\phi = \phi_- - \phi_+, \tag{10}$$

one obtains

$$|\psi(n)\rangle \approx (|\phi_+\rangle + e^{(-i2\pi n\Delta\phi/\bar{k})}|\phi_-\rangle)/\sqrt{2}. \tag{11}$$

At

$$n = \bar{k}/(2\Delta\phi) \tag{12}$$

periods, the state will form the antisymmetric superposition of Floquet states and thus is localized on the other fixed point

at $-p_0$. In other words the atoms have tunneled from one of the fixed points to the other. This is reminiscent of barrier tunneling between two wells, where a particle in one well, in a superposition of symmetric and antisymmetric energy eigenstates, oscillates between wells with a frequency given by the energy difference between the eigenstates.

Tunneling can also occur when the initial state has significant overlap with two nonsymmetric states. For example, if the initial state is localized on two Floquet states, one localized inside the classical chaotic region and one inside the region of regular motion, a distinct oscillation in the stroboscopic evolution of the mean momentum may be visible. The frequency of this tunneling oscillation depends on the spacing of the corresponding quasi-eigenenergies in the Floquet spectrum. In many cases multiple tunneling frequencies occur in the stroboscopic evolution of the mean momentum some of which are due to tunneling between nonsymmetric states.

Quantum dynamical tunneling may be defined in that a particle can access a region of phase space in a way that is forbidden by the classical dynamics. This implies that it crosses a Kolmogorov-Arnold-Moser (KAM) surface [12,13]. The clearest evidence of dynamical tunneling can be obtained by choosing the scaled Planck's constant $\bar{\kappa}$ sufficiently small so that the atomic wave function is much smaller than the region of regular motion (the size of the wave function is given by $\bar{\kappa}$). Furthermore, it should be centered inside the region of regular motion. However, even if the wave packet is larger than the region of regular motion and also populates the classical chaotic region of phase space one can still analyze quantum-classical correspondence and tunneling. One assumes a classical probability distribution of point particles with the same size as the quantum wave function and compares the classical evolution of this point particle probability distribution with the quantum evolution of the wave packet. A distinct difference between the two evolutions results from the occurrence of tunneling assuming that the quantum evolution penetrates a KAM surface visibly.

C. Comparison

Using the Gross-Pitaevskii equation one can exactly simulate the experiment because the momentum or position representation is used. Therefore the theoretical simulation can be directly compared with the experimental result. In contrast Floquet states do not have a straightforward experimental intuitive analog. In the Floquet states analysis one can compare the quasienergy splitting between the tunneling Floquet state with the experimentally measured tunneling period. The occurrence of multiple frequencies in the experimentally observed tunneling oscillations might also be explained with the presence of more than two dominant Floquet states, the tunneling frequencies being the energy splitting between different participating Floquet states. Using the Gross-Pitaevskii approach one can simulate the experiment with high precision. The same number of populated wells as in the experiment can be used and the turn-on of the standing wave can be simulated using an appropriate turn-on Hamiltonian. Therefore one can obtain the correct initial state with high precision. Furthermore, the mean-field interaction is simulated which is not contained in the Floquet approach.

III. NUMERICAL SIMULATIONS OF THE EXPERIMENTS

A. Gross-Pitaevskii simulations

In this section experimental results that were discussed in a previous paper [1] are compared with numerical simulations of the Gross-Pitaevskii (GP) equation.

In the experiment [1] the atomic wave function was prepared initially to be localized around a period-1 region of regular motion. Figure 2 shows the stroboscopically measured mean momentum as a function of the interaction time with the standing wave for modulation parameter $\varepsilon=0.29$, scaled well depth $\kappa=1.66$, modulation frequency $\omega/2\pi=250$ kHz, and a phase shift of $\varphi=0.21\times 2\pi$. (a) and (b) correspond to the two different interaction times $n+0.25$ (standing wave modulation ends at a maximum of the amplitude modulation) and $n+0.75$ modulation periods (standing wave modulation ends at a minimum of the amplitude modulation), respectively. Results from the simulations (solid line, circles) are compared with the experimental data (dashed line, diamonds). Dynamical tunneling manifests itself as a coherent oscillation of the stroboscopically observed mean momentum. This occurs in contrast to the classical prediction in which atoms should retain their momentum state when observed stroboscopically (time step is one modulation period). There is good agreement between experiment and theory as far as the tunneling period is concerned. However, the experimentally measured tunneling amplitude is smaller than the theoretical prediction.

It should be noted that the theoretical simulations do not take account of any possible spatial and temporal variations of the scaled well depth (e.g., light intensity), which could possibly lead to the observed discrepancy. It was decided to produce simulations without using any free parameters. However, the uncertainty associated with the experiment would allow small variations of the modulation parameter ε and the scaled well depth κ. There was a 10% uncertainty in the value of the scaled well depth κ and a 5% uncertainty in the modulation parameter ε (all reported uncertainties are 1 standard deviation combined systematic and statistical uncertainties). Both temporal and spatial uncertainty during one run of the experiment are contained in these values as well as the systematic total measurement uncertainty. It was verified that there are no important qualitative changes when varying the parameters in the uncertainty regime for the simulations presented here. However, the agreement between experiment and theory often can be optimized (not always nonambiguously, meaning that it is sometimes hard to decide which set of parameters produces the best fit). Although the theoretical simulation presented does not show any decay in the mean momentum curve, a slight change of parameters inside the experimental uncertainty can lead to decay which is most likely caused by another dominant Floquet state whose presence leads to the occurrence of a beating of the tunneling oscillations which appears as decay (and revival on

longer time scales). A detailed analysis of the corresponding Floquet states and their meaning will be presented in Sec. III C. [An example of how a change of parameters inside the experimental uncertainty in the simulations can optimize the agreement between theory and experiment is shown in Figs. 6 and 7. Both figures are described in more detail later in this section.] Another reason for the observed discrepancy could be the evolution of noncondensed atoms that is not contained in the GP approach and the interaction of noncondensed atoms with the condensate. With a sufficiently long adiabatic turn-on time of the far detuned standing wave the production of noncondensed atoms should be negligible. The interaction of the condensate with noncondensed atoms should also be negligible due to the low atomic density (note that in the experiments the condensate is expanded before the standing wave is turned on). However, further studies are needed to give an exact estimate of these effects.

The position representation of the atomic wave function $|\Psi(x)|^2$ is plotted stroboscopically after multiples of one modulation period in Fig. 3 for the same parameters as Fig. 2. The position of the standing wave wells is also shown (dotted line), their amplitude is given in arbitrary units. The position axis is scaled with the mean Thomas-Fermi diameter. The initial modulation phase is chosen so that the wave packet should be located classically approximately at its highest point of the potential well [2]. Choosing this stroboscopic phase the two regions of regular motion are always maximally separated in position space. Using this phase for the stroboscopic plots enables the observation of dynamical tunneling in position space as the two regions of regular motion are located to the left and to the right of the minimum of the potential well, being maximally spatially separated. In contrast, in the experiments, tunneling is always observed in momentum space (the standing wave is turned off when the regions of regular motion are at the bottom of the well, overlapping spatially but having oppositely directed momenta) as it is difficult to optically resolve individual wells of the standing wave. The first picture in Fig. 3 ($t=0T$) shows the initial wave packet before the modulation is turned on. Subsequent pictures exemplify the dynamical tunneling process. At $t=2T$, half the atoms have tunneled; most of the atoms are in the other region of regular motion at $t=5T$. The atoms have returned to their initial position at about $t=9T$. The double peak structure at $t=5T$ and the small central peak at $t=2T$ could indicate that Floquet states other than the two dominant ones are also loaded which is likely as a relatively large Planck's constant was used enabling the initial wave packet to cover a substantial phase space area.

Figure 4 shows simulations of the stroboscopically measured momentum distributions $|\Psi(p)|^2$ as bar graphs for the same parameters as Fig. 3. Corresponding experimental data from Ref. [1] are also included as insets. The momentum distributions are plotted at $n+0.25$ modulation periods, where n is an integer. At this modulation phase the amplitude modulation is at its maximum and atoms in a period-1 region of regular motion are classically at the bottom of the well having maximum momentum. The two period-1 regions of regular motion can be distinguished in their momentum representation at this phase as they have opposite momenta. At $t=0.25T$ the atoms which were located initially halfway up the potential well as shown in Fig. 3 at $t=0T$ have "rolled" down the well having acquired negative momentum. Momentum distributions for subsequent times illustrate the dynamical tunneling process. At $t=5.25$ modulation periods most atoms have reversed their momentum and they return to their initial momentum state at approximately $t=9.25T$. The simulations are in reasonable agreement with the experimentally measured data.

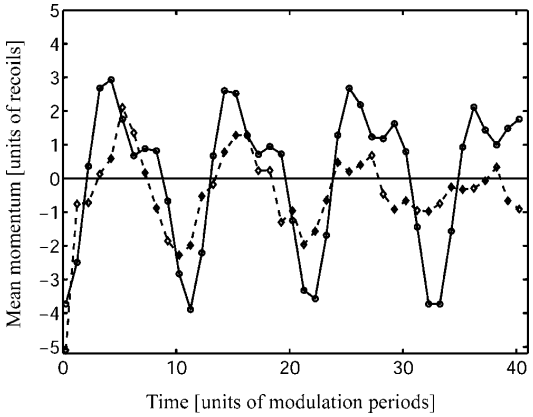

FIG. 5. Mean momentum as a function of the interaction time with the modulated standing wave measured in modulation periods, n, for $\varepsilon=0.28$, $\kappa=1.49$, $\omega/2\pi=250$ kHz, and $\varphi=0.22\times2\pi$. The points are plotted stroboscopically with an interaction time of $n+0.25$ modulation periods which corresponds to turning off the standing wave at maximum. Results from the dynamic evolution of the Gross-Pitaevskii equation are plotted as a solid line (circles) and the experimental data is plotted as a dashed line (diamonds).

Dynamical tunneling is sensitive to the modulation parameter, the scaled well depth, and the scaled Planck's constant. To illustrate this, tunneling data along with the appropriate evolution of the Gross-Pitaevskii equation will be shown for another two parameter sets. Even though this represents only a small overview of the parameter dependency of the tunneling oscillations it may help to appreciate the variety of features in the atomic dynamics. Figure 5 shows the theoretical simulation and the experimental data for $\varepsilon=0.28$, $\kappa=1.49$, $\omega/2\pi=250$ kHz, and $\varphi=0.22\times2\pi$. The mean momentum is plotted stroboscopically with the intensity modulation at maximum ($n+0.25$ modulation periods, n being an integer). The solid line (circles) is produced by a Gross-Pitaevskii simulation and the dashed line (diamonds) consists of experimental data. There are approximately 3.5 tunneling periods in 40 modulation periods in the theoretical curve. Figure 6 shows the mean momentum as a function of the interaction time with the standing wave for modulation parameter $\varepsilon=0.30$, scaled well depth $\kappa=1.82$, modulation frequency $\omega/2\pi=222$ kHz, and phase shift $\varphi=0.21\times2\pi$. For these parameters the tunneling frequency is larger than for the parameters shown in Fig. 5.

The simulation shows good agreement with the experiment. However, the theoretical mean momentum tunneling amplitude is larger than the one measured in the experiment and the theoretical tunneling frequency for this set of param-

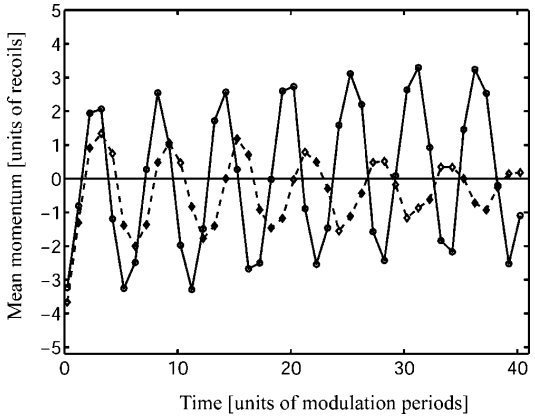

FIG. 6. Mean momentum as a function of the interaction time with the modulated standing wave measured in modulation periods, n, for modulation parameter $\varepsilon=0.30$, scaled well depth $\kappa=1.82$, modulation frequency $\omega/2\pi=222$ kHz, and phase shift $\varphi=0.21\times2\pi$. The points are plotted stroboscopically with an interaction time of $n+0.25$ modulation periods which corresponds to turning off the standing wave at maximum. Results from the dynamic evolution of the Gross-Pitaevskii equation are plotted as a solid line (circles) and the experimental data is plotted as a dashed line (diamonds).

eters is slightly larger than the experimentally measured one. Figure 7 illustrates that one can achieve much better agreement between experiment and simulation if one of the parameters is varied inside the experimental regime of uncertainty. The theoretical curve in this figure is obtained using the same parameters as in Fig. 6, but the modulation parameter ε is reduced from 0.30 to 0.28. The tunneling amplitude and frequency is now very similar to the experimental re-

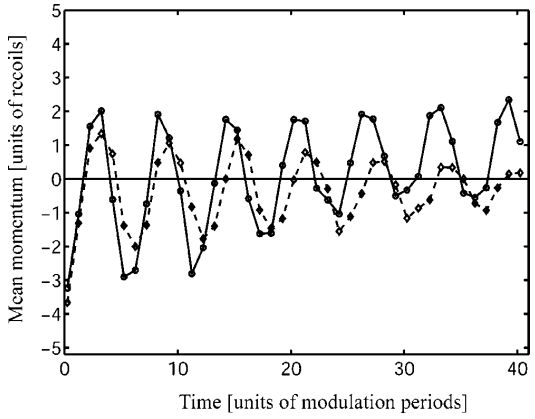

FIG. 7. Mean momentum as a function of the interaction time with the modulated standing wave measured in modulation periods, n, using the same parameters as Fig. 6 but the modulation parameter ε is reduced from 0.30 to 0.28 for the theoretical simulation. A much better fit is obtained.

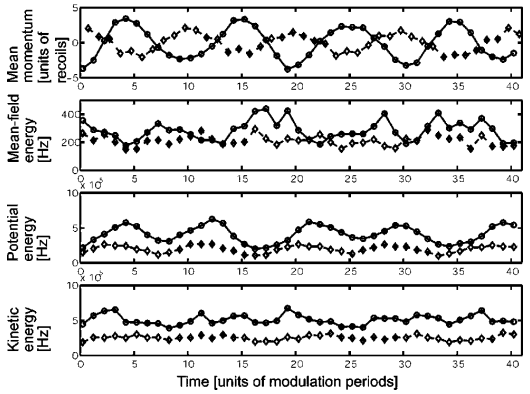

FIG. 8. Stroboscopic evolution of mean-field energy, the kinetic energy, and the potential energy. The energies are given in Hz (energy is scaled with Planck's constant). For comparison the mean momentum is also shown as a function of the interaction time with the standing wave (in units of modulation periods). The solid (circles) and dashed (diamonds) curves correspond to the two different interaction times $n+0.25$ and $n+0.75$ modulation periods, respectively. The evolution is plotted for modulation parameter $\varepsilon=0.29$, scaled well depth $\kappa=1.66$, modulation frequency $\omega/2\pi=250$ kHz, and a phase shift $\varphi=0.21\times2\pi$.

sults. Note that the experimental data is not centered at zero momentum. This is also the case in the theoretical simulations for both $\varepsilon=0.28$ and $\varepsilon=0.30$. The mean momentum curve appears much more sinusoidal than the one for $\varepsilon=0.29$, $\kappa=1.66$, $\omega/2\pi=250$ kHz and $\varphi=0.21\times2\pi$ (Fig. 2). This could imply that the initial wave function has support on fewer Floquet states.

B. Stroboscopic evolution of the system energies

Calculating the expectation values of the relevant system energies can give important information about the relevant energy scales and it might also help to obtain a deeper insight into the stroboscopic evolution of a Bose-Einstein condensate in a periodically modulated potential. Figure 8 shows the energy, expectation values for the mean-field energy, the potential energy, and the kinetic energy given in Hz (scaled by Planck's constant). For comparison the stroboscopic mean momentum expectation values are also shown. The energy and momentum expectation values are plotted stroboscopically and the solid (circles) and dashed (diamonds) curves correspond to the two different interaction times $n+0.25$ and $n+0.75$ modulation periods, respectively. Figure 8 is plotted for modulation parameter $\varepsilon=0.29$, scaled well depth $\kappa=1.66$, modulation frequency $\omega/2\pi=250$ kHz, and a phase shift of $\varphi=0.21\times2\pi$ which corresponds to Fig. 2. The mean-field energy is three orders of magnitude smaller than the potential or the kinetic energy. While the kinetic energy does not show a distinct oscillation, an oscillation is clearly visible in the stroboscopic potential energy evolution. This oscillation frequency is not equal to the tunneling frequency but it is smaller as can be seen in Fig. 8. One obtains a period

of approximately 8.9 modulation periods compared to a tunneling period of approximately 10.0 modulation periods. Considering the energy scales one should note that this oscillation is also clearly visible in the stroboscopic evolution of the total energy of the atoms. The origin of this oscillation is not known yet and will be the subject of future investigation.

C. Floquet analysis for some experimental parameters

Time and spatial periodicity of the Hamiltonian allow utilization of the Bloch and Floquet theorems [11,14]. Because of the time periodicity, there still exist eigenstates of the evolution operator over one period (Floquet theorem). Its eigenvalues can be written in the form $e^{-i2\pi\phi_n\tau/\bar{k}}$ where ϕ_n is called the quasienergy of the states. n is a discrete quantum number. Due to the spatial $\lambda/2$-periodicity, in addition to n, these states are labeled by a continuous quantum number, the so-called quasi-momentum $\vartheta \in [-2\pi/\lambda, 2\pi/\lambda]$ (Bloch theorem). The quasienergy spectrum $\phi_n(\vartheta)$ is therefore made of bands labeled by n (see for instance Fig. 10). More precisely, the states can be written as

$$|\phi_{n,\vartheta}(\tau)\rangle = e^{[-i2\pi\phi_n(\vartheta)\tau/\bar{k}]}e^{(-i\vartheta q)}|\psi_{n,\vartheta}(\tau)\rangle \qquad (13)$$

where $\{|\psi_{n,\vartheta}(\tau)\rangle\}$ is now strictly periodic in space and time (i.e., not up to a phase).

The evolution of the initial atomic wave function can be easily computed from its expansion on the $|\phi_{n,\vartheta}(0)\rangle$ once the Floquet operator has been diagonalized. The $|\psi_{n,\vartheta}(\tau)\rangle$, are the eigenstates of the modified Floquet-Bloch Hamiltonian

$$\mathcal{H} = (p + \bar{k}\vartheta)^2/2 + 2\kappa(1 - 2\varepsilon \sin \tau)\sin^2(q/2) \qquad (14)$$

subjected to strictly periodic space-time boundary conditions.

Dominant Floquet states may be determined by calculating the inner product of the Floquet states with the initial atomic wave function. To obtain a phase space representation of Floquet states in momentum and position space one can calculate the Husimi or Q-function. It is defined as

$$Q(q,p,\tau) = \frac{1}{2\pi\bar{k}}|\langle q + ip|\phi\rangle|^2, \qquad (15)$$

where $|q+ip\rangle$ is the coherent state of a simple harmonic oscillator with frequency ω_0 chosen as $\sqrt{\kappa}$ in scaled units. The position representation $\langle q'|q+ip\rangle$ of the coherent state [15,16] is given by

$$\langle q'|q + ip\rangle = \left(\frac{\omega_0}{\pi\bar{k}}\right)^{1/4} \exp\left\{-\left[\frac{q' - q}{2\Delta}\right]^2 + ip\frac{q}{\bar{k}}\right\} \qquad (16)$$

up to an overall phase factor and where $\Delta = \sqrt{\bar{k}/2\omega_0}$. Floquet analysis will be shown for some of the experimental parameters which were presented in the previous section. Figure 9 shows contour plots of the Husimi functions of two Floquet states with opposite parity [(a) and (b)] for these parameters whose presence allows dynamical tunneling to occur. Both of them are approximately localized on the classical period-1

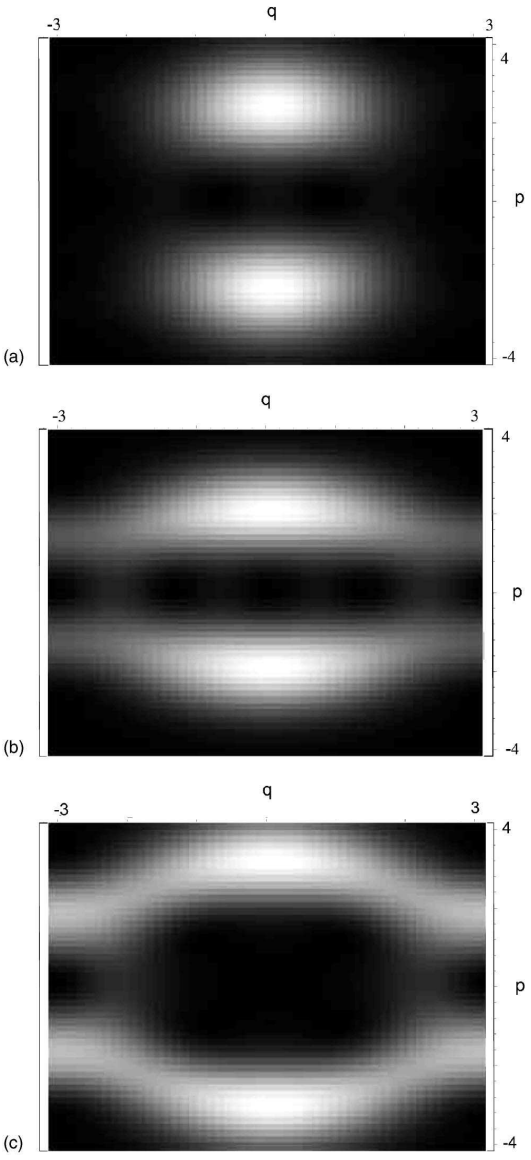

FIG. 9. Phase space representations of two Floquet states for $\vartheta = 0$ that are involved in the dynamical tunneling are shown in (a) and (b). The Floquet states correspond to the experimental parameters: modulation parameter $\varepsilon = 0.29$, scaled well depth $\kappa = 1.66$, and modulation frequency $\omega/2\pi = 250$ kHz, which were utilized to obtain the experimental results shown in Fig. 2. A third state, shown in (c) also has significant overlap with the initial experimental state.

regions of regular motion and they were selected so that the initial atomic wave function has significant overlap with them (26% and 44%, respectively). The initial experimental state has also significant overlap (22%) with a third state that is shown in Fig. 9(c). The overlap is calculated using a

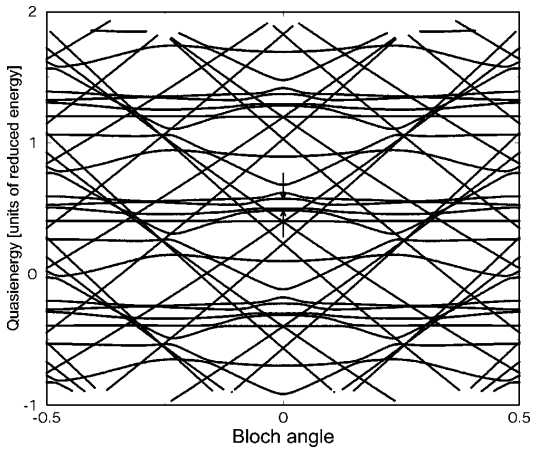

FIG. 10. Quasi-eigenenergy spectrum for parameters: modulation parameter $\varepsilon=0.29$, scaled well depth $\kappa=1.66$, and modulation frequency $\omega/2\pi=250$ kHz. The quasi-eigenenergy is measured in reduced energy units and it is a function of the Bloch angle. The Bloch angle is equal to the quasi-momentum multiplied with the spatial period $\lambda/2$ of the lattice. Each line corresponds to one Floquet state labeled by n [see Eq. (13)]. The quasi-eigenenergy of most Floquet states is strongly dependent on the quasi-momentum but it is not the case for the states of the tunneling doublet. Recall that the quasi-momentum ϑ is proportional to the phase taken by a state when spatially translated by $\lambda/2$. In other words, fixing ϑ imposes on the states some conditions on the boundary of one elementary cell $[q,q+\lambda/2]$. If a state is localized deep inside a cell, changing the boundary conditions (i.e., ϑ) will not affect the state so much and the corresponding quasienergies appear as curves that are approximately parallel to the ϑ axis. However, one should expect a strong ϑ-dependence for a state that spreads over at least $\Delta q\sim\lambda/2$.

coherent state that is centered on the periodic region of regular motion, which is a good approximation of the initial experimental state. The quasi-eigenenergy spectrum for this set of parameters is shown in Fig. 10. The quasi-eigenenergies are plotted as a function of the quasi-momentum (Bloch angle). Each line corresponds to one Floquet state labeled by n [see Eq. (13)]. The arrows point to the two Floquet states shown in Figs. 9(a) and 9(b) that correspond to the tunneling splitting in Eq. (10). Most of the other lines correspond to Floquet states which lie in the classical chaotic phase space region. Examples of phase space representations of such Floquet states can be found in Ref. [11]. Note that the spectrum is $\bar{\kappa}$ periodic in quasienergies. For quasi-momentum $\vartheta=0$ the splitting between the two states that are shown in Fig. 9 is approximately 0.08 in reduced units (energy in frequency units, $[\text{energy}/(2\pi\hbar)]$). With a modulation frequency $\omega/2\pi=250$ kHz one obtains a scaled Planck's constant $\bar{\kappa}$, therefore the tunneling period T_{tun} which follows from Eq. (12) is 10 which is in good agreement with the experiment.

The quasi-momentum plays a significant role in the experiments. The quasi-momentum ϑ is approximately equal to the relative velocity v between the wave packet (before the lattice is turned on) and the lattice, $v=\vartheta/m$ [17] if the standing wave is adiabatically turned on. It was found in [11] that it is of importance to populate a state whose quasi-momentum average is equal to zero. Moreover, quasi-momentum spread is also of importance. It has been shown in [18] that if the thermal velocity distribution is too broad, then the tunneling oscillation disappears. As can be seen in Fig. 10 the quasi-eigenenergies of the two contributing Floquet states depend on the quasi-momentum (or Bloch angle). The tunneling period (which is inversely proportional to the separation between these two quasi-eigenenergies) depends on the quasi-momentum. Using a thermal atomic cloud one obtains a statistical ensemble of many quasi-momenta as they initially move in random directions with respect to the optical lattice. Atoms localized in individual wells can be described by a wave packet in the plane wave basis and therefore they are characterized by a superposition of many quasi-momenta. The resulting quasi-momentum width washes out the tunneling oscillations (see [18], Fig. 3). In fact in another experiment Steck *et al.* [3] found that the amplitude of the mean momentum oscillations resulting from a tunneling process between two librational islands of stability decreased when the initial momentum width of the atomic cloud was increased.

Figure 11 shows contour plots of Husimi functions for the two dominant Floquet states for the modulation parameter $\varepsilon=0.30$, scaled well depth $\kappa=1.82$, and modulation frequency $\omega/2\pi=222$ kHz, which corresponds to experimental results shown in Fig. 6. The states are selected to have maximum overlap with the initial wave packet (38% and 44%). In contrast to the experimental results shown in Fig. 2 there are only two dominant Floquet states. The quasi-eigenenergy spectrum for this set of parameters (not shown) reveals a level splitting of approximately 0.15 in reduced units, the calculated tunneling period is 6 modulation periods which is in good agreement with the experiment.

When comparing the stroboscopic evolution of the mean momentum shown in Fig. 2 (modulation parameter $\varepsilon=0.29$, scaled well depth $\kappa=1.66$, and modulation frequency $\omega/2\pi=250$ kHz) with the one shown in Fig. 6 (modulation parameter $\varepsilon=0.30$, scaled well depth $\kappa=1.82$, and modulation frequency $\omega/2\pi=222$ kHz), one finds that it is less sinusoidal. This can be explained in the Floquet picture. While there are three dominant Floquet states for the first case (Figs. 2 and 9) (three Floquet states with significant overlap with the initial experimental state), there are only two dominant Floquet states for the second case (Figs. 6 and 11) resulting in a more sinusoidal tunneling oscillation.

D. Loading analysis of the Floquet superposition state

The initial atomic wave packet is localized around the classical period-1 region of regular motion by inducing a sudden phase shift to the standing wave. This enables the observation of dynamical tunneling. In the Floquet picture the observation of dynamical tunneling requires that the initial state has support on only a few dominant Floquet states, preferably populating only two with a phase space structure as shown in Fig. 9. Optimizing the overlap of the initial state

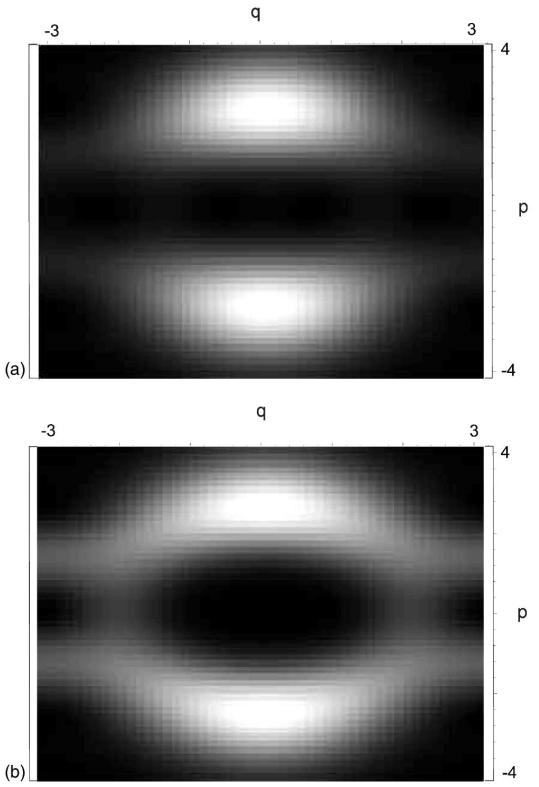

FIG. 11. Phase space representations of two Floquet states whose presence can lead to the occurrence of dynamical tunneling. The Floquet states correspond to the experimental parameters: modulation parameter $\varepsilon=0.30$, scaled well depth $\kappa=1.82$, and modulation frequency $\omega/2\pi=222$ kHz, which were utilized to obtain the experimental results shown in Fig. 6.

with these Floquet "tunneling" states should maximize the observed tunneling amplitude. Here we carry out analysis confirming this prediction. This corresponds to optimizing the overlap of the initial experimental state with the period-1 regions of regular motion. Figure 12 shows the mean atomic momentum as a function of the interaction time with the standing wave which is plotted for a range of the initial phase shift φ of the standing wave. The solid line (circles) corresponds to an interaction time with the standing wave of $n+0.25$ modulation periods and the dashed line (diamonds) corresponds to an interaction time of $n+0.75$ modulation periods. The simulations are made using the Gross-Pitaevskii equation for modulation parameter $\varepsilon=0.29$, scaled well depth $\kappa=1.66$, and modulation frequency $\omega/2\pi=250$ kHz which corresponds to Fig. 2. A phase shift $\varphi=0$ corresponds to localizing the wave packet exactly at the bottom of the well and $\varphi=\pi$ corresponds to localizing it exactly at the maximum of the standing wave well. Symmetry dictates that no tunneling oscillation can occur for these two loading phases. This is also shown in Fig. 12 (the mean momentum curve for $\varphi=\pi$ is not shown but it is the same as for $\varphi=0$). The amplitude of the tunneling oscillations changes strongly when the initial phase shift φ of the standing wave is changed. The best overlap with the tunneling Floquet states is obtained for the phase shift φ somewhere in between $0.25\times2\pi$ and $0.30\times2\pi$ which corresponds to placing the wave packet halfway up the standing wave well. This result is in good agreement with the structure of the tunneling Floquet states as shown in Fig. 9. When changing φ there is no change in the observed tunneling period. This is to be expected as mainly the loading efficiency for the "tunneling" Floquet states varies when φ is varied. It should be noted that the simulations are carried out for a relatively large scaled Planck's constant $\bar{\kappa}$ which means that the wave packet size is rather large compared to characteristic classical phase space features like the period-1 regions of regular motion. This analysis shows that the tunneling amplitude sensitively depends on the loading efficiency of the tunneling Floquet states and that there is a smooth dependency of the tunneling amplitude on this loading parameter.

IV. PARAMETER DEPENDENCY OF THE TUNNELING OSCILLATIONS

The scaled parameter space for the dynamics of the system is given by the scaled well depth κ and the modulation parameter ε. Both parameters will significantly change the structure and number of the contributing Floquet states. It has been found that a strong sensitivity of the tunneling frequency on the system parameters is a signature of chaos-assisted tunneling [11,18] where a third state associated with the classical chaotic region interacts with the tunneling Floquet states. A Floquet state that is localized inside a region of regular motion that surrounds another resonance can also interact with the tunneling doublet (two tunneling Floquet states), this phenomenon is known as resonance-assisted tunneling [19].

Comprehensively exploring the parameter space and its associated phenomena is out of the scope of this paper. Instead an analysis associated with our experiments will be presented here showing one scan of the scaled well depth κ and another scan of the modulation parameter ε around the experimental parameter regime. The results are shown in the form of plots of the mean momentum as a function of the interaction time with the modulated standing wave. The solid line (circles) corresponds to an interaction time with the standing wave of $n+0.25$ modulation periods and the dashed line (diamonds) corresponds to an interaction time of $n+0.75$ modulation periods.

Figure 13 shows the scaled well depth κ being varied from 1.10 to 1.75. The other parameters are held constant (modulation parameter $\varepsilon=0.29$, modulation frequency $\omega/2\pi=250$ kHz, and phase shift $\varphi=0.21\times2\pi$). The momentum distribution evolution is shown to illustrate intricate changes in the tunneling dynamics when the parameters are varied. Both the tunneling frequency spectrum and the tunneling amplitude are strongly dependent on κ. Often one can see more than just one dominant tunneling frequency. For example, for $\kappa=1.35$ the two dominant tunneling frequencies

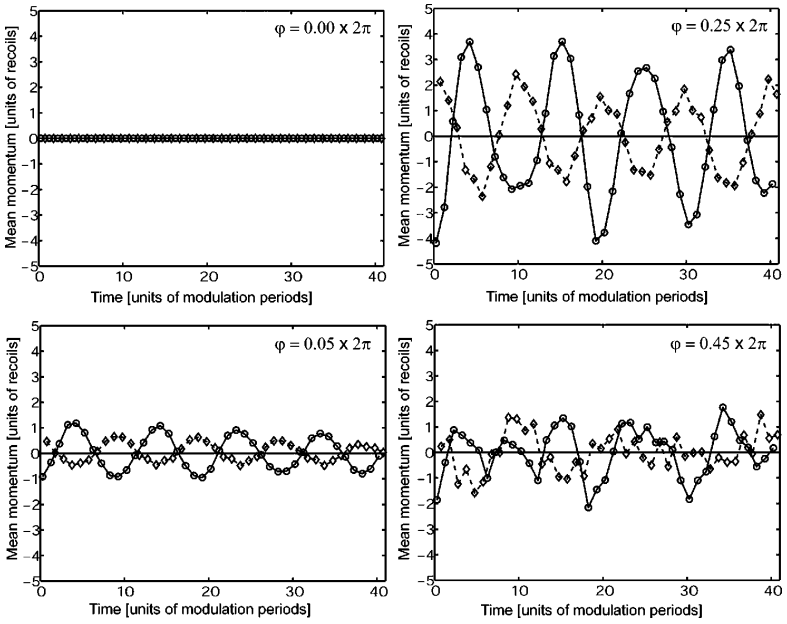

FIG. 12. Mean atomic momentum as a function of the interaction time with the standing wave plotted for a range of the initial phase shift φ of the standing wave. The solid line (circles) corresponds to an interaction time with the standing wave of $n+0.25$ modulation periods and the dashed line (diamonds) corresponds to an interaction time of $n+0.75$ modulation periods.

which contribute to the tunneling oscillation have a period of approximately 3.9 and 34 modulation periods. In the interval of approximately $\kappa=1.5$ and 1.8 the tunneling oscillations have a more sinusoidal shape indicating the presence of only approximately two dominant tunneling states. In this interval the tunneling frequency is peaked at $\kappa=1.55$ with a tunneling period of approximately 8.9 modulation periods. In order to analyze further the behavior of the tunneling frequency, we show the low frequency (diamonds) and the high frequency component (squares) of the tunneling frequency as a function of the scaled well depth κ in Fig. 14. The high frequency component is plotted only for values of κ where it is visible in the stroboscopic momentum evolution shown in Fig. 13. The occurrence of multiple tunneling frequencies results from the presence of more than two dominant Floquet states. The minimum of the low frequency component of the tunneling frequency is due to the level crossing of two contributing Floquet states (see squares and filled circles at $\kappa=1.25$ in Fig. 15). The error bars result from the readout uncertainty of the tunneling period from the simulations. This analysis reveals some of the intricate features of the tunneling dynamics. Instead of a smooth parameter dependency a distinct rise and fall (in the low frequency component) in the tunneling frequency versus scaled well depth appears. The tunneling frequency minimum is centered at $\kappa\approx 1.3$. Note that a rise and fall in the tunneling frequency is often understood as a signature of chaos-assisted tunneling. However, it is not a sufficient criterion for chaos-assisted tunneling. One needs to choose an approximately ten times smaller scaled Planck's constant to use the terminology of chaos-assisted tunneling [18]. The size of the Floquet states is given by the scaled Planck's constant. If the states are much larger than phase space features like regions of regular motion, then it is impossible to make a classification of Floquet states as chaotic or regular, which is needed for chaos-assisted tunneling.

Another interesting feature of dynamical tunneling can be derived from Fig. 14. It shows that for a certain parameter regime the tunneling frequency decreases with decreasing scaled well depth. This is the contrary of what one would expect for spatial energy barrier tunneling. This feature has been also observed in recent experiments [4]. Floquet spectra provide alternative means of analyzing the tunneling dynamics. The dependence of the tunneling frequency on the scaled well depth κ can be understood using the appropriate Floquet spectrum. Figure 15 shows the quasi-eigenenergies of different Floquet states as a function of the scaled well depth κ. The Floquet states with maximum overlap are marked with bullets. Figure 15 also shows phase space representations (Husimi functions) of some of these Floquet states for different values of κ. The shape and structure of these Floquet states depend on the value of the scaled well depth. In fact Floquet states can undergo bifurcations. This may be seen as the quantum analog of classical phase bifurcations. Classical phase space bifurcations have been reported in Ref. [20]. In this case the shapes of the Floquet states change in such a way that different Floquet states have non-negligible overlap with the initial experimental state as the scaled well depth κ is varied. The separation between the quasi-eigenenergies of the two states with maximum overlap will determine a dominant tunneling frequency. Note that often more than two states have relevant overlap with the initial experimental states which leads to the occurrence of multiple tunneling frequencies.

Figure 16 shows effects of a variation of the modulation parameter ε. To obtain these simulations all other parameters are held constant (scaled well depth $\kappa=1.66$, modulation frequency $\omega/2\pi=250$ kHz, and phase shift $\varphi=0.21\times 2\pi$). For

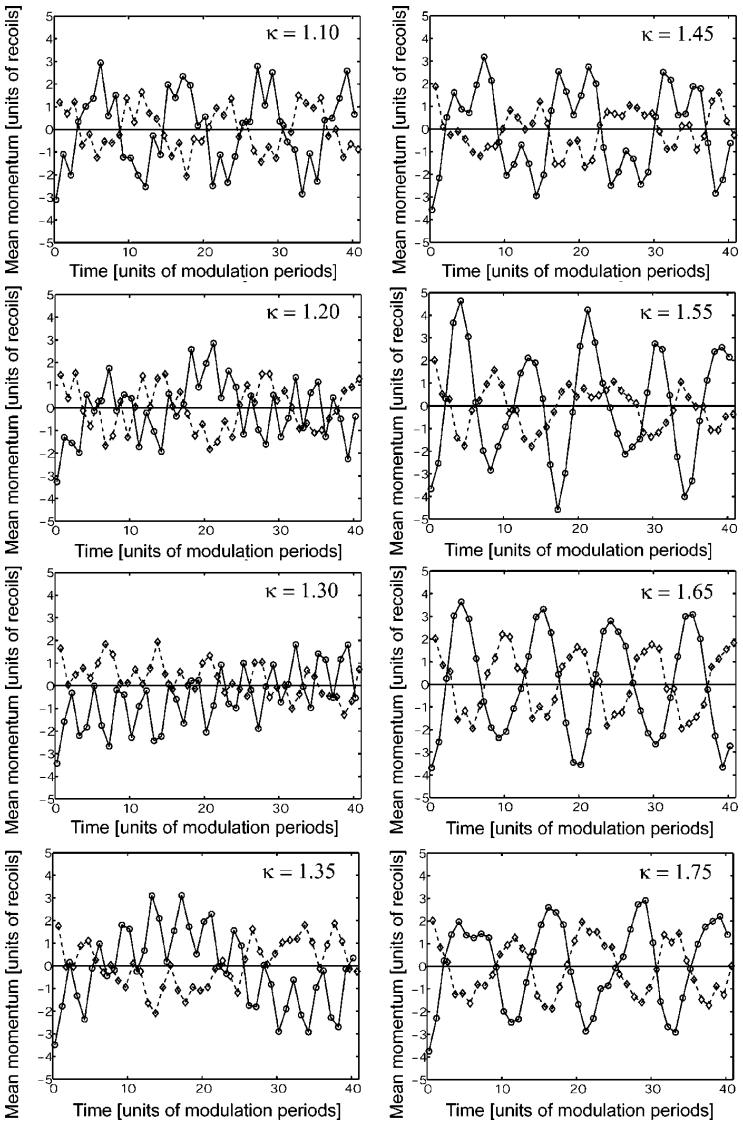

FIG. 13. Mean momentum as a function of the interaction time with the modulated standing wave for different values of the scaled well depth κ (modulation parameter $\varepsilon=0.29$, modulation frequency $\omega/2\pi=250$ kHz, and phase shift $\varphi=0.21\times 2\pi$). The solid line (circles) corresponds to an interaction time with the standing wave of $n+0.25$ modulation periods and the dashed line (diamonds) corresponds to an interaction time of $n+0.75$ modulation periods.

smaller values of ε the corresponding classical phase space is mainly regular. There is no distinct oscillation at $\varepsilon=0.10$ which is centered at zero momentum. Distinct tunneling oscillations start to occur at $\varepsilon=0.14$ with a gradually increasing tunneling frequency. While there is a tunneling period of approximately 67 modulation periods at $\varepsilon=0.14$, the tunneling period is only approximately 7.7 modulation periods at $\varepsilon=0.38$. For larger values of the modulation parameter ε the oscillations become less sinusoidal indicating the presence of an increasing number of dominant Floquet states. The error bars result from the readout uncertainty of the tunneling period from the simulations.

V. MOVING THE QUANTUM SYSTEM TOWARDS THE CLASSICAL LIMIT

A fundamental strength of the experiments which are discussed here is that they are capable of exploring the transition of the quantum system towards the classical limit by decreasing the scaled Planck's constant $\bar{\kappa}$.

Here a quantum system with mixed phase space exhibiting classically chaotic and regular regions of motion is moved towards the classical limit. By adjusting the scaled Planck's constant $\bar{\kappa}$ of the system, the wave and particle character of the atoms can be probed although some experi-

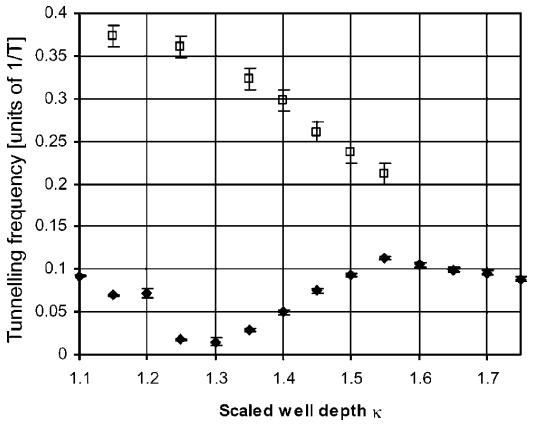

FIG. 14. Tunneling frequency as a function of the scaled well depth κ (modulation parameter $\varepsilon=0.29$, modulation frequency $\omega/2\pi=250$ kHz, and phase shift $\varphi=0.21\times 2\pi$) taken from Fig. 13. Diamonds and squares denote low and high frequency components, respectively.

mental and numerical restrictions limit the extent of this quantum-classical probe. This should enhance our understanding of nonlinear dynamical systems and provide insight into their quantum and classical origin. It is out of the scope of this paper to present anything more than a short analysis relevant to the experimental results. The quantum-classical borderland is analyzed by considering the mean momentum as a function of the interaction time with the modulated standing wave for different values of the scaled Planck's constant $\bar{\kappa}$. Figure 17 shows results for modulation parameter $\varepsilon=0.29$, scaled well depth $\kappa=1.66$, and phase shift $\varphi=0.21\times 2\pi$ which corresponds to experimental results shown in Fig. 2. The scaled Planck's constant $\bar{\kappa}$ is varied by adjusting the modulation frequency $\omega/2\pi$ and leaving the scaled well depth κ, the modulation parameter ε, and the initial phase shift φ constant. Results are shown for the scaled Planck's constant $\bar{\kappa}$ ranging from 0.40 ($\omega/2\pi=500$ kHz) to 1.33 ($\omega/2\pi=150$ kHz). The error bars result from the readout uncertainty of the tunneling period from the simulations. As shown in previous work [21], the momentum of the regions of regular motion is proportional to the modulation frequency. Note that this is a purely classical feature that would disappear if the scaled momentum would be plotted instead

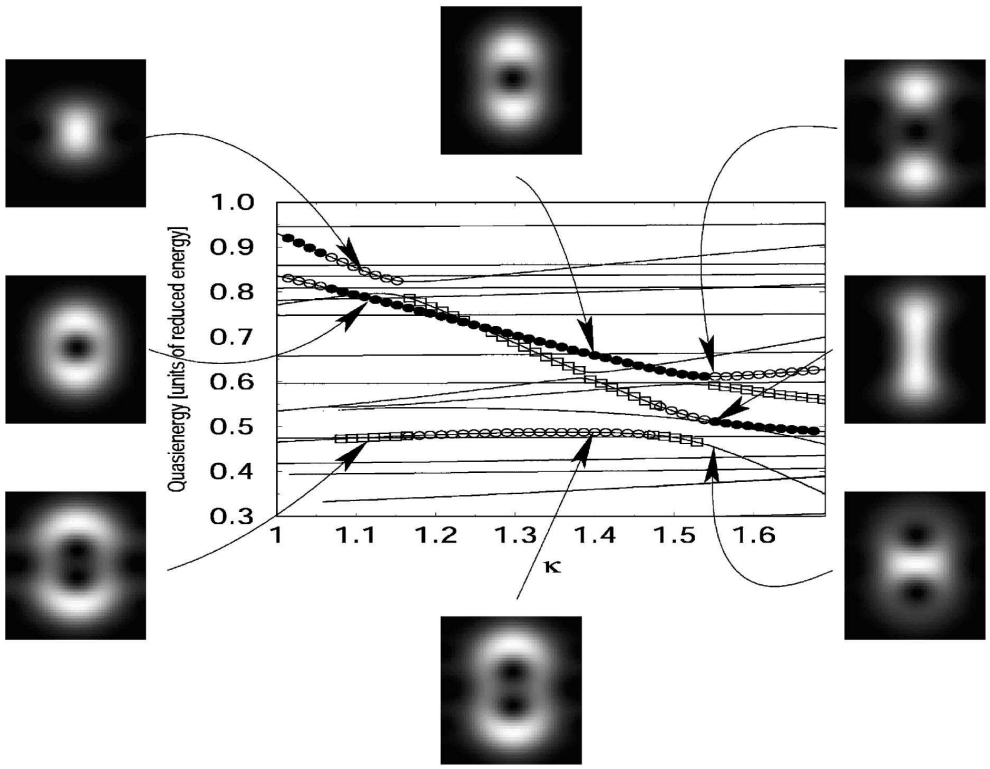

FIG. 15. Floquet spectrum as a function of the scaled well depth κ (modulation parameter $\varepsilon=0.29$, modulation frequency $\omega/2\pi=250$ kHz, and phase shift $\varphi=0.21\times 2\pi$. The Floquet states with maximum overlap are marked by black bullets, white bullets are used for second most overlap, and white squared bullets show third most overlap. Phase space representations (Husimi functions) of some of the Floquet states for different values of κ are also shown.

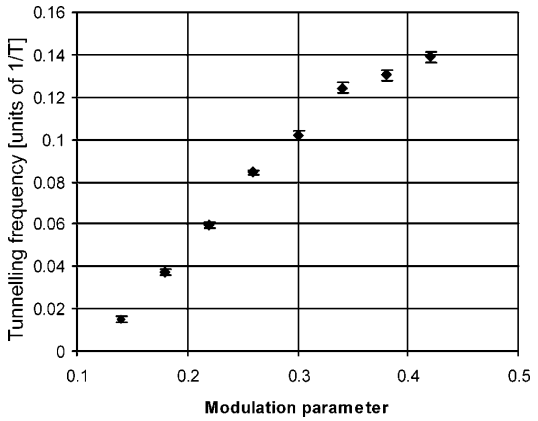

FIG. 16. Tunneling frequency as a function of the modulation parameter ε (scaled well depth $\kappa=1.66$, modulation frequency $\omega/2\pi=250$ kHz, and phase shift $\varphi=0.21\times 2\pi$). The error bars result from the readout uncertainty of the tunneling oscillations from the simulations. The high frequency component that is present in the data for $0.00<\varepsilon<0.18$ is not shown.

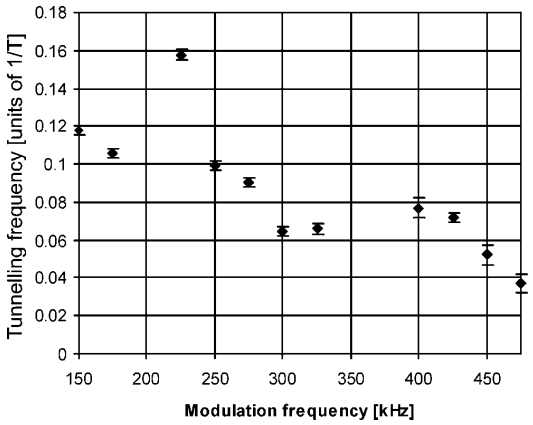

FIG. 17. Dominant tunneling frequency as a function of the modulation frequency $\omega/2\pi$ for modulation parameter $\varepsilon=0.29$, scaled well depth $\kappa=1.66$, and phase shift $\varphi=0.21\times 2\pi$ which corresponds to experimental results shown in Fig. 2. As expected, the overall tendency consists of a decreasing of the tunneling frequency as the modulation frequency increases and therefore as the scaled Planck's constant decreases, however, the transition is not as smooth as one might expect.

of the real momentum. Intuitively one would expect the tunneling frequency to decrease as the system becomes more classical. However, a different quite surprising phenomenon occurs. Considering the modulation frequency interval between 225 and 325 kHz the tunneling frequency gradually decreases as the system becomes more classical. The same applies for the interval between 150 and 175 kHz and the interval from 425 to 475 kHz. Qualitative changes occur at approximately 200, 350 (375), and 500 kHz where the tunneling oscillation shows multifrequency contributions and the tunneling frequency then significantly increases as the effective Planck's constant is further decreased. A more detailed analysis will be the subject of future study. The three intervals where the tunneling frequency decreases appear as three arms in the graph. At $\omega/2\pi=200$, 350, and 375 kHz the system cannot be well described using one dominant tunneling frequency, therefore no data is shown at these frequencies.

The results of this first analysis indicate that the transition from quantum to classical physics contains many fascinating details to be explored. The results for the driven pendulum in atom optics shows that the transition from quantum to classical dynamics is not smooth.

VI. CONCLUSION

Recent dynamical tunneling experiments [1] were analyzed using simulations of the Gross-Pitaevskii equation and the corresponding Floquet theory. The main features of the experiments can be explained by a two or three state framework that is provided by Floquet theory. We have identified the relevant Floquet states and shown their Husimi functions. Note that the mean-field interaction was negligible in the experiments. Tunnelling period and amplitude are in good agreement with GP simulation and Floquet theory.

An analysis of the parameter space has shown that tunneling frequency is strongly dependent on the system parameters scaled well depth κ, modulation parameter ε, and the scaled Planck's constant $\bar{k}$. While we find an approximately linear dependence of the tunneling frequency on the modulation parameter ε for the set of experimental parameters, there is a distinct spike in the tunneling frequency as a function of the scaled well depth κ.

However, this cannot be interpreted as a signature of chaos-assisted tunneling essentially because the states cannot be clearly identified with chaotic or regular regions of the classical phase space, therefore the notion of chaos-assisted tunneling is difficult to use in this context. We note that it is important to decrease the scaled Planck's constant by at least an order of magnitude [18] for an observation of chaos-assisted tunneling to be nonambiguous. We have simulated when the system is moved towards the classical limit. A bifurcationlike behavior results which can be understood in terms of quantum bifurcations of the contributing Floquet states.

ACKNOWLEDGMENTS

This work was supported by the Australian Research Council. The experimental results that are shown here were accomplished by W. K. Hensinger, H. Häffner, A. Browaeys, N. R. Heckenberg, K. Helmerson, C. McKenzie, G. J. Milburn, W. D. Phillips, S. L. Rolston, H. Rubinsztein-Dunlop, and B. Upcroft in the context of Ref. [1] and we would like to thank the authors. The corresponding author W. K. H. would like to acknowledge interesting discussions with William D. Phillips and Steven Rolston during the preparation of

theoretical results presented in this paper. W. K. H. would like to thank NIST and Laboratoire Kastler-Brossel for hospitality during part of the work for this paper. Laboratoire Kastler Brossel de l'Université Pierre et Marie Curie et de l'Ecole Normale Supérieure is Unité Mixte de Recherche 8552 du CNRS. Laboratoire de mathématiques et de physique théorique de l'Université François Rabelais is Unité Mixte de Recherche 6083 du CNRS.

[1] W. K. Hensinger *et al.*, Nature (London) **412**, 52 (2001).
[2] W. K. Hensinger, N. R. Heckenberg, G. J. Milburn, and H. Rubinsztein-Dunlop, J. Opt. B: Quantum Semiclassical Opt. **5**, R83 (2003).
[3] D. A. Steck, W. H. Oskay, and M. G. Raizen, Science **293**, 274 (2001).
[4] D. A. Steck, W. H. Oskay, and M. G. Raizen, Phys. Rev. Lett. **88**, 120406 (2002).
[5] R. Luter and L. E. Reichl, Phys. Rev. A **66**, 053615 (2002).
[6] V. Averbukh, S. Osovski, and N. Moiseyev, Phys. Rev. Lett. **89**, 253201 (2002).
[7] F. L. Moore, J. C. Robinson, C. F. Bharucha, B. Sundaram, and M. G. Raizen, Phys. Rev. Lett. **75**, 4598 (1995).
[8] F. Dalfovo, S. Giorgini, L. P. Pitaevskii, and S. Stringari, Rev. Mod. Phys. **71**, 463 (1999).
[9] A. S. Parkins and D. F. Walls, Phys. Rep. **303**, 1 (1997).
[10] S. Dyrting, G. J. Milburn, and C. A. Holmes Phys. Rev. E **48**, 969 (1993).
[11] A. Mouchet, C. Miniatura, R. Kaiser, B. Grémaud, and D. Delande, Phys. Rev. E **64**, 016221 (2001).
[12] M. V. Berry, in *Topics in Nonlinear Dynamics—A Tribute to Sir Edward Bullard*, edited by S. Jorna (AIP, New York, 1978), Vol. 46, pp. 16–120, reprinted in R. S. Mackay and J. D. Meiss, *Hamiltonian Dynamical Systems* (Adam Hilger, Bristol, 1987).
[13] V. I. Arnold, *Mathematical Methods of Classical Mechanics* (Springer-Verlag, New York, 1979).
[14] N. W. Ashcroft and N. D. Mermin, *Solid State Physics* (Saunders College, Philadelphia, 1976).
[15] J. R. Klauder and B.-S. Skagerstam, *Coherent States—Applications in Physics and Mathematical Physics* (World Scientific, Singapore, 1985).
[16] C. Cohen-Tannoudji, B. Diu, and F. Laloë, *Quantum Mechanics* (Wiley-Interscience, New York, 1977).
[17] J. H. Denschlag, J. E. Simsarian, H. Häffner, C. McKenzie, A. Browaeys, D. Cho, K. Helmerson, S. L. Rolston, and W. D. Phillips, J. Phys. B **35**, 3095 (2002).
[18] A. Mouchet and D. Delande Phys. Rev. E **67**, 046216 (2003).
[19] O. Brodier, P. Schlagheck, and D. Ullmo, Phys. Rev. Lett. **87**, 064101 (2001).
[20] W. K. Hensinger, B. Upcroft, C. A. Holmes, N. R. Heckenberg, G. J. Milburn, and H. Rubinsztein-Dunlop, Phys. Rev. A **64**, 063408 (2001).
[21] W. K. Hensinger, A. G. Truscott, B. Upcroft, M. Hug, H. M. Wiseman, N. R. Heckenberg, and H. Rubinsztein-Dunlop, Phys. Rev. A **64**, 033407 (2001).

I.7 Influence des résonances classiques sur l'effet tunnel chaotique

Dans ce dernier article sur l'effet tunnel, écrit en collaboration avec Peter SCHLAGHECK et Christopher ELTSCHKA (groupe *Complex Quantum Systems* de l'université de Regensburg (Allemagne) dirigé par Klaus RICHTER), nous nous éloignons des expériences physiques pour revenir à des concepts théoriques étayés par des expériences numériques. Nous confirmons le rôle central joué par les résonances dans l'effet tunnel chaotique et nous apportons un nouvel éclairage sur la correspondance entre ces résonances, les fonctions d'onde impliquées dans l'effet tunnel chaotique et leur représentation dans l'espace des phases. À noter aussi que nous réfutons quantitativement une proposition désinvolte[30] de PODOLSKIY & NARIMANOV (2003) pour estimer le doublet $\Delta\varepsilon$ exprimé en fonction de l'aire des îlots.

[30] Dans un *Phys. Rev. Lett.*, en escamotant sans le dire des facteurs multiplicatifs de plusieurs ordres de grandeurs et en renvoyant à un argument absent de la référence citée !

PHYSICAL REVIEW E **74**, 026211 (2006)

Influence of classical resonances on chaotic tunneling

Amaury Mouchet
Laboratoire de Mathématiques et de Physique Théorique, CNRS UMR 6083, Université François Rabelais Avenue Monge, Parc de Grandmont 37200 Tours, France

Christopher Eltschka and Peter Schlagheck
Institut für Theoretische Physik, Universität Regensburg, 93040 Regensburg, Germany
(Received 9 June 2006; published 22 August 2006)

Dynamical tunneling between symmetry-related stable modes is studied in the periodically driven pendulum. We present strong evidence that the tunneling process is governed by nonlinear resonances that manifest within the regular phase-space islands on which the stable modes are localized. By means of a quantitative numerical study of the corresponding Floquet problem, we identify the trace of such resonances not only in the level splittings between near-degenerate quantum states, where they lead to prominent plateau structures, but also in overlap matrix elements of the Floquet eigenstates, which reveal characteristic sequences of avoided crossings in the Floquet spectrum. The semiclassical theory of resonance-assisted tunneling yields good overall agreement with the quantum-tunneling rates, and indicates that partial barriers within the chaos might play a prominent role.

DOI: 10.1103/PhysRevE.74.026211 PACS number(s): 05.45.Mt, 05.60.Gg, 32.80.Qk, 05.45.Pq

I. INTRODUCTION

Since the very first quantitative studies of tunneling in a chaotic system [1,2], it has been clear that a minute scrutiny of the associated classical dynamics was required in order to understand even the most coarse features of the quantum behavior of such systems. In essence, tunneling is a semiclassical concept since it refers to a quantum process—typically a decay or the oscillation of an averaged observable—that is forbidden at a classical level. But, despite the numerous successes of semiclassical computations in quantum chaos, the questions of which and how classical objects can be used to understand tunneling and to compute, say, their characteristic time scales, have been remaining widely open for sixteen years. The stakes in the battle are important since nonintegrability is the generic rule of multidimensional systems and tunneling may play a crucial role in their transport properties. Moreover, it is one of its signatures that chaotic tunneling can be modified on several orders of magnitude by the slightest variation of any classical or quantum parameter; therefore a deep understanding of chaotic tunneling is required to control the process, what may be an advantage in delicate quantum experiments and, hopefully, give rise to an extremely sensitive quantum tool. Some promising clues have been provided in this direction by numerical studies and experiments with cold atoms [3–6], but also with microwave cavities [7,8] where tunneling signatures for processes that are forbidden by ray optics were observed.

Of course, in order to capture the typical exponentially small tunneling effects, it is expected that the classical dynamics should be complexified. It is well known [9,10] that the complex solutions of Hamilton's equations are actually involved in the interpretation of tunneling of autonomous systems with one degree of freedom. In the mid 1990's, the first observations [11–14] that complex periodic orbits allow one to reproduce quantitatively some feature of chaotic tunneling gave hope that a semiclassical strategy was indeed possible, even though the complexified classical tori are generically destroyed in chaotic systems [15]. But to deal with tractable semiclassical trace formulas à la Gutzwiller, a general criterion for selecting the complex periodic orbits was still lacking; this need became an emergency when it was unexpectedly discovered [16,17] that chaos reveals itself in the complex phase space through some fractal structures, the so-called Laputa islands, that look like agglomerates of complex trajectories. It is only recently that some encouraging significant steps were done for retaining the relevant semiclassical skeleton [18]. A lot of work remains to be done in that direction, especially if one wants to deal with continuous systems where time can (and must) be complexified as well, unlike what occurs in discrete maps.

The second strategy to cope with chaotic tunneling is not purely semiclassical, but rather calls up random matrix theory. Since the seminal work presented in Ref. [19], a fruitful approach of quantum chaos is to replace a chaotic but deterministic Hamiltonian by a random element of an ensemble of matrices that only encapsulates the global symmetries. These hybrid techniques, with both semiclassical and statistical ingredients, first allowed us to qualitatively understand the so-called chaos-assisted tunneling, i.e., the observation [20] that tunneling is increased *on average* as the transport through chaotic regions grows [21–23]. However, the extreme sensitivity of tunneling renders the predictions very difficult even if just an order of magnitude is required. This is also true for the seemingly simple case of *near-integrable* dynamics where it was shown, on a discrete quasi-integrable quantum map, that the internal resonances may enhance the transitions by several orders of magnitudes [24,25]. This resonance-assisted tunneling is also at work in discrete systems where chaos is much more developed [26]. The aim of the present paper is to show that the ideas in Refs. [26,27] are strengthened, now in a continuous system, by a systematic analysis of level dynamics and the phase-space representation of the quantum states.

We shall begin in Sec. II with a short presentation of the general framework of chaotic tunneling and the model we chose in order to study it. We will be concerned with a typical signature of tunneling, namely, the period of Rabi oscillations between two wells that are separated by a dynamical barrier. In Sec. III we will show with a simple argument, that the attempt to reproduce the average tunneling periods presented in Ref. [28] is far from being complete precisely because it ignores the resonances, among other things. In Sec. IV we will give an illuminating illustration of a characteristic feature of chaotic tunneling [29]: it appears to be a collective effect in level dynamics where not just one third state crosses a tunneling doublet. We will give a phase-space picture of resonance-assisted tunneling and confirm that taking into account the resonances is unavoidable if we want to reproduce or predict the average behavior of tunneling transitions. In Sec. V, we show that the ideas of Refs. [26,27] actually provide a good estimate for the average tunneling rate in our model.

II. GENERAL FRAMEWORK OF CHAOTIC TUNNELING

The simplest nonintegrable Hamiltonian models are either time-dependent one-dimensional (1D) systems or, equivalently, autonomous systems with two degrees of freedom where the Hamiltonian is the only constant of motion. Seen from the classical point of view, a generic potential induces a cascade of nonlinear resonances whose overlap generates chaos [30,31]. One minimal continuous model that encapsulates these typical properties is a 1D time-dependent system whose Hamiltonian is

$$H(p,q;t) = \frac{p^2}{2} - \frac{\gamma_+}{2}\cos(q + 2\pi t/\tau) - \frac{\gamma_-}{2}\cos(q - 2\pi t/\tau), \tag{1}$$

where p and q denote canonical action-angle variables that are coordinates on a phase-space having the topology of a cylinder: it is 2π-periodic in position (angle) q and infinitely extended in the momentum (action) direction. The model (1) can be seen as the most natural normal form where we keep only two overlapping resonances, i.e., the first two time-dependent Fourier components of the potential. The Hamiltonian H can also be interpreted, provided a change of frame is performed, as a pendulum driven by a periodic wave. Moreover, it is actually very similar to the effective Hamiltonian that can be realized in experiments on cold atoms [32]. We shall consider the period $\tau \equiv 2\pi$ in the following.

The two parameters $\gamma_\mp$ control the size of the two stable islands $\mathcal{I}_\pm$ located in a phase space near $p = \pm 1$, respectively. When increasing the γ's from zero, we leave the quasi-integrable freelike motion and rapidly (at $\gamma \sim 0.2$) reach a mixed regime where the two stable resonance islands are fully surrounded by a chaotic sea. If an initial condition lies inside one island, the classical motion will remain trapped forever within a very thin quasi-one-dimensional layer without the possibility of escape (this evasion is the forbidden process that tunneling will be concerned with [33]). Alternatively, a trajectory starting in between the two islands is chaotic: without being fully ergodic since it cannot enter the islands, the absence of a sufficiently large number of constants of motion allows the system to explore large areas and to develop an exponential sensitivity on initial conditions. Still increasing the γ's, the cascade of secondary resonances inside the islands erode gradually the regular zones and make them dissolve completely in the chaotic sea. Figure 1 shows some Poincaré sections of the classical dynamics, i.e., views taken stroboscopically at every integer multiple of the time period $\tau = 2\pi$ of Eq. (1).

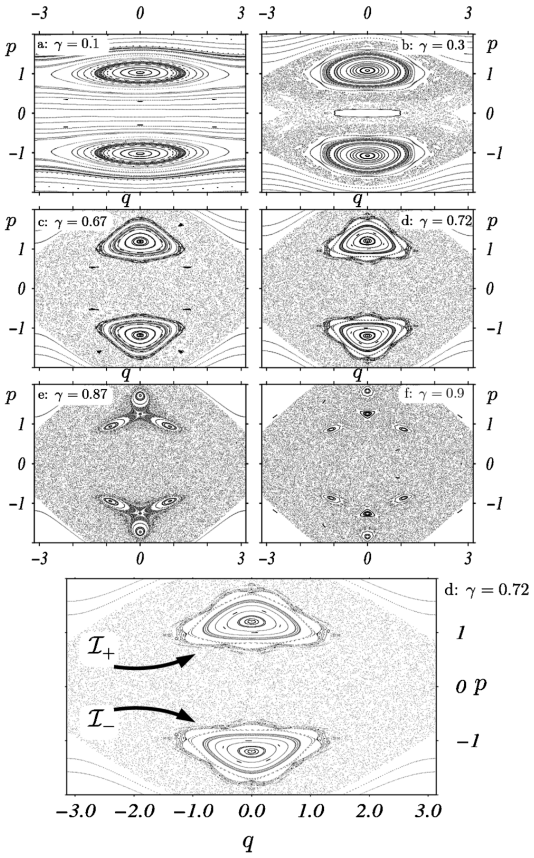

FIG. 1. Some Poincaré sections ($\tau = 2\pi$-stroboscopic plots) corresponding to Hamiltonian (1) for several values of $\gamma_+ = \gamma_- = \gamma$. Increasing γ, between $\gamma \simeq 0.1$ and $\gamma \simeq 0.3$, the two resonances at $(p,q) \simeq (\pm 1, 0)$ start to significantly overlap, and the systems enter in a mixed regime where both regular and chaotic dynamics coexist. From $\gamma \sim 0.3$ to $\gamma \sim 0.8$, the two stable islands $\mathcal{I}_\pm$ are completely surrounded by a chaotic sea, and although they are related by the time-reversal symmetry, they are disconnected from each other at a classical level, since dynamical barriers prevent the real classical trajectories starting in one island to escape from it. For $\gamma \sim 0.72$, $\mathcal{I}_\pm$ have developed a relatively wide 3/7 resonance, which is not the case for $\gamma \sim 0.67$, where the corresponding 3/7 resonance chain is hardly visible. The insets in Fig. 2 show magnifications of the islands in these last two cases.

At a quantum level, the quantization of a Hamiltonian like Eq. (1) has, for a long time, been employed as a very natural continuous model for studying tunneling [34–36]. The time dependence is implemented within the Floquet theory where the phases ϵ of the eigenvalues of the evolution operator at time τ play the role of the energies for autonomous systems. The eigenvectors associated with these so-called quasienergies ϵ will be called the (eigen)states of the system. When $\hbar$ is small enough compared to the typical size of the stable islands, some states, the *regular* states $\{|\phi_n\rangle\}_{n\in\{0,1,\ldots\}}$, appear to have their Husimi distribution localized on the two main stable islands while other states, the *chaotic* states, are found to be delocalized in the chaotic sea.

Following the same route that is explained in great detail in Ref. [[29], Secs. II and III], we will keep a discrete twofold symmetry, namely, the time-reversal symmetry, by considering $\gamma_+=\gamma_-=\gamma$ throughout this paper [37]. This allows us to clearly identify the tunneling process through the existence of small energy scales, the doublet splittings $\Delta\epsilon_n$, which are associated with large time scales, namely, the periods $2\pi\hbar/\Delta\epsilon_n \gg \tau$ of tunneling oscillations between the stable islands. In other words, the magnitude of the splittings $\Delta\epsilon_n=|\epsilon_n^+-\epsilon_n^-|$ between the states that are symmetric ($|\phi_n^+\rangle$) and antisymmetric ($|\phi_n^-\rangle$) with respect to the time-reversal symmetry measure the importance of tunneling between the two stable islands. The actual challenge of chaotic tunneling is to understand and hopefully predict the behavior of $\Delta\epsilon_n$ as a classical (γ) or quantum ($\hbar$) parameter is varied within a regime where the quantum scalesare small enough to resolve the classical scales of the chaotic structures.

Unlike what occurs for integrable multidimensional systems where $\Delta\epsilon_n$ is a smooth monotonic function given by $\Delta\epsilon \propto e^{-A/\hbar}$ [38] with A being a typical classical action that characterizes the tunneling barriers, the splittings can display huge fluctuations in the mixed regular-chaotic case, which were soon identified as a signature of chaos [22,34]. But, as far as *isolated* fluctuations are observed, this point of view must be amended. One isolated fluctuation is clearly associated with a third state whose (quasi)energy nearly degenerates with the doublet [34,36] as γ or $\hbar$ is varied. Chaos is not necessarily relevant here since such fluctuations can be observed when the chaotic layers are too small (and $\hbar$ too large) to be resolved by the quantum waves. It may happen that the third state is also a regular state localized on another regular Einstein Brillouin Keller (EBK) torus, possibly belonging to another stable island. What deserves the name of chaotic tunneling is a radical change of regime where the fluctuations are not isolated anymore and where the coarse-grained behavior of $\Delta\epsilon$ does not follow a monotonic law. It was shown in Ref. [[29], Sec. V], that there actually exists a rather abrupt transition between a quasi-integrable tunneling regime and a chaotic regime and that this transition occurs precisely when the quantum eyes can resolve the chaotic classical structures.

While the study of statistics of the splittings is necessary to give an insight into chaotic tunneling [23,39], we will focus here on the *average* behavior of the splittings. It is far from obvious that we can conceptually justify the distinction between "large" scales (the average) and "small" scales (the fluctuations) in the variations of $\Delta\epsilon$. Most probably, there may exist a whole hierarchy of such variations. From the numerical point of view, however, there seems to be an overall modulation of $\Delta\epsilon$, both observed in maps ([[40], Fig. 3], [[26], Figs. 1 and 2]) and in continuous systems [[3], Fig. 7]. This modulation is precisely the very object of Ref. [26] (see also Ref. [27]) and of the present paper.

III. KEY ROLE OF RESONANCES

In the general context recalled in the previous section, where tunneling transitions occur between two symmetric but disconnected stable classical islands, the following estimate has been proposed for a typical chaotic tunneling splitting [[28], Eq. (4)]:

$$\Delta\epsilon \simeq \hbar\,\Omega\frac{\Gamma(2N,4N)}{\Gamma(2N+1;0)}. \tag{2}$$

Here, Γ stands for the incomplete gamma function, $N=A/(2\pi\hbar)$ denotes the semiclassical estimate of the number of states localized in one island of area A, and Ω represents an unknown prefactor, with the dimension of an inverse time scale, which does not depend on $\hbar$. Though the origin of the formula remains obscure as Eq. (2) is not explicitly proven by their authors, it gave, in Ref. [28], good agreement with numerical computations provided we are ready to accept an unreasonably large ambiguity on the unspecified proportionality factor: for $\hbar^{-1}\simeq 40$, the estimate (2) varies by five orders of magnitude (10^{-1} vs 10^{-6}) in the two cases considered in Fig. 2 of Ref. [28] where the areas A of the stable islands are of the same order. More recent calculations within the "kicked Harper" model, however, revealed substantial deviations between Eq. (2) and the exact quantum-tunneling rates in the semiclassical regime, where a reasonable agreement was only found in the deep quantum limit of large $\hbar$ [27].

Indeed, no good estimate of $\Delta\epsilon$ can be obtained if the only classical parameter on which the theory depends is the area A of the island. As shown in Fig. 2, the internal classical structure of the islands must be involved in one way or another. We have plotted here the splitting $\Delta\epsilon_0$ between the two "central" states $|\phi_0^\pm\rangle$ localized in the two islands; more precisely, they both were selected by the criterion of having the maximal overlap with a coherent state that is located on the central stable periodic orbit of period τ. The two graphs, $\Delta\epsilon_0$ as a function of $1/\hbar$, are shown for the two classical parameters $\gamma=0.67$ and $\gamma=0.72$ [see also Figs. 1(c) and 1(d)]. In these cases, the stable symmetric islands $\mathcal{I}_\pm$ have an area A of the same order of magnitude, but exhibit a rather distinct internal structure: for $\gamma=0.72$, $\mathcal{I}_\pm$ have developed a wide 3/7-resonance chain compared to the $\gamma=0.67$ case. In the logarithmic plot, the two graphs strongly differ. Not only the fluctuations of $\Delta\epsilon_0$ hardly match, but also the average behavior is completely distinct in a semiclassical regime where $1/\hbar > 10$. A discrepancy of about five orders of magnitude can be clearly observed for $1/\hbar \simeq 16$: for $\gamma=0.72$, we have $\Delta\epsilon_0 \sim 10^{-6}$ compared to $\Delta\epsilon_0 \sim 10^{-11}$ for $\gamma=0.67$. At $1/\hbar \sim 25$, on the other hand, the splittings for $\gamma=0.72$ are about 10^{-3} smaller than for $\gamma=0.67$.

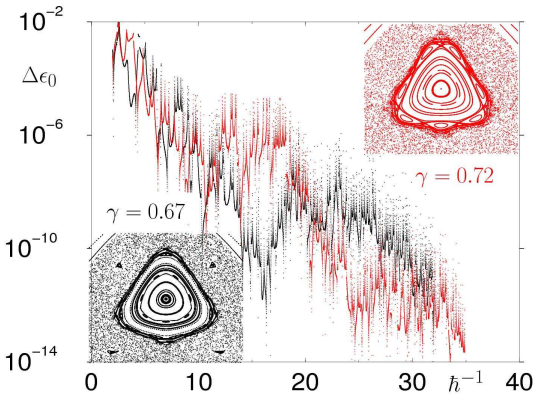

FIG. 2. (Color online) Comparison of the tunneling splittings $\Delta\epsilon_0$ for γ=0.72 (black line) and γ=0.67 (gray/red line). The corresponding stable islands, magnified in both cases with the same scaling factor, are shown in the insets [see Figs. 1(c) and 1(d)] for a full Poincaré surface of section). The exponentially large difference between the two curves is explained by the different internal structure of the islands: for γ=0.72, the 3/7-resonance chain is much more developed than for γ=0.67.

In any case, no estimate formula $\Delta\epsilon_0(A,\hbar)$, which would produce approximately the same graphs for γ=0.67 and γ=0.72, can be satisfactory. At this stage it is more than plausible that the internal structure of $\mathcal{I}_\pm$ must be taken into account in any attempt to estimate $\Delta\epsilon_n$ with the help of classical ingredients.

IV. MULTILEVEL CROSSING

To obtain more insight, we analyze in this section the "level dynamics," i.e., the changes of the quasienergy spectrum as $1/\hbar$ or γ is varied. This can, for instance, explain individual fluctuation spikes, which correspond to the crossing of the tunneling doublet with a third state (or an unresolved doublet) ([[22], Fig. 7], [[34], Fig. 1], [[29], Fig. 4]). As far as the average of $\Delta\epsilon$ is concerned, we can also establish a correspondence between its behavior as a function of $1/\hbar$ and some features of the level dynamics. First, a technical point should be mentioned at this stage. For τ-periodic systems whose classical phase-space is unbounded, it is expected that the quasienergy spectrum becomes a dense set because of the foldings of an infinite spectrum in the finite Floquet zone $]-\pi\hbar/\tau,\pi\hbar/\tau]$. Hence, we need a criterion to select only those states that are relevant in the level dynamics. Numerically, the truncation of the Floquet matrices at high $|p|$'s is not sufficient, especially for small $\hbar$, since more and more regular and chaotic states are *a priori* potentially implicated in the tunneling dynamics. To select the levels that are actually involved, we will use a simple criterion based on the systematic computation of the overlaps σ_m between the states $|\psi_m\rangle$ and a coherent state centered on the island: $\sigma_m \overset{\text{def}}{=} |\langle z_{\text{stable orbit}}|\psi_m\rangle|$. Retaining only those states whose σ_m is larger than a given threshold σ_{filter} will filter the levels that are the best candidates to play a role in the tunneling process, precisely because their wave functions are not negligible in the area where the tunneling doublet wave functions live.

Let us fix the classical dynamics at γ=0.72 where, as we have seen in the previous section, the internal 3/7 resonance is suspected to provoke the enhancement of average tunneling for $11\lesssim 1/\hbar\lesssim 19$ (see Fig. 2). When we look at this plateau more carefully, we can identify two "bumps" that are visualized in Fig. 3. One corresponds to $11\lesssim 1/\hbar\lesssim 13.5$ followed by a wider one for $13.5\lesssim 1/\hbar\lesssim 19$. These two bumps are in one-to-one correspondence with two bunches of levels with significant overlaps σ_m crossing the tunneling doublet $\epsilon_0^\pm$. In general, we have observed in many cases, with such a level-dynamics point of view, that there seems to be a clear change of regime: for a given σ_{filter}, when the average of $\Delta\epsilon_n$ stops decreasing, the states $|\psi_m\rangle$ whose quasienergies are in the neighborhood of $\epsilon_n^\pm$ and whose σ_m are larger than σ_{filter}, become significantly more numerous. For instance, in Fig. 3 where we chose $\sigma_{\text{filter}}\simeq 7\times 10^{-3}$, or in Fig. 4 with a five times more rough filter $\sigma_{\text{filter}}\simeq 1.4\times 10^{-3}$, just after the end of the large plateau at $1/\hbar\gtrsim 20$, the crossings with relevant levels become suddenly scarce. To put it in a different way, the average enhancement of tunneling appears to be the outcome of a collective dynamics involving numerous states that can be seen in the spectrum through their crossing with the tunneling doublet.

In order to be more convincing, this qualitative observation can be strengthened by a phase-space analysis. In addition to the unresolved tunneling doublet $\epsilon_\pm^0$, we can clearly see, in the level dynamics in Fig. 4, two other unresolved doublets $\epsilon_5^\pm$ and $\epsilon_7^\pm$ for $1/\hbar\gtrsim 20$, whose Husimi distribution is mainly located near the boundary of the stable islands $\mathcal{I}_\pm$. In fact, the doublet $\epsilon_5^\pm$ can be followed along a quasicontinuous line even for $1/\hbar\lesssim 20$ whereas the other one cannot be identified unambiguously in that region of $\hbar$ corresponding to the plateau: when $1/\hbar$ is decreased from about 19, the doublet line $\epsilon_7^\pm$ encounters many avoided crossings and ramifies into the bunch of levels we have precisely associated with the bump. Therefore, even if their Husimi plots both look very similar, one doublet is dramatically involved in the tunneling process while the other remains a bystander. If we compute the overlap of these states with the harmonic states inside the islands, that is, the eigenstates of the harmonic approximation of the Hamiltonian (1) near the corresponding stable periodic orbits, we find that the bystander doublet $\epsilon_5^\pm$ is indeed the fifth excited doublet in $\mathcal{I}_\pm$ whereas the other $\epsilon_7^\pm$ is the seventh. This can also be checked in the Floquet spectrum. Indeed, we expect that the levels of the local eigenmodes of the island (which is locally equivalent to a harmonic oscillator) approximately differ from each other by multiples of $\hbar\omega_0$ where $\omega_0\simeq 0.4$ denotes the frequency oscillations around the center of the island at $(p,q)\simeq(\pm 1.20,0)$. This yields $\epsilon_l^\pm\simeq\epsilon_0^\pm+l\hbar\omega_0$ modulo a Floquet width $2\pi\hbar/\tau$ for the levels. The fact that it is precisely the quantum number ℓ=7, which is involved in the emergence of the plateau, is not a coincidence. This ℓ is exactly the order of the resonance 3/7 that dominates in $\mathcal{I}_\pm$ for γ=0.72.

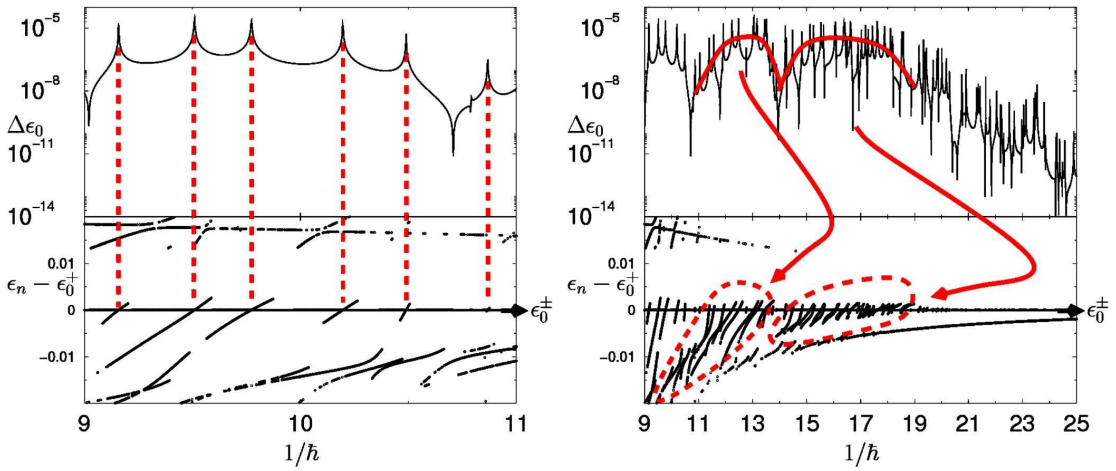

FIG. 3. (Color online) The upper panels show $\Delta\epsilon_0$ as a function of $1/\hbar$ for $\gamma=0.72$ and the lower panels display a part of the corresponding Floquet spectrum. Only the quasienergies associated with states whose overlaps are $\sigma_m \geq 7\times 10^{-3}$ are shown, once calibrated with respect to the tunneling doublet $\epsilon_0^\pm$ (unresolved in the lower panels). For relatively large $\hbar$ (on the left-hand side), the huge fluctuations of $\Delta\epsilon_0$ are in one-to-one correspondence with the crossings of the tunneling doublet by one isolated doublet. On the right-hand side, the upper panel shows a magnification of the plateau in $\Delta\epsilon_0$ occurring at $\gamma=0.72$ between $\hbar\simeq 11$ and $\hbar\simeq 19$ (see also Fig. 2). The lower right panel displays a part of the corresponding Floquet spectrum. The plateau in $\Delta\epsilon_0$ corresponds to a large number of crossings where we can even identify by eye two families of levels (encircled by the dashed lines) that give rise to the two bumps in the average of $\Delta\epsilon_0$ (red/gray thick continuous line in the upper right panel). Beyond the point where the plateau ends, i.e., for $\hbar^{-1}\gtrsim 19$, no more crossings can be identified, and the only other state apart from $\epsilon_0^\pm$ that significantly overlaps with the Husimi function in the island is the bystander doublet $\epsilon_5^\pm$ (see also Fig. 4).

The quantitative details of how the classical resonances may be implemented in order to reproduce the average behavior of $\Delta\epsilon_0$ will be described in the next section. Even though the approximations that are involved are not always under rigorous control, we can see here the resonances at work. Suppose that the classical parameters are such that one *classical* resonance s/ℓ dominates the others in the stable islands $\mathcal{I}_\pm$ (s being an integer and ℓ a strictly positive integer, the order of the resonance). This precisely means that one torus is actually broken into a chain of ℓ subislands centered about a stable periodic orbit of period $2\pi/\omega_0=\ell\tau/s$. A *quantum* resonance occurs when two quasienergies ϵ_m and ϵ_0 are nearly degenerate, i.e., differ by an integer number s' of Floquet widths: $\epsilon_m-\epsilon_0\simeq s'\hbar 2\pi/\tau$. As mentioned above, we also have $\epsilon_m-\epsilon_0\simeq m\hbar\omega_0+s''2\pi/\tau$ from a semiclassical argument (s'' being an integer). Hence, we immediately see that m must be an integer multiple of ℓ.

The analysis given so far, however, shows that the tunneling enhancement cannot be explained with just one crossing of the $\epsilon_0^\pm$ doublet by $\epsilon_m^\pm$. This global crossing is actually made up of many elementary crossings whose contributions cannot be individually distinguished. In effect, this game involves many players among which are the states that are completely delocalized in the chaotic sea. There are also states ("beach" states [41,42] or "Janus" states) that are strongly coupled on one side to the regular states and on the other side to the chaotic ones. It is scarcely surprising that these states have their Husimi distribution localized near the borderline between the stable islands and the chaotic sea (see Fig. 5).

V. RESONANCE-ASSISTED TUNNELING

The above discussion has provided overwhelming evidence for the relevance of nonlinear resonances in the dynamical tunneling process. We now focus on the quantitative evaluation of the influence of such resonances, which was presented in detail in Refs. [24–27]. To this end, we formally introduce an integrable Hamiltonian that approximately reproduces the dynamics within the regular island. For the upper island at $p\simeq 1$, such an integrable system can be explicitly obtained by leaving out the γ_+-dependent term in the Hamiltonian (1). Performing the time-dependent canonical transformation $q\mapsto\tilde{q}=q-t$ to the frame that co-propagates with the resonant orbit, this integrable Hamiltonian reads

$$H_0(p,\tilde{q}) = \frac{(p-1)^2}{2} - \frac{\gamma_-}{2}\cos(\tilde{q}). \tag{3}$$

Canonical perturbation theory [31] can be applied on the basis of Eq. (3) in order to obtain an improved integrable description that is in good agreement with the motion in the regular island also at finite values of γ.

In the dynamics generated by H_0, the regular island is embedded in a phase-space domain of bounded elliptic motion in momentum space. Within this bounded domain, action-angle variables (I,θ) can be introduced, which, respectively, correspond to the area enclosed by an elliptic invariant orbit as well as to the propagation time that elapses along this orbit. In this action-angle variable representation, we have $H_0(p,\tilde{q})\equiv H_0(I)$, and the full time-dependent

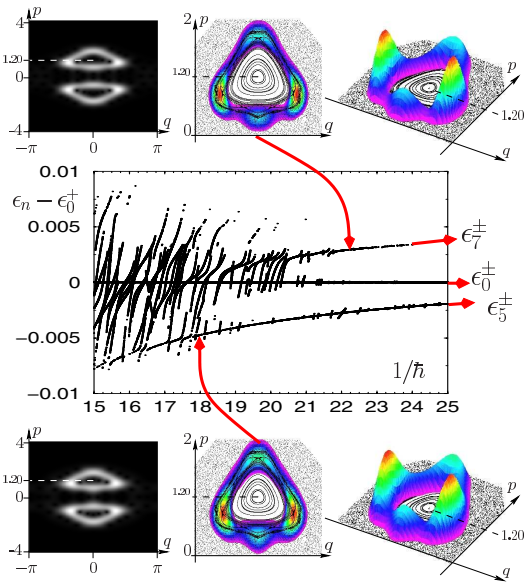

FIG. 4. (Color online) The level dynamics for $\gamma=0.72$ calibrated with respect to the tunneling doublet $\epsilon_0^\pm$ (unresolved). Compared to Fig. 3, more states are plotted since we take a smaller $\sigma_{\text{filter}} \simeq 1.4 \times 10^{-3}$. When looking at the crossings with the tunneling doublet, there still is a clear transition of regime for $\hbar^{-1}$ below or above 20, which corresponds to the end of the plateau in $\Delta\epsilon_0$. The three upper views show the Husimi distribution of the state, $|\phi_7^+\rangle$, whose quasienergy is ϵ_7^+, for $\hbar^{-1}>20$. A comparison with the Poincaré surface of section in the neighborhood of the stable island $\mathcal{I}_+$ is shown. The three lower views (which are, actually, very similar to the upper ones at this resolution) correspond to $|\phi_5^+\rangle$, the symmetric state whose quasienergy is ϵ_5^+ can be followed for every $\hbar^{-1}$. Unlike $|\phi_7^\pm\rangle$, the doublet $|\phi_5^\pm\rangle$ does not cross and has no influence on the tunneling doublet. $|\phi_7^+\rangle$ (respectively, $|\phi_5^+\rangle$) is localized near the boundary of the two islands and indeed corresponds to the symmetric combination of the seventh (respectively, fifth) excited regular state in $\mathcal{I}_\pm$.

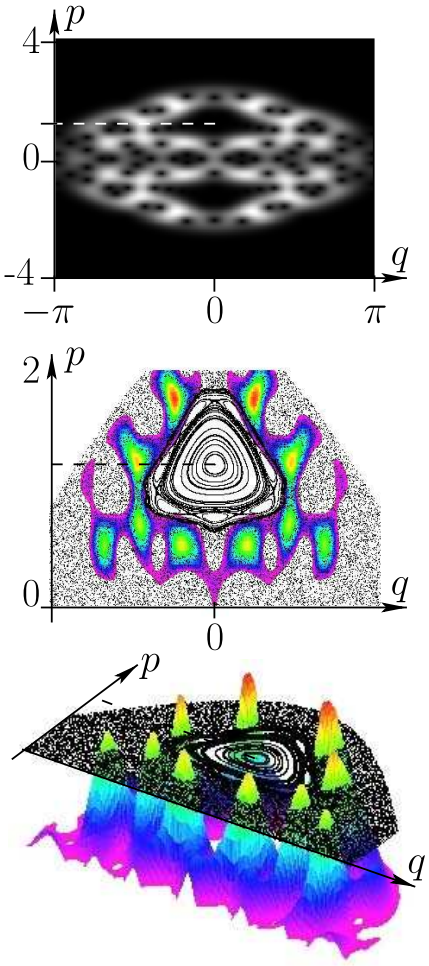

FIG. 5. (Color online) Janus state: it is strongly coupled to the most excited resonant state in the stable island and to the chaotic states. In the random matrix model, it is "seen" as chaotic from the regular states and almost "regular" from the chaotic sea. Here we plot several views of the Husimi distribution of a Janus state and compare its localization with the classical phase-space structures ($\gamma=0.72$, $\hbar^{-1}=30$, and $\epsilon=-0.007\,774$).

Hamiltonian (1) is formally written as $H(I,\theta,t)=H_0(I)+V(I,\theta,t)$ where V represents a weak perturbation within the island.

We now assume the presence of a prominent s/ℓ resonance within the regular island, where s oscillations around the island's center match ℓ periods of the driving. This resonance condition is satisfied at $\ell\omega_0(I)=s$ where $\omega_0 \equiv dH_0/dI$ is the oscillation frequency along the bounded orbit with action variable I. The dynamics in the vicinity of such a resonance can be approximately described by the pendulumlike integrable Hamiltonian

$$H_{\text{eff}}(I,\vartheta) = \frac{(I-I_0)^2}{2m_0} + 2V_0\cos(\ell\vartheta), \tag{4}$$

which is derived from $H(I,\theta,t)$ using secular perturbation theory [31]. Here, $\vartheta=\theta-(s/\ell)t$ is the (slowly varying) angle variable that corotates with the resonance. The resulting phase-space structure of H_{eff} is plotted in Fig. 6.

Following the lines of Ref. [43], we now evaluate the influence of such a resonance in the corresponding quantum system by a direct quantization of the effective pendulum Hamiltonian (4) in the modified angle variable ϑ. Apart from a phase factor containing the Maslov index, the unperturbed eigenstates of H_0 are then given by the plane waves $\langle\vartheta|n\rangle=\exp(in\vartheta)$. In the co-rotating frame, their eigenenergies approximately read

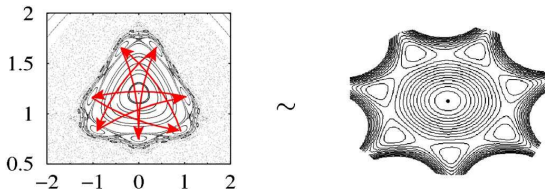

FIG. 6. (Color online) Left panel: classical phase space in the vicinity of the regular island. The straight solid lines indicate in which order the subislands are "visited" in the course of time evolution. The right panel shows the phase-space structure that would result from the pendulumlike Hamiltonian (4) describing the dynamics in the vicinity of the 3/7 resonance.

$$E_n = \frac{[\hbar(n+1/2) - I_0]^2}{2m_0}, \tag{5}$$

using the fact that $I_n = \hbar(n+1/2)$ are the quantized action variables within a regular island of elliptic shape. The ϑ-dependent term in Eq. (4) introduces couplings between the states $|n\rangle$ and $|n \pm \ell\rangle$ with the coupling matrix element V_0. These couplings give rise to perturbative chains by means of which eigenstates with low and high excitations within the bounded domain are connected to each other.

The pendulum Hamiltonian (4) can be considered to be appropriate for $I < I_c$ where I_c denotes the action variable of the outermost invariant elliptic curve of the regular island. The regime beyond this "chaos border" is characterized by the presence of multiple overlapping resonances, which implies that the unperturbed states with $I_n > I_c$ can be assumed to be strongly coupled to each other by many different matrix elements. Such couplings would also occur between "bound" and "unbound" eigenstates of the integrable Hamiltonian H_0 (which are, respectively, located within and outside the domain of bounded motion that embeds the regular island) as well as between states that are located in the vicinity of the two different islands at $p \simeq 1$ and $p \simeq -1$. In this way, an efficient two-step mechanism is introduced by which two symmetry-related quasimodes that are localized in the upper and lower island, respectively, are coupled to each other: the nonlinear resonance connects those quasimodes to the states in the chaotic domain, and the latter "see" each other via strong matrix elements of the full (Floquet) Hamiltonian of the driven system.

Figure 7 schematically displays the effective Hamiltonian matrix that governs this resonance- and chaos-assisted tunneling process between the two "central states" of the islands (i.e., given by $|n=0\rangle$ in the above notation). The matrix is restricted to basis states of one particular symmetry class—i.e., to states that are "even" or "odd" with respect to time-reversal symmetry—and includes, for the sake of clarity, only those regular components to which the central state is perturbatively connected via the s/ℓ resonance. Altogether, k_c regular states are included in the matrix, where the integer k_c is defined such that $I_{(k_c-1)\ell} < I_c < I_{k_c\ell}$ holds true, i.e., $|(k_c-1)\ell\rangle$ is still located in the island, whereas $|k_c\ell\rangle$ is dissolved in the chaotic part.

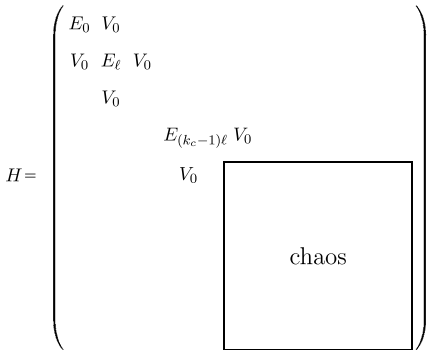

FIG. 7. Sketch of the effective Hamiltonian matrix that describes the coupling between the regular island and the chaotic domain for one particular symmetry class (i.e., for even or odd states with respect to time-reversal symmetry). The regular part (upper left band) includes only components that are coupled to the island's central state by the s/ℓ resonance. In the simplest possible approximation, the chaotic part consists of a full subblock with equally strong couplings between all basis states with actions beyond the outermost invariant torus of the island.

We can now prediagonalize the upper left "regular" block of the Hamiltonian. This yields, in lowest nonvanishing order in the perturbation strength $|V_0|$ (which is much smaller than all relevant energy differences), the modified central state as

$$|\tilde{0}\rangle = |0\rangle + \sum_{k=1}^{k_c-1} \left(\prod_{k'=1}^{k} \frac{V_0}{E_0 - E_{k'\ell}} \right) |k\,\ell\rangle. \tag{6}$$

This perturbed central now exhibits a nonvanishing matrix element with one of the states that are contained within the chaotic domain: we obtain

$$V_{\text{eff}} \equiv \langle k_c\,\ell\,|H|\tilde{0}\rangle = V_0 \prod_{k=1}^{k_c-1} \frac{V_0}{E_0 - E_{k\ell}}, \tag{7}$$

which can be interpreted as the effective resonance-induced matrix element between the central state and the chaotic domain. In this way, our effective Hamiltonian matrix can be related to the phenomenological matrix models that constitute the starting point of the statistical theory of chaos-assisted tunneling [21–23].

In the simplest possible approach, we assume that the "chaos block" is essentially homogeneous and can be well modeled by a random matrix from the Gaussian orthogonal ensemble (GOE). This assumption does not account for the influence of prominent partial barriers to the classical transport, which can arise from broken invariant tori (so-called "Cantori" [44]) as well as from unstable periodic orbits in the chaotic sea, and which would lead to an effective division of the chaotic Hamiltonian into several subblocks that are weakly connected to each other [21]. Neglecting those partial barriers and performing the random matrix average over the eigenvectors and eigenvalues of the chaos block gives rise to the Cauchy distribution

$$P(\Delta E_0) = \frac{2}{\pi}\frac{\overline{\Delta E_0}}{(\Delta E_0)^2 + (\overline{\Delta E_0})^2} \tag{8}$$

for the level splitting between the "even" and "odd" combination of central states that are associated with the pair of regular islands [22,23]. This distribution is characterized by the scale

$$\overline{\Delta E_0} = \frac{2\pi V_{\rm eff}^2}{N_c \Delta_c}, \tag{9}$$

which contains the most dominant effective matrix element (7) between the island's central state and one of the chaotic states, the total number N_c of chaotic states, as well as the mean level spacing Δ_c in the chaos block. In our case of a periodically driven system, the latter is given by $\Delta_c = \hbar/N_c$, due to the fact that the chaotic states are, in the framework of the Floquet approach, uniformly distributed at random in an energy window of the size $2\pi\hbar/\tau = \hbar$ (we recall that the period of the driving equals $\tau = 2\pi$). As a consequence, we obtain $\overline{\Delta E_0} = 2\pi V_{\rm eff}^2/\hbar$.

The distribution (8) is, strictly speaking, valid only for $\Delta E_0 \ll V_{\rm eff}$ and exhibits a cutoff at $\Delta E_0 \sim 2V_{\rm eff}$ [23], which ensures that the statistical expectation value $\langle \Delta E_0 \rangle = \int_0^\infty x P(x) dx$ does not diverge. However, since tunneling rates and their parametric variations are typically studied on a logarithmic scale (see Fig. 2), we compute from Eq. (8) not the mean value $\langle \Delta E_0 \rangle$, but rather the average of the *logarithm* of ΔE_0. Our "average" level splitting $\langle \Delta E_0 \rangle_g$ is therefore defined by the *geometric* mean $\langle \Delta E_0 \rangle_g \equiv \exp[\langle \ln(\Delta E_0) \rangle]$, the evaluation of which does not involve the above cutoff; we obtain the expression

$$\langle \Delta E_0 \rangle_g = \overline{\Delta E_0} = \frac{2\pi V_{\rm eff}^2}{\hbar}, \tag{10}$$

which, notably, is free of any adjustable parameter. Hence, up to a trivial prefactor, the mean value of splittings is, in a logarithmic-scale representation, given by the square of the coupling matrix element (7) between the island's central state and the chaos [26,27].

Figure 8 shows the comparison with the exact quantum splittings at $\gamma = 0.72$, calculated by the numerical diagonalization of the Floquet matrix. The semiclassical prediction (10) (the solid line in Fig. 8) was evaluated on the basis of the prominent 3/7 resonance, for which the relevant parameters I_0, m_0, and V_0 that enter into the pendulum Hamiltonian (4) were entirely determined from classical dynamics of the system: As in Ref. [26], we compute for this purpose the trace of the monodromy matrix associated with a stable or unstable periodic point of the 3/7 resonance, as well as the phase-space areas that are enclosed by the inner and outer separatrices of the resonance. Indeed, those quantities remain invariant under the canonical transformation to the action-angle variables (I, ϑ), which means that the latter need not be explicitly evaluated in order to obtain the effective coupling matrix element $V_{\rm eff}$.

We see that the semiclassical theory reproduces quite well the two plateaus that arise in the quantum splittings. The drop in the semiclassical splittings at $1/\hbar \simeq 24$ occurs due to

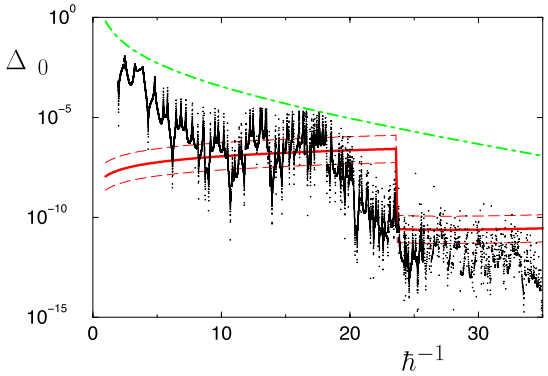

FIG. 8. (Color online) Comparison between the numerically calculated splittings of the driven pendulum at $\gamma = 0.72$ (black dots) and the semiclassical prediction according to Eq. (10) (red, solid line). The semiclassical theory, which is based on the prominent internal 3/7 resonance within the regular island, reproduces quite well the positions and heights of the two plateaus that appear in the exact quantum splittings. The dashed lines indicate the size of the logarithmic standard deviation according to Eq. (11). The (green) dot-dashed line displays the prediction that would be obtained from Eq. (12) with $\Omega = 1$.

the fact that the island supports more than seven locally quantized eigenstates beyond this critical value of $1/\hbar$; hence, two perturbative steps instead of one are required in order to connect the central state of the island to the chaotic domain. This drop is considerably softened in the quantum splittings, but can still be identified, which confirms the relevance of the resonance-assisted coupling mechanism in this tunneling process. Since nonlinear resonances represent a general feature of nonintegrable Hamiltonian systems, we expect that the appearance of such steplike sequences of plateaus is a *generic* phenomenon, which is not restricted to one particular system, but arises in various chaos-assisted tunneling processes. This expectation is indeed confirmed by previous studies on the kicked Harper [40], on the decay of nondispersive wave packets in driven hydrogen [45], as well as on the dynamical tunneling process of cold atoms [3,46], where significant plateau structures were encountered in numerically calculated tunneling rates.

In addition to the mean value for the splittings, the probability distribution (8) can also be used in order to calculate the expectation value for their *logarithmic variance* characterizing the average size of fluctuations on a logarithmic scale; we obtain

$$\langle (\ln \Delta E_0 - \ln \overline{\Delta E_0})^2 \rangle = \pi^2/4. \tag{11}$$

This result is *universal* in the sense that it does not depend on system-specific parameters nor on $\hbar$. The size of the corresponding standard deviation is indicated by the dashed lines in Fig. 8, which are generated by multiplying $\overline{\Delta E_0}$ with $e^{\pm\pi/2}$. Clearly, the "window" defined by those dashed lines is exceeded near local avoided crossings with chaotic states, where a large enhancement as well as a complete suppres-

sion of the splittings may be induced [2]. Apart from those exceptional events, however, the scale of the average fluctuations of the splittings is well described by Eq. (11). The green dot-dashed line in Fig. 8 displays the prediction for the splittings that would be obtained from Eq. (2) according to Ref. [28]. Here, the asymptotic expression

$$\Delta\epsilon \simeq \frac{\hbar\Omega}{16\pi N^3} e^{-2(1-\ln 2)N} \tag{12}$$

of Eq. (2), valid for $N \equiv A/(2\pi\hbar) \gg 1$, was evaluated with the numerically calculated size A of the island. Being an entirely classical ($\hbar$-independent) quantity, the system-dependent prefactor Ω was set equal to unity. We clearly note a substantial disagreement between this semiclassical estimation and the quantum splittings.

The theory of resonance-assisted tunneling does not reproduce the splittings in the deep quantum regime of larges values of $\hbar$, where a different mechanism, possibly in the spirit of Ref. [28], might induce the transition to the chaos. Moreover, the critical value of $1/\hbar$, at which the drop of the splittings from the first to the second plateau occurs, is significantly overestimated by our semiclassical approach. This could be due to the presence of *partial barriers* in the chaotic phase-space domain, such as "Cantori" [44], which are known to inhibit the quantum flux at not too small values for $\hbar$ [47,48]. If such a Cantorus is manifested in the vicinity of the regular island, the effective "quantum" size of the island could be considerably enhanced as compared to A, which would reduce the value of $1/\hbar$ at which exactly ℓ quantum states are localized around the island. This observation is indeed in accordance with the manifestation of Janus states [41,42] in the spectral analysis (see Sec. IV).

Significant deviations of the splittings from the semiclassical prediction (10) are also to be expected in the deep semiclassical regime where a multitude of steps ($k \gg 1$) would be needed to connect the central state to the chaotic domain according to the expression (7). In this regime, the coupling via the s/ℓ resonance—which also represents a dynamical tunneling process, as was pointed out in Ref. [25]—can again be assisted by the presence of another nonlinear s'/ℓ' resonance, as long as this is permitted by the associated selection rule ($n \mapsto n+\ell'$). Such a s'/ℓ' resonance would generally exhibit a lower effective coupling strength V_0' and is typically of higher order than the s/ℓ resonance (i.e., ℓ' and s' are typically larger than ℓ and s, respectively). The relevance of this multiresonance coupling mechanism was demonstrated in the near-integrable kicked Harper model where the semiclassical tunneling process involves a sequence of three nonlinear resonances [24,25,27].

In the case of the driven pendulum at $\gamma=0.72$, such multiresonance processes cannot be observed within the range of values for $1/\hbar$ at which precise quantum calculations of the splittings can be performed. This is different, however, for $\gamma=0.67$. At this value of the coupling parameter, the regular island $\mathcal{I}_\pm$ exhibits two nonlinear resonances of almost equal importance: a 3/7 resonance, located closer to the center of the island than at $\gamma=0.72$, and a 5/11 resonance, located close to the chaos border (see Fig. 9). This implies that a two-step tunneling process involving both resonances can be encountered at finite values for $1/\hbar$. Assuming that each resonance contributes with one single-perturbative step (which is the case at the values of $1/\hbar$ considered here), the corresponding matrix element that connects the central state to the chaotic domain would read

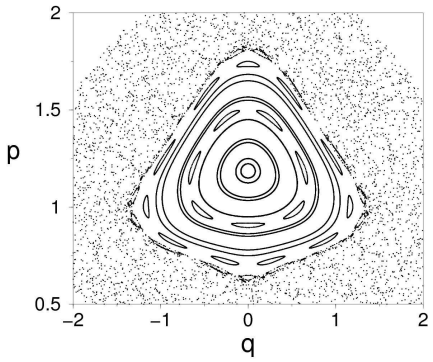

FIG. 9. Classical phase space at $\gamma=0.67$ in the vicinity of the regular island $\mathcal{I}_+$. The two chains of subislands correspond to the 3/7 as well as to the 5/11 resonance (inner and outer chain, respectively).

$$V_{\text{eff}} = \frac{V_0^{(3/7)}}{E_0^{(3/7)} - E_7^{(3/7)}} V_0^{(5/11)}. \tag{13}$$

Here, $V_0^{(s/\ell)}$ represents the pendulum-coupling strength of the effective Hamiltonian (4), and $E_n^{(s/\ell)}$ denotes the energies (5) in the corotating frame that is defined with respect to the s/ℓ resonance. This expression requires that the seventh excited state, i.e., the first state to which the central state of the island is coupled via the 3/7 resonance, is located *in between* the two resonances, which implies that the action variable I_7 of this state ought to be lower than the action variable $I_0^{(5/11)}$ of the 5/11 resonance. This condition turns out to be valid for $1/\hbar > 28.8$.

Figure 10 displays the quantum splittings at $\gamma=0.67$. The red solid line denotes the semiclassical prediction (10) for the splittings, which is for $1/\hbar < 28.8$ calculated by the single-step process via the 5/11 resonance (which has the larger matrix element $V_0^{(s/\ell)}$ and should therefore dominate compared to the 3/7 resonance) and for $1/\hbar > 28.8$ obtained through the two-step process that is described by Eq. (13). As in the case of $\gamma=0.72$, the overall agreement between the semiclassical and the quantum splittings is quite good, with significant deviations arising only in the deep quantum regime at $1/\hbar < 10$ as well as in the vicinity of the crossover between the single- and the two-step process, which is artificially sharp in the semiclassical calculation. Striking evidence for the validity of the two-step process is the appearance of a pronounced peak in the quantum splittings at $1/\hbar \simeq 43$, which arises due to a vanishing denominator in Eq. (13), i.e., due to the fact the central state and the seventh excited state become near-degenerate in the corotating frame.

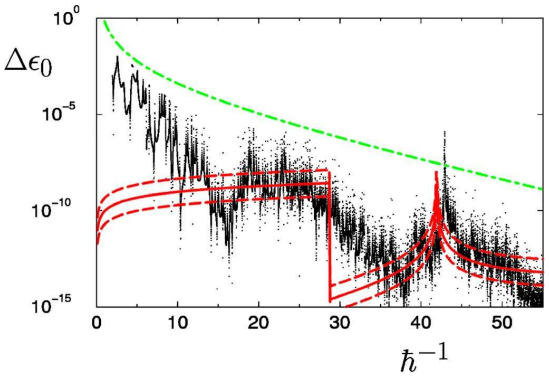

FIG. 10. (Color online) Comparison between the numerically calculated splittings of the driven pendulum at $\gamma=0.67$ (black dots) and the semiclassical prediction (red, solid line). The latter was evaluated by a single-resonance process via the 5/11 resonance for $1/\hbar < 28.8$, and by a two-resonance process, according to Eq. (13), involving also the 3/7 resonance for $1/\hbar > 28.8$. As in Fig. 8, the dashed lines indicate the size of the logarithmic standard deviation according to Eq. (11), and the green dot-dashed line displays the prediction obtained from Eq. (12).

The position and height of this peak are fairly well reproduced by the semiclassical theory.

VI. CONCLUSION

In summary, we provided clear evidence of the significance of nonlinear resonances in the dynamical tunneling process within the driven pendulum. Indeed, the signature of the 3/7 resonance that is dominantly manifested in the regular island at $\gamma=0.72$ is identified in various ways: (a) The characteristic plateau structure in the level splittings sensitively depends on whether or not the resonance is well developed within the regular island; (b) Floquet states that exhibit an appreciable overlap with the central Husimi wave function of the island energetically correspond to the seventh excited eigenstate within the island; and (c) a semiclassical expression for the tunneling-induced splittings that is based on the resonance-assisted coupling scheme is in good agreement with the exact quantum data. The validity of the resonance-assisted tunneling mechanism is furthermore confirmed by a striking peak in the quantum splittings at $\gamma=0.67$, which arises due to a two-step process involving two different nonlinear resonances within the regular island. Both in the spectral analysis and in the semiclassical comparison, we identify traces of Janus states that are located in the chaotic vicinity of the islands. This indicates that partial barriers in the chaotic domain could still be relevant in our system at the values of $\hbar$ under consideration.

The present approach is presumably not suited for a full-blown semiclassical theory of mixed regular-chaotic tunneling in terms of complexified orbits, for which the ansatz of Refs. [16–18] provides a more convenient framework. Our findings, however, provide essential ingredients to the *interpretation* of such semiclassical theories, in the sense that "direct" and "resonance-assisted" processes ought to be somehow represented in relevant combinations of such complex orbits. Moreover, specific quantitative predictions for tunneling rates, using only easily accessible quantities of the classical dynamics of the system, can be made on the basis of our approach, provided $\hbar$ is small enough for the most dominant resonance to become relevant (which is roughly the case if $\ell/2$ states fit into the island). We therefore believe that the principle of resonance-assisted couplings will represent the relevant paradigm also in the context of more complex dynamical tunneling processes, e.g., within systems that have two or more degrees of freedom.

ACKNOWLEDGMENTS

It is a pleasure to thank Denis Ullmo for sharing with us his extensive experience on tunneling. A.M. acknowledges the generous hospitality of Dominique Delande at Laboratoire Kastler-Brossel and his relevant remarks after reading the first proof of this manuscript. P.S. acknowledges support from the Bayerisch-Französisches Hochschulzentrum (BFHZ) and from the Deutsche Forschungsgemeinschaft (DFG).

[1] W. A. Lin and L. E. Ballentine, Phys. Rev. Lett. **65**, 2927 (1990).
[2] F. Grossmann, T. Dittrich, P. Jung, and P. Hänggi, Phys. Rev. Lett. **67**, 516 (1991).
[3] A. Mouchet, C. Miniatura, R. Kaiser, B. Grémaud, and D. Delande, Phys. Rev. E **64**, 016221 (2001).
[4] W. K. Hensinger, H. Häffner, A. Browaeys, N. R. Heckenberg, K. Helmerson, C. McKenzie, G. J. Milburn, W. D. Phillips, S. L. Rolston, H. Rubinsztein-Dunlop, and B. Upcroft, Nature (London) **412**, 52 (2001).
[5] D. A. Steck, H. O. Windell, and M. G. Raizen, Science **293**, 274 (2001).
[6] W. K. Hensinger, A. Mouchet, P. S. Julienne, D. Delande, N. R. Heckenberg, and H. Rubinsztein-Dunlop, Phys. Rev. A **70**, 013408 (2004).
[7] C. Dembowski, H.-D. Gräf, A. Heine, R. Hofferbert, H. Rehfeld, and A. Richter, Phys. Rev. Lett. **84**, 867 (2000).
[8] R. Hofferbert, H. Alt, C. Dembowski, H.-D. Gräf, H. L. Harney, A. Heine, H. Rehfeld, and A. Richter, Phys. Rev. E **71**, 046201 (2005).
[9] L. D. Landau and E. M. Lifshitz, in *Quantum Mechanics (Non-relativistic Theory)*, Course of Theoretical Physics Vol. 3 (Pergamon Press, Oxford, 1958).
[10] R. Balian and C. Bloch, Ann. Phys. **84**, 559 (1974).
[11] M. Kuś, F. Haake, and D. Delande, Phys. Rev. Lett. **71**, 2167 (1993).

[12] P. Leboeuf and A. Mouchet, Phys. Rev. Lett. **73**, 1360 (1994).
[13] R. Scharf and B. Sundaram, Phys. Rev. E **49**, R4767 (1994).
[14] S. C. Creagh and N. D. Whelan, Phys. Rev. Lett. **77**, 4975 (1996).
[15] For multidimensional nonseparable but integrable systems, these tori are precisely the relevant classical structures that allow us to generalize JWKB 1D tunneling [38].
[16] A. Shudo and K. S. Ikeda, Phys. Rev. Lett. **74**, 682 (1995).
[17] A. Shudo and K. S. Ikeda, Physica D **115**, 234 (1998).
[18] A. Shudo, Y. Ishii, and K. S. Ikeda, J. Phys. A **35**, L225 (2002).
[19] O. Bohigas, M.-J. Giannoni, and C. Schmit, Phys. Rev. Lett. **52**, 1 (1983).
[20] O. Bohigas, D. Boosé, R. E. de Carvalho, and V. Marvulle, Nucl. Phys. A **560**, 197 (1993).
[21] O. Bohigas, S. Tomsovic, and D. Ullmo, Phys. Rep. **223**, 43 (1993).
[22] S. Tomsovic and D. Ullmo, Phys. Rev. E **50**, 145 (1994).
[23] F. Leyvraz and D. Ullmo, J. Phys. A **29**, 2529 (1996).
[24] O. Brodier, P. Schlagheck, and D. Ullmo, Phys. Rev. Lett. **87**, 064101 (2001).
[25] O. Brodier, P. Schlagheck, and D. Ullmo, Ann. Phys. **300**, 88 (2002).
[26] C. Eltschka and P. Schlagheck, Phys. Rev. Lett. **94**, 014101 (2005).
[27] P. Schlagheck, C. Eltschka, and D. Ullmo, in *Progress in Ultrafast Intense Laser Science I*, edited by K. Yamanouchi, S. L. Chin, P. Agostini, and G. Ferrante (Springer, Berlin, 2006), p. 107.
[28] V. A. Podolskiy and E. E. Narimanov, Phys. Rev. Lett. **91**, 263601 (2003).
[29] A. Mouchet and D. Delande, Phys. Rev. E **67**, 046216 (2003).
[30] B. Chirikov, Phys. Rep. **52**, 263 (1979).
[31] A. J. Lichtenberg and M. A. Lieberman, in *Regular and Stochastic Motion*, Applied Mathematical Sciences Vol. 38 (Springer-Verlag, New York, 1983).
[32] The only difference is that a third resonance term must be added to Eq. (1) in order to fulfill some experimental constraints on the laser's configuration. How this can be done is explained in Refs. [3–5] but the present paper, devoted to theoretical considerations only, will not introduce this irrelevant third term.
[33] M. J. Davis and E. J. Heller, J. Phys. Chem. **85**, 307 (1981).
[34] M. Latka, P. Grigolini, and B. J. West, Phys. Rev. E **50**, 596 (1994).
[35] V. Averbukh, N. Moiseyev, B. Mirbach, and H. J. Korsh, Z. Phys. D: At., Mol. Clusters **35**, 247 (1995).
[36] L. Bonci, A. Farusi, P. Grigolini, and R. Roncaglia, Phys. Rev. E **58**, 5689 (1998).
[37] For the same reason we will not consider the different possible boundary conditions offered by Bloch's theorem. The wave functions in the q representation will always be taken to be strictly 2π spatially periodic, i.e., without acquiring any phase factor when winding around the cylinder.
[38] S. C. Creagh, J. Phys. A **27**, 4969 (1994).
[39] R. E. de Carvalho and A. P. Mijolaro, Phys. Rev. E **70**, 056212 (2004).
[40] R. Roncaglia, L. Bonci, F. M. Izrailev, B. J. West, and P. Grigolini, Phys. Rev. Lett. **73**, 802 (1994).
[41] E. Doron and S. D. Frischat, Phys. Rev. Lett. **75**, 3661 (1995).
[42] S. D. Frischat and E. Doron, Phys. Rev. E **57**, 1421 (1998).
[43] A. M. Ozorio de Almeida, J. Phys. Chem. **88**, 6139 (1984).
[44] R. S. MacKay, J. D. Meiss, and I. C. Percival, Phys. Rev. Lett. **52**, 697 (1984).
[45] K. Hornberger and A. Buchleitner, Europhys. Lett. **41**, 383 (1998).
[46] For this latter case, we have indications that the prominent plateau structure in the level splittings at γ=0.18 (see Fig. 7 in Ref. [3]) is induced by a nonlinear 1/4 resonance that is already contained within the *chaotic* part of the phase space. Since our numerical approach to calculate the coupling matrix element V_0 is perturbative by nature and relies on a well-preserved separatrix structure of the resonance, we are, at present, unable to make a quantitative semiclassical reproduction of this particular plateau.
[47] T. Geisel, G. Radons, and J. Rubner, Phys. Rev. Lett. **57**, 2883 (1986).
[48] N. T. Maitra and E. J. Heller, Phys. Rev. E **61**, 3620 (2000).

I.8 Perspectives à court et moyen termes

a) Des expériences

À ma connaissance, il n'existe pas de projets expérimentaux visant à améliorer les résultats de Dembowski *et al.* (2000), Hensinger *et al.* (2001), Steck *et al.* (2001) en atteignant un régime indiscutablement semiclassique qui permettrait d'observer la transition abrupte de régime, effet tunnel intégrable $\leftrightharpoons$ effet tunnel chaotique, que l'on peut observer sur les figures p. I.5. Par exemple le programme proposé par (Delande & Zakrzewski, 2003) est pour l'instant resté lettre morte. Il faut reconnaître qu'en l'absence d'applications à court terme prometteuses et compte-tenu du coût des expériences, le jeu n'en vaut peut-être plus la chandelle. Diminuer $\hbar$ d'un facteur 10 implique de travailler avec des intensités de laser 100 fois plus élevées (communication privée de W. Phillips) ce qui est prohibitif en l'absence de nouvelles idées (*cf.* cependant le§ I.5). Il faut aussi signaler que les recherches autour de l'information quantique mobilisent plus facilement les chercheurs, les bailleurs de fonds(31) et l'intérêt public. Bref, tant qu'il n'y aura pas de percées théoriques et technologiques notables, il semblerait que les expériences portant directement sur l'étude de l'effet tunnel chaotique soient échouées provisoirement dans le calme plat d'une crique, en attendant une nouvelle marée ou un bon coup de vent.

b) De la théorie

b.1) État des lieux

En revanche, l'activité théorique autour de l'effet tunnel chaotique est plus que jamais extrêmement vivante ; pour ne retenir qu'un seul exemple significatif, en août 2005, fût organisée à Kusatsu (Japon), une conférence dévolue exclusivement aux problèmes liés à la complexification de la dynamique. Elle réunissait pour la première fois autour de ce même thème à la fois des mathématiciens, des physiciens, des chimistes, théoriciens et expérimentateurs venus du monde entier. Cette conférence permit de révéler à beaucoup d'entre-nous une variété de points de vue dont certes nous connaissions l'existence, mais devant lesquels nous n'avions pas pris le temps de nous arrêter jusqu'alors.

Un très grand besoin se fait sentir, me semble-t-il, de nouer des liens explicites entre les différentes approches théoriques, chacune à leur façon et satisfaisante et frustrante, comme le point de vue de l'école japonaise, les approches s'appuyant sur la formule de Herring (Creagh, 1994; Smith & Creagh, 2006), les résultats purement semiclassiques ou hybrides dont il a été question dans ce mémoire(32). On pressent bien, dans ce foisonnement, l'existence d'une certaine unité, mais ces convergences restent, à mes yeux en tous cas, floues et encore trop partielles.

(31) Bill Phillips jubilait à l'idée que ses très belles expériences de physique quantique fondamentale étaient financées en partie par la nsa !

(32) Dans certaines situations qui semblent très spécifiques, d'autres pistes ont été tentée. Par exemple la complexification proposé par Doron & Frischat (1995) dans le cas du billard annulaire.

b.2) Quelques résultats préliminaires quantitatifs encourageants ?

Un programme de recherche dont on ne pourra, comme toujours, véritablement juger la pertinence qu'une fois bien avancé, a pour point de départ une volonté d'approfondir plus outre les relations entre effet tunnel, trajectoires classiques complexes et résonances. En reprenant une vieille idée qui remonte aux instantons (McLaughlin, 1972; Polyakov, 1977; Coleman, 1985; Patrascioiu, 1981; Burgess, 1991, entre autres) et en essayant de comprendre quelques principes qui régissent la complexification, je me suis récemment aperçu que le prolongement analytique du temps τ dans le cas d'une application quantique discrète (*cf.* note 22 p. 24) de la forme

$$\hat{U}(\tau) \;=\; \mathrm{e}^{-\mathrm{i}\tau f(\hat{p})/\hbar}\mathrm{e}^{-\mathrm{i}\tau g(\hat{q})/\hbar} \tag{I.8–1}$$

permettait d'éroder les pics dans le comportement des doublets tunnel $\Delta\varepsilon$ [33]. Plus précisément, en supposant l'existence d'une symétrie $\hat{S}$, disons représentant la parité $(p,q)\mapsto(-p,-q)$, commutant avec $\hat{U}(\tau)$, le spectre de ce dernier est constitué de doublets $\{u_n^{\pm}\}$ à partir desquels on peut définir les quasi-énergies complexes

$$\varepsilon_n^{\pm} \;\stackrel{\text{def}}{=}\; \frac{\mathrm{i}\hbar}{\tau}\ln(u_n^{\pm}) \tag{I.8–2}$$

et les doublets (insensibles à l'ambiguïté provenant de la détermination du logarithme)

$$\Delta\varepsilon_n \;\stackrel{\text{def}}{=}\; \varepsilon_n^- - \varepsilon_n^+ \,. \tag{I.8–3}$$

Dans une perspective semiclassique, la dynamique classique associée sera gouvernée par l'application $\Phi : (p_0,q_0)\mapsto(p_1,q_1)$ définie par les équations de Hamilton discrètes :

$$\Phi\begin{cases} p_1 = p_0 - \tau g'(q_0)\,; \\ q_1 = q_0 + \tau f'(p_1)\,. \end{cases} \tag{I.8–4}$$

Quand τ est réel, ces équations engendrent une dynamique génériquement mixte qui devient intégrable lorsque $\tau\to 0$ puisqu'alors le hamiltonien pulsé qui gouverne Φ se lisse en

$$H(p,q)\stackrel{\text{def}}{=} f(p)+g(q) \tag{I.8–5}$$

indépendant de τ.

Il est facile de choisir f et g pour obtenir une situation typique d'effet tunnel chaotique. Le choix du pendule pulsé (*kicked pendulum*) pour lequel Φ est l'application standard (*standard map*), correspondant à

$$f(p)=p^2/2\,; \qquad g(q)=\gamma\cos 2q\,; \quad \gamma\in\mathbb{R}\,, \tag{I.8–6}$$

semble posséder plusieurs avantages :

[33] Mais, faute d'avoir approfondi la littérature, je ne saurais affirmer que c'est la première fois que l'on tente de complexifier le temps dans le cas d'une application discrète.

(i) Classiquement, en repliant l'espace des phases sur un cylindre de période 2π, on obtient effectivement deux points fixes centrés en $p = 0, q = \pm\pi/2$ quel que soit γ et autour desquels s'accrochent des îlots stables tant que

$$\tau \in \left]-1/\sqrt{\gamma}\,,\,1/\sqrt{\gamma}\right[. \tag{I.8–7}$$

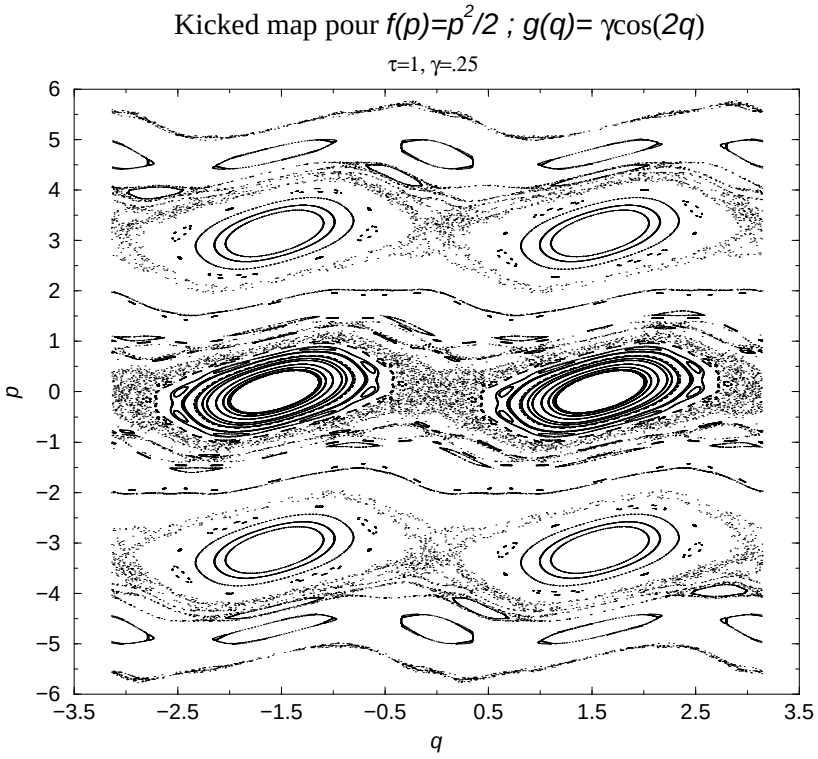

FIG. I.8–1 : *Section de POINCARÉ (réelle) pour le choix* (I.8–6) *avec* $\tau = 1$ *et* $\gamma = 1/4$.

(ii) Il se trouve que la dynamique classique est π-périodique également en p (*cf.* figure I.8–1), ce qui peut présenter une simplification puisque toute l'information sur les trajectoires réelles est contenue alors dans un espace compact([34]).

(iii) Certains aspects de la dynamique classique complexe sont connus, *cf.* figure I.1–9 23 ou (GREENE & PERCIVAL, 1981, Figs. 1 et 3). Plus généralement, beaucoup de propriétés classiques et quantiques de ce modèle sont bien établies dans la littérature.

([34]) Le modèle de HARPER pulsé introduit par LEBŒUF, KURCHAN, FEINGOLD & AROVAS (1990) — pour lequel $f(x) = g(x) \propto \cos x$ — utilisé avec succès pour rendre compte de l'effet tunnel (RONCAGLIA, BONCI, IZRAILEV, WEST & GRIGOLINI, 1994; LEBŒUF & MOUCHET, 1994; BRODIER, SCHLAGHECK & ULLMO, 2001) possède aussi cet avantage. L'inconvénient, s'il en est, réside dans le fait que quantiquement $\hbar$ ne peut varier continûment.

(iv) Une rotation de Wick $\tau = -\mathrm{i}|\tau|$ (voir plus loin) conduit essentiellement à la même dynamique classique réelle translatée de $\pi/2$ en q (contrairement à ce qui se passe pour le problème à double puits). Les instantons ont donc des propriétés qui se calquent sur celles des trajectoires du cas purement réel.

(v) Quantiquement les éléments de matrice de $\hat{U}(\tau)$ se calculent facilement dans la base propre de $\hat{p}$ en terme de fonctions de Bessel, même pour $\tau \in \mathbb{C}$. La diagonalisation numérique est relativement rapide.

(vi) On peut aussi rêver peut-être (*perchance to dream*) en rappelant que des expériences peuvent être conduites avec cette dynamique sous-jacente.

On peut transposer pas à pas à ce système l'analyse faite dans (Mouchet, Eltschka & Schlagheck, 2006) pour τ réel et calculer, en particulier, le comportement de $\Delta\varepsilon_n$ en fonction de $1/\hbar$ (n numérote les états localisés dans les îlots). Les pics aussi bien que les oscillations plus lentes de $\Delta\varepsilon_n$ s'interprètent en terme de résonances quantiques (et probablement classiques) : lorsqu'une ou plusieurs $u_n^{\pm}$ se rapprochent sur le cercle unité (les quasi-énergies $\varepsilon_n^{\pm}$ différent alors quasiment d'une zone de Floquet c.-à-d. d'un nombre entier de fois $2\pi\hbar/\tau$).

Lorsque l'on donne une partie imaginaire à τ ([35]), par exemple en le faisant tourner

$$\tau = |\tau| \mathrm{e}^{-\mathrm{i}\theta}, \tag{I.8–8}$$

les $\{u_n^{\pm}\}$ s'éloignent du cercle unité et se répartissent au voisinage de la spirale logarithmique définie paramétriquement par

$$\mathcal{S}_\tau \overset{\text{def}}{=} \left\{ \mathrm{e}^{-\mathrm{i}\tau s/\hbar}, \quad s \in \mathbb{R} \right\}. \tag{I.8–9}$$

Compréhensible dans le cas quasi-intégrable (γ ou τ petits), cette observation persiste même dans le régime fortement chaotique correspondant à la section de Poincaré I.8–1, *cf.* la figure I.8–2. Ainsi, en «éclatant» le cercle unité, on dispose d'un moyen de séparer des valeurs propres les unes des autres et de détruire les résonances quantiques. C'est bien ce que l'on observe sur les graphes de $|\Delta\varepsilon_0|$ (*cf.* figure I.8–3). Pour τ réel ($\theta = 0$), on reconnaît le comportement déjà rencontré des fluctuations géantes : pics et oscillations plus lentes en échelle semi-logarithmique plutôt qu'un comportement linéaire à la Wilkinson (équations I.1–2 ou (I.1–6)). Donner une toute petite partie imaginaire à τ ($\theta \sim 10^{-3}$) suffit à éroder les pics les plus pointus. Pour $\theta \simeq 0.03$ seules les lentes oscillations ont résisté à l'érosion puis les courbes convergent rapidement vers une décroissance linéaire dont la pente se stabilise à partir d'une valeur de θ que l'on peut estimer à quelques fractions de π (en tous cas bien avant $\pi/4$). La figure (I.8–4) permet de se convaincre que les pentes limites $-A(\gamma)$ de ces droites sont en accord avec la loi

$$A(\gamma) \simeq 4\sqrt{\gamma}\,. \tag{I.8–10}$$

([35]) Par un argument semiclassique, on comprend qu'il faille la choisir négative pour avoir un opérateur $\hat{U}(\tau)$ borné à un facteur multiplicatif inessentiel près (mais on perd bien sûr l'unitarité).

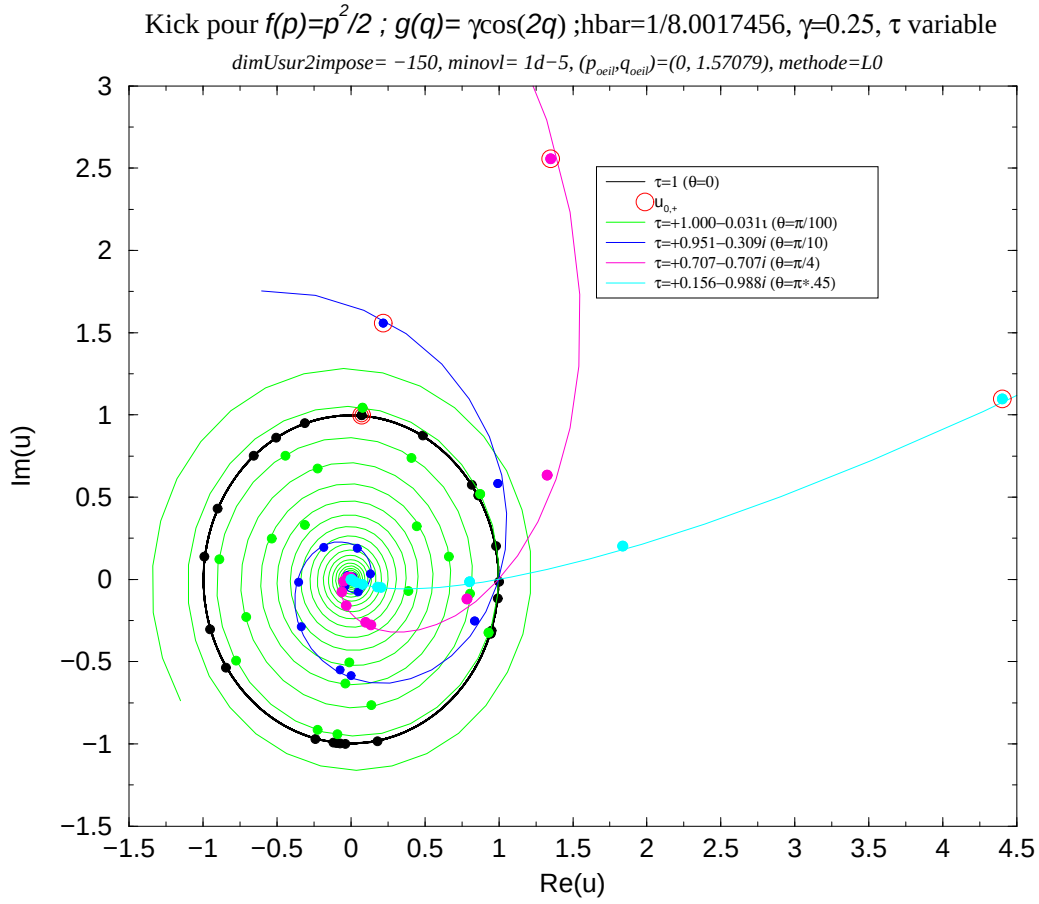

FIG. I.8–2 : *(couleur recommandée) Répartition dans le plan complexe des valeurs propres de* $\hat{U}(\tau)$ *pour différentes valeurs de l'angle de rotation* θ *(équation* (I.8–8)*) et pour le pendule pulsé. Les valeurs* $|\tau| = 1$ *et* $\gamma = 1/4$ *sont les mêmes que pour la figure I.8–1 et l'on a choisi* $1/\hbar \simeq 8.0$*. Les disques pleins sont les valeurs propres* $\{u_n^{\pm}\}$ *(les doublets tunnel ne peuvent être résolus à cette échelle, on peut voir sur la figure I.8–3 qu'ils sont de l'ordre de* 10^{-6} *pour* $\theta = 0$*) et l'on entoure d'un cercle la valeur propre* u_0^+ *correspondant à l'état ayant le plus grand recouvrement avec un état cohérent centré sur* $(p = 0, q = \pm\pi/2)$*. Les courbes continues sont les spirales* (I.8–9).

Non seulement la rotation (I.8–8) conduit à une loi du genre (I.1–2), mais encore, il est facile de vérifier que (I.8–10) correspond à l'action

$$A = \int p(q, E)\, \mathrm{d}q \tag{I.8–11}$$

de l'instanton du modèle continu régi par (I.8–5) et reliant en un temps infini les deux points fixes instables situés en $p = 0$. En vertu de la propriété (iv) énoncée ci-dessus. A représente également la demi-aire de l'un des îlots stables dans la limite intégrable.

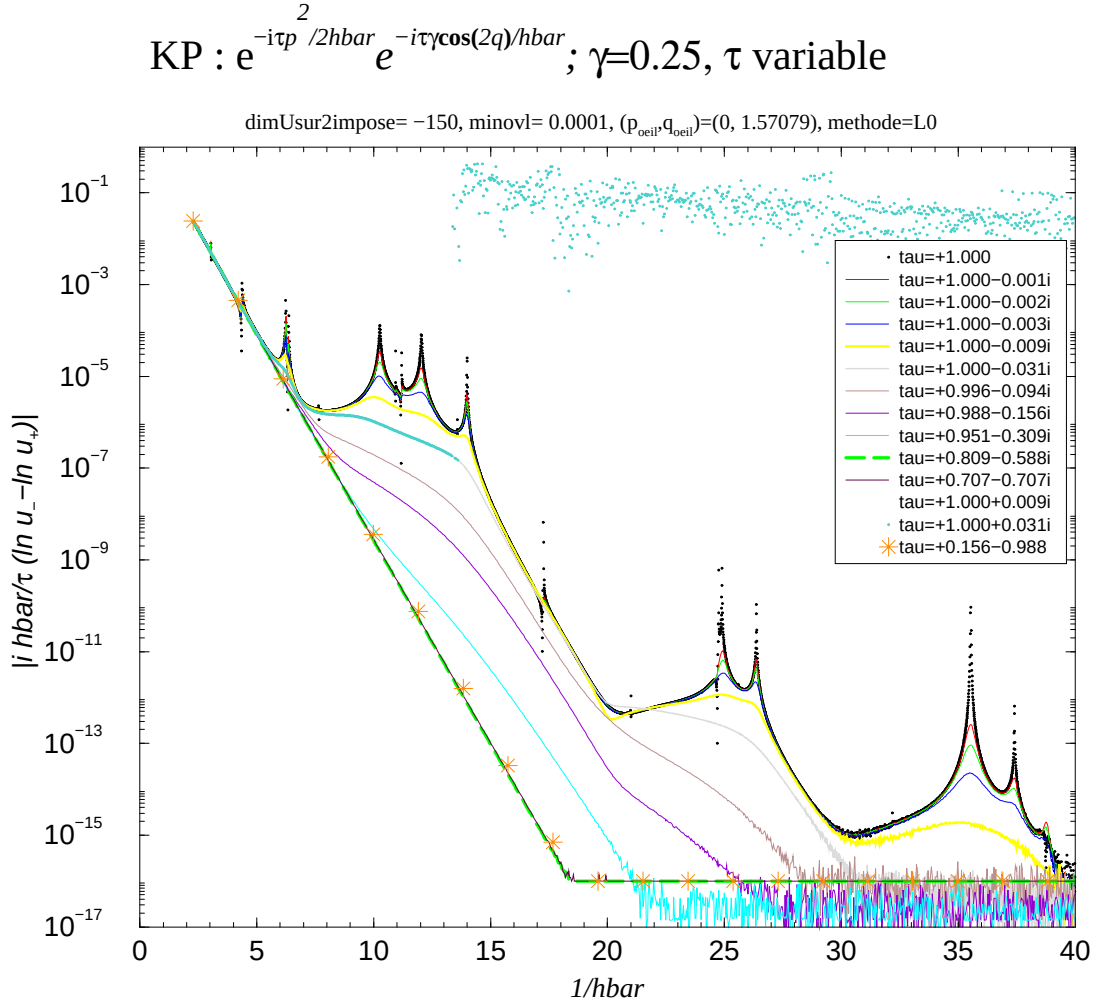

FIG. I.8–3 : *(couleur recommandée) Graphes de $|\Delta\varepsilon_0|$ en fonction de $1/\hbar$ pour différentes valeurs de l'angle de rotation θ. Les valeurs $|\tau| = 1$ et $\gamma = 1/4$ sont les mêmes que pour la figure I.8–1.*

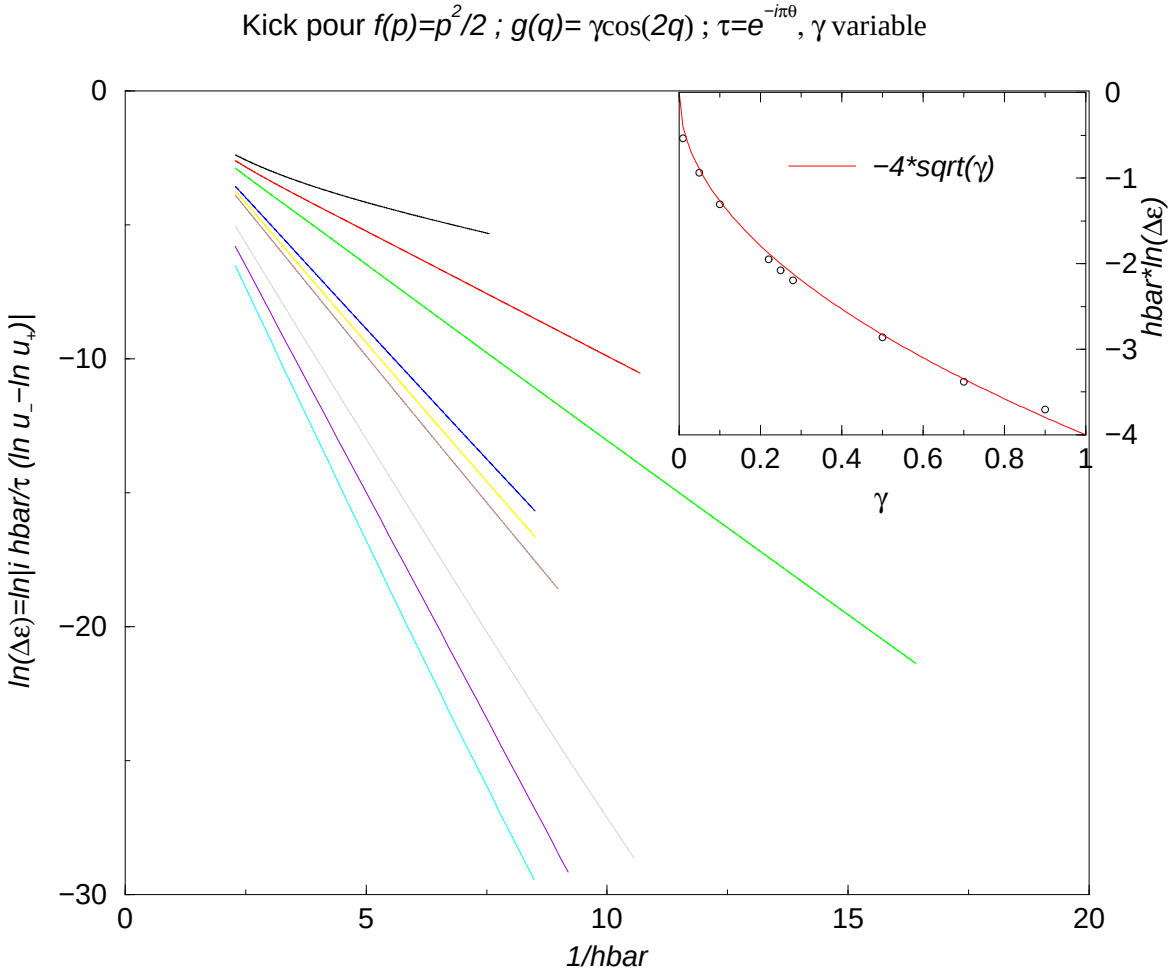

FIG. I.8–4 : *Quand θ croît à partir de zéro, les graphes de $\ln|\Delta\varepsilon_0|$ en fonction de $1/\hbar$ tendent rapidement vers des droites limites. Dans le cadre principal, ces droites sont tracées pour différentes valeurs de γ. Dans l'encart, on reporte les valeurs des pentes en fonction de γ (disques) et l'on constate qu'elles suivent assez correctement la loi* (I.8–10) *(courbe continue) même dans le cas fortement chaotique où $\gamma \lesssim 1$ (pour $\theta = 0$, les îlots tunnels disparaissent en perdant leur stabilité pour $\gamma = 1/\tau^2 = 1$).*

b.3) Quelques questions

Si les résultats présentés ci-dessus peuvent sembler encourageants, leur interprétation reste encore largement à faire et de nombreuses questions se posent. Par exemple,

(i) Comment caractériser précisément la dynamique classique complexe obtenue lors d'une rotation (I.8–8) ? C'est-à-dire les orbites qui extrémalisent une fonctionnelle du genre

$$S[p,q] \stackrel{\text{def}}{=} \int_0^1 \Big[p(s)\frac{\mathrm{d}q}{\mathrm{d}s} - |\tau| \mathrm{e}^{-\mathrm{i}\theta} H\big(p(s),q(s)\big)\Big]\mathrm{d}s\,, \tag{I.8–12}$$

où sa version discrète adaptée aux applications Φ données par (I.8–4),

$$S\big(\{p_n\},\{q_n\}\big) \stackrel{\text{def}}{=} \sum_n \big[p_{n+1}(q_{n+1}-q_n) - |\tau| \mathrm{e}^{-\mathrm{i}\theta} H(p_{n+1},q_n)\big]\,. \tag{I.8–13}$$

(ii) En particulier, comment se fait-il que la complexification de τ dont on s'attend qu'elle déstabilise génériquement les orbites périodiques stables[36] conduit, du moins tant que les doublets sont concernés, à un comportement qui ressemble étrangement à celui qu'on attendrait d'un système intégrable ?

(iii) D'après ce qui précède, on retrouve une théorie de type instanton. Il semblerait donc que ce soient les orbites *primitives* de périodes très longues qui jouent un rôle. Est-ce que cela ne serait pas un signe qu'il est illusoire de chercher un développement semiclassique ordonné suivant les périodes croissantes des orbites primitives ? Par exemple à partir de l'estimation du type[37]

$$\Delta\varepsilon_0 \;\sim\; \frac{2\mathrm{i}\hbar}{N\tau}\,\frac{\mathrm{tr}\,\big(\hat{S}\hat{U}^N(\tau)\big)}{\mathrm{tr}\,\big(\hat{U}^N(\tau)\big)} \tag{I.8–15}$$

pour N entier avec $N\,\mathrm{Im}\,\tau$ assez grand pour que le doublet (u_0^+,u_0^-) soit suffisamment éloigné des autres doublets (*cf.* figure I.8–2) pour les dominer exponentiellement même dans la trace de $\hat{S}\hat{U}^N(\tau)$.

(iv) Pourquoi les courbes $\Delta\varepsilon(1/\hbar)$ convergent-t-elles si rapidement vers le résultat donné par l'instanton intégrable bien avant que la rotation de Wick ne soit achevée ?

---

(36) Pour τ complexe les traces des matrices de monodromies $\mathrm{tr}\,M^n = 2\cosh(n\tau\lambda)$ partent génériquement dans le plan complexe. en particulier, la condition de stabilité (I.8–7) n'est plus remplie, même si $|\tau| < 1/\sqrt{\gamma}$.

(37) $\hat{S}$ est la symétrie tunnel. Il n'est pas absolument certain que l'estimation (I.8–15) soit correcte à cause des batailles d'exponentielles. Des vérifications numériques restent à faire pour s'assurer que dans

$$\mathrm{tr}\,\big(\hat{S}\hat{U}^N(\tau)\big) = \sum_n \Big(\mathrm{e}^{-\mathrm{i}N\tau\varepsilon_n^+/\hbar} - \mathrm{e}^{-\mathrm{i}N\tau\varepsilon_n^-/\hbar}\Big)\,, \tag{I.8–14}$$

on puisse trouver un régime où ce soient les termes pour $n=0$ qui dominent.

(v) Dans quelle mesure ces observations dépendent-ils du modèle ? Suivant une suggestion de Dominique Delande il faudrait en premier lieu s'assurer que les observations qui précèdent ne découlent pas simplement de la structure en p^2 du choix de f. Changer le terme cinétique en $f(p) \propto p^4$ est particulièrement intéressant pour tenter de préserver une résonance pour toute valeur de θ. En effet, il se trouve que, dans ce cas, l'origine est toujours un point marginalement stable $\operatorname{tr} M = 2$. Les courbes limites obtenues par rotation de θ ne s'écrasent pas en droites mais ont une structure plus riche qui trahit, j'en suis persuadé (une analyse par les représentations de Husimi devrait se faire à très court terme), la présence d'une résonance persistance c.-à-d. d'un état Janus qui s'accroche sur l'origine.

(vi) Comment recomposer ces questions dans le cadre de l'effet tunnel amplifié par résonance (classique) et s'assurer que les cascades fractales de résonances classiques qui sont à l'origine du chaos reflètent la forêt de pics ? Comment comprendre que la rotation de τ de la dynamique classique complexe semble estomper assez rapidement les résonances classiques réelles.

(vii) Quels liens établir avec la complexification des formes normales au voisinage des bifurcations où naissent les résonances (Bazzani & Turchetti, 1992) ?

(viii) Quels liens établir avec les ensembles de Julia de l'école japonaise ?

(ix) Quels liens établir avec la littérature récente sur l'effet tunnel multidimensionnel (Benderskii, Vetoshkin, Kats & Trommsdorff, 2003, et ses références) et le seul travail, à ma connaissance, qui évoque les instantons en régime chaotique (Kuvshinov, Kuzmin & Shulyakovsky, 2003).

On peut également songer à d'autres questions à beaucoup plus longue échéance, encore largement spéculatives, comme :

(x) Si ces résultats se renforcent et se comprennent mieux, est-ce que cela n'implique pas qu'il faille prendre la rotation de Wick avec des pincettes quand on affirme, comme très souvent en théorie quantique des champs relativistes, qu'il suffit de faire une rotation de Wick pour transposer aisément les résultats en métrique euclidienne vers la métrique minkowskienne et réciproquement ? Déjà, dans les systèmes ayant le moins de degrés de liberté possible, les effets des non-linéarités peuvent être affectés sur plusieurs ordres de grandeurs par une rotation de Wick (voir aussi la note 15 p. 19).

À l'interface avec les mathématiques :

(xi) Peut-on faire progresser notre compréhension des propriétés spectrales des opérateurs de type (I.8–1). En particulier, peut-on comprendre la disparition des résonances à partir des généralisations des formules de Campbell-Baker-Hausdorff faisant explicitement apparaître le problème des petits dénominateurs (Scharf, 1988, eq. 2.13') ?

c) Interactions

On voit donc se profiler un programme de recherche précis qui nécessitera à coup sûr un travail collectif impliquant de nombreux acteurs. L'arrivée à Tours, à la rentrée 2006 de l'un des trois pionniers de l'effet tunnel amplifié par résonance, Olivier Brodier, laisse espérer qu'ensemble, nous pourrions engager une collaboration fructueuse. Par ailleurs, certaines des questions ci-dessus peuvent raisonnablement motiver un travail de thèse qui peut être initié au préalable par le stage à temps complet d'un semestre qu'offre la seconde année du master recherche *Phénomènes non-linéaires* de Tours (*cf.* aussi § 6 c) p. 8).

Il n'est pas impossible non plus que les spécialistes du laboratoire en théorie des champs, particulièrement les experts des systèmes intégrables n'aient pas leur mot à dire à propos, par exemple du point (x). Les mathématiciens du laboratoire issus de la théorie spectrale peuvent être aussi concernés par le point (xi). Comme toujours, les discussions informelles qui électrisent la vie d'un laboratoire ouvrent des perspectives que souvent l'on attendait pas.

Bien entendu, les liens étroits que j'entretiens depuis dix ans avec l'équipe de *Dynamiques des systèmes coulombiens* de Dominique Delande du Laboratoire Kastler-Brossel (Paris) continueront de plus belle. En particulier, avec Benoît Grémaud, nous essayons actuellement de nous attaquer aux questions (v) et (vi).

La proximité de l'un des groupes de chaos quantique les plus dynamiques (forcément !) du monde, au Laboratoire de Physique Théorique et de Modèles Statistiques autour d'Oriol Bohigas, Eugène Bogomolnyi, Patricio Lebœuf et Denis Ullmo (avec une pensée émue pour le regretté Charles Schmit qui vient de nous quitter en septembre 2006) est la garantie d'une source de discussions toujours nourrissantes.

À partir des trois sommets de ce triangle français (Tours, Paris, Orsay), on peut d'ores et déjà voir se tisser des liens européens avec l'Allemagne grâce à mes collaborateurs directs, Peter Schlagheck, Christopher Eltschka, mais aussi Andreas Buchleitner chef d'équipe du groupe *Nonlinear Dynamics in Quantum Systems* du *Max Planck für Physik Komplexer Systeme* de Dresde, directeur de post-doc d'O. Brodier et le Royaume-Uni par l'intermédiaire de Stephen Creagh de la *School of Mathematical Sciences Division of Theoretical Mathematics* de Nottingham. Compte-tenu des affinités thématiques et humaines qui nous lient, j'envisage mal un avenir scientifique sans une collaboration avec chacun d'entre eux.

Élargissons encore plus le cercle disciplinaire et l'orbe géographique : en septembre 2006, j'ai été invité par Akira Shudo de la *Tokyo Metropolitan university* à participer, avec K.S. Ikeda, K. Takahashi, Y. Ishii, W.H. Miller, E. Bedford, S. Marmi, S.C. Creagh à l'élaboration d'un projet sur l'*effet tunnel chaotique* d'une durée de deux ou trois ans, visant à obtenir le soutien du ministère de la science japonais pour financer des voyages et des conférences internationales sur ce sujet.

La méthode différentielle

II.1 Le contexte

La méthode différentielle est une technique qui vise à encadrer toute valeur propre d'un opérateur (ou d'une matrice) dont le vecteur propre associé est réel et ne change pas de signe (propriété de positivité). En quantique, il s'agira essentiellement de donner à la fois une borne supérieure et inférieure à l'énergie fondamentale d'un système dont il est inutile, ici, de rappeler l'importance physique. Cette méthode se démarque très nettement d'autres approches, perturbatives ou variationnelles, qui remontent à Rayleigh au moins et largement éprouvées depuis (sans oublier les algorithmes de diagonalisation directe). Elle ne fait intervenir aucune intégrale ou calcul de norme, ce qui est à priori un avantage lorsque les espaces de configuration possèdent de multiples dimensions, comme typiquement un problème à N corps ou à fortiori une théorie des champs. L'information globale sur l'espace de configuration contenue dans la valeur propre recherchée se retrouve dans la détermination des extrémums globaux d'une fonction donnée explicitement, $q \mapsto E_{\text{loc}}(q)$, l'énergie locale dans le cas quantique. Ces extrémums correspondent précisément aux bornes cherchées.

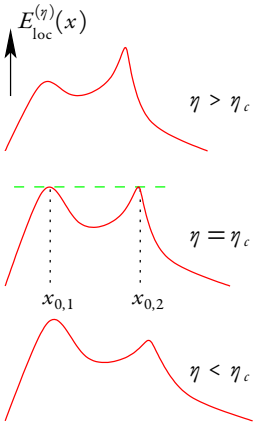

Fig. II.1–1 : *Exemple de bifurcation globale (Arnold, 1984, chap. 10). En variant le paramètre de contrôle η, il se produit un échange de maximums globaux sans que ce dernier puisse être détecté localement.*

Dans les espaces multidimensionnels, on n'a pas forcément gagné au change : il peut être aussi difficile, si ce n'est plus, de déterminer analytiquement ou numériquement un extrémum absolu qu'une intégrale. L'avantage est qu'une fois ces extrémums déterminés, la méthode différentielle permet au moins en principe d'améliorer substantiellement les bornes à coup de ravaudage local tant que l'opération ne provoque pas de bifurcations globales où un échange d'extrémums de $q \mapsto E_{\text{loc}}(q)$ se produit. Pour contourner cette difficulté il faudrait déterminer aussi tous les extrémums locaux, ce qui peut être prohibitif si l'algorithme les multiplie un peu trop rapidement (*cf.* figure 2 p. 110). D'un certain point de vue, la méthode différentielle tend à rester aussi locale que possible, d'où le choix du qualificatif qui fait référence également à la géométrie différentielle, cadre naturel de la théorie des bifurcations et autres catastrophes (Demazure, 1989, l'un des cours de mathématiques les mieux écrits que je connaisse).

L'idée de départ, due à Hector GIACOMINI du LMPT (communication privée 2004) était d'utiliser la propriété de positivité dans le cas d'une équation de SCHRÖDINGER à une dimension avec un potentiel polynômial pour trouver, à partir de fonctions d'essai φ, des inégalités algébriques imposées par la nécessité d'avoir au moins un zéro réel pour un certain polynôme ; ces inégalités permettaient alors d'obtenir des bornes pour le niveau fondamental. En fait, il s'est avéré que non seulement on obtenait systématiquement des bornes supérieures et inférieures mais que l'on y parvenait par un argument ridiculement simple, capable d'être étendu à des potentiels quelconques en dimension quelconque sans que, d'ailleurs, l'opérateur soit nécessairement un opérateur de SCHRÖDINGER. En fait, comme l'avait déjà soupçonné H. GIACOMINI, le point clef nécessaire était bien la propriété de positivité. Il est apparu qu'elle est dans une très large mesure suffisante. Du coup, on pouvait espérer obtenir des résultats intéressants, même en physique, pour des systèmes multidimensionnels complexes où les méthodes traditionnelles progressent avec peine et prix. Il était clair dès le début que la jeune méthode différentielle ne pourrait jamais faire mieux que les méthodes traditionnelles dans les cas à petit nombre de degrés de liberté(1).

En fait, les inégalités obtenues par la méthode différentielle apparaissent comme une très large généralisation d'inégalités dues à BARTA (1937) qui concernaient au départ le mode fondamental de vibration d'un billard bi-dimensionnel (valeur propre principale du laplacien). Les inégalités de BARTA sont très connues et utilisées dans la littérature mathématique en théorie spectrale ; elles ont été généralisées à des opérateurs de LAPLACE agissant sur des fonctions de carré intégrable définies sur des variétés riemanniennes, ou encore à des opérateurs de SCHÖDINGER de la forme $-\Delta + V$. Mais si, dans ce dernier cas, la littérature est relativement clairsemée (une demi-douzaine d'articles depuis la promesse, apparemment non tenue de BARTA, de généraliser ses résultats originaux), c'est parce que non seulement la dérivation des inégalités, reposait trop fortement sur la spécificité des formes quadratiques, mais encore qu'aucun des auteurs pré-cités n'avait en tête la stratégie que je décris dans l'article qui suit (très souvent l'une des deux bornes était perdue) et qui a permis dès les premières tentatives d'application d'améliorer notablement les résultats existants.

La démonstration, en quelques lignes, que je donne dans les trois articles de ce chapitre et ne retenant, je l'ai dit, que l'hypothèse de positivité, n'a étonnamment jamais été formulée explicitement à l'exception du cas matriciel de la référence (BARNSLEY & DUFFIN, 1980) signalée par un rapporteur bienveillant de l'article (MOUCHET, 2006B) et dont on comprendra aisément par son titre pourquoi elle avait échappé à mes moteurs de recherche.

(1) À titre d'exemple, citons la détermination numérique par le groupe de D. DELANDE des niveaux d'énergie des systèmes coulombiens à trois corps (hélium, la molécule H_2^+) avec un nombre de chiffres significatifs pouvant dépasser la quadruple précision. Par comparaison, dans le cas de l'atome d'hydrogène en champ magnétique, l'encadrement que je propose sur la figure 1 p. 109 peut faire pâle figure si l'on se cantonne au résultat brut.

La propriété de positivité de la fonction d'onde du fondamental est bien connue pour les opérateurs de Schrödinger sous le nom de théorème de Krein-Rutman([2]) ou des matrices à coefficients positifs (théorème de Perron-Frobenius).

II.2 Une méthode différentielle pour encadrer l'énergie de l'état fondamental

Il s'agit ici du premier article sur le sujet, plutôt élémentaire et aussi peu technique que possible. Il présente les premiers exemples non triviaux de l'application de la méthode différentielle auxquels j'ai pensés. Il s'agit, on ne s'en étonnera pas, de dynamique complexe des systèmes simples, cas d'écoles du chaos quantique suffisamment différents pour couvrir un spectre assez large de situations (billard annulaire, atome d'hydrogène en champ magnétique, problème coulombien). Après de nombreux tâtonnements, il s'est avéré que finalement le cas coulombien avec charges électriques était très subtil à traiter (sauf à deux corps !). Rien que pour l'hélium, la méthode différentielle ne conduit pas à des résultats très excitants et surtout semble résister à toutes mes tentatives d'amélioration des bornes, pour des raisons auxquelles j'appris à m'habituer plus tard (Mouchet, 2006a) : les répulsions inévitables le rendent trop fragile. Pour finir, ce n'est que sur un exemple trop simple (comme par hasard, le double puits à une dimension) que je suis parvenu à des résultats concrets concernant la mise en œuvre d'un algorithme possible (mais trop primitif). J'essaie de discuter les problèmes de convergence de l'« algorithme de principe » qu'offre la méthode. La publication de cet article a influencé, de son propre aveu, Handy (2006) qui propose de contourner certains obstacles liés à l'algorithme en question par la méthode des moments.

En plus de l'impulsion initiale fournie par H. Giacomini, j'ai pu bénéficier ici des calculs numériques exacts de D. Delande et B. Grémaud (lkb) et d'une discussion féconde avec Michel Caffarel (alors au Lab. de Chimie Théorique de l'université Paris-6).

([2]) Par souci de complétude je rappelle brièvement l'argument : Si $\Phi_0(q)$ est la fonction d'onde fondamentale du hamiltonien $H = -\Delta + V(q)$ agissant sur les fonctions de carré intégrable s'annulant sur le bord $\partial\mathcal{Q}$ de l'espace de configuration, alors, quitte à la combiner avec Φ_0^*, autre fonction propre de H, on peut supposer Φ_0 réelle et de norme unité. Elle donne un minimum absolu à la fonctionnelle $E[\Phi] \stackrel{\text{def}}{=} \langle\Phi|H|\Phi\rangle = \int_{\mathcal{Q}}(-\Phi^*\Delta\Phi + V|\Phi|^2)\mathrm{d}q$. La dérivation de la valeur absolue produit une distribution de Dirac ayant pour support $\mathcal{Z}$, l'ensemble des zéros de Φ_0 à l'intérieur de $\mathcal{Q}$: $\Delta|\Phi_0| = \mathrm{sgn}(\Phi_0)\Delta\Phi_0 + 2\,\delta(\Phi_0)(\boldsymbol{\nabla}\Phi_0)^2$. Cette distribution ne modifie pas $E[|\Phi_0|]$ parce que, précisément, elle intervient comme un produit avec $|\Phi_0|$. La fonction $|\Phi_0|$ est donc elle aussi une fonction d'onde fondamentale de H. L'équation aux valeurs propres écrite pour $|\Phi_0|$ fait apparaître le terme en $\delta(\Phi_0)(\boldsymbol{\nabla}\Phi_0)^2$ supplémentaire qui doit donc s'annuler identiquement, c.-à-d. que $\boldsymbol{\nabla}\Phi_0$ s'annule précisément sur $\mathcal{Z}$. Le théorème de Green, permettant de reconstruire Φ_0 en tous points à partir de Φ_0 et de son gradient donnés sur une sous-variété de $\mathcal{Q}$ de codimension un, montre qu'alors Φ_0 est identiquement nulle si l'on choisit $\mathcal{Z}$ comme étant cette sous-variété où à la fois Φ_0 et $\boldsymbol{\nabla}\Phi_0$ s'annulent. La seule situation possible est que $\mathcal{Z}$ soit vide, ce qui implique, puisque Φ_0 est continue, que la propriété de positivité est vérifiée pour Φ_0. On voit que cet argument repose crucialement sur la structure purement quadratique de l'énergie cinétique et donc qu'il n'est pas immédiatement applicable à des hamiltoniens plus généraux comme ceux impliquant un champ magnétique.

INSTITUTE OF PHYSICS PUBLISHING JOURNAL OF PHYSICS A: MATHEMATICAL AND GENERAL

J. Phys. A: Math. Gen. **38** (2005) 1039–1047 doi:10.1088/0305-4470/38/5/006

A differential method for bounding the ground state energy

Amaury Mouchet

Laboratoire de Mathématiques et de Physique Théorique (CNRS UMR 6083), Université François Rabelais Avenue Monge, Parc de Grandmont 37200 Tours, France

E-mail: mouchet@phys.univ-tours.fr

Received 20 October 2004, in final form 25 November 2004
Published 19 January 2005
Online at stacks.iop.org/JPhysA/38/1039

Abstract

For a wide class of Hamiltonians, a novel method for obtaining lower and upper bounds for the lowest energy is presented. Unlike perturbative or variational techniques, this method does not involve the computation of any integral (a normalization factor or a matrix element). It just requires the determination of the absolute minimum and maximum in the whole configuration space of the local energy associated with a normalizable trial function (the calculation of the norm is not needed). After a general introduction, the method is applied to three non-integrable systems: the asymmetric annular billiard, the many-body spinless Coulombian problem, the hydrogen atom in a constant and uniform magnetic field. Being more sensitive than the variational methods to any local perturbation of the trial function, this method can be used to systematically improve the energy bounds with a local skilled analysis; an algorithm relying on this method can therefore be constructed and an explicit example for a one-dimensional problem is given.

PACS numbers: 03.65.Db, 05.45.Mt, 02.30.Tb

1. Introduction

In a large variety of interesting physical problems, finding the discrete spectrum of an operator can be done with approximate methods only. Moreover, in most cases, it is a rather difficult task to estimate errors. Perturbative techniques often lead to non-convergent series and an evaluation of the discrepancies with the exact result is usually beyond their scope. For semibounded operators (bounded from below, say), variational methods naturally provide upper bounds for the lowest eigenvalue and require much more work for providing a lower bound with Temple-like methods (Reed and Simon 1978, XIII.2). Another source of difficulties when dealing with perturbative and/or variational techniques, is that they both involve the calculation of integrals on the configuration space $\mathcal{Q}$: the norm of the wavefunctions

0305-4470/05/051039+09$30.00

and some matrix elements of operators. This reflects the fact that the discrete spectrum of a differential operator encapsulates some global information on $\mathcal{Q}$ within the boundary conditions imposed on the normalizable wavefunctions. In this paper, I want to propose an approximate method that will overcome these two obstacles: it can rigorously provide both lower and upper bounds without any kind of integration. Like the variational techniques, it will involve a (set of) trial normalizable function(s) with the appropriate boundary conditions and will concern in practice the lowest eigenvalue only. The bounds are given by the absolute extrema of a function defined on $\mathcal{Q}$ (the so-called local energy). In a sense, this method allows us to stay as local as possible in the configuration space $\mathcal{Q}$: in order to improve the bounds, a local analysis near the extrema (or near the possible singular points) of the local energy is sufficient and necessary. This paper is organized as follows. In section 2, I give the proof of the inequalities that will be the starting point of the differential method. A comparison with what already exists in the literature follows and the guidelines of the method are presented. Sections 3, 4 and 5 show how the method can be applied to three non-integrable quantum systems. Before the concluding remarks, in section 6, I explicitly show on the quartic oscillator how the sensitivity of the differential method to local perturbations of the trial functions can be exploited to systematically improve the bounds of the ground state energy with an elementary algorithm.

2. Bounding the ground state energy with the local energy

Let us start with a quantum system whose Hamiltonian $\hat{H}$ acts on the Hilbert space of functions defined on a configuration space $\mathcal{Q}$. Let us suppose that $\hat{H}$ has an eigenstate $|\Phi_0\rangle$ associated with an element E_0 of the discrete spectrum. For any state $|\varphi\rangle$, the Hermiticity of $\hat{H}$ implies the identity $\langle\Phi_0|(\hat{H}-E_0)|\varphi\rangle = 0$. If we choose $|\varphi\rangle$ such that its configuration space representation $\varphi(q)$ is a smooth real normalizable wavefunction, we obtain

$$\int_{\mathcal{Q}} \Phi_0^*(q)(H - E_0)\varphi(q)\,\mathrm{d}q = 0. \tag{1}$$

The crucial *positivity hypothesis* is to assume that we can choose one eigenstate such that its eigenfunction Φ_0 remains real and positive or zero in the whole $\mathcal{Q}$. This generally applies to the ground state for which it has been shown in many cases that it is strictly positive in the interior of $\mathcal{Q}$ (Reed and Simon 1978, XIII.12). Then, the real part of (1) involves an integrand that is a smooth, real function constructed from the real part H_R of the differential operator H. Then there exists a q in $\mathcal{Q}$ such that $\Phi_0(q)(H_R - E_0)\varphi(q)$ changes its sign. Therefore,

$$\exists q \in \mathcal{Q} \quad \text{such that} \quad (H_R - E_0)\varphi(q) = 0. \tag{2}$$

Let us now introduce a function on $\mathcal{Q}$ that is known as the *local energy*[1]

$$E_{\mathrm{loc}}^{[\varphi]}(q) \stackrel{\mathrm{def}}{=} \frac{H_R\varphi(q)}{\varphi(q)}. \tag{3}$$

From condition (2), we immediately obtain that for all smooth real and normalizable states φ,

$$\inf_{\mathcal{Q}}\left(E_{\mathrm{loc}}^{[\varphi]}(q)\right) \leqslant E_0 \leqslant \sup_{\mathcal{Q}}\left(E_{\mathrm{loc}}^{[\varphi]}(q)\right). \tag{4}$$

Surprisingly, these two inequalities are sparsely known in the literature (Barnsley 1978, Baumgartner 1979, Thirring 1979, Crandall and Reno 1982, Schmutz 1985) and always under some more restricted conditions (the upper bound is often missing).

[1] The usual motivation for introducing the local energy is just to roughly estimate the dispersion in energy obtained for an approximated eigenfunction. For instance, when using Monte Carlo methods for computing expectation values. The derivation of inequality (4) shows that for the ground state this qualitative approach can be made rigorous.

The original proof presented here links the inequalities to the non-negativity of the ground state without referring to the detailed structure of the Hamiltonian. In particular, it does not require the Hamiltonian to have the purely quadratic form

$$\hat{H} = \sum_{i,j} a_{i,j}\,\hat{p}_i\,\hat{p}_j + V(\hat{q}) \tag{5}$$

where a is a definite positive real matrix and V a well-behaved potential. Inequalities (4) still apply (with the appropriate definition (3) of the local energy) in the presence of a singular potential, when there is a magnetic field and for an infinite number of freedoms (as in the non-relativistic quantum field describing a BEC condensate). Besides, it is not required for φ to be nonvanishing. It simply says that where φ vanishes faster than $H_R\varphi$, one or both of the bounds can be infinite and therefore useless.

The first form of inequalities (4) (with its two bounds) is due to Barta (1937) and was derived for the fundamental vibration mode of an elastic membrane. Though Barta writes that his method will be generalized in subsequent publications, I was not able to find any extensions of his original work before an article of Duffin (1947) where a Schrödinger operator of the form $H = -\Delta + V$ is considered. Duffin shows that the Dirichlet boundary conditions imposed on the trial function φ can be relaxed but he loses the upper bound. One obtains the equalities in (4) for a flat local energy, i.e. for $\varphi = \Phi_0$; hence we will try to work with a φ that mimics the exact ground state best. Therefore, generalizing the Barta inequalities by increasing the size of the functional space of φ can be irrelevant. One should instead keep working with a restricted set of trial functions that respects some *a priori* known properties of Φ_0, such as its boundary conditions, its symmetries and its positivity[2].

More precisely, we will explain in the last part of this paper that, once a φ that bounds the local energy is found, it is expected that there is only a *finite* number of independent directions in the functional space along which the bounds can be improved. In the following, we will actually deal with a finite-dimensional submanifold of trial functions φ_λ where λ stands for a small number of control parameters varying in a control space $\mathcal{C}$. Accordingly, the strategy is clear: for, say, obtaining an optimized lower bound we will try to find $\sup_{\lambda\in\mathcal{C}}(\inf_{q\in\mathcal{Q}}(E_{\rm loc}(\lambda;q)))$ where $E_{\rm loc}(\lambda;q)$ stands for $E_{\rm loc}^{[\varphi_\lambda]}(q)$. As long as the extremal values of $q \mapsto E_{\rm loc}(\lambda;q)$ can be followed smoothly with λ (in particular, the Morse points are generically stable), the problem is reduced to local differential calculations in $\mathcal{C}\times\mathcal{Q}$ in the neighbourhood of the critical points: adding to a trial function an infinitesimal perturbation that is localized far away from the extremal point does not affect the energy bounds. One recovers the global sensitivity of the eigenvalue problem because the critical points of the local energy generically bifurcate for finite variations of λ (Poston and Stewart 1978, Demazure 2000) and can jump to other distant points when a degeneracy occurs (Arnold 1984, chapter 10, especially figure 50).

In mathematical physics literature, Barta's inequalities are always considered within the context of the billiards systems (Laplacian spectra on a Riemannian manifold), even in the most recent papers (for instance (Bessa and Montenegro 2004)). As far as I could search, the most advanced extension to other physical problems has been made (tentatively) by Barnsley (1978)

[2] A technicality should be mentioned here: if one chooses the trial states $|\varphi\rangle$ such that for all $q\in\mathcal{Q}$, $\langle q|\varphi\rangle > 0$ except, perhaps, for the *a priori* known zeros of $\langle q|\Phi_0\rangle$, we can deal with systems where the configuration variable q includes some discrete parameter such as a spin index (the somewhat loose notation $H_R\varphi(q)$ must be understood as the real part of $\langle q|\hat{H}|\varphi\rangle$ and $\mathrm{d}q$ is the measure on $\mathcal{Q}$ possibly having a continuous and/or a discrete part). Indeed, under the positivity hypothesis, from (1) we deduce that there must be a couple (q,q') in $\mathcal{Q}^2$ such that $\varphi(q)>0$, $\varphi(q')>0$, $(H_R-E_0)\varphi(q)\geqslant 0$, $(H_R-E_0)\varphi(q')\leqslant 0$. Therefore inequalities (4) remain valid. For instance, if H_R is a (possibly finite) matrix, the local energy consists of a discrete (finite) set of real numbers.

but, for the same reasons as Duffin's (1947), he systematically loses the upper bound. Besides, he acknowledges he is unable to produce any non-trivial bound for the helium atom.

One can easily understand Barnsley's failure: with variational methods, a very rough estimation of the exact ground state wavefunction can lead to a reasonably good agreement for E_0 while a simple local perturbation of the exact wavefunction can even make the local energy unbounded. Therefore, at first sight, one could see the sensitivity of the local energy as a major drawback of the method: variational methods are more robust to local perturbations of the trial function. But this argument can be reversed: compared to the rigidity of the variational methods, the differential method offers the possibility of improving the estimations at low cost provided we are able to implement a skilled strategy (eliminating the singularities, controlling the behaviour at infinity with JWKB techniques, increasing the absolute minima, etc). In the following, I explicitly show in many non-trivial cases that once we have this strategy in mind, we can obtain interesting results for complex systems. For instance, not only can we improve Barnsley's trivial bound for the ground state energy of the helium atom, but it will be shown in section 4 how this result generalizes to any number of Coulombian particles. The calculations can be made analytically with a surprising simplicity.

As far as the upper bound is concerned, the variational method leads *a priori* to a better approximation than the differential method since, for any normalized function φ,

$$\int_{\mathcal{Q}} \varphi^*(q) H\varphi(q)\,\mathrm{d}q = \int_{\mathcal{Q}} |\varphi(q)|^2 E_{\mathrm{loc}}^{[\varphi]}(q)\,\mathrm{d}q \leqslant \sup_{\mathcal{Q}} \left(E_{\mathrm{loc}}^{[\varphi]}(q)\right). \tag{6}$$

Nevertheless, being free of any integration, the absolute maximum of the local energy is a quantity that is more easily accessible to analytical or numerical computations than the average value of H.

3. Application to billiards; the example of the 2D-annular billiard

As a first illustration of the differential method, let us consider the problem of finding the lowest eigenvalue of $H = -\Delta/2$ in a connected finite region $\mathcal{Q}$ with the Dirichlet boundary conditions imposed on $\mathcal{B} \stackrel{\text{def}}{=} \partial\mathcal{Q}$. Suppose that the boundary $\mathcal{B}$ is given by an implicit smooth scalar equation of the form $b(q) = 0$ while the interior of $\mathcal{Q}$ is defined to be the set of points q such that $b(q) < 0$. Then, trial functions can be taken of the form $\varphi = fb$ for any arbitrary smooth function f that does not vanish inside $\mathcal{Q}$. The only possible singular points of $q \mapsto E_{\mathrm{loc}}^{[\varphi]}(q)$ are located on $\mathcal{B}$ and can be removed if f is chosen with appropriate behaviour in the neighbourhood of $\mathcal{B}$. Imposing this behaviour for f is *a priori* a simpler task than solving the eigenvalue problem on the global $\mathcal{Q}$: one dimension has been spared since we have to deal with some local properties of f near $\mathcal{B}$. For instance, by generalizing Barta's trick (Barta 1937), one can easily check by simple equation counting that when $\mathcal{Q}$ is algebraic, i.e. when b is a polynomial, provided that we choose f to be a polynomial of sufficiently high degree n whose zeros are outside $\mathcal{Q}$, we can find a polynomial g of degree $n-2$ such that $\Delta(fb) = gb$. Therefore, $E_{\mathrm{loc}}^{[\varphi]} = -g/(2f)$ is bounded and finite upper and lower bounds of E_0 can be found. Let us apply this method to the asymmetric annular billiard that is an elegant paradigmatic model in quantum chaos (Bohigas *et al* 1993). $\mathcal{B}$ is made of two circles of radius 1 and $r < 1$ whose centres are distant by $\delta < 1 - r$. $\mathcal{Q}$ is the 2D domain in between the circles. The simplest choice of trial function is to take $\varphi(x, y) = b(x, y) = [x^2+y^2-r^2][(x-\delta)^2+y^2-1]$. One can check analytically that the lower bound of $E_{\mathrm{loc}}^{[\varphi]}$ is

$$\inf_{\mathcal{Q}} \left(\frac{-\Delta\varphi}{2\varphi}\right) = \sup_{\mathcal{Q}} \left(\frac{8[(x-\delta/2)^2 + y^2 - (1+r^2)/4]}{[x^2+y^2-r^2][(x-\delta)^2+y^2-1]}\right). \tag{7}$$

For $r = 3/4$ and $\delta = 0.1$, a simple numerical computation shows that (7) is finite and obtained at $(x, y) \simeq (0.86, 0)$ and leads to $E_0 \geqslant 28.390$ to be compared with the exact result $E_0 \simeq 42.94$. As one could have expected with the rough trial function chosen above, the estimation is not very precise but the calculations required here to get this result are much simpler than the ones involved in a variational method (that provides the complementary upper bound 55.32 with the same test function) or by the exact numerical resolution that requires finding the smallest root of an infinite determinant made of Bessel functions.

4. The many-body Coulombian problem

The next examples, presented in this section and in the following, will illustrate that the first strategy for obtaining finite bounds is to get rid of the singularities that may appear in the local energy. When $\mathcal{Q}$ is not bounded, one must have a control over the behaviour of the trial functions as q goes to infinity. For a multidimensional, nonseparable, Schrödinger Hamiltonian, a JWKB-like asymptotic expression is generally not available (Maslov and Fedoriuk 1981, introduction). Nevertheless, the differential method is less demanding than the semiclassical approximations: we need the local energy to be bounded at infinity but we will not require it to tend to the *same* limit in all directions. As already shown in the annular billiard problem, for the sake of simplicity one could start with a less ambitious program and try to obtain just one nontrivial inequality in (4).

The second example is to consider a system of N non-relativistic, spinless, charged particles living in a D-dimensional infinite space. Their kinetic energy is given by $\sum_{i=0,\ldots,N-1} \hat{p}_i^2/(2m_i)$ and they interact with each other via a two-body Coulombian interaction $e_i e_j/\hat{r}_{ij}$. We will assume that the masses m_i and the charges e_i allow the existence of a bound state. Once the free motion of the centre of mass is discarded, we are led to a $D(N-1)$-dimensional configuration space that can be described by the relative positions $q = \{\mathbf{r}_{0,i}\}_{i=1,\ldots,N-1}$ with respect to one distinguished particle. The Hamiltonian is given by

$$\hat{H} = \sum_{i=1}^{N-1} \frac{1}{2m_{0,i}} \hat{\mathbf{p}}_i^2 + \frac{1}{2m_0} \sum_{\substack{i,\,j=1 \\ i \neq j}}^{N-1} \hat{\mathbf{p}}_i . \hat{\mathbf{p}}_j + \frac{1}{2} \sum_{\substack{i,\,j=0 \\ i \neq j}}^{N-1} \frac{e_i e_j}{\hat{r}_{i,j}}. \tag{8}$$

The notation $m_{i,j}$ stands for the reduced mass $m_i m_j/(m_i + m_j)$. For $D \geqslant 2$, one can eliminate the Coulombian simple poles $r_{i,j} = \|\mathbf{r}_{0,i} - \mathbf{r}_{0,j}\| = 0$ in the local energy by choosing the trial function as follows:

$$\varphi(q) = \exp\left(-\frac{1}{2} \sum_{\substack{i,\,j=0 \\ i \neq j}}^{N-1} \lambda_{i,j} r_{i,j} \right) \tag{9}$$

with $\lambda_{i,j} = -2m_{i,j} e_i e_j/(D-1)$. When this choice does not provide a normalizable function, it should be understood that the exponent is just the first order of a Taylor expansion near $r_{i,j} = 0$. Whenever (9) is actually square integrable on $\mathcal{Q}$, the local energy reads

$$E_{\mathrm{loc}}^{[\varphi]} = -\sum_{\substack{i,\,j=0 \\ i<j}}^{N-1} \frac{\lambda_{i,j}^2}{2m_{i,j}} - \sum_{\widehat{j,i,k}} \frac{\lambda_{i,j}\lambda_{i,k}}{m_i} \cos(\widehat{j,i,k}). \tag{10}$$

The last sum involves all the $N(N-1)(N-2)/2$ angles $\widehat{j,i,k}$ that can be formed with all the triangles made of three distinct particles. This expression treats all the particles on an equal

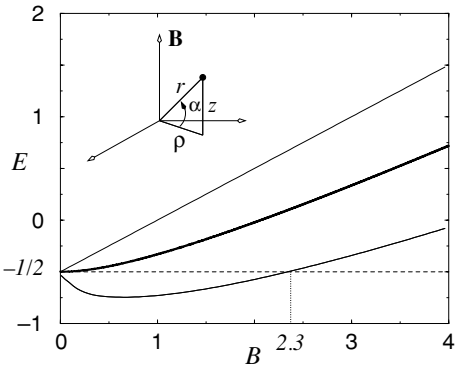

Figure 1. Upper and lower bounds of the ground state energy (thick line) for hydrogen in a Zeeman configuration.

footing and it is clear that the local energy is bounded everywhere. For $N = 2$, we recover the exact ground state since the last sum is absent and the local energy is constant. For a helium-like atom ($D = 3$, $N = 3$) of charge $(Z-2)e$ with the nucleus considered as infinitely massive compared to the electron mass, only two angular terms survive and we get (in atomic units) $E_{\rm loc} = -Z^2 - 1/4 + Z(\cos\theta_1 + \cos\theta_2)/2$. The two angles are taken at the vertices made by the two electrons: the sum of their cosines is bound from below by 0 and from above by 2 (diametrically opposed electrons). The lower bound of the local energy is $-Z^2 - 1/4$; this is not an interesting piece of information since we know that E_0 is larger than the energy $-Z^2$ obtained by neglecting the strictly positive repulsion of the electrons. On the other hand, the bound $E_0 \leqslant -(Z - 1/2)^2$ provides a simple, analytical, nontrivial result.

5. The hydrogen atom in a magnetic field

The third application of the differential method to a non-integrable system will concern the hydrogen atom in a constant and uniform magnetic field $B\vec{u}_z$. While the positivity of the ground state wavefunction was guaranteed by the so-called Krein–Rutman theorem in all the previous examples (applicable for any Hamiltonian of the form (5), see for instance (Reed and Simon 1978, XIII.12)), it is no longer valid for an arbitrary potential when a magnetic field is present (Helffer *et al* 1999). Nevertheless, for the hydrogen atom, the attractive interaction between the nucleus and the electron keeps the orbital momentum L_z of the ground state at zero for any arbitrary value of B (Avron *et al* 1977) and the Krein–Rutman theorem applies when restricted to the $L_z = 0$ subspace. In order to preserve the symmetry of the ground state, the trial function will be chosen to be strictly positive and even with respect to z; hence we can work in the half space where $z \geqslant 0$. With a vanishing paramagnetic term, φ depends on the coordinates $q = (\rho, r)$ only (see figure 1). In atomic units, the local energy is given by $E_{\rm loc}^{[\varphi]} = V - \Delta\varphi/(2\varphi)$ where the effective potential is $V(\rho, r) = B^2\rho^2/8 - 1/r$. In order to eliminate the Coulomb singularity, one must impose some local conditions on the logarithmic derivatives of φ. More precisely, with $S \stackrel{\rm def}{=} \ln\varphi$, we must have $\partial_r S(0,0) = -1$ and $\partial_\rho S(0, r) = 0$ for all $r \geqslant 0$. Assuming that S is smooth enough near $\rho = 0$, it takes the general form $S(\rho, r) = -r + r^2 l(r) + \rho^2 h(\rho, r)$ where l and h are two smooth functions. Choosing $l \equiv 0$ and $h \equiv -B/4$ (resp. $h \equiv 0$) will bound from above (resp. below) the local energy: $-1/2 \leqslant E_0 \leqslant -1/2 + B/2$. As in the previous example the lower bound is useless

Figure 2. Increasing $E_{\rm loc}^{[\varphi_0]}$ (dashed line) with one local perturbation is limited. When adding to $\ln(\varphi_0)$, say, a Gaussian perturbation localized near an isolated minimum of the local energy, we can increase the value of the absolute minimum by a finite amount (solid line in the left figure). But if the magnitude of the Gaussian is increased too much, the minima created by passing through a bifurcation can decrease below the original minimum (solid line in the right figure).

since it can be guessed from the very beginning. The real challenge here is to improve the lower bound without introducing a divergence as $r \to \infty$ in any direction characterized by α. After a detailed examination of the possible balance between the asymptotic behaviour of l and h as $r \to \infty$, a trial function can be constructed in order to improve the trivial lower bound for B large enough. Namely if we take $S = -r - B\rho^2/4 + \rho^2\big(r - \sqrt{r^2 - \rho^2}\big)/(\rho^2 + 5r/\sqrt{B})$ we improve the trivial lower bound for $B \gtrsim 2.3$ (see figure 1). Note that for very large B we recover a wavefunction that mimics a Landau state.

6. A local algorithm for improving the bounds; application to the quartic oscillator

Assume now that $\varphi_0 = \exp(S_0)$ bounds the local energy. Is there any systematic strategy to improve the bounds and, one day, compete with the very high precision of the secular variational and perturbative methods or numerical diagonalization of truncated matrices? Of course one can always combine these four approaches but let us look, for the moment, how the local character of the differential method can be exploited further. Suppose that q_0 is a point where $q \mapsto E_{\rm loc}^{[\varphi_0]}(q)$ reaches its lowest non-degenerate value. Among all the possible infinitesimal perturbations of S_0, only those that are localized in the neighbourhood of q_0 are relevant since adding a perturbation far away from q_0 will not affect the absolute minimum. The appropriate framework for local studies in an infinite functional space is bifurcation theory. Since the local energy, the determination of the critical points and their stability involve a finite number of derivatives, we expect that the number of relevant control parameters λ remains finite for low-dimension configuration space very much like the central result of catastrophe theory (Poston and Stewart 1978, Demazure 2000). We will leave this quantitative study for future investigations. For the moment, let us keep the discussion at a qualitative level only with a 1D Hamiltonian of the form $H = -\Delta/2 + V$ and take $S = S_0 + \delta S$ with a Gaussian perturbation $\delta S(q) = s\exp(-(q-a)^2/\sigma^2)$ controlled by three parameters $\lambda = (s, a, \sigma)$. The specific choice of the form of δS is not important here; only a finite number of pointwise derivatives will matter for locally improving the bounds as long as δS does not change the normalizability of the trial function. The choice of a Gaussian is particularly simple: it will modify the local energy in a neighbourhood of a whose size is governed by σ and by the magnitude s. This perturbation is qualitatively reproduced in figure 2. The value of $E_{\rm loc}$ at $q = a$ is increased (resp. decreased) for a small but finite positive (resp. negative) s. We can apply this procedure near the absolute minimum (resp. maximum) of $E_{\rm loc}$ and repeat it for the possible absolute extrema that may have emerged during the previous step. We get an iteration sequence that may systematically improve the bounds. Still, this algorithm is slowed down because if we try to 'lift up the dress' too much, a 'prudish censor' lowers it on both sides of $q = a$ (this phenomenon is not specific to 1D).

To be more precise, consider a quartic potential given by $V(q) = r^2q^2(q^2 + \eta\delta^2)/2$ where $\eta = \pm 1$. In order to bound the local energy as $|q| \to \infty$, we can use a JWKB-like expansion

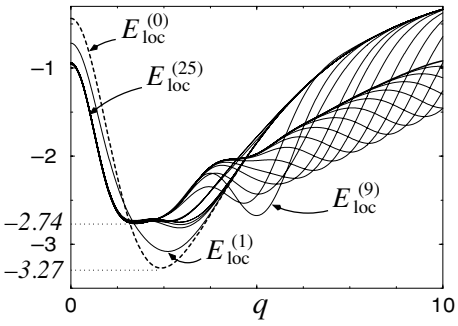

Figure 3. Adding n Gaussians to S_0 allows us to increase the minimum of the local energy when constructing the sequence $E^{(n)}_{\rm loc}$. For each iteration, only one scalar parameter is optimized (the amplitude of the Gaussian being added).

for S_0. If we want a uniformly smooth expression, we can take

$$S_0(q) = -\tfrac{1}{3}r(q^2+\delta^2)^{3/2} + \tfrac{1}{2}r\delta^2(1-\eta)(q^2+\delta^2)^{1/2} - \tfrac{1}{2}\ln(q^2+\delta^2) - \tfrac{1}{2}r\delta^4(q^2+\delta^2)^{-1/2}. \tag{11}$$

The last term is chosen to improve the trivial lower bound given by the minimum of V. For the arbitrary choice $r = 1/\sqrt{2}$, $\eta = -1$ and $\delta^2 = 8$, figure 3 shows how the lower bound can be improved from -3.27 up to -2.74 (the exact result is -2.66) when adding to S_0 enough Gaussians that are equi-spaced by 0.5 with a fixed $\sigma = 1$. Only their magnitudes s are numerically optimized here, one after another. One can see a second advantage of the differential method when numerically implemented: not only is no integral required but also, provided we keep under control the instabilities that are illustrated in figure 2, the optimization algorithm concerns a small number of parameters at each step (just one in the example given in figure 3) to be compared with the large number of parameters to be optimized at one go in the final step of the variational method.

7. Conclusion

The differential method appears to be a new kind of general theoretical tool for obtaining rigorous information on a ground state energy. Its local character makes it quite different from the traditional ones (to put it succinctly, the variational, the perturbation and the numerical diagonalization techniques). In this paper, I have given some qualitative and quantitative arguments to show how simple and efficient it can be. However, I should insist that even in the cases where the variational or perturbative techniques can be applied, the aim of the paper is not to seek for performance: for the moment the differential method is too young to compete by itself with the traditional methods. One short term possibility is to calculate the extrema of the local energy constructed with the trial function given by the other methods. The idea of locally modifying the local energy or any local function of the same type—for instance, those currently used in Monte Carlo methods—may be fruitful as well (Caffarel 2004). Actually, in order to convince the reader that the method is indeed applicable in a wide field of physics and furnishes some reasonable results, I had to compare them with some more precise ones and therefore I dealt with situations where the exact ground state energy was already known with the help of other methods. The algorithm that is presented in section 6 is chosen to prove how

the local sensitivity of the local energy can be exploited to systematically improve the bounds. The feasibility is in itself not obvious and is worth demonstrating even in the simplest cases.

Acknowledgments

This work could not have been started without Hector Giacomini's brilliant intuition that some relevant information on E_0 could be extracted from (2). I am very indebted to Dominique Delande and Benoît Grémaud for sharing their penetrating thoughts, their skilled numerical calculations in Coulombian problems and, not least, their kind hospitality at the Laboratoire Kastler Brossel.

References

Arnold V I 1984 *Catastrophe Theory* (New York: Springer)
Avron J, Herbst I and Simon B 1977 The Zeeman effect revisited *Phys. Lett.* A **62** 214–6
Barnsley M 1978 Lower bounds for quantum mechanical energy levels *J. Phys. A: Math. Gen.* **11** 55–68
Barta J 1937 Sur la vibration fondamentale d'une membrane *C. R. Acad. Sci. Paris* **204** 472–3 (in French)
Baumgartner B 1979 A class of lower bounds for Hamiltonian operators *J. Phys. A: Math. Gen.* **12** 459–67
Bessa G P and Montenegro J F 2003 An extension of Barta's theorem and geometric applications *Preprint* math/0308099
Bohigas O, Boosé D, Egydio de Carvalho R and Marvulle V 1993 Quantum tunneling and chaotic dynamics *Nucl. Phys.* A **560** 197–210
Caffarel M 2004 Private communication
Crandall R E and Reno M H 1982 Ground state energy bounds for potentials $\|x\|^\nu$ *J. Math. Phys.* **23** 64–70
Crandall R E and Reno M H 1982 *J. Math. Phys.* **23** 1737 (erratum)
Demazure M 2000 *Bifurcations and Catastrophes* (Berlin: Universitext, Springer)
Duffin R J 1947 Lower bounds for eigenvalues *Phys. Rev.* **71** 827–8
Helffer B, Hoffmann-Ostenhof T and Owen M 1999 Nodal sets for groundstates of the Schrödinger with zero magnetic fields in a non simply connected domain *Commun. Math. Phys.* **202** 629–49
Maslov V P and Fedoriuk M V 1981 *Semi-Classical Approximation in Quantum Mechanics (Mathematical Physics and Applied Mathematics* vol 7*)* (Dordrecht: Reidel)
Poston T and Stewart I 1978 *Catastrophe Theory and its Applications* (London: Pitman)
Reed M and Simon B 1978 *Analysis of Operators (Methods of Modern Mathematical Physics* vol 4*)* (New York: Academic)
Schmutz M 1985 The factorization method and ground state energy bounds *Phys. Lett.* A **108** 195–6
Thirring W 1979 *Quantum Mechanics of Atoms and Molecules (A Course in Mathematical Physics* vol 3*)* (New York: Springer)

II.3 Encadrement de l'énergie de l'état fondamental d'un système à N corps à l'aide de la méthode différentielle

Pour l'instant, c'est pour le problème coulombien purement attractif que j'ai pu obtenir les résultats les plus probants de la méthode différentielle. Physiquement, on quitte alors les échelles de physique atomique pour plonger au cœur des noyaux ou même des hadrons. J'ai beaucoup bénéficié de discussions avec J.-M. Richard (Laboratoire de Physique Subatomique et de Cosmologie de Grenoble) ; les méthodes astucieuses d'encadrement qu'il a utilisées avec ses collaborateurs (J.-L. Basdevant., A. Martin et T. T. Wu) m'ont permis de m'assurer que, pour ces systèmes, la méthode différentielle tenait bien la route et donnait des résultats équivalents aux leurs.

Available online at www.sciencedirect.com
SCIENCE DIRECT®
ELSEVIER
Nuclear Physics A 765 (2006) 319–341
NUCLEAR PHYSICS A

Bounding the ground-state energy of a many-body system with the differential method

Amaury Mouchet

Laboratoire de Mathématiques et de Physique Théorique (CNRS UMR 6083), Université François Rabelais, Avenue Monge, Parc de Grandmont, 37200 Tours, France

Received 29 June 2005; received in revised form 28 October 2005; accepted 31 October 2005

Available online 28 November 2005

Abstract

This paper promotes the differential method as a new fruitful strategy for estimating a ground-state energy of a many-body system. The case of an arbitrary number of attractive Coulombian particles is specifically studied and we make some favorable comparison of the differential method to the existing approaches that rely on variational principles. A bird's-eye view of the treatment of more general interactions is also given.

PACS: 24.10.Cn; 12.39.Jh; 03.65.Db; 05.30.Jp

1. Introduction

There is little need to stress the great importance of the ground-state in many domains of quantum physics. Nevertheless, computing the lowest energy of most systems cannot be done analytically and approximations are required. Some techniques, being very general, have been well known for several decades. For instance, the variational methods (Rayleigh–Ritz) or the perturbative series (Rayleigh–Schrödinger) have their roots in the pre-quantum era; much later, numerical algorithms (numerical diagonalizations as well as Monte Carlo computations), supported by the increasing power of computers, have been able to provide a tremendous precision on the ground-state of a large variety of very complex systems. However, it is a much more difficult task to rigorously estimate the discrepancies between the exact ground-state energy E_0 and the approximated one. In particular, though variational methods naturally provide upper bounds on E_0, obtaining lower estimates requires more sophisticated techniques (for instance,

E-mail address: mouchet@phys.univ-tours.fr (A. Mouchet).

0375-9474/$ – see front matter
doi:10.1016/j.nuclphysa.2005.10.015

the Temple-like methods [19, Section XIII.2]), some of them being very system-dependent (e.g., the moment method proposed in [10] for rational-fraction potentials or the Riccati–Padé method proposed in [7] for one-dimensional Schrödinger equations).

1.1. The optimized variational methods

For a many-body system governed by pairwise interactions, an interesting strategy is to approximate E_0 from below in terms of the ground-states of the two-body subsystems [8]. Such an approach has been successfully applied to Coulombian (bosonic and fermionic) systems of charged particles [12] or self-gravitating bosons [1,13]. Clever refinements have been proposed that provide some very accurate lower bounds of E_0 for the three-body [3] and the four-body systems [4]. Though not easily generalizable to an arbitrary number of particles, these last optimized variational methods can be applied to interactions that are not necessarily Coulombian and may be relevant for quarks models [2] where some inequalities between baryon and meson masses represent theoretical, numerical and experimental substantial information ([17,20], and references therein). In practice, the optimized variational methods allow to efficiently treat some models that have simple scaling properties, for instance, when the two-body interaction can be described by a purely radial potential of the form $v(r) \propto \mathrm{sign}(\beta) r^{\beta}$. The main reason relies in the fact that, except the Coulombian ($\beta = -1$) and the harmonic ($\beta = 2$) interactions, the exact form of the ground-state energy of the two-body problem is not known. Yet, one can still take advantage of the power-law behavior of v to obtain worthwhile lower bounds for the *ratio* between the N-body and the 2-body ground-state energies.

1.2. The differential method

Besides the variational and perturbative techniques that are mentioned above, there exists a third very general method for approximating the ground-state energy of a quantum system, namely the differential method (see [15,16], and references therein for a historical track) whose starting point is recalled in Section 2 for the sake of completeness. As for the variational methods, the differential method call on a family of trial functions that supposedly mimic the ground-state and that allow for the construction of a function (the average of the Hamiltonian in the former case, the so-called local energy in the latter case) whose absolute extrema within the chosen trial family provide bounds on the exact ground-state energy E_0. One of the main advantages of the differential method over the other ones is that no integral is required, then it allows to work, even analytically, with rather complicated trial functions by encapsulating some rich structure of the potential. It is also worth mentioning that the same test function leads to both upper and lower bounds on E_0: the estimate comes with a rigorous window. Though applicable to many models (to systems involving a magnetic field, to discrete systems, to non-Schrödinger equations, etc.) the major inconvenient of the differential method is that it requires, as a crucial hypothesis, the exact eigenfunction to remain non-negative in the configuration space (it must be real without sign changes). Therefore, it excludes any ground-state whose spatial wave-function is antisymmetric under some permutations of its arguments. As far as fermionic systems are involved, the differential method will concern only those whose ground-state eigenfunction remains symmetric under permutations of the spatial positions of the identical particles.

The aim of this paper is to apply the differential method specifically to a system made of N non-relativistic particles of masses m_i in a D-dimensional space whose Hamiltonian has the form

$$\tilde{H} = \sum_{i=0}^{N-1} \frac{\mathbf{p}_i^2}{2m_i} + V(\mathbf{r}_0, \ldots, \mathbf{r}_{N-1}). \tag{1}$$

When the N particles located at $\{\mathbf{r}_i\}_{i=0,\ldots,N-1}$ interact only through pairwise potentials $v_{ij} = v_{ji}$, V is given by

$$V = \sum_{\substack{i,j=0 \\ i<j}}^{N-1} v_{ij}(\mathbf{r}_{ij}), \tag{2}$$

where $\mathbf{r}_{ij} \stackrel{\text{def}}{=} \mathbf{r}_j - \mathbf{r}_i$. The spin-dependent interactions, if any, are assumed to be included somehow in the scalar potential V and $\tilde{H}$ will be supposed to act on spatial wave-functions only; in other words, the possible spin configuration have been factorized out in one way or another. When $N = 3$ and $N = 4$ and for power-law potentials, this is the same kind of systems to which the optimized variational method applies also. We will consider the Coulombian case in Section 3 and systematically compare the estimates given by the variational methods and the differential method. In Section 4, general interactions are considered (not necessarily power-law v_{ij}'s). This is of course relevant for estimating the ground-state energy of a system where the spin-independent strong interactions are dominant; for heavy enough quarks for instance, it is known [11] that the non-relativistic form (1) may be pertinent.[1] At atomic scales, the method could be applied to clouds made of neutral atoms where short-range interactions govern the dynamical properties.

2. The differential method

2.1. The general strategy

The necessary but sufficient condition for the differential method to work is the following: the Hamiltonian H has one bound state $|\Phi_0\rangle$, associated with energy E_0, such that $\Phi_0(q) \stackrel{\text{def}}{=} \langle q|\Phi_0\rangle$ remains real and non-negative in an appropriate q-representation, say of spatial positions. For a N-body system governed by the Hamiltonian (1), the dynamics in the center-of-mass frame corresponds to a reduced Hamiltonian H whose ground-state[2] Φ_0 has precisely this positivity property in the whole configuration space $\mathcal{Q}_N$ of the $(N-1)D$ relative coordinates $q_N \stackrel{\text{def}}{=} (\mathbf{r}_1 - \mathbf{r}_0, \ldots, \mathbf{r}_{N-1} - \mathbf{r}_0)$. This is the Krein–Rutman theorem (see [19, Section XIII.12]). For each

[1] Possible relativistic corrections may be included (for instance, by considering the spinless Salpeter equation) since the differential method does not require a quadratic kinetic energy.

[2] We will only consider the cases where at least one bound state exists. Physically, this can be achieved with a confining external potential (a "trap" is currently used in experiments involving cold atoms). Formally, this can be obtained in the limit of one mass, say m_0, being much larger than the others. The external potential appears to be the v_{0i}'s, created by such an infinitely massive motionless device. It will trap the remaining $N-1$ particles in some bound states if the v_{0i}'s increase sufficiently rapidly with the r_{0i}'s.

state $|\varphi\rangle$, the hermiticity of H implies the identity $\langle\Phi_0|(H-E_0)|\varphi\rangle = 0$. If we choose $|\varphi\rangle$ such that its representation $\varphi(q_N)$ is a smooth normalizable real wave-function, we obtain

$$\int_{\mathcal{Q}_N} \Phi_0^*(q_N)(H-E_0)\varphi(q_N)\,dq_N = 0. \tag{3}$$

Taking into account the positivity of Φ_0 on $\mathcal{Q}_N$, there necessarily exists some q_N such that $(H-E_0)\varphi(q_N) \geqslant 0$ and some other configurations for which $(H-E_0)\varphi(q_N) \leqslant 0$. Choosing $\varphi > 0$ on $\mathcal{Q}_N$, we get both an upper and a lower bound on E_0:

$$\inf_{\mathcal{Q}_N}\big(E_{\rm loc}^{[\varphi]}(q_N)\big) \leqslant E_0 \leqslant \sup_{\mathcal{Q}_N}\big(E_{\rm loc}^{[\varphi]}(q_N)\big), \tag{4}$$

where the local energy is defined by

$$E_{\rm loc}^{[\varphi]}(q_N) \stackrel{\rm def}{=} \frac{H\varphi(q_N)}{\varphi(q_N)}. \tag{5}$$

In other words, the differential method provides an estimate

$$E_0^{(\rm d.m.)} \stackrel{\rm def}{=} \frac{1}{2}\Big[\sup_{\mathcal{Q}_N}\big(E_{\rm loc}^{[\varphi]}(q_N)\big) + \inf_{\mathcal{Q}_N}\big(E_{\rm loc}^{[\varphi]}(q_N)\big)\Big], \tag{6}$$

that comes with a rigorous windows $\pm\Delta E_0^{(\rm d.m.)}$, where

$$\Delta E_0^{(\rm d.m.)} \stackrel{\rm def}{=} \frac{1}{2}\Big[\sup_{\mathcal{Q}_N}\big(E_{\rm loc}^{[\varphi]}(q_N)\big) - \inf_{\mathcal{Q}_N}\big(E_{\rm loc}^{[\varphi]}(q_N)\big)\Big]. \tag{7}$$

Unlike for the variational method, the determination of the absolute extrema of the local energy does not require the computation of any integral. Even the norm of the test function φ is not required provided it remains finite. The two inequalities (4) become equalities (the local energy becomes a flat function) when $\varphi = \Phi_0$ and therefore we will try to construct a test function that mimics Φ_0 at best. We will choose φ that respects the a priori known properties of Φ_0: its positivity, its boundary conditions and its symmetries if there are any. Since for each test function the error on E_0 is controlled by inequalities (4), the strategy for obtaining decent approximations is clear. First, we must choose or construct φ to eliminate all the singularities of the local energy in order to work with a bounded function. For instance, when the Hamiltonian has the form $p^2 + V$ with V being unbounded at some finite or infinite distances, the first kinetic term of the local energy $E_{\rm loc}^{[\varphi]} = -\Delta\varphi/\varphi + V$ must compensate the singular behavior of V for the corresponding configurations (we will work systematically with units such that $\hbar = 1$). Once a bounded local energy, say $E_{\rm loc}^{[\varphi_0]}$, is obtained, we can proceed to a second step: perturb the test function, $\varphi_0 \to \varphi = \varphi_0 + \delta\varphi$, in the neighborhood of the absolute minimum (respectively, maximum) of $E_{\rm loc}^{[\varphi_0]}$ in order to increase $\min E_{\rm loc}^{[\varphi_0]}$ (respectively, decrease $\max E_{\rm loc}^{[\varphi_0]}$). Up to the end of this article, we will focus on the first step: we will show how obtaining a bounded local energy furnishes some sufficiently constrained guidelines for obtaining reasonable bounds on E_0.[3] We will keep for future work the systematic local improvements of the absolute extrema of the local energy. In [15, Section 6], I have shown on a simple example how this can be done.

[3] One can understand it from the extreme sensitivity of the local energy to any local perturbation of the test function: while, in the variational methods, the quantity $\langle\varphi|H|\varphi\rangle/\langle\varphi|\varphi\rangle$ is quite robust to local perturbations because it represents precisely an average on the configuration space, the local energy may become unbounded quite easily by canceling locally φ faster than $H\varphi$.

2.2. Illustration in the two-body case

Before coping with much complex systems, let us first consider the case of the two-body problem that can be reducible to a one single non-relativistic particle of unit mass in an external potential V. The local energy is

$$E_{\rm loc}^{[\varphi]} = -\frac{\Delta\varphi}{2\varphi} + V = -\frac{1}{2}\Delta S - \frac{1}{2}(\nabla S)^2 + V, \tag{8}$$

where $S \stackrel{\rm def}{=} \ln(\varphi)$ is a well-defined function when $\varphi > 0$.

For the D-Coulombian potential $V(r) = \kappa/r$ ($D > 1$), the singularity at $r = 0$ controls the local behavior of the test function if one wants a bounded local energy. If $\lim_{r\to 0} S(r)$ is finite, by possibly subtracting an irrelevant constant term, we can suppose that this limit vanishes. Therefore, without too much loss of generality, we assume that S, can be asymptotically expanded near $r = 0$ on a family of power functions (for $D = 1$, the logarithmic functions should be considered) whose dominant term can be written like $S(r) \underset{r\to 0}{\sim} s_0 r^{\sigma+1}/(\sigma+1)$ with $\sigma \neq -1$ and $s_0 \neq 0$. Balancing the dominant terms in the local energy, it is therefore straightforward, to check that the only choice for the parameters s_0 and σ to get rid of the Coulombian singularity is too take $\sigma = 0$ and $s_0 = 2\kappa/(D-1)$. It happens that for S exactly equal to $2\kappa r/(D-1)$, we obtain a global constant local energy, namely, $-2\kappa^2/(D-1)^2$. Therefore, we have obtained the exact wave-function of the ground-state provided we eventually check that the wave-function is square-integrable which is true for $\kappa < 0$.

For the harmonic oscillator $V(r) = \omega^2 r^2/2$, V is unbounded as r increases ($r = +\infty$ is a singular point for V). If we tentatively look for an S whose asymptotic expansion at $r \to +\infty$ has a leading term of the form $s_0 r^{\sigma+1}/(\sigma+1)$, we necessarily get $\sigma = 1$ and $s_0 = -\omega$ (the cases where $\sigma \leqslant -1$ are ruled out by the square-integrable property). The local energy $D\omega/2$ is actually constant for all r's and indeed represents the exact ground-state energy. More generally, with the help of standard linear algebra arguments, for V being any definite positive quadratic form, we can always find a quadratic form S for which the local energy is globally constant.

2.3. Formulation for the many-body problem

When the potential V has the form (2), a natural choice of trial function is to take (for variational techniques in a few nuclear body context, such a choice has been used by [18,23] for instance)

$$\varphi(q_N) = \prod_{\substack{i,j=0 \\ i<j}}^{N-1} \phi_{ij}(\mathbf{r}_{ij}), \tag{9}$$

where each of the $N(N-1)/2$ functions $\phi_{ij}(\mathbf{r}) = \phi_{ji}(-\mathbf{r})$ depends on D coordinates.[4]

[4] The present paper wants mainly to stress the simplicity of the differential method. It does not seek for a real performance at the moment and we will not try to improve the choice of coordinates. Working with Jacobi coordinates, for instance, or constructing optimized coordinates as done in [4] may lead to better results. Anyway, we will see that the numerical results of Section 3 are satisfactory enough for validating the approach by the differential method.

It is straightforward to check that this choice describes a state with a fixed center-of-mass: indeed, we have $(\sum_{i=0}^{N-1}\mathbf{p}_i)|\varphi\rangle = \mathbf{0}$. Hence, $\tilde{H}\varphi = H\varphi$ and the local energy is given by

$$E_{\rm loc}^{[\varphi]}(q_N) = \sum_{\substack{i,j=0\\ i<j}}^{N-1}\left(-\frac{1}{2m_{ij}}\frac{\Delta\phi_{ij}(\mathbf{r}_{ij})}{\phi_{ij}(\mathbf{r}_{ij})} + v_{ij}(\mathbf{r}_{ij})\right) - \sum_{\widehat{j,i,k}}\frac{1}{m_i}\frac{\boldsymbol{\nabla}\phi_{ij}(\mathbf{r}_{ij})}{\phi_{ij}(\mathbf{r}_{ij})}\cdot\frac{\boldsymbol{\nabla}\phi_{ik}(\mathbf{r}_{ik})}{\phi_{ik}(\mathbf{r}_{ik})}, \quad (10)$$

where m_{ij} stands for the reduced masses $m_i m_j/(m_i+m_j)$. The last sum involves all the $N(N-1)(N-2)/2$ angles $(\widehat{j,i,k})$ between $\mathbf{r}_{ij}$ and $\mathbf{r}_{ik}$ that can be formed with all the triangles made of three particles having three distinct labels ($i\neq j$, $i\neq k$, $j\neq k$). Let us now take ϕ_{ij} to be a positive solution of the two-body spectral equation

$$-\frac{1}{2m_{ij}}\Delta\phi_{ij} + v_{ij}\phi_{ij} = \epsilon_{ij}\phi_{ij}. \quad (11)$$

The local energy becomes

$$E_{\rm loc}^{[\varphi]}(q_N) = \sum_{\substack{i,j=0\\ i<j}}^{N-1}\epsilon_{ij} - \sum_{\widehat{j,i,k}}\frac{1}{m_i}\boldsymbol{\nabla}S_{ij}(\mathbf{r}_{ij})\cdot\boldsymbol{\nabla}S_{ik}(\mathbf{r}_{ik}), \quad (12)$$

where $S_{ij} \stackrel{\rm def}{=} \ln(\phi_{ij})$. The trial wave-function (9) of the global system must be kept square-integrable but it is not necessary for *all* two-body subsystems to have a bound state when isolated.[5] For instance, for two electric charges having the same sign a positive but non-normalizable solution of (11) can be found. When v_{ij} admits at least one bound state (see also footnote 2), thanks to the Krein–Rutman theorem, we are certain to get a positive ϕ_{ij} when taking the ground-state of the two-body system and ϵ_{ij} its corresponding energy. At finite distances, if the possible singularities of v_{ij} are not too strong, we expect that ϕ_{ij} and then S_{ij} to be smooth enough for $E_{\rm loc}$ to remain bounded. At infinite distances, $E_{\rm loc}$ is expected to become infinite if v_{ij} does not tend to a constant sufficiently quickly. To see that, one can take purely radial potentials. i.e., $v_{ij}(\mathbf{r}) = v_{ij}(r)$ where $r \stackrel{\rm def}{=} \|\mathbf{r}\|$, and consider the asymptotic behavior of S_{ij} given by the semiclassical (JWKB) theory (see, for instance, [14]). Its derivative is given by $S'_{ij}(r) \underset{r\to\infty}{\sim} -\sqrt{2m_{ij}[v_{ij}(r)-\epsilon_{ij}]}$ and is not bounded if v_{ij} is not (at infinite distances). Strictly speaking, it is only for short-distant potentials that we can hopefully obtain rigorous non-trivial inequalities (4) while keeping the choice (9) with (11). However, as will be discussed in Section 4, the ground-state energy may be generally not be very sensitive to the potential at large distances (far away where Φ_0 is localized) and this physical assumption may be implemented by introducing a cut-off length from the beginning.

For purely radial potentials (12) simplifies in

$$E_{\rm loc}^{[\varphi]}(q_N) = \sum_{\substack{i,j=0\\ i<j}}^{N-1}\epsilon_{ij} - \sum_{\widehat{j,i,k}}\frac{1}{m_i}S'_{ij}(r_{ij})S'_{ik}(r_{ik})\cos(\widehat{j,i,k}). \quad (13)$$

Yet, for a multidimensional, non-separable, Schrödinger equation like (11), a JWKB-like asymptotic expression is generally not available [14, Introduction]. Nevertheless, the differential

[5] But for some pairing, (11) must have a normalizable solution. The cases of Borromean states where no two-body binding is possible [21] cannot be described by the form (9) if we keep (11).

method is less demanding than the semiclassical approximations: we will try to keep the local energy, like the one given by (12), bounded at infinity but we will not necessarily require it to tend to the *same* limit in all directions.

3. The Coulombian problem

The purely Coulombian problem in $D > 1$ dimensions corresponds to the situation where all v_{ij}'s are radial potentials and have the form

$$v_{ij}(r) = \frac{e_{ij}}{r} \tag{14}$$

for $N(N-1)/2$ coupling constants e_{ij} that may be or may be not constructed from individual quantities like charges. Provided a N-body ground-state exists, we can solve exactly (11) making use of $\Delta\phi(r) = \phi''(r) + (D-1)\phi'(r)/r$. We obtain a bounded local energy given by

$$E_{\rm loc}^{[\varphi]}(q_N) = \sum_{\substack{i,j=0\\ i<j}}^{N-1} -\frac{2m_{ij}e_{ij}^2}{(D-1)^2} - \frac{4}{(D-1)^2} \sum_{\widehat{(j,i,k)}} \frac{m_{ij}m_{ik}e_{ij}e_{ik}}{m_i} \cos(\widehat{j,i,k}). \tag{15}$$

For obtaining upper and lower bounds on E_0, one has just to calculate the absolute extrema of such a function. It can be done by standard optimization routines up to quite large N and even analytically in some cases (see below). The recipe is therefore simple and systematic: as far as only Coulombian interactions are involved, we can work with generic masses and coupling constants for which (9) is normalizable. The remaining of this section will concern the quality of these bounds and then we will accord our attention to cases that have been treated by other methods, mainly those treated in the references cited in the second paragraph of the introduction. More specifically, in order to leave aside the problem of the existence of a ground-state we will consider the case of attractive interactions only[6] (all e_{ij}'s being negative).

3.1. Arbitrary number of identical attractive particles

In this section we consider one species of particles only: for all i and j we denote $m_i = m$ and $e_{ij} = -g^2$. The local energy (15) becomes

$$E_\varphi(q_N) = -\frac{\epsilon_0}{(D-1)^2}\left(\frac{1}{2}N(N-1) + F_N(q_N)\right), \tag{16}$$

where $\epsilon_0 \stackrel{\rm def}{=} mg^2$. The function

$$F_N(q_N) \stackrel{\rm def}{=} \sum_{\widehat{(j,i,k)}} \cos(\widehat{j,i,k}) \tag{17}$$

[6] For an immediate application in the case of charged electric particles see [15] where the Helium atom is discussed. While the differential method provides an analytical non-trivial upper bound for the ground-state of the helium-like atoms, $E_0 \leqslant -(Z-1/2)^2$ in the simplest model ($D=3$, non-relativistic, spinless and with an infinitely massive nucleus of charge Z in atomic units), in the case of more delicate systems like the positronium ion (e^+, e^-, e^-), a systematic improvement is clearly required but is beyond the scope of this paper as explained at the end of Section 2.1. Indeed, for (e^+, e^-, e^-) if we content ourselves with eliminating the singularities, we obtain, for $D=3$, $-9m\alpha^2/8 \leqslant E_0 \leqslant 0$ (α being the fine structure constant). The upper bound is trivial while the lower bound is even worse compared to $-3m\alpha^2/4$ obtained in [2, Eq. (6.4)] or to $-3m\alpha^2/4$ obtained by a simple crude argument [2, Eq. (6.6)] (the exact result is $E_0 \lesssim -m\alpha^2/4$).

is invariant under translations and rotations but also under dilations of the particle configuration. For $N = 3$, the Appendix A proofs that $\sup_{\mathcal{Q}_3} F_3 = 3/2$ is reached when the three particles make an equilateral triangle and $\inf_{\mathcal{Q}_3} F_3 = 1$ is obtained when they are aligned. From this last result we are able to provide the lower bounds for F_N for any N: by a decomposition of F_N into a sum on $N(N-1)(N-2)/6$ triangle contributions,

$$F_N(q_N) = \sum_{\substack{\{i_1,i_2,i_3\} \\ 1\leqslant i_1<i_2<i_3\leqslant N}} \underbrace{\cos(\widehat{i_3,i_1,i_2}) + \cos(\widehat{i_1,i_2,i_3}) + \cos(\widehat{i_2,i_3,i_1})}_{= F_3(\mathbf{r}_{i_1},\mathbf{r}_{i_2},\mathbf{r}_{i_3})}, \tag{18}$$

all the F_3's in the sum reach their minimum simultaneously when all the particles are aligned, and for this configuration we have $\inf_{\mathcal{Q}_N} F_N = N(N-1)(N-2)/6$. From (16), we deduce that for each N

$$E_0 \leqslant -\frac{\epsilon_0}{6(D-1)^2}\, N(N-1)(N+1). \tag{19}$$

For $D = 3$, the same exponential test-functions lead to the better variational estimate [13, Eq. (17)]

$$E_0 \leqslant -\epsilon_0 \frac{25}{512} N(N-1)^2 \tag{20}$$

($25/512 \simeq 0.0488 \gtrsim 1/24 \simeq 0.0417$). This was expected from the general identity valid for any normalized function φ,

$$\int_{\mathcal{Q}} \varphi^*(q) H\varphi(q)\, dq = \int_{\mathcal{Q}} \big|\varphi(q)\big|^2 E_{\mathrm{loc}}^{[\varphi]}(q)\, dq \leqslant \sup_{\mathcal{Q}} \big(E_{\mathrm{loc}}^{[\varphi]}(q)\big). \tag{21}$$

The differential method always gives worse upper bounds than the variational method with the same test-functions but, in the last case, one still has to be able to compute the integrals and one cannot generally estimate how far from the exact value the average Hamiltonian is. For a different choice of test functions, a better variational upper-bound has been obtained [1, Eq. (16)],

$$E_0 < -0.0542 N(N-1)^2. \tag{22}$$

As far as lower estimates are concerned, bounding F_N from above will allow us to improve the existing results, namely (for $D = 3$),

$$E_0 \geqslant -\frac{1}{16} N^2(N-1) \tag{23}$$

obtained in [1, Eq. (12)].

First, when N is not too large for the numerical computation to remain tractable, the direct calculation of $\sup_{\mathcal{Q}_N} F_N$ shows (see Fig. 1) that it gives better lower estimates than (23). For very large N, we can nevertheless benefit from the maximum of F_M for smaller M. Indeed, for $M \leqslant N$ we can decompose F_N into contributions of M-clusters as follows:

$$F_N(q_N) = \sum_{M\text{-subclusters}} \frac{(M-3)!(N-M)!}{(N-3)!} F_M(q_M), \tag{24}$$

where the sum is taken on all the M-subclusters, labeled by the coordinates q_M, that can be formed with the given configuration q_N. This sum involves exactly $N!/M!/(N-M)!$ terms and we have

$$\sup_{\mathcal{Q}_N} F_N \leqslant \frac{N(N-1)(N-2)}{M(M-1)(M-2)} \sup_{\mathcal{Q}_M} F_M. \tag{25}$$

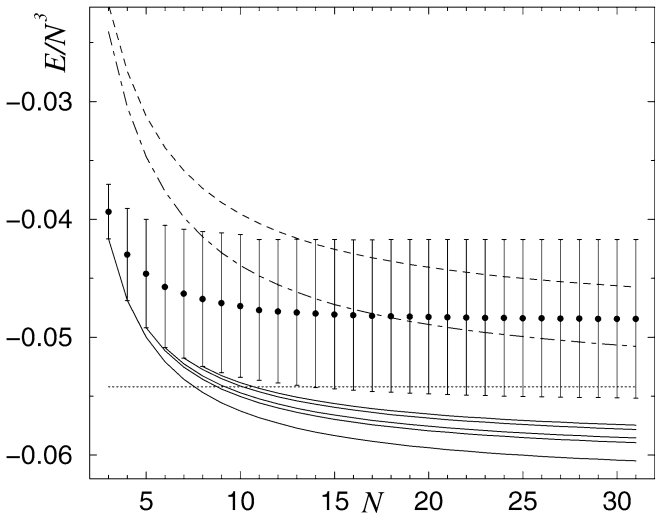

Fig. 1. Estimations of ground-state energy for N identical attractive Coulombian particles (rescaled by a factor N^3). The differential method provides $E_0^{(\mathrm{d.m.})}$ defined by (6) (black disks) with exact error bars whose half-width are given by (7). Each solid line starting at M corresponds to the lower bounds (27). For $M = 3$ and $M = 4$, there is only one solid curve given by (23). The dashed line corresponds to the upper bound (20) given by [13, Eq. (17)]. The dot-dashed line corresponds to the upper bound (22) given by [1, Eq. (16)] that tends, when $N \to \infty$, to the thin dotted horizontal line located at -0.0542.

This leads to define

$$\alpha_M \stackrel{\text{def}}{=} \frac{\sup_{\mathcal{Q}_M} F_M}{M(M-1)(M-2)}, \tag{26}$$

and from (16) we find

$$E_0 \geqslant -\frac{\epsilon_0}{(D-1)^2} N(N-1)\left(\frac{1}{2} + \alpha_M(N-2)\right). \tag{27}$$

Since, from (25), α_M is decreasing when M increases, the larger M the better the lower estimate of E_0.

For $M = 3$ we have already seen that $\alpha_3 = 1/4$; for $D = 3$, (27) reproduces exactly (23). No better estimate is obtained when considering $M = 4$. Indeed, the configuration of particles that maximizes F_4 corresponds to the regular tetrahedron because its faces, that are equilateral triangles, maximize the contributions of all the 3-subclusters simultaneously. We obtain $\sup_{\mathcal{Q}_4} F_4 = 6$ and hence $\alpha_4 = \alpha_3$.

For $M = 5, 6, 7, 8$ and $D = 3$, the configurations that maximize F_M can be seen in Fig. 2. Crossed numerics and analytical studies lead to very plausible conjectures on the geometrical description of the configuration for $M = 5$ and $M = 8$ for which explicit analytical value of α_M can be proposed [16]. The lower bound for (27), for $N \geqslant M$, is strictly improved when increasing M from 5 and in particular is better than (23).

However, the sequence of improvements obtained this way seems to saturate up to $\alpha_\infty = 2/9$:

$$\alpha_3 = \alpha_4 = \frac{1}{4} \geqslant \alpha_5 \simeq 0.2432 \geqslant \alpha_6 \simeq 0.2414 \geqslant \alpha_7 \simeq 0.2382 \geqslant \alpha_8 \simeq 0.2366 \geqslant \cdots \geqslant \alpha_{30} \simeq 0.2266 \cdots \geqslant \alpha_\infty = \frac{2}{9} \simeq 0.2222. \tag{28}$$

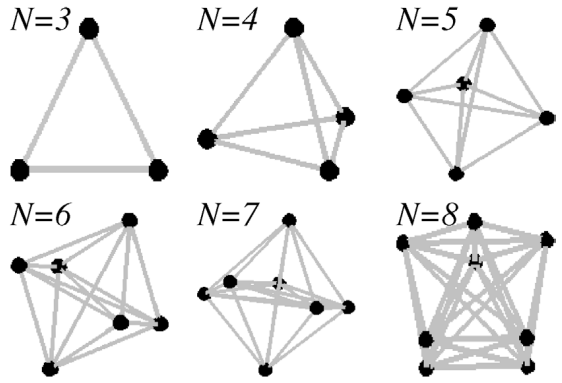

Fig. 2. The configurations that maximize F_N defined by (17) for identical Coulombian attractive particles.

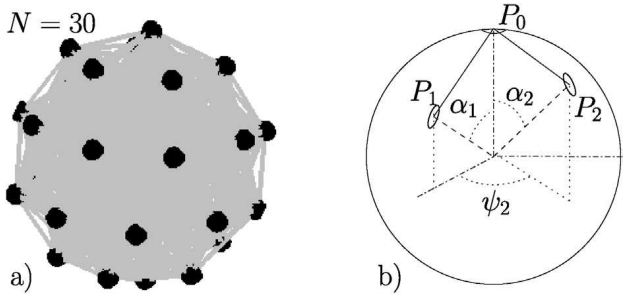

Fig. 3. For large N, F_N is maximized for a configuration where the N points seems, numerically, to distribute uniformly on a sphere (with the well-known caveat concerning the ambiguity of such a notion [22]). Such an optimal configuration for $N = 30$ is shown in (a). The continuous limit of F_N/N^3 when $N \to \infty$ can be computed with the help of figure (b).

From the optimized configuration obtained with N about several tens (see Fig. 3(a)), we can hopefully guess that the limit $N \to \infty$ leads to a continuous and uniform distribution of the particles on the same sphere. The continuous limit of $\sup_{\mathcal{Q}_N} F_N$ varies as N^3 with N. If, on the unit sphere $\mathcal{S}$, the N particles get distributed uniformly with density $\sigma = N/4\pi$, the continuous limit of $\sup_{\mathcal{Q}_N} F_N$ is given by ($\mathrm{d}S_i$ is an infinitesimal portion of the sphere near the point P_i, $i = 0, 1, 2$; see Fig. 3(b))

$$\sup_{\mathcal{Q}_N} F_N \sim \int_{\mathcal{S}} \sigma \,\mathrm{d}S_0 \frac{1}{2} \int_{\mathcal{S}} \sigma \,\mathrm{d}S_1 \int_{\mathcal{S}} \sigma \,\mathrm{d}S_2 \cos(\widehat{P_1, P_0, P_2})$$

$$\sim \frac{1}{2}\sigma^3 8\pi^2 \int_0^{\pi} \mathrm{d}\alpha_1 \int_0^{\pi} \mathrm{d}\alpha_2 \int_0^{2\pi} \mathrm{d}\psi_2 \sin(\alpha_1)\sin(\alpha_2)\cos(\widehat{P_1, P_0, P_2}).$$

When $\cos(\widehat{P_1, P_0, P_2}) = \frac{\mathbf{P_0P_1}}{||\mathbf{P_0P_1}||} \cdot \frac{\mathbf{P_0P_2}}{||\mathbf{P_0P_2}||}$ is expressed as a function of α_1, α_2 and ψ_2, we straightforwardly get $\sup_{\mathcal{Q}_N} F_N/N^3 \underset{N\to\infty}{\simeq} 2/9 = \alpha_\infty$. For infinite N, this last result supplement the upper bound given by (22) and we have

$$N \to \infty, \quad -\frac{1}{18} \simeq -0.0556 \lesssim \frac{E_0}{N^3} \lesssim -0.0542. \tag{29}$$

3.2. Three particles with one different from the two others

Without loss of generality, we can choose units where $e_{12} = e_{13} = e_{23} = -1$, $m_1 = m_2 = 1$, $m_0 = m$. For $D = 3$ the local energy (15) simplifies into

$$E_{\mathrm{loc}}^{[\varphi]}(q_3) = -\frac{5m+1}{4(m+1)} - \frac{m}{2(m+1)}\left(\cos\theta_1 + \cos\theta_2 + \frac{2}{m+1}\cos\theta_3\right). \tag{30}$$

The general study of Appendix A applied for $(a_1, a_2, a_3) = (1, 1, \frac{2}{m+1})$ allows to get the following analytic bounds on E_0:

$$0 \leqslant m \leqslant 1, \quad -\frac{1}{4} - \frac{m}{8} - \frac{m(m+2)}{(m+1)^2} \leqslant E_0 \leqslant -\frac{1}{4} - \frac{m(2m+1)}{(m+1)^2}, \tag{31a}$$

$$1 \leqslant m \leqslant 3, \quad -\frac{1}{4} - \frac{m}{8} - \frac{m(m+2)}{(m+1)^2} \leqslant E_0 \leqslant -\frac{1}{4} - \frac{m(m+2)}{(m+1)^2}, \tag{31b}$$

$$3 \leqslant m, \quad -\frac{1}{4} - \frac{m(2m+1)}{(m+1)^2} \leqslant E_0 \leqslant -\frac{1}{4} - \frac{m(m+2)}{(m+1)^2}. \tag{31c}$$

For $m \leqslant 3$, the lower bound on E_0 corresponds to a configuration where the particles make a non-degenerate isosceles triangle whose three angles are given by $\cos\theta_1 = \cos\theta_2 = (m+1)/4$ and $\cos\theta_3 = 1 - (m+1)^2/8$. The other bounds correspond to configurations where the particles are aligned. For $m \gg 1$, the bounds saturates to $-9/4 \lesssim E_0 \lesssim -5/4$ which is quite rough compared to the numerical value $E_0 > -1.8$ obtained for $m = 20$ with the optimized variational method; yet it is better than the results given by the improved (Hall–Post) variational method [3, Table 2] with which it coincides for $m \leqslant 1$. For small m both upper and lower bounds tend to the 2-body exact energy and provide acceptable bounds: for instance, when $m = 0.05$, the differential method gives $-0.34922 \leqslant E_0 \leqslant -0.29989$ while the other ones [3, Table 2] give $-0.59525 \leqslant E_0$ (naive variational method) , $-0.34922 \leqslant E_0$ (improved variational method), $-0.34666 \leqslant E_0$ (optimized variational method) and $E_0 \leqslant -0.3375$ (variational with hyperspherical expansion up to $L = 8$). See Fig. 4.

As already mentioned, the differential method, though being less precise for $N = 3$ than the improved or hyperspherical variational approaches, has several advantages: it is much simpler, it provides analytic upper and lower bounds that furnish an explicit estimation of the errors and, at last but not least, can be easily extended to larger N (see below); though possible in principle, the generalization of the improved variational method has not been done beyond $N = 4$.

3.3. Several examples of four-body systems

The optimized variational method has been successfully proposed for $N = 4$ in [4] for potentials with scaling-law behavior. For Coulombian interactions with a common coupling constant set to -1, tables and Figs. 5 and 6 compare the variational results to those obtained from the differential method when $D = 3$. The same conclusion as in the previous section can be drawn and here are some examples of explicit analytic bounds that are obtained by partitioning F_4 in subclusters made of 3 particles:

Let us take $m_1 = m_2 = m_3 = 1$ and $m_0 = m$. We have

$$0 \leqslant m \leqslant 1, \quad -\frac{9}{8} - \frac{3m(m^2+6m+13)}{8(m+1)^2} \leqslant E_0, \tag{32a}$$

m	Naive	Hall–Post	Optimized	Variational	$E_0^{(\mathrm{d.m.})}$	$\Delta E_0^{(\mathrm{d.m.})}$	$E_0^{(\mathrm{d.m.})} - \Delta E_0^{(\mathrm{d.m.})}$
0.05	−0.59525	−0.34922	−0.34666	−0.3375	−0.3246	0.02467	−0.3492
0.1	−0.6818	−0.436055	−0.43434	−0.423465	−0.3926	0.04344	−0.4361
0.2	−0.8333	−0.58055	−0.58045	−0.55915	−0.5125	0.06806	−0.5806
0.5	−1.16667	−0.86805	−0.86705	−0.8242	−0.7813	0.08681	−0.8681
1	−1.5	−1.125	−1.125	−1.067	−1.0625	0.06250	−1.1250
2	−1.83333	−1.3889	−1.37135	−1.30225	−1.2639	0.12500	−1.3889
5	−2.16667	−1.8472	−1.61705	−1.53935	−1.5000	0.27778	−1.7778
10	−2.3182	−2.49175	−1.731	−1.6495	−1.6136	0.37190	−1.9855
20	−2.40475	−3.74775	−1.7972	−1.7134	−1.6786	0.43084	−2.1094

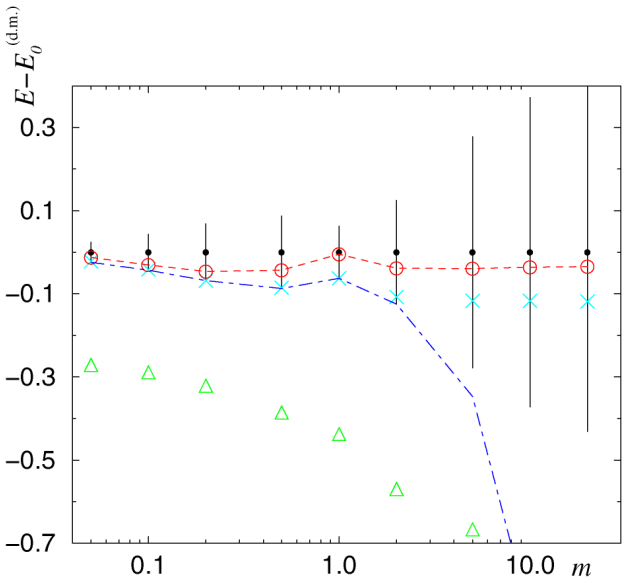

Fig. 4. Estimations for the ground-state energy E_0 of an attractive Coulombian system made of three particles with masses $(m, 1, 1)$. Naive (△), Hall–Post (also called improved, dashed-dotted link) and Optimized (×) provide lower bounds on E_0 while Variational (open circles with a dashed link) provides an upper bound. The corresponding data are taken from [3]. In the graph, the value of $E_0^{(\mathrm{d.m.})}$ has been subtracted. The error-bars are centered at zero (filled-circles) and have a width $2\Delta E_0^{(\mathrm{d.m.})}$.

$$1 \leqslant m \leqslant 2\sqrt{3}-1, \quad -\frac{9}{8} - \frac{3m(m^2+6m+13)}{8(m+1)^2} \leqslant E_0 \leqslant -\frac{5m^2+13m+2}{2(m+1)^2}, \tag{32b}$$

$$2\sqrt{3}-1 \leqslant m, \quad -\frac{9}{8} - \frac{3m(m^2+6m+13)}{8(m+1)^2} + \frac{3m(m+1-2\sqrt{3})^2}{8(m+1)^2} \leqslant E_0 \leqslant -\frac{5m^2+13m+1}{2(m+1)^2}. \tag{32c}$$

The configuration that minimizes $E_{\mathrm{loc}}^{[\varphi]}(q_4)$ given by (15) corresponds to a tetrahedron with an equilateral basis made by particles 1, 2 and 3. The three other faces, with particle 0 at one vertex, are identical isosceles triangles, namely those which maximize (30) when $m \leqslant 3$. Such a tetrahedron can indeed be constructed provided the angles at particle 0 are lower than $2\pi/3$ which requires $m \leqslant 2\sqrt{3}-1 \simeq 2.464$. For $m \geqslant 2\sqrt{3}-1$, the configuration that minimizes $E_{\mathrm{loc}}^{[\varphi]}(q_4)$

m	Naive	Hall–Post	Optimized	Variational	$E_0^{(\mathrm{d.m.})}$	$\Delta E_0^{(\mathrm{d.m.})}$	$E_0^{(\mathrm{d.m.})} - \Delta E_0^{(\mathrm{d.m.})}$
0.01	−2.29455	−1.17301	−1.17283	−1.108281	−1.10	0.07	−1.1730
0.1	−2.65909	−1.54679	−1.54167	−1.45802	−1.39	0.16	−1.5468
0.5	−3.75	−2.47917	−2.47618	−2.28857	−2.20	0.28	−2.4792
1	−4.5	−3	−3	−2.78762	−2.7500	0.2500	−3.0000
3	−5.625	−3.9375	−3.73167	−3.45553	−3.3024	0.6149	−3.9173
10	−6.3409	−6.48655	−4.20877	−3.90826	−3.6691	1.0575	−4.7266
100	−6.70545	−40.1395	−4.4673	−4.154310	−3.8412	1.3266	−5.1678
500	−6.741	−190.128	−4.49338	−4.17914	−3.8574	1.3545	−5.2119
$+\infty$	−6.75	$-\infty$	−4.5	−4.19259	−3.8615	1.3615	−5.2231

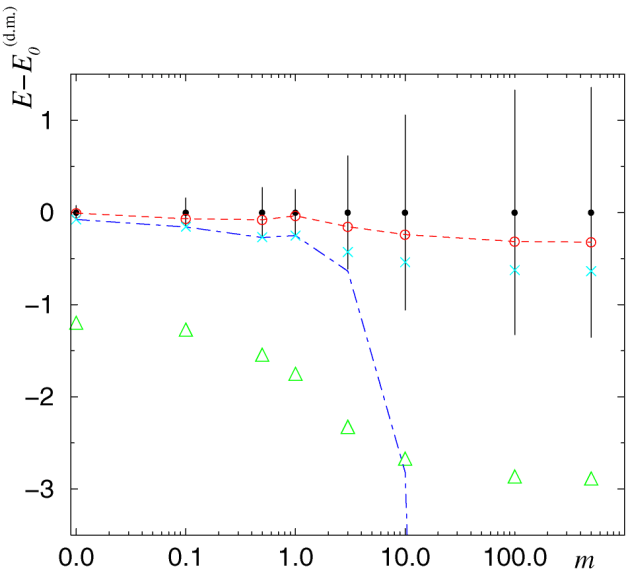

Fig. 5. Same conventions as in Fig. 4 for an attractive Coulombian system made of four particles with masses $(m, 1, 1, 1)$.

seems numerically to correspond to an equilateral triangle made by particles 1, 2 and 3 with particle 0 at its center (the flat tetrahedron obtained when $m = 2\sqrt{3} - 1$). This simple configuration allows to conjecture the analytic lower bound in (32c). For $m \geqslant 1$, the upper bound is obtained when the four particles are aligned with the 0th at one extremity. For $m \leqslant 1$, I am not able to propose an analytic expression for the upper bound.

For $m_2 = m_3 = 1$ and $m_0 = m_1 = m$, a tetrahedron that maximizes all the contributions of its faces simultaneously can be constructed for $m_\star^{-1} \leqslant m \leqslant m_\star \stackrel{\text{def}}{=} (-1 + \sqrt{17} + \sqrt{14 - 2\sqrt{17}})/2$. Two identical faces (see Fig. 7) corresponding to particles with masses $(1, 1, m)$ have their three angles given by $\cos\theta_1 = \cos\theta_2 = (m+1)/4$ and $\cos\theta_3 = 1 - (m+1)^2/8$. The angles $(\theta_1' = \theta_2', \theta_3')$ of the two other faces corresponding to particles with masses $(m, m, 1)$ are obtained replacing m by m^{-1} in the previous expressions. For $1/3 \leqslant m \leqslant 3$ such faces can indeed be constructed but the pairs of identical faces can be put together to construct one tetrahedron provided only that $\theta_3 \leqslant 2\theta_1'$. This last condition leads to $m^4 + 2m^3 - 14m^2 + 2m + 1 \leqslant 0$. $m_\star$ and $m_\star^{-1}$ are the two positive roots of the four-degree-polynomial, the two others being negative. We get

$$m_\star^{-1} \simeq 0.3622 \leqslant m \leqslant m_\star \simeq 2.7609, \quad -\frac{m^2 + 10m + 1}{2(m+1)} \leqslant E_0. \tag{33}$$

m	Naive	Hall–Post	Optimized	Variational	$E_0^{(\mathrm{d.m.})}$	$\Delta E_0^{(\mathrm{d.m.})}$	$E_0^{(\mathrm{d.m.})} - \Delta E_0^{(\mathrm{d.m.})}$
0.001	−0.756745	−0.504495	−0.25557	−0.25492	−0.2543	0.0021	−0.2564
0.002	−0.763475	−0.508985	−0.26114	−0.25985	−0.2587	0.0042	−0.2629
0.005	−0.7836	−0.5224	−0.277805	−0.2746	−0.2717	0.0104	−0.2820
0.01	−0.816905	−0.544605	−0.305465	−0.32403	−0.2931	0.0204	−0.3135
0.05	−1.07322	−0.715475	−0.519635	−0.50503	−0.4581	0.0913	−0.5494
0.1	−1.37045	−0.913635	−0.76439	−0.7308	−0.6492	0.1594	−0.8086
0.2	−1.9	−1.26666	−1.17921	−1.10975	−0.9893	0.2448	−1.234
0.5	−3.125	−2.08333	−2.06426	−1.91867	−1.7847	0.2986	−2.0833†
0.8	−4.01666	−2.67778	−2.67552	−2.48094	−2.4034	0.2744	−2.6778†
1	−4.5	−3	−3	−2.78736	−2.7500	0.2500	−3.0000†

† Lower bounds (33).

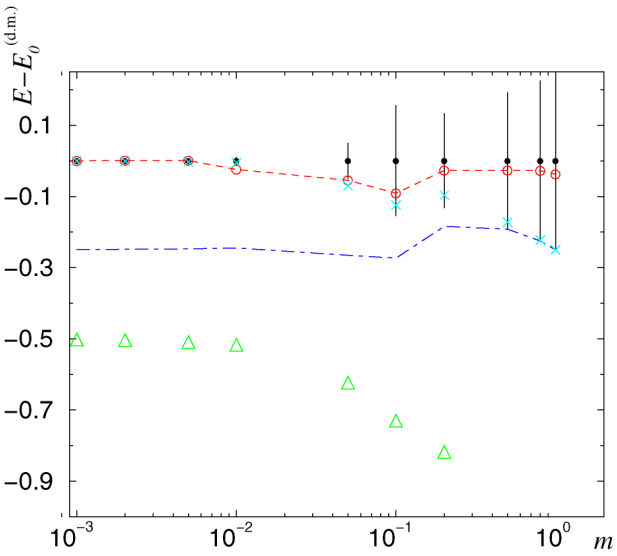

Fig. 6. Same conventions as in Fig. 4 for an attractive Coulombian system made of four particles with masses $(m, m, 1, 1)$.

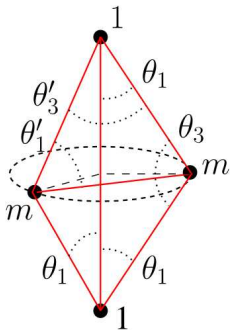

Fig. 7. For a special range of m, a four-body configuration with masses $(m, m, 1, 1)$ that minimizes the local energy can be constructed from the optimal configurations of each of its three-body subsystems.

3.4. Arbitrary number of identical particles plus one different from the others

As we have already seen for identical particles, the possibility of partitioning the local energy in contributions involving more than two particles allow to get some bounds on the ground-state energy of systems made of an arbitrary number N of particles. For $N \geqslant 5$, this is beyond the scope of the existing optimized variational methods. To see one more last example, let us generalize both cases of Sections 3.1 and 3.2 and consider a system made of one particle with mass $m_0 = m$ and $N-1$ identical particles of mass $m_1 = \cdots = m_{N-1} = 1$. All the identical particles interact with the same coupling constants $e_{ij} = -1$ and the 0th interact with $e_{0,i} = -g^2$. The local energy is given by (15) as

$$E_{\text{loc}}^{[\varphi]}(q_N) = -\frac{1}{(D-1)^2}\left\{\frac{2mg^4}{m+1}(N-1) + \frac{1}{2}(N-1)(N-2) + F_{N-1}(q_{N-1}) + a\big(m^{-1}\big)\sum_{\substack{i,j=1\\ i<j}}^{N-1}\big[\cos(\widehat{0ij}) + \cos(\widehat{0ji}) + a(m)\cos(\widehat{i0j})\big]\right\}, \tag{34}$$

where now q_{N-1} stands for the configuration of the $N-1$ identical particles, $a(m) \overset{\text{def}}{=} 2g^2/(m+1)$. By simultaneously bounding the contributions of the triangles that include the 0th particle and the contribution of the remaining cluster of the identical particles, we immediately have analytic expressions for bounds on E_0. For instance, the lower bound is given by

$$E_0 \geqslant -\frac{1}{(D-1)^2}\left\{\frac{2mg^4}{m+1}(N-1) + \frac{1}{2}(N-1)(N-2) + \sup_{\mathcal{Q}_{N-1}} F_{N-1} + \frac{1}{2}a\big(m^{-1}\big)(N-1)(N-2)F_3^{\max}\big(1,1,a(m)\big)\right\}, \tag{35}$$

where $F_3^{\max}$ is given by (A.4) and $\sup_{\mathcal{Q}_{N-1}} F_{N-1}$ has been explicitly estimated in Section 3.1.

4. Arbitrary two-body interaction

4.1. Behavior at large distances

Considering attractive Coulombian interactions is relevant for heavy quarks models at short distances but, of course, other kinds of effective potentials are required in most models. Since in general no analytic expressions are known for the two-body ground-state energies ϵ_{ij}, no method is expected to provide explicit non-trivial bounds on E_0. However, if one has some experimental clues about ϵ_{ij} (by measuring 2-body masses or dissociation energies) or numerical estimates as well, it is always interesting to obtain some relations between the ϵ's and the ground-state energies of larger systems. As mentioned in the introduction, this have been achieved in [2] for $N = 3$ and in [4] for $N = 4$ when the interactions are of the form $v_{ij}(r) \propto \text{sign}(\beta) r^\beta$.

For $\beta > 0$, the semiclassical argument given at the end of Section 2 shows that (13) is expected to be unbounded; then (4) gives no information. If we want to take the advantage of the simple form (13) (that is, to keep the choice (9) with (11) for the test functions), we have to work with finite range potentials. When at large distances, the potential is still confining ($\beta = 2$ for harmonic forces or $\beta = 1$ for interquark force in quantum chromodynamics [9], and [5] for an

up-to-date review), some different ansatz for φ must be constructed in order to eliminate the singular behavior of the v_{ij}'s at infinite distances. Actually, the Coulombian case considered in the previous section can be seen as an example of a problem where simple poles at finite distances can be eliminated. Anyway, in many situations, the 2-body ground-state is expected to depend on the behavior of the potential at large distances by exponentially small terms only. If, in the integral (3), we decide to keep only those configurations q_N whose size remains in a physical domain bounded by a cut-off length Λ, then we expect to make an exponentially small error on the estimates of E_0; this is due to the exponential decay of Φ_0 when two or more particles separate off. Like the ϵ_{ij}'s, Λ is typically obtained from a 2-body dynamics but its precise value is irrelevant if the extremal values of the local energy do not depend on it. It is precisely the case of the Coulombian interactions (more exactly, interactions that can be modeled by Coulombian potential at the energy scale where the ground-state exists) for which the local energy (15) is invariant under dilations.

Since, in the present section, we just want to sketch some main guidelines without working through the details neither being exhaustive, we will consider only the cases where

$$v(r) \underset{r\to+\infty}{\longrightarrow} 0. \tag{36}$$

4.2. Fitting the 2-body ground-state wavefunction

What is new, here, is that the differential method allows us to choose directly the 2-body ground-state wave-functions, or rather their logarithms S_{ij}. Once some numerical estimate of ϵ_{ij} is obtained in one way or another, we can completely bypass the problem of modeling the 2-body potential uniformly. Being free of any integration, the differential method can deal with rather complicated, and therefore rather realistic two-body test functions. An explicit choice of S_{ij}'s provides an explicit form for the local energy (13).

It frequently happens that we know from experiments the behavior of the two-body potential in some specific regimes (most generally, at short and large distances) but not uniformly. We can therefore, in each of these regimes, tentatively obtain, with the help of the differential equation (11), the local functional form of the two-body ground-state wave-function. Matching these local solutions together, and then dealing with quite complicated global expression for S and v, do not represent a serious obstacle for the computation of (13).

To be a little less speculative, let us consider N identical particles with unit mass, interacting with a two-body radial potential $v(r)$ such that $v(r) \to 0$ when $r \to \infty$ and

$$v(r) \underset{r\to0^+}{\longrightarrow} v_0 r^\beta \tag{37}$$

for some v_0, and with considering only one case, say, $\beta > 0$. The two-body stationary Schrödinger equation (11) becomes

$$-\left(\frac{\mathrm{d}^2}{\mathrm{d}r^2} + \frac{D-1}{r}\frac{\mathrm{d}}{\mathrm{d}r}\right)\phi + v\phi = \epsilon_0\phi, \tag{38}$$

where $\epsilon_0 < 0$ will denote an estimate of the two-body ground-state energy; it can be considered as another parameter that should fit the experiments involving two bodies. Let us guess the behavior of $S(r) \overset{\text{def}}{=} \ln\phi(r)$ at short distances by writing for $\sigma \neq -1$:

$$S(r) \underset{r\to0^+}{\longrightarrow} \frac{s_0}{\sigma+1} r^{\sigma+1}. \tag{39}$$

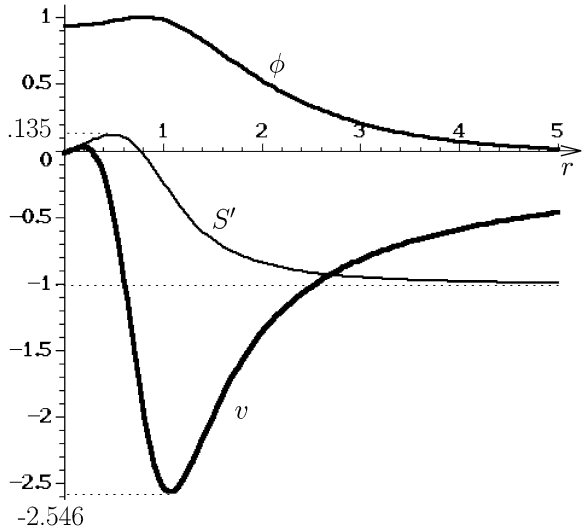

Fig. 8. $D = 3$, $\epsilon_0 = -1$, $v_0 = 1$, $\beta = 1.5$, the function S' given by (42) is plotted as well as the corresponding wavefunction $\phi = \exp S$ which is the ground-state of the potential v for energy ϵ_0. The latter can be reconstructed from ϕ with the Schrödinger equation.

Identifying the leading orders after having reported (39) in (38), we necessarily get (for $D > 1$) $\sigma = 1$ and $s_0 = -\epsilon_0/D$. The next term in the development of S can also be determined. For $0 < \beta < 2$, it depends only on the leading term (37) and we have

$$S(r) \underset{r\to 0^+}{\longrightarrow} -\frac{\epsilon_0}{2d} r^2 + \frac{v_0}{(D+\beta)(2+\beta)} r^{2+\beta} + o\big(r^{2+\beta}\big). \tag{40}$$

This local asymptotic series must be matched with the semiclassical behavior at large r

$$S(r) \underset{r\to+\infty}{\longrightarrow} -\sqrt{-\epsilon_0}\, r, \tag{41}$$

since we have supposed (36). The additive constant in S is irrelevant since the local energy does not depend on the normalization of ϕ. A simple choice that ensures the local energy to remain uniformly bounded is to take for S' a fraction like

$$S'(r) = \frac{-\frac{\epsilon_0}{D} r + \frac{v_0}{D+\beta} r^{1+\beta} - \sqrt{-\epsilon_0}\, r^{1+2\beta}}{1 + r^{1+2\beta}}. \tag{42}$$

Fig. 8 show the corresponding ϕ for an arbitrary choice of parameters together with the corresponding v whose complicated analytic expression on $[0, +\infty[$ is not needed.

4.3. Crude bounds

From Eq. (13), an immediate upper bound on E_0 is given by:

$$\begin{aligned} &\frac{1}{2}N(N-1)\epsilon_0 - \frac{1}{2}N(N-1)(N-2)\sigma^2 \\ &\quad \leqslant E_0 \leqslant \frac{1}{2}N(N-1)\epsilon_0 + \frac{1}{2}N(N-1)(N-2)\sigma^2, \end{aligned} \tag{43}$$

where

$$\sigma \stackrel{\text{def}}{=} \sup_{[0,+\infty[} |S'|. \tag{44}$$

Because the constraints between the angles $\widehat{j,i,k}$ are not taken into account, these inequalities are expected to be rather rough and their quality deteriorate for large N: when positive, the upper bound becomes irrelevant since we already know that $E_0 \leqslant 0$. Indeed, the decreasing of the σ^2 term with N does not guarantee that the lower bound is better than the Hall–Post bound $N(N-1)\tilde{\epsilon}_0/2$ or even than the naive one $N(N-1)\tilde{\tilde{\epsilon}}_0/2$ [4, Sections 2.1 and 2.2] where $\tilde{\tilde{\epsilon}}_0$ (respectively, $\tilde{\epsilon}_0$ and ϵ_0) is the ground-state energy for a particle of mass $(N-1)/2$ (respectively, $N/4$ and 1/2) in the central potential v (recall $\tilde{\tilde{\epsilon}}_0 < \tilde{\epsilon}_0 < \epsilon_0$).

4.4. Reduction to a finite number of Coulombian cases

In fact, we can find some bounds of (13) by reducing the problem to a finite number of Coulombian-like cases, that is, where the function to be bound involves constant factors in front of the cosine (compare (15) with (13)). To see this, split the coordinates q_N into a scaling factor $\lambda \geqslant 0$ and some angle variables θ among which $(N-1)D-1$ are independent. Each distance writes $r_{ij} = \lambda\rho_{ij}(\theta)$ where the ρ_{ij}'s are functions that do not depend on the global size of the configuration but on its shape only. Now, from (13), we define (recall $m_i = 1$)

$$G_N(q_N) \stackrel{\text{def}}{=} \sum_{\widehat{(j,i,k)}} S'(r_{ij})S'(r_{ik})\cos(\widehat{j,i,k}), \tag{45}$$

and we have

$$\inf_{q_N}\big(G_N(q_N)\big) = \inf_{\theta}\big(\tilde{G}_N(\theta)\big), \tag{46}$$

where

$$\tilde{G}_N(\theta) = \inf_{\lambda} \sum_{\widehat{(j,i,k)}} S'\big[\lambda\rho_{ij}(\theta)\big]S'\big[\lambda\rho_{ik}(\theta)\big]\cos(\widehat{j,i,k}). \tag{47}$$

Analogous relations are obtained for the maxima. For fixed θ, when λ varies from 0 to $+\infty$, the map $\lambda \mapsto (S'[\lambda\rho_{ij}(\theta)])_{0\leqslant i<j\leqslant N-1}$ defines a curve $\mathcal{C}_\theta$ in a n-dimensional space with $n = N(N-1)/2$. $\mathcal{C}_\theta$ is bounded if S' is bounded. More precisely, $\mathcal{C}_\theta$ is inside the n-dimensional hypercube $\mathcal{B} \stackrel{\text{def}}{=} [\sigma_{\min}, \sigma_{\max}]^n$ where

$$\sigma_{\min} \stackrel{\text{def}}{=} \inf_{[0,+\infty[} S', \tag{48a}$$

$$\sigma_{\max} \stackrel{\text{def}}{=} \sup_{[0,+\infty[} S'. \tag{48b}$$

If S' has the form shown in Fig. 8, $\mathcal{C}_\theta$ starts at the origin ($S'(0) = 0$) and ends at the point $(-1,\ldots,-1)$. Taking all the points in $\mathcal{B}$ rather than the points of $\mathcal{C}_\theta$ leads to a lower bound of $\tilde{G}_N$:

$$\inf_{\vec{s}\in\mathcal{B}} \sum_{\widehat{(j,i,k)}} s_{ij}s_{ik}\cos(\widehat{j,i,k}) \leqslant \tilde{G}_N(\theta), \tag{49}$$

where $\vec{s} = (s_{ij})_{0 \leqslant i < j \leqslant N-1}$. Now, whatever the values of the cosines may be, the quadratic function in $\vec{s}$ appearing in the left-hand side of (49) reaches its minimum at a vertex of $\mathcal{B}$.[7] Let us denote by $\mathcal{V}$, the finite set of the 2^n vertices $\vec{s}$ of $\mathcal{B}$ (i.e., for all $\vec{s}$ in $\mathcal{V}$, each s_{ij} is either $\sigma_{\min}$ or $\sigma_{\max}$). We have

$$\inf_{\vec{s}\in\mathcal{V}}\Big[\inf_{\theta}\big(F_N^{(\vec{s})}(\theta)\big)\Big] \leqslant \inf_{q_N}\big(G_N(q_N)\big), \tag{50}$$

where

$$F_N^{(\vec{s})}(\theta) \stackrel{\text{def}}{=} \sum_{\widehat{(j,i,k)}} s_{ij}s_{ik}\cos(\widehat{j,i,k}). \tag{51}$$

In fact, what we have done by obtaining the left-hand side of (50) is to make the values of $S'(r_{ij})$ independent from those of θ. It follows that the inequality (50) will be strict if the value of $\vec{s}$ at the minimizing vertex are incompatible with the geometrical constraints on the configuration of the N points. We will illustrate this point in the next subsection. We have obtained

$$E_0 \leqslant \frac{1}{2}N(N-1)\epsilon_0 - \inf_{\vec{s}\in\mathcal{V}}\Big[\inf_{\theta}\big(F_N^{(\vec{s})}(\theta)\big)\Big], \tag{52a}$$

and similarly

$$\frac{1}{2}N(N-1)\epsilon_0 - \sup_{\vec{s}\in\mathcal{V}}\Big[\sup_{\theta}\big(F_N^{(\vec{s})}(\theta)\big)\Big] \leqslant E_0. \tag{52b}$$

The function $F_N^{(\vec{s})}(\theta)$ has the same form as the second sum of the right-hand side of (15). Therefore, the computation of the bounds in (52) is equivalent to a finite number of Coulombian problems (with not necessarily attractive interactions since the sign of s_{ij} may change) where we must consider all the possible $\vec{s}$ whose components are either $\sigma_{\min}$ or $\sigma_{\max}$.

4.5. Three bodies

As we have seen in Section 3, even in the purely attractive Coulombian cases, an analytic expression of the extrema of F_N is not known in general. Anyway, one can always group in clusters the terms involved in (51) like in (24), then use inequalities like (25) and reduce the number of particles. Let us then consider $N = 3$. It can be shown[8] that

$$\inf_{\vec{s}\in\mathcal{V}}\Big[\inf_{\theta}\big(F_3^{(\vec{s})}(\theta)\big)\Big] = 2\sigma_{\min}\sigma_{\max} - \sigma^2 \tag{53}$$

[7] For any constant A, any n-dimensional vector $\vec{B}$ and any symmetric $(n \times n)$-matrix C with vanishing diagonal coefficients, the critical points of $f_n(\vec{s}) = \vec{s}\cdot C\vec{s} + \vec{B}\cdot\vec{s} + A$ are always saddle points: the direction $s_2 = \pm\,\mathrm{sign}(C_{12})s_1$ and $s_i = 0$ for $i > 2$ makes f increase/decrease as $\pm|C_{12}|s_1^2$ from its critical value. Therefore, the extrema of f are reached on the boundary of the domain of $\vec{s}$. For $\vec{s}$ restricted to a n-dimensional squared box whose faces are given by fixing one s_i, the restriction of f_n to one face, i.e., to a $(n-1)$-dimensional box, leads to a function f_{n-1} to which the above argument may be applied again. By repetition down to $n = 1$, we see that the maximum and the minimum of f is necessarily reached at one of the vertices of the original n-box.

[8] The extrema of $F_3^{(\vec{s})}(\theta)$ when θ varies can be calculated with the help of the appendix with $a_3 = s_{01}s_{02}$, $a_2 = s_{02}s_{12}$ and $a_1 = s_{01}s_{12}$. From (A.3), we get $f(a_1,a_2,a_3) = \frac{1}{2}(s_{01}^2 + s_{02}^2 + s_{12}^2)$ which is always positive and larger than $a_1 + a_2 - a_3$, $-a_1 + a_2 + a_3$ and $a_1 - a_2 + a_3$ corresponding to the three aligned configurations for different ordering of the particles. From (A.4), the minimum of $F_3^{(\vec{s})}(\theta)$ must therefore correspond to an aligned configuration. Its maximum is reached for the configuration described just after Eq. (57).

with definitions (44) and (48). $\inf_\theta F_3^{(\vec{s})}(\theta)$ is obtained for an aligned configuration which is generically incompatible with $\vec{s}$ being a vertex of the cube $[\sigma_{\min},\sigma_{\max}]^3$. For instance, suppose that S' has the shape depicted in Fig. 8 where $\sigma=-\sigma_{\min}>\sigma_{\max}>0$; the value $2\sigma_{\min}\sigma_{\max}-\sigma_{\min}^2$ is obtained for $\vec{s}=(s_{01},s_{02},s_{12})=(\sigma_{\min},\sigma_{\min},\sigma_{\max})$ and should be realized for $r_{01}\gg 1$, $r_{02}\gg 1$ and $r_{12}\simeq r_{\max}$ (the unique finite distance at which S'' vanishes); but this is incompatible with the alignment condition $\cos(\widehat{1,0,2})=-1$ where particle 0 is in between the two others which implies $r_{12}=r_{01}+r_{02}$. The inequality (50) is therefore strongly strict. It can be improved by reducing the size of the cube $\mathcal{B}$ to make its minimizing vertices compatible with the aligned configuration. It can be shown that for S' of the form shown in Fig. 8, we have

$$2\sigma_{\max}S'(2r_0)-\sigma_{\max}^2\leqslant\inf_{q_3}\bigl(G_3(q_3)\bigr), \tag{54}$$

where r_0 is the unique strictly positive distance where S' vanishes.[9] Even though the inequality is still strict because $r_{12}=2r_0\neq r_{01}+r_{02}=2r_{\max}$ in general, the bound is much better than (53). For instance, if we take the value of the parameters corresponding to Fig. 8 we have

$$2\sigma_{\min}\sigma_{\max}-\sigma_{\min}^2\simeq-1.2705<2\sigma_{\max}S'(2r_0)-\sigma_{\max}^2\simeq-0.205, \tag{55}$$

to be compared with the result of the numerical minimization of G_3

$$\inf_{q_3}\bigl(G_3(q_3)\bigr)\simeq-0.1150, \tag{56}$$

obtained for the aligned configuration where $r_{01}=r_{02}=r_{12}/2\simeq 0.6107$.

The other bound

$$\sup_{q_3}\bigl(G_3(q_3)\bigr)=\sup_{\vec{s}\in\mathcal{V}}\Bigl[\sup_\theta\bigl(F_3^{(\vec{s})}(\theta)\bigr)\Bigr]=\frac{3}{2}\sigma^2 \tag{57}$$

is actually obtained at the vertex $\vec{s}=(\sigma,\sigma,\sigma)$ for an equilateral configuration where the common distance $r_{01}=r_{02}=r_{12}$ is where $|S'|$ reaches its maximum. For S' like in Fig. 8, it corresponds to a very large triangle ($r_{01}\gg 1$) where $\sigma\simeq 1$. For $D=3$, $\epsilon_0=-1$, $v_0=1$, $\beta=1.5$, from (50) and results (56), (57), the inequalities (52) give

$$-3-\frac{3}{2}=-4.5\leqslant E_0\leqslant-3+0.1150=-2.885, \tag{58}$$

corresponding to a relative error of $\Delta E_0^{(\mathrm{d.m.})}/E_0^{(\mathrm{d.m.})}\simeq 22\%$. This not really impressive (again we emphasize that we are not looking for numerical performance at this stage of development of the differential method) but can be seen as an encouraging starting point since the interactions involved so far in the three-body system are highly not trivial. It would have required much more numerical work to obtain a rigorous window for E_0 with variational methods (specially a lower bound since the potential considered here does not follow a power-law behavior).

5. Conclusion

The differential method appears to offer a completely new strategy for estimating a ground-state energy. For many-body systems, we have seen on several examples how this approach can

[9] Any aligned configuration with $r_{01}\simeq r_{02}\lesssim r_0$ and $r_{12}=r_{01}+r_{02}>r_0$ corresponds to a negative G_3. Therefore, as far as its minimum is concerned, the configurations leading to a positive $\inf_\theta F_3^{(\vec{s})}$ can be forgotten (see footnote 8). It is straightforward to check that all the possible relative positions of r_{ij} with respect to $r_{\max}$ and r_0 that are compatible with $r_{12}=r_{01}+r_{02}$ provide a G_3 such that (54).

be fruitful. For attractive Coulombian particles, it can compete with existing others methods (that are based on the variational principle) on several levels: it provides upper *and* lower bounds with comparable numerical precision, its simplicity renders the analytic calculations tractable even for large N and/or allows a low cost of numerical computation. Beyond purely Coulombian systems, the differential method, being so general, offers a remarkable flexibility. As have been sketched in the previous section, one can deal with systems where interactions can be very rich (possibly short-ranged with an a priori cut-off); several regimes which are valid at different scales can be implemented at once. There is some hope that future works successfully apply the differential methods for proper realistic potentials.

Unfortunately, I have not been able to generalize the differential method to fermionic systems where the ground-state spatial wave-function is antisymmetric. In such cases, the presence of non-trivial nodal lines [6] breaks down the proof of inequalities (4).

There is a lot of work to be done regarding a systematic improvement of the bounds, once some finite ones have been found with a φ given at first attempt. In this paper, we have not considered some free parameters on which a (family) of test functions, say φ_ζ, may depend. As shown for a one-dimensional system [15], the locality of the differential method may require a very few number of ζ's at each optimization step (unlike for the variational test functions) for obtaining substantial improvements of the bounds by calculating, say, $\sup_\zeta[\inf_q(E_{\rm loc}^{[\varphi_\zeta]}(q))]$. A precise proof that this approach is efficient for several dimensions remains an open interesting problem.

Acknowledgements

I thank Jean-Marc Richard for a critical reading of the first proof of this manuscript and acknowledge the generous hospitality of Dominique Delande and Benoît Grémaud of the group "Dynamique des systèmes coulombiens" at the Laboratoire Kastler-Brossel.

Appendix A. Extrema for the three-body Coulombian problem

For the three-body Coulombian problem, as can be seen from the second sum in the right-hand side of (15), we must find

$$F_3^{\max}(a_1,a_2,a_3) \stackrel{\text{def}}{=} \sup_{\text{triangles}} [a_1\cos\theta_1 + a_2\cos\theta_2 + a_3\cos\theta_3], \tag{A.1}$$

$$F_3^{\min}(a_1,a_2,a_3) \stackrel{\text{def}}{=} \inf_{\text{triangles}} [a_1\cos\theta_1 + a_2\cos\theta_2 + a_3\cos\theta_3], \tag{A.2}$$

where the θ's are the angles at the three vertices of the triangle made of the three particles. The a's are some real parameters that depend on the masses and the coupling constants. Let us define

$$f(a_1,a_2,a_3) \stackrel{\text{def}}{=} \frac{1}{2}\left(\frac{a_1a_2}{a_3} + \frac{a_1a_3}{a_2} + \frac{a_2a_3}{a_1}\right), \tag{A.3}$$

then we have

$$F_3^{\max\min}(a_1,a_2,a_3) = \stackrel{\max}{\min}\{a_1+a_2-a_3, a_1-a_2+a_3, -a_1+a_2+a_3, f(a_1,a_2,a_3)\}. \tag{A.4}$$

f is considered in the list (A.4) if and only if the following three conditions are satisfied simultaneously:

$$\frac{1}{2}\left|\frac{a_2}{a_3}+\frac{a_3}{a_2}-\frac{a_2a_3}{a_1^2}\right|\leqslant 1,$$
$$\frac{1}{2}\left|\frac{a_1}{a_2}+\frac{a_2}{a_1}-\frac{a_1a_2}{a_3^2}\right|\leqslant 1,\qquad \frac{1}{2}\left|\frac{a_3}{a_1}+\frac{a_1}{a_3}-\frac{a_1a_3}{a_2^2}\right|\leqslant 1. \tag{A.5}$$

Here is the proof. We will restrict the values of the θ's to $[0,\pi]$ and the constraint $\theta_1+\theta_2+\theta_3=\pi$ is implemented by the Lagrange multiplier method. We are led to extremalize the function $G_3(\theta_1,\theta_2,\theta_3)\stackrel{\text{def}}{=}a_1\cos\theta_1+a_2\cos\theta_2+a_3\cos\theta_3+\ell(\theta_1+\theta_2+\theta_3-\pi)$ for unconstrained $(\theta_1,\theta_2,\theta_3)\in[0,\pi]^3$, ℓ being the Lagrange multiplier. The three conditions $\partial_{\theta_i}G_3=0$ for $i=1,2,3$ lead to $\ell=a_1\sin\theta_1=a_2\sin\theta_2=a_3\sin\theta_3$. The case $\ell=0$ corresponds to the alignment of the three particles and gives the three first values in the list (A.4) corresponding to $(\theta_1,\theta_2,\theta_3)=(0,0,\pi)$ and its circular permutations.

Taking into account the constraint on the angles, we have $\ell=a_3\sin\theta_3=a_3\sin\theta_1\cos\theta_2+a_3\sin\theta_2\cos\theta_1=\ell(a_3\cos\theta_2/a_1+a_3\cos\theta_1/a_2)$. Therefore, when $\ell\neq 0$, we find $a_1\cos\theta_1+a_2\cos\theta_2=a_1a_2/a_3$ as well as the other relations that are obtained by circular permutations of the indices. From the decomposition $F_3=\frac{1}{2}(a_1\cos\theta_1+a_2\cos\theta_2)+\frac{1}{2}(a_2\cos\theta_2+a_3\cos\theta_3)+\frac{1}{2}(a_1\cos\theta_1+a_3\cos\theta_3)$, we obtain the value (A.3) that must be considered in (A.4) if and only if there exists some θ's such that

$$a_1\sin\theta_1=a_2\sin\theta_2=a_3\sin\theta_3\quad\text{and}\quad\theta_1+\theta_2+\theta_3=\pi. \tag{A.6}$$

Solving these three equations leads to the values for the three $|\cos\theta_i|$ that are precisely given by the left-hand sides of the inequalities (A.5).

References

[1] J.-L. Basdevant, A. Martin, J.-M. Richard, Improved bounds on many-body Hamiltonians. I. Self-gravitating bosons, Nucl. Phys. B 343 (1) (1990) 60–68.
[2] J.-L. Basdevant, A. Martin, J.-M. Richard, Improved bounds on many-body Hamiltonians. II. Baryons from mesons in the quark model, Nucl. Phys. B 343 (1) (1990) 69–85.
[3] J.-L. Basdevant, A. Martin, J.-M. Richard, T.T. Wu, Optimized lower bounds in the three-body problem, Nucl. Phys. B 393 (1993) 111–125.
[4] A. Benslama, A. Metatla, A. Bachkhaznadji, S.R. Zouzou, A. Krikeb, J.-L. Basdevant, J.-M. Richard, T.T. Wu, Optimized lower bound for four-body Hamiltonians, Few-Body Systems 24 (1) (1998) 39–54.
[5] N. Brambilla, et al., Heavy quarkonium physics, hep-ph/0412158, 2004.
[6] D.M. Ceperley, Fermion nodes, J. Stat. Phys. 63 (5/6) (1991) 1237–1267.
[7] F.M. Fernández, Q. Ma, R.H. Tipping, Eigenvalues of the Schrödinger equation via the Riccati–Padé method, Phys. Rev. A 40 (11) (1989) 6149–6153.
[8] M.E. Fisher, D. Ruelle, The stability of many-particle systems, J. Math. Phys. 7 (2) (1966) 260–270.
[9] A.K. Grant, J.L. Rosner, E. Rynes, An updated description of quarkonium by power-law potentials, Phys. Rev. D 47 (5) (1993) 1981–1987.
[10] C.R. Handy, D. Bessis, Rapidly convergent lower bounds for the Schrödinger-equation ground-state energy, Phys. Rev. Lett. 55 (9) (1985) 931–934.
[11] G. Jaczko, L. Durand, Understanding the success of nonrelativistic potential models for relativistic quark–antiquark bound states, Phys. Rev. D 58 (11) (1998) 114017.
[12] A. Lenard, F.J. Dyson, Stability of matter I, J. Math. Phys. 8 (3) (1967) 423–434.
[13] J.-M. Lévy-Leblond, Nonsaturation of gravitational forces, J. Math. Phys. 10 (5) (1969) 806–812.
[14] V.P. Maslov, M.V. Fedoriuk, Semi-Classical Approximation in Quantum Mechanics, Mathematical Physics and Applied Mathematics, vol. 7, Reidel, Dordrecht, 1981.
[15] A. Mouchet, A differential method for bounding the ground state energy, J. Phys. A 38 (2005) 1039–1047.
[16] A. Mouchet, Upper and lower bounds for an eigenvalue associated with a positive eigenvector, math.SP/0505541.
[17] S. Nussinov, Baryon–meson mass inequality, Phys. Rev. Lett. 51 (23) (1983) 2081–2084.

[18] A.R. Bodmer, A. Shamsher, A self-consistent two-body method for three-body systems and the hypernucleus ${}_{\Lambda}\mathrm{Be}^{9}$, Nucl. Phys. 54 (1964) 657–682.
[19] M. Reed, B. Simon, Analysis of Operators, Methods of Modern Mathematical Physics, vol. 4, Academic Press, New York, 1978.
[20] J.-M. Richard, Few-body problems in hadron spectroscopy, Nucl. Phys. A 689 (2001) 235–246.
[21] J.-M. Richard, Borromean binding, nucl-th/0305076.
[22] E.B. Saff, A.B. Kuijlaars, Distributing many points on a sphere, Math. Intelligencer 19 (1) (1997) 5–11.
[23] P. Van Dyke, R. Folk, Two-body equations for four-nucleon problems, Phys. Rev. 178 (4) (1969) 1537–1542.

II.4 Bornes supérieures et inférieures d'une valeur propre associée à un vecteur propre positif

Cet article est la mise en forme de la méthode différentielle en suivant des critères de rigueur plus mathématiques. Les discussions avec les mathématiciens du LMPT, notamment Émmanuel LESIGNE à propos de la répartition de points sur une sphère et bien sûr les experts de géométrie riemanienne comme Ahmad ELSOUFI, Saïd ILIAS ou de théorie spectrale et d'équations aux dérivées partielles, notamment Laurent VÉRON et Evans HARRELL de la *School of Mathematics & Associate Dean College of Sciences* (Georgia Institute of Technology, Atlanta) m'ont convaincu que ce travail pouvait intéresser les mathématiciens et justifiaient ainsi un effort de « traduction » auquel je ne suis pas habitué.(3)

(3) Il n'y a pas que pour le grand public que l'on doive faire un effort pour se faire comprendre (*cf.* § I.4 p. 46). Essayer de briser les cloisons interdisciplinaires ou des résistances culturelles requiert souvent des efforts encore plus considérables.

JOURNAL OF MATHEMATICAL PHYSICS **47**, 022109 (2006)

Upper and lower bounds for an eigenvalue associated with a positive eigenvector

Amaury Mouchet[a)]
Laboratoire de Mathématiques et de Physique Théorique (CNRS UMR 6083), Université François Rabelais Avenue Monge, Parc de Grandmont 37200 Tours, France

(Received 28 October 2005; accepted 14 December 2005;
published online 28 February 2006)

When an eigenvector of a semibounded operator is positive, we show that a remarkably simple argument allows to obtain upper and lower bounds for its associated eigenvalue. This theorem is a substantial generalization of Barta-type inequalities and can be applied to non-necessarily purely quadratic Hamiltonians. An application for a magnetic Hamiltonian is given and the case of a discrete Schrödinger operator is also discussed. It is shown how this approach leads to some explicit bounds on the ground-state energy of a system made of an arbitrary number of attractive Coulombian particles. © *2006 American Institute of Physics.*
[DOI: 10.1063/1.2168124]

I. INTRODUCTION

In most situations, the principal eigenvalue of a semibounded operator cannot be obtained explicitly whereas it plays a crucial role in physics: the smallest vibration frequency of an elastic system, the fundamental mode of an electromagnetic cavity, the ground-state energy of a quantum system with a finite number of degrees of freedom, the energy of the vacuum in a quantum field theory, the equilibrium state at zero temperature in statistical physics, etc. There are actually very few ways—which are usually specific to a restricted class of systems[1]—to obtain accurate approximations of an eigenvalue with a rigorous control on the errors and a reasonable amount of numerical computations. For instance, in a typical Dirichlet-Laplacian problem defined for an open connected set $\mathcal{Q}\subset\mathbb{R}^d$; $d\in\mathbb{N}$; Barta's inequalities (Barta, 1937) allow to bound to the lowest eigenvalue e_0: The determination of a lower (respectively, upper) bound requires the finding of the absolute minimum (respectively, maximum) of a smooth function defined on $\mathcal{Q}$. Compared to the general and traditional methods like the Rayleigh-Schrödinger perturbative series and the Rayleigh-Ritz or Temple variational methods, an advantage of Barta's approach is not only to naturally provide both an upper and a lower bound, but also does not involve the calculation of any integral. Therefore, generalizations of Barta's inequalities can lead to interesting spectral information. This generalization has been carried out in two directions:

(i) For Laplacian operators acting on square integrable functions defined on a Riemannian manifold (for a recent work on this subject, see Bessa and Montenegro, 2004).

(ii) For Schrödinger operators of the form $-\Delta+V$ acting on square integrable functions defined on an open set of $\mathbb{R}^d$ (Barnsley, 1978; Baumgartner, 1979; Thirring, 1979; Crandall and Reno, 1982; Schmutz, 1985) or more generally second order elliptic operators (Protter and Weinberger, 1966; Berestycki *et al.*, 1994; Harrell II, 2005).

[a)]mouchet@phys.univ-tours.fr

[1]Finding lower bounds for the smallest eigenvalue of a typical Hamiltonian is far more difficult than finding upper bounds. For successful attempts, see for instance the moment method proposed by Handy and Bessis, 1985, the Riccati-Padé method proposed in Fernández *et al.*, 1989 and the lower bounds obtained for few-body systems by Benslama *et al.*, 1998.

In both cases, the proofs of Barta's inequalities involve the use of a Kato-type inequality and therefore rely extensively on the somehow specific properties of the purely quadratic differential operator. In this paper, we propose a significant extension of Barta's inequalities that will rely on the properties of one eigenvector only. More precisely, with a remarkably simple argument, we will show that we can obtain upper and lower bounds for the eigenvalue e_0 associated with the eigenvector Φ_0 of an operator, under the only hypothesis that Φ_0 is real and non-negative. This result includes cases (i) and (ii) because the Krein-Rutman theorem guarantees the positivity of Φ_0 (Reed and Simon, 1978a, Sec. XIII.12) for the smallest eigenvalue e_0,[2] but also applies for a much wider class of operators including the following.

(iii) the Schrödinger operators involving a magnetic field, e.g., the hydrogen atom in a Zeeman configuration;

(iv) discrete Hamiltonians, e.g., the one occurring in the Harper model;[3]

(v) some integral or pseudodifferentiable operators, e.g., the Klein-Gordon or spinless Salpeter Hamiltonians.

The next section fixes the notations, proves the main general results (theorems 1 and 2). Section III shows how the original argument given in Sec. II actually embraces and generalizes the Barta-type inequalities that have been already obtained in the literature and furnishes guidelines to numerically improve the bounds on e_0. Sections IV and V provide two applications in the differentiable case (many-body problem) and in the discrete case, respectively.

II. BOUNDING THE PRINCIPAL EIGENVALUE WITH THE LOCAL ENERGY

A. General inequalities

In the following, $\mathcal{Q}$ will be a locally compact space endowed with a positive Radon measure μ. $\langle\psi|\varphi\rangle$ will denote the scalar product between two elements ψ and φ belonging to the Hilbert space of the square integrable complex functions $\mathsf{L}^2(\mathcal{Q},\mu)$,

$$\langle\psi|\varphi\rangle = \int_{\mathcal{Q}} \bar{\psi}(q)\varphi(q)\mathrm{d}\mu(q).$$

$\mathsf{D}(H)$ will denote the domain of the operator H acting on $\mathsf{L}^2(\mathcal{Q},\mathrm{d}\mu)$. The crucial hypothesis on H is the following.

Hypothesis 1: The operator H is symmetric and has one real eigenvector $\Phi_0 \in \mathsf{D}(H)$ *such that* $\Phi_0 \geqslant 0$ (*almost everywhere with respect to* μ) *on* $\mathcal{Q}$.

If e_0 stands for the eigenvalue of H associated with Φ_0, the symmetry of H implies that, for all $\varphi \in \mathsf{D}(H)$, we have $\langle\Phi_0|(H-e_0)\varphi\rangle=0$ that is

$$\varphi \in \mathsf{D}(H), \quad \int_{\mathcal{Q}} \overline{\Phi_0}(q)(H-e_0)\varphi(q)\mathrm{d}\mu(q) = 0.$$

Taking the real part of the integral, we can see that the support of $q\mapsto \underline{\mathrm{Re}}[\overline{\Phi_0}(q)(H-e_0)\varphi(q)]$ either is empty, either contains two disjoints open sets $\mathcal{Q}_\pm$ such that $\mathrm{Re}(\overline{\Phi_0}(H-e_0)\varphi) \gtrless 0$ and $\mu(\mathcal{Q}_\pm)>0$. The hypothesis of positivity of Φ_0 implies that on $\mathcal{Q}_\pm$, we have $\mathrm{Re}[(H-e_0)\varphi] \gtrless 0$. The last results motivates the following definition.

Definition 1 (*local energy): For any* φ *in* $\mathsf{D}(H)$, *the* local energy *is the function* $E_\varphi\colon \mathcal{Q}\to\bar{\mathbb{R}}$ *defined by*

[2]The positivity of Φ_0 is also required for the traditional proofs of Barta's inequalities; this explains why, in case (i) and (ii), they concern the lowest eigenvalue only.

[3]After the first version of this paper was written, the author became aware of the paper by Barnsley and Duffin, 1980 where a similar argument as the one presented here was proposed (Theorem 7) for the bounds on an eigenvalue of a finite matrix.

$$E_\varphi(q) = \frac{\mathrm{Re}(H\varphi(q))}{\mathrm{Re}(\varphi(q))}. \tag{1}$$

Therefore from what precedes, we have obtained the main theorem.

Theorem 1: *For any symmetric operator H on $\mathsf{L}^2(\mathcal{Q},\mu)$ having an eigenvalue e_0 whose corresponding eigenfunction is non-negative almost everywhere on $\mathcal{Q}$, we have*

$$\varphi \in \mathsf{D}(H) \text{ such that } \mathrm{Re}(\varphi) \geqslant 0, \quad \inf_{\mathcal{Q}}(E_\varphi) \leqslant e_0 \leqslant \sup_{\mathcal{Q}}(E_\varphi). \tag{2}$$

Actually, for a nonsymmetric operator K, we can keep working with its adjoint K^* and easily generalize the above argument.

Theorem 2: *Let K being an operator on $\mathsf{L}^2(\mathcal{Q},\mu)$ having an eigenvalue k_0 whose corresponding eigenfunction is real and non-negative almost everywhere on $\mathcal{Q}$, we have* $\varphi \in \mathsf{D}(K^*)$ such that $\varphi > 0$,

$$\inf_{\mathcal{Q}}\left[\frac{\mathrm{Re}(K^*\varphi)}{\varphi}\right] \leqslant \mathrm{Re}(k_0) \leqslant \sup_{\mathcal{Q}}\left[\frac{\mathrm{Re}(K^*\varphi)}{\varphi}\right], \tag{3a}$$

$$\inf_{\mathcal{Q}}\left[-\frac{\mathrm{Im}(K^*\varphi)}{\varphi}\right] \leqslant \mathrm{Im}(k_0) \leqslant \sup_{\mathcal{Q}}\left[-\frac{\mathrm{Im}(K^*\varphi)}{\varphi}\right]. \tag{3b}$$

This generalization may be of physical relevance. There are some models (e.g., the so-called "kicked" systems, or quantized maps) where the dynamics are described "stroboscobically", i.e., implemented by a unitary operator (the Floquet evolution operator) that cannot be constructed from a smooth Hamiltonian. However, we will not consider this possibility here, and up to the end of this paper, H will denote a symmetric operator.

B. Optimization strategy

Since generally, the eigenfunction Φ_0 is not known exactly, it will be approximated with the help of test functions that belong to a trial space $\mathsf{T}(H) \subset \mathsf{D}(H)$, very much like the variational method. Since we want a test function to mimic Φ_0 at best, we will restrict $\mathsf{T}(H)$ to functions that respect the *a priori* known properties of Φ_0: its positivity, its boundary conditions and its symmetries if there are any. For each test function the error on e_0 is controlled by inequalities (2). Therefore, the strategy for obtaining reasonable approximations is clear: First, we must choose or construct φ to eliminate all the singularities of the local energy in order to work with a bounded function and second, perturb the test function in the neighborhood of the absolute minimum (respectively, maximum) of the local energy in order to increase (respectively, decrease) its value. For practical and numerical computations, this perturbation will be implemented by constructing a diffeomorphism $\Lambda \to \mathsf{T}(H), \lambda \mapsto \varphi_\lambda$ from a finite dimensional differentiable real manifold Λ of control parameters λ and the optimized bounds for e_0 will be

$$\sup_{\Lambda}\inf_{\mathcal{Q}}(E_{\varphi_\lambda}) \leqslant e_0 \leqslant \inf_{\Lambda}\sup_{\mathcal{Q}}(E_{\varphi_\lambda}). \tag{4}$$

III. INEQUALITIES IN THE DIFFERENTIABLE CASE: OLD AND NEW

A. General considerations

When H is a local differential operator, i.e., involves a finite number of derivatives in an appropriate representation (for instance in position or in momentum representation), one can therefore construct an algorithm that does not require any integration but differential calculus only. In an analytic and in a numerical perspective, this may be a significant advantage on the pertur-

bative or variational methods even though it is immediate to see[4] that the upper bound given by (2) is always larger than $\langle\varphi|H\varphi\rangle/\langle\varphi|\varphi\rangle$. The global analysis appears only through the determination of the singularities and the *absolute* extrema of the local energy that may have bifurcated when the control parameter λ varies smoothly. For a Schrödinger operator, the possible singularities of the potential on $\bar{\mathcal{Q}}$ like a Coulombian divergence or an unbounded behavior at infinite distances may furnish a strong guideline for constructing relevant test functions (see Sec. III D below). We have given in Mouchet, 2005, some heuristic and numerical arguments to show how this strategy can be fruitful. In the present paper, the main focus will concern rigorous results and will explain how some of them can be obtained with great simplicity even for systems as complex as those involved in the many-body problem.

B. Case (i) Barta's inequalities

They immediately appear as a particular case of Theorem 1.

Theorem 3 (Barta, 1937): *Let $\mathcal{Q}$ be a connected bounded Riemannian manifold endowed with the metric g and H, the opposite of the Laplacian Δ_g acting on the functions in $\mathsf{L}^2(\mathcal{Q},\mu)$ that satisfy Dirichlet boundary conditions on the boundary $\partial\mathcal{Q}$. The lowest eigenvalue e_0 of H is such that, for all positive $\varphi\in\mathcal{C}^2(\mathcal{Q})$,*

$$\inf_{\mathcal{Q}}\left(-\frac{\Delta_g\varphi}{\varphi}\right)\leqslant e_0\leqslant\sup_{\mathcal{Q}}\left(-\frac{\Delta_g\varphi}{\varphi}\right). \tag{5}$$

Proof: It follows directly from Theorem 1, with the local energy given by $E_\varphi=-\Delta_g\varphi/\varphi$: The spectrum of H is discrete and the Krein-Rutman theorem assures that Hypothesis 1 is fulfilled for e_0 being the lowest (and simple) eigenvalue. ■

Remark 1: The Dirichlet boundary conditions are not essential and can be replaced by any other type of boundary conditions provided that Hypothesis 1 remains fulfilled. However, as explained in Sec. II B, *for obtaining interesting bounds on e_0 extending $\mathsf{T}(H)$ to test functions that do not fulfill the boundary conditions (as proposed by Duffin, 1947) seems not appropriate.*

C. Case (ii) Duffin-Barnsley-Thirring inequalities

Extensions of Barta's inequalities for Schrödinger operators have been obtained partially by Duffin (Duffin, 1947) and Barnsley (Barnsley, 1978) (for the lower bound only) and completely (lower and upper bound) by Thirring (Thirring, 1979) using Kato's inequalities (see also Schmutz, 1985).

Theorem 4 (Duffin, 1947; Barnsley, 1978; Thirring, 1979): *Let $H=-\Delta+V$ be a Schrödinger operator acting on $\mathsf{L}^2(\mathbb{R}^d)$ having an eigenvalue below the essential spectrum. Then the lowest eigenvalue e_0 of H is such that for any strictly positive $\varphi\in\mathsf{D}(H)$,*

$$\inf_{\mathbb{R}^d}\left(V-\frac{\Delta\varphi}{\varphi}\right)\leqslant e_0\leqslant\sup_{\mathbb{R}^d}\left(V-\frac{\Delta\varphi}{\varphi}\right). \tag{6}$$

The proof is similar to the one presented above with the local energy being now $E_\varphi=V-\Delta\varphi/\varphi$. This argument has the advantage on the existing ones that it does not involve the specific properties of the Laplacian and can be immediately transposed to the larger class of the differential operators (not necessarily of second order) that fulfill Hypothesis 1.

D. Case (iii) magnetic Schrödinger operators

In the presence of a magnetic field, Schrödinger operators take the form $H=(\mathrm{i}\partial_q+A(q))^2+V(q)$ with $A:\mathcal{Q}\to\mathbb{R}^d$ being a smooth magnetic potential vector and $V:\mathcal{Q}\to\mathbb{R}$ a smooth scalar

[4]For each positive φ, it follows from $\langle\varphi|H\varphi\rangle=\mathrm{Re}[\langle\varphi|H\varphi\rangle]=\int_{\mathcal{Q}}\varphi(q)\mathrm{Re}[H\varphi(q)]\mathrm{d}\mu(q)=\int_{\mathcal{Q}}\varphi^2(q)E_\varphi(q)\mathrm{d}\mu(q)\leqslant\langle\varphi|\varphi\rangle\sup_{\mathcal{Q}}(E_\varphi(q))$.

potential. The Krein-Rutman theorem may not apply whereas there still exists a non-negative real eigenfunction (e_0 may be not simple nor the lowest eigenvalue) (Helffer *et al.*, 1999).

In the particular case of the hydrogen atom in a constant and uniform magnetic field, Hypothesis 1 is fulfilled for all values of the magnetic field (Avron *et al.*, 1977; Avron *et al.*, 1978) and indeed concerns the lowest eigenvalue. Therefore Theorem 1 applies and furnishes relevant analytical bounds that can be improved numerically as shown in (Mouchet, 2005).

Proposition 1: The smallest eigenvalue e_0 of the (3d-)Zeeman Hamiltonian

$$H = \frac{1}{2}\left(-i\vec{\nabla} + \frac{1}{2}\vec{r}\times\vec{B}\right)^2 - \frac{1}{r} \tag{7}$$

is such that

$$B \geqslant 0, \quad e_0 \leqslant -1/2 + B/2. \tag{8}$$

Proof: In cylindrical coordinates (ρ, θ, z) where the magnetic field is $\vec{B}=B\vec{u}_z$, the test function of the form $\varphi=\exp(-\sqrt{\rho^2+z^2}-B\rho^2/4)$ is constructed, according to the strategy explained in Sec. II B, in order to respect the rotational invariance of the ground state (Avron *et al.*, 1977) and eliminate both singularities at $r\to 0$ and at $\rho\to\infty$. Indeed such a choice leads straightforwardly to the bounded local energy

$$E_\varphi = -1/2 + B/2 - \frac{\rho^2 B}{2\sqrt{\rho^2+z^2}}. \tag{9}$$

The upper bound follows. ■

IV. APPLICATION TO THE MANY-BODY PROBLEM

A. Expression of the local energy in terms of two-body functions

We will consider in this section a N-body nonrelativistic bosonic system in d dimensions; $(d,N)\in(\mathbb{N}\backslash\{0,1\})^2$; whose Hamiltonian is given by

$$\widetilde{H} = \sum_{i=0}^{N-1} -\frac{1}{2m_i}\Delta_i + V(\vec{r}_0, \ldots, \vec{r}_{N-1}) \tag{10}$$

acting on $\mathsf{L}^2(\mathbb{R}^{Nd})$, endowed with the canonical Lebesgue measure, and where $i\in\{0,\ldots,N-1\}$, $\vec{r}_i\in\mathbb{R}^d$. Δ_i is the Laplacian in the $\vec{r}_i$ variables and $m_i\in\mathbb{R}^+\backslash\{0\}$ the mass of the ith particle. The spinless bosons interact only by the two-body radial potentials $v_{ij}=v_{ji}:\mathbb{R}\to\mathbb{R}$, i.e., V is given by

$$V = \sum_{\substack{i,j=0\\ i<j}}^{N-1} v_{ij}(r_{ij}), \tag{11}$$

where $r_{ij}=r_{ji}=\|\vec{r}_j-\vec{r}_i\|$. Once the center of mass is removed, the Hamiltonian $\widetilde{H}$ leads to a reduced Hamiltonian H acting on $\mathsf{L}^2(\mathbb{R}^{(N-1)d})$ [see for instance Sec. XI.5 of (Reed and Simon, 1978b)] and we will suppose in the following that H has at least one eigenvector.[5] Therefore, Hypothesis 1 is fulfilled for e_0 being the lowest (and simple) eigenvalue. A natural choice for test functions is to consider factorized ones of the form

[5]Physically, this can be achieved with a confining external potential (a "trap" is currently used in experiments involving cold atoms). Formally, this can be obtained in the limit of one mass, say m_0, being much larger than the others. The external potential appears to be the $v_{0,i}$'s, created by such an infinitely massive motionless device. It will trap the remaining $N-1$ particles in some bounded states if the $v_{0,i}$'s increase sufficiently rapidly with the $r_{0,i}$'s.

$$\varphi(\vec{r}_0,\dots,\vec{r}_{N-1}) = \prod_{\substack{i,j=0\\ i<j}}^{N-1} \phi_{ij}(r_{ij}), \tag{12}$$

where $\phi_{ij} \in \mathsf{L}^2(\mathbb{R}^+)$ and $\phi_{ji}=\phi_{ij}>0$. One can check easily that the total momentum of such a test function vanishes. The corresponding local energy (1) is given by

$$E_\varphi(q_N) = \sum_{\substack{i,j=0\\ i<j}}^{N-1} \left[\frac{-1}{2m_{ij}\phi_{ij}(r_{ij})} \left(\phi''_{ij}(r_{ij}) + \frac{d-1}{r_{ij}} \phi'_{ij}(r_{ij}) \right) + v_{ij}(r_{ij}) \right] - \sum_{(\widehat{j,i,k})} \frac{1}{m_i} S'_{ij}(r_{ij}) S'_{ik}(r_{ik}) \cos(\widehat{j,i,k}), \tag{13}$$

where $q_N \in \mathcal{Q}_N = \mathbb{R}^{(N-1)d}$ stands for the $(N-1)d$ relative coordinates $(\vec{r}_1-\vec{r}_0,\dots,\vec{r}_{N-1}-\vec{r}_0)$, m_{ij} for the reduced masses $m_i m_j/(m_i+m_j)$, S'_{ij} is the derivative of $S_{ij}=\ln(\phi_{ij})$. The last sum involves all the $N(N-1)(N-2)/2$ angles $(\widehat{j,i,k})$ between $\vec{r}_j-\vec{r}_i$ and $\vec{r}_k-\vec{r}_i$ that can be formed with all the triangles made of three distinct particles.

Whenever each v_{ij} allows for a two-body bounded state, we can choose ϕ_{ij} to be the eigenvector of $-(2m_{ij})^{-1}\Delta+v_{ij}$ having the smallest eigenvalue $\epsilon^{(2)}_{ij}$. Moreover, if $v_{ij}(r)$ is bounded when $r\to\infty$, from an elementary semiclassical analysis [see for instance (Maslov and Fedoriuk, 1981)] it follows that S'_{ij} is also bounded since asymptotically we have $S'_{ij}(r)\sim_{r\to\infty} -\sqrt{2m_{ij}[v_{ij}(r)-\epsilon^{(2)}_{ij}]}$. It follows that the local energy is also bounded and finite lower and upper bounds on e_0 can be found. For instance, directly from expression (13), we have the following.

Proposition 2: If, for all $(i,j)\in\{0,\dots,N-1\}^2$, $i\neq j$, $v_{ij}(r)$ *is bounded when* $r\to\infty$ *and* $-(2m_{ij})^{-1}\Delta+v_{ij}$ *has a smallest eigenvalue* $\epsilon^{(2)}_{ij}$ *obtained for* $\phi_{ij}=\exp S_{ij}$, *then the smallest eigenvalue* e_0 *of the N-body Hamiltonian in the center-of-mass frame is bounded by*

$$\sum_{\substack{i,j=0\\ i<j}}^{N-1} \epsilon^{(2)}_{ij} - \frac{s^2}{2m} N(N-1)(N-2) \leqslant e_0 \leqslant \sum_{\substack{i,j=0\\ i<j}}^{N-1} \epsilon^{(2)}_{ij} + \frac{s^2}{2m} N(N-1)(N-2), \tag{14}$$

where $m=\min_i m_i$ *and* $s=\max_{i,j}\sup_{\mathbb{R}^+}|S'_{ij}|$.

For potentials that are relevant in physics [see for instance the effective power-law potentials of the form $v_{ij}(r)=\mathrm{sign}(\beta)r^\beta$; $\beta\in\mathbb{R}$; between massive quarks as studied by Benslama *et al.*, 1998], the analytic form of the two-body eigenvector is not known in general and some numerical computations are required to obtain the absolute maximum and minimum of the local energy (13).

B. The local energy for a general Coulombian problem

When N is large, the estimation (14) is quite rough, in particular it does not take into account the constraints between the several angles. More precise results are obtained for the Coulombian problem where $v_{ij}(r)=e_{ij}/r$ with $e_{ij}\in\mathbb{R}$ and $d>1$. In that case, provided a bounded state exists and that we keep the test function (12) in $\mathsf{L}^2(\mathbb{R}^{(N-1)d})$, we choose a constant derivative $S'_{ij}=2e_{ij}m_{ij}/(d-1)$ in order to get rid of the Coulombian singularities of V. We obtain a bounded local energy given by

$$E_\varphi(q_N) = \sum_{\substack{i,j=0\\ i<j}}^{N-1} -\frac{2m_{ij}e_{ij}^2}{(d-1)^2} - \frac{4}{(d-1)^2} \sum_{(\widehat{j,i,k})} \frac{m_{ij}m_{ik}e_{ij}e_{ik}}{m_i} \cos(\widehat{j,i,k}). \tag{15}$$

C. Identical purely attractive Coulombian particles

The case where all the N particles are identical and attract each other, i.e., when $(i,j)\in\{0,\dots,N-1\}^2$, $i\neq j$, $m_i=1$ and $e_{ij}=-1$, has been extensively studied in the literature, in particular the asymptotic behavior of e_0 with large N may have some dramatic consequences on the

thermodynamical limit (Fisher and Ruelle, 1966; Lenard and Dyson, 1967; Lévy-Leblond, 1969; Lieb, 2005). The local energy method allows to obtain in a much simpler way energy bounds that are comparable to those already obtained by other methods. Actually, (15) simplifies to

$$E_\varphi(q_N) = -\frac{1}{(d-1)^2}\left[\tfrac{1}{2}N(N-1) + F_N(q_N)\right] \tag{16}$$

with $F_2 \equiv 0$ and for $N \geqslant 3$,

$$F_N(q_N) = \sum_{\widehat{(j,i,k)}} \cos(\widehat{j,i,k}). \tag{17}$$

The angular function F_N depends only on the geometrical configuration of the N vertices $(\vec{r}_0, \ldots, \vec{r}_{N-1})$, i.e., it is invariant under the group of Euclidean isometries and the scale invariance of the Coulombian interaction makes it invariant under dilations as well.

Lemma 1: $\inf_{\mathcal{Q}_3} F_3 = 1$ *is obtained when the three points are aligned.* $\sup_{\mathcal{Q}_3} F_3 = 3/2$ *is obtained when the three points make an equilateral triangle.*

Proof: The extrema of F_3 correspond to the extrema of the function defined by $(\theta_0, \theta_1, \theta_2) \mapsto \cos\theta_0 + \cos\theta_1 + \cos\theta_2$ under the constraint $\theta_0 + \theta_1 + \theta_2 = \pi$ for $(\theta_0, \theta_1, \theta_2)$ being the three angles $(\widehat{1,0,2})$, $(\widehat{0,1,2})$, $(\widehat{0,2,1})$, respectively. The Lagrange multiplier method leads to the determination of the extrema of the function $[0;\pi]^3 \to \mathbb{R}$ defined by $(\theta_0, \theta_1, \theta_2) \mapsto \cos\theta_0 + \cos\theta_1 + \cos\theta_2 + l(\theta_0 + \theta_1 + \theta_2 - \pi)$; $l \in \mathbb{R}$. We immediately obtain that the extremal points are located at $(\theta_0, \theta_1, \theta_2) = (\pi/3, \pi/3, \pi/3)$ and $(\theta_0, \theta_1, \theta_2) = (0, 0, \pi)$ together with the solutions that are obtained by circular permutations. It is easy to check that the first solution provides an absolute maximum for F_3 and the second ones an absolute minimum. ■

An immediate consequence of the preceding lemma is the following.

Proposition 3: The lowest energy e_0 *of* $N \geqslant 2$ *identical attractive Coulombian spinless particles in* $d > 1$ *dimensions is such that*

$$e_0 \leqslant -\frac{1}{(d-1)^2}\frac{1}{6}N(N-1)(N+1) \tag{18}$$

when the individual masses equal to unity and the attractive potential is $-1/r$.

Proof: The sum on the angles that defines F_N in (17) can be written as a sum of $N(N-1)(N-2)/6$ F_3-terms calculated for all the triangles that belong to the N-uplet made of the N vertices. Since, from Lemma 1 the absolute minimum of F_3 is obtained for a flat configuration, when all the N points are aligned all the F_3-terms reach their absolute minimum simultaneously and the absolute minimum of F_N is obtained. We have

Lemma 2: $\inf_{\mathcal{Q}_N} F_N = \frac{1}{6}N(N-1)(N-2)$ *is obtained when all the N points are aligned.*

The upper bound (18) follows from (16). ■

More generally, for a given N-uplet (i.e., a set of exactly N points), clustering the sum (17) in M-uplets $(N \geqslant M \geqslant 3)$ allows to find bounds on F_N from bounds on F_M. Indeed, we can write

$$F_N(q_N) = \sum_{q_M} \frac{(M-3)!\,(N-M)!}{(N-3)!} F_M(q_M), \tag{19}$$

where the sum is taken on all the M-uplets, labeled by the coordinates q_M, that belong to the given N-uplet. This sum involves exactly $N!/(M!(N-M)!)$ terms and we have, therefore,

Lemma 3: $(N, M) \in \mathbb{N}^2$ *such that* $N \geqslant M \geqslant 3$,

$$\sup_{\mathcal{Q}_N} F_N \leqslant \frac{N(N-1)(N-2)}{M(M-1)(M-2)} \sup_{\mathcal{Q}_M} F_M. \tag{20}$$

For a given N, $\sup_{\mathcal{Q}_N} F_N$ is not known exactly but the ordered sequence

$$\frac{\sup_{\mathcal{Q}_N} F_N}{N(N-1)(N-2)} \leqslant \frac{\sup_{\mathcal{Q}_{N-1}} F_{N-1}}{(N-1)(N-2)(N-3)} \leqslant \cdots \leqslant \frac{\sup_{\mathcal{Q}_M} F_M}{M(M-1)(M-2)} \leqslant \cdots \leqslant \frac{\sup_{\mathcal{Q}_3} F_3}{3.2.1} = \frac{1}{4} \tag{21}$$

shows that in order to improve the lower bounds on (16), we must try to find $\sup_{\mathcal{Q}_M} F_M$ with M being the largest as possible. However, when considering identity (19) for $N=4$ and $M=3$ together with Lemma 1 we have the following.

Lemma 4: $\sup_{\mathcal{Q}_4} F_4 = 6$ *is obtained when the four points make a regular tetrahedron.*

Then $\sup_{\mathcal{Q}_4} F_4/(4.3.2) = \sup_{\mathcal{Q}_3} F_3/(3.2.1) = 1/4$ and no better estimate is obtained when considering $M=4$ rather than $M=3$. Numerical investigations lead to the following conjectures.

Conjecture 1: (C_5) *When* $d=3$,

$$\sup_{\mathcal{Q}_5} F_5 = \frac{9}{2} + \frac{6(h_0+1)}{\sqrt{h_0^2+\frac{1}{3}}} - \frac{1}{h_0^2+\frac{1}{3}} \simeq 14.591\,594$$

with

$$6h_0 = 1 + \sqrt{-1 + \sqrt[3]{7+4\sqrt{3}} + \frac{1}{\sqrt[3]{7+4\sqrt{3}}}} + \sqrt{-2 - \sqrt[3]{7+4\sqrt{3}} - \frac{1}{\sqrt[3]{7+4\sqrt{3}}} + 8\frac{1}{\sqrt{-1+(7+4\sqrt{3})^{1/3}+(7+4\sqrt{3})^{-1/3}}}} \tag{22}$$

is obtained when the five points make two mirror-symmetric tetrahedrons sharing one common equilateral basis, their other faces being six isosceles identical triangles.

Remark 2: The only free parameter of the specific configuration can be chosen to be the height h of one tetrahedron (the length of the edges of the common equilateral basis being fixed to one). The maximum of $h \mapsto F_5$ *is reached for* h_0 *being the greatest solution of* $9h^4-6h^3+3h^2-2h+1/3$ *that is precisely given by* (22).

Remark 3: The pyramidal configurations with a squared basis leads to a local maximum that gives $F_5 = 15/2+5\sqrt{2} \simeq 14.57$.

Conjecture 2: (C_6) *When* $d=3$, $\sup_{\mathcal{Q}_6} F_6 = 12(1+\sqrt{2})$ *is obtained when the six points make a regular octahedron.*

Conjecture 3: (C_8) *When* $d=3$,

$$\sup_{\mathcal{Q}_8} F_8 = 16\left[\frac{4}{5} + \frac{1}{\sqrt{2}} + \frac{1}{\sqrt{5}} + \frac{4(1+\sqrt{2})}{\sqrt{5}\sqrt{5+4\sqrt{2}}} + \frac{3+2\sqrt{2}}{\sqrt{5+4\sqrt{2}}} - \frac{1}{5+4\sqrt{2}}\right] \simeq 79.501$$

is obtained when the eight points make two identical squares (whose edges have length one) lying in two parallel planes separated by a distance $h = \sqrt{1+2\sqrt{2}}/2$. *The axis joining the centers of the two squares is perpendicular to the squares and the two squares are twisted one from the other by a relative angle of* $\pi/4$.

Remark 4: The cube corresponds to $F_8 = 8(3\sqrt{2}+\sqrt{3}+3/2+\sqrt{6}) \simeq 79.393$.

Conjecture 4: (C_∞) *When* $d=3$ *and* $N \to \infty$, *the configuration that maximizes* F_N *corresponds to N points uniformly distributed on a sphere and* $\sup_{\mathcal{Q}_N} F_N \sim \frac{2}{9}N^3 + o(N^3)$.

Remark 5: The ambiguity of distributing N points uniformly on a sphere (Saff and Kuijlaars, 1997 and references therein) vanishes for large N as far as a uniform density is obtained. Assuming such a uniform density, the continuous limit of F_N/N^3 *is a triple integral on the sphere than can be computed exactly to* $2/9$.

The upper bound (18) for $d=3$ is slightly above the one obtained by Lévy-Leblond, 1969, Eq. (17), p. 807, namely $-(5/8)^2 N(N-1)^2/8$, and the numerical estimate $-0.0542N(N-1)^2$ by Basdevant *et al.*, 1990, Eq. (16), p. 63. For the lower bounds, from Lemmas 1 or 4, we have obtained the following.

Proposition 4: The lowest energy e_0 of $N \geqslant 2$ identical attractive Coulombian spinless particles in $d > 1$ dimensions is such that

$$-\frac{1}{(d-1)^2}\frac{1}{4}N^2(N-1) \leqslant e_0 \tag{23}$$

when the individual masses equal to unity and the attractive potential is $-1/r$.

The same result has been obtained for $d=3$ by Basdevant *et al.*, 1990, Eq. (11), p. 62 and is slightly better than $-N(N-1)^2/8$ given by Lévy-Leblond, 1969 Eq. (13), p. 807. For $N \geqslant M \geqslant 4$, this lower bound can be improved to

$$-\frac{1}{(d-1)^2}N(N-1)\left(\frac{1}{2}+\alpha_M(N-2)\right) \leqslant e_0 \tag{24}$$

with

$$\alpha_M = \frac{\sup_{\mathcal{Q}_M} F_M}{M(M-1)(M-2)} \leqslant \frac{1}{4}. \tag{25}$$

If conjecture (C_5) [respectively (C_6), (C_8), and (C_∞)] is correct we get, when $d=3$, $\alpha_5 \simeq 0.2432$ (respectively, $\alpha_6 \simeq 0.2414$, $\alpha_8 \simeq 0.2366$, and $\alpha_\infty \sim 2/9$) and the lower bounds are, therefore, improved.

Some numerical investigations, in particular a systematic comparison with the lower bounds obtained with variational methods in (Benslama *et al.*, 1998) for $N=3$ and $N=4$ Coulombian particles will be given elsewhere (Mouchet, 2006).

V. APPLICATION TO DISCRETE HAMILTONIANS

Where $q \in \mathbb{Z}^d$; $d \in \mathbb{N}$; the discretized analog of a local differential operator corresponds to a Hamiltonian that couples at most a finite number of basis vectors (e.g., the nearest neighbors on the lattice $\mathbb{Z}^d$). For instance, when $d=1$, it can be seen as a Hermitian band matrix (finite or infinite) of finite half-width in an appropriate basis. Possibly with renumbering the q's, on $\ell^2(\mathbb{Z}^d)$ H has the form:

$$(H\varphi)_q = \sum_{\substack{\nu \in \mathbb{Z}^d \\ |\nu|_\infty \leqslant N_b}} H_{q,q+\nu}\varphi_{q+\nu}, \tag{26}$$

where $N_b \in \mathbb{N}$, $(q,q') \in \mathbb{Z}^d \times \mathbb{Z}^d$, $H_{q',q} = \bar{H}_{q,q'} \in \mathbb{C}$ and $|\nu|_\infty$ stands for $\max(|\nu_1|,\ldots,|\nu_d|)$. φ will be taken as a discrete set of real strictly positive numbers, and the local energy $E_\varphi(q)$ is computed, for a given q, with elementary algebraic operations whose number is finite and all the smaller than N_b are small: its value at a given q depends on $(2N_b)^d+1$ components of φ at most. Under hypothesis 1,[6] if, say, for a given test vector φ, the absolute maximum of E_φ occurs only at a unique finite q_m, one can immediately improve the upper bound by a finite amount, for instance just by varying φ_{q_m} only, until $E_\varphi(q_m)$ is not an absolute maximum anymore. Only $(2N_b)^d+1$ values of the local energy will be affected by the variation of just one component of φ. One can see easily that this approach leads to a wide variety of algorithms where a sequence of optimization steps is constructed; each step involves a number of optimization parameters and functions that is usually much smaller [of order $(2N_b)^d$ or less] than the dimension of the original matrix.

Discrete Schrödinger operators are important particular cases of Hamiltonians (26) with $N_b = 1$. They are relevant models for the description of quantum (quasi-) particles evolving in periodic crystals. For $d=1$, they can be written as

[6]We have seen at the end of Sec. II A that the symmetry hypothesis can be relaxed.

$$(H\varphi)_q = -\varphi_{q+1} - \varphi_{q-1} + V(q)\varphi_q, \tag{27}$$

where the potential V is a real bounded function on $\mathbb{Z}$. By possibly subtracting a constant positive real number to V, the bounded operator $-H$ can be made positive and ergodic: First, for any positive and non-identically vanishing φ and φ' in $\ell^2(\mathbb{Z})$, $-H\varphi$ remains positive. Second, $\langle\varphi'|(-H)^{|q'-q|}\varphi\rangle = \varphi'_{q'}\varphi_q + (\text{positive terms}) \neq 0$ for any given pair of strictly positive components $\varphi'_{q'}$ and φ_q with $q' \neq q$. [In the marginal case where φ and φ' both vanish everywhere but on the same point, we have $\langle\varphi'|(-H)\varphi\rangle) \neq 0$. Therefore Theorem XIII.43 of (Reed and Simon, 1978a) applies: if H has indeed one eigenvalue, hypothesis 1 is fulfilled for e_0 being the smallest eigenvalue of H. In that case, inequalities (2) takes the following form:

Proposition 5: When the discrete Schrödinger operator (27) *admits at least one eigenvalue and when V is bounded, then the smallest eigenvalue* e_0 *is such that,* $\varphi \in \ell^2(\mathbb{Z})$ *such that* $\varphi > 0$,

$$\inf_{q\in\mathbb{Z}}\left(-\frac{\varphi_{q+1}+\varphi_{q-1}}{\varphi_q} + V(q)\right) \leqslant e_0 \leqslant \sup_{q\in\mathbb{Z}}\left(-\frac{\varphi_{q+1}+\varphi_{q-1}}{\varphi_q} + V(q)\right). \tag{28}$$

When V is actually a N-periodic real function, the spectral problem (see Reed and Simon, 1978a for instance) leads to the search of complex series $(u_q)_{q\in\mathbb{Z}}$ such that

$$\eta = (\eta_1, \eta_2) \in [0;1[^2 \quad \begin{cases} -u_{q+1} - u_{q-1} + V(q+\eta_2)u_q = e(\eta)u_q, \\ u_{q+N} = e^{i2\pi\eta_1}u_q. \end{cases} \tag{29}$$

The spectrum of H is the bounded set $\sigma(H) = \{e(\eta)\,|\,\eta \in [0;1[^2\} \subset \mathbb{R}$. It is given by the reunion for all η's of the N eigenvalues of finite $N\times N$ Hermitian matrices $H^{(\eta)}$ obtained after transforming (29) with the one-to-one mapping $u_q \mapsto u_q \exp(-i2\pi q\,\eta_1/N)$. As far as positive solutions of (29) are concerned, we will take $\eta_1 = 0$ and will look for the smallest eigenvalue $e_0(\eta_2)$ of

$$H^{(0,\eta_2)} = \begin{pmatrix} V(\eta_2) & -1 & 0 & \cdots & 0 & -1 \\ -1 & V(1+\eta_2) & -1 & 0 & \cdots & 0 \\ 0 & -1 & V(2+\eta_2) & -1 & \cdots & \cdots \\ 0 & \cdots & \cdots & & \cdots & \cdots \\ -1 & 0 & \cdots & 0 & -1 & V(N-1+\eta_2) \end{pmatrix}. \tag{30}$$

Remark 6: The (rational) Harper model (Harper, 1955b; Harper, 1955a) [*also called the almost Mathieu equation (Bellissard and Simon, 1982)*] *corresponds to* $V(q) = -V_0\cos(2\pi qM/N)$ *where* $V_0 > 0$, (M,N) *being strictly positive coprimes integers. For a given N and M,* $\sigma(H)$ *appears to be made of N bands. The union of these bands for each rational number M/N between 0 and 1 produces the so-called Hofstadter butterfly (Hofstadter, 1976).*

We are therefore able to produce two nontrivial bounds on the lowest eigenvalue $e_0(\eta_2)$ without any diagonalization:

Proposition 6: When V is N-periodic, $\eta_2 \in [0;1[$, *the smallest eigenvalue* $e_0(\eta_2)$ *of* (30) *is such that* $\varphi \in (\mathbb{R}^+\backslash\{0\})^N$,

$$\min_{q\in\{0,\ldots,N-1\}}\left(-\frac{\varphi_{q+1}+\varphi_{q-1}}{\varphi_q} + V(q+\eta_2)\right) \leqslant e_0(\eta_2) \tag{31a}$$

and

$$e_0(\eta_2) \leqslant \max_{q\in\{0,\ldots,N-1\}}\left(-\frac{\varphi_{q+1}+\varphi_{q-1}}{\varphi_q} + V(q+\eta_2)\right) \tag{31b}$$

(the indices labeling the components of φ *are taken modulo N).*

Therefore, we can bound the bottom of the Hofstadter butterfly with the help of any test function.

Corollary 1: For the rational Harper Hamiltonian

$$H\varphi_q = -\varphi_{q+1} - \varphi_{q-1} - V_0 \cos\left(2\pi q \frac{M}{N}\right)\varphi_q, \tag{32}$$

we have $\varphi \in (\mathbb{R}^+\backslash\{0\})^N$

$$\min_{q\in\{0,\ldots,N-1\}}\left[-\frac{\varphi_{q+1}+\varphi_{q-1}}{\varphi_q} - V_0\cos\left(2\pi q\frac{M}{N}\right)\right] \leqslant \inf[\sigma(H)] \tag{33a}$$

and

$$\inf[\sigma(H)] \leqslant \max_{q\in\{0,\ldots,N-1\}}\left[-\frac{\varphi_{q+1}+\varphi_{q-1}}{\varphi_q} - V_0\cos\left(2\pi q\frac{M}{N}\right)\right]. \tag{33b}$$

Proof: In the Harper model, for each rational number M/N, the lowest eigenvalue is obtained for $\eta=(0,0)$. It is a direct application of Reed and Simon, 1978a, Theorem XIII.89(e) and thus inequalities (33) follow directly from (31). ■

Choosing for φ, at first guess, semiclassical approximations (i.e., corresponding to large N) constructed from Mathieu functions are therefore expected to provide numerical reasonable bounds.

VI. CONCLUSION

It has been shown on various examples how theorem 1 can be used to obtain rigorous estimates on the principal value of any symmetric operator. Its simplicity, its low cost in computations and its wide domain of applications make the method presented in this article a powerful tool for controlling bounds. In many situations, it provides nontrivial complementary information to those obtained by traditional or more system-dependent methods. Unfortunately, this paper does not extend the method to fermionic systems (see for instance, Sigal, 1995 and references therein) where the spatial wave function of the ground state has generically nontrivial nodes (Ceperley, 1991) that cannot be known *a priori* even with some considerations on symmetries.

This paper presents some clues for further developments of optimization algorithms. However it remains an open question whether such algorithms really bear the potential of an efficient treatment and will overcome the possible difficulties one may face in realistic problems.

ACKNOWLEDGMENTS

The author thanks Laurent Véron for a critical reading of the paper, Evans Harrell for fruitful discussions, Saïd Ilias for providing useful knowledge on references on the generalizations of Barta's inequalities, Emmanuel Lesigne for attracting my attention to the paper by Saff and Kuijlaars, 1997 and Michel Caffarel for the paper by Ceperley, 1991. The author is also grateful to the Laboratoire Kastler Brossel for its warm hospitality.

Avron, J., Herbst, I., and Simon, B., "The Zeeman effect revisted," Phys. Lett. **62A**(4), 214–216. (1977).
Avron, J., Herbst, I., and Simon, B., "Schrödinger operators with magnetic fields. I. General interactions," Duke Math. J. **45**(4), 847–883 (1978).
Barnsley, M. F., "Lower bounds for quantum mechanical energy levels," J. Phys. A **11**(1), 55–68 (1978).
Barnsley, M. F. and Duffin, R. J., "Bounds for the *r*th characteristic frequency of a beaded string or an electrical filter," Proc. Natl. Acad. Sci. U.S.A. **77**(6), 3120–3124 (1980).
Barta, J., "Sur la vibration fondamentale d'une membrane," C. R. Acad. Sci. **204**(7), 472–473 (1937) (in French).
Basdevant, J. L., Martin, A., and Richard, J. M., "Improved bounds on many-body Hamiltonians. I. Self-gravitating bosons," Nucl. Phys. B **343**(1), 60–68 (1990).
Baumgartner, B., "A class of lower bounds for Hamiltonian operators," J. Phys. A **12**(4), 459–467 (1979).
Bellissard, J. and Simon, B., "Cantor spectrum for the almost Mathieu equation," J. Funct. Anal. **48**, 408–419 (1982).
Benslama, A., Metatla, A., Bachkhaznadji, A., Zouzou, S. R., Krikeb, A., Basdevant, J. L., Richard, J. M., and Wu, T. T.,

"Optimized lower bound for four-body Hamiltonians," Few-Body Syst. **24**(1), 39–54 (1998).
Berestycki, H. and Nirenberg, L., "The principal eigenvalue and maximum principle for second-order elliptic operators in general domains," Commun. Pure Appl. Math. **47**(1), 47–92 (1994).
Bessa, G. P. and Montenegro, J. F., "An extension of Barta's theorem and geometric applications," arXiv: math-ph/0308099 (2004).
Ceperley, D. M., "Fermion nodes," J. Stat. Phys. **63**(5/6), 1237–1267 (1991).
Crandall, R. E. and Reno, M. H., "Ground state energy bounds for potentials $\|x\|^{\nu}$," J. Math. Phys. **23**(1), 64–70 (1982); **23**, 1737 (1982).
Duffin, R. J., "Lower bounds for eigenvalues," Phys. Rev. **71**, 827–828 (1947).
Fernández, F. M., Ma, Q., and Tipping, R. H., "Eigenvalues fo the Schrödinger equation via the Riccati-Padé method," Phys. Rev. A **40**(11), 6149–6153 (1989).
Fisher, M. E. and Ruelle, D., "The stability of many-particle systems," J. Math. Phys. **7**(2), 260–270 (1966).
Handy, C. R. and Bessis, D., "Rapidly convergent lower bounds for the Schrödinger-equation ground-state energy," Phys. Rev. Lett. **55**(9), 931–934 (1985).
Harper, P. G., "Single band motion of conduction electrons in a uniform magnetic field," Proc. R. Soc. London, Ser. A **68**, 879–892 (1955a).
Harper, P. G., "The general motion of conduction electrons in a uniform magnetic field, with application to the diamagnetism of metals," Proc. R. Soc. London, Ser. A **68**, 874–878 (1955b).
Harrell II, E. M., "Geometric lower bounds for the spectrum of elliptic PDEs with Dirichlet conditions in part" (unpublished).
Helffer, B., Hoffmann-Ostenhof, M., Hoffmann-Ostenhof, T., and Owen, M. P., "Nodal sets for groundstates of Schrödinger operators with zero magnetic fields in a non simply connected domain," Commun. Math. Phys. **202**, 629–649 (1999).
Hofstadter, D. R., "Energy levels and wave functions of Bloch electrons in rational and irrational magnetic fields," Phys. Rev. B **14**(6), 2239–2249 (1976).
Lenard, A. and Dyson, F. J., "Stability of matter. I," J. Math. Phys. **8**(3), 423–434 (1967).
Lévy-Leblond, J. M., "Nonsaturation of gravitational forces," J. Math. Phys. **10**(5), 806–812 (1969).
Lieb, E. H., *The Stability of Matter: From Atoms to Stars*, 4th ed. (Springer-Verlag, Berlin, 2005).
Maslov, V. P. and Fedoriuk, M. V., *Semi-Classical Approximation in Quantum Mechanics*, Mathematical Physics and Applied Mathematics, Vol. 7 (D. Reidel, Dordrecht, 1981).
Mouchet, A., "Bounding the ground-state energy of a many-body system with the differential method," Nucl. Phys. A **765**, 319–341 (2006).
Mouchet, A., "A differential method for bounding the ground state energy," J. Phys. A **38**, 1039–1047 (2005).
Protter, M. H. and Weinberger, H. W., "On the spectrum of general second order operators," Bull. Am. Math. Soc. **72**, 251–255 (1966).
Reed, M. and Simon, B., *Analysis of Operators*, Methods of modern mathematical physics, Vol. 4 (Academic, New York, 1978a).
Reed, M. and Simon, B., *Scattering theory*, Methods of modern mathematical physics, Vol. 3 (Academic, New York, 1978b).
Saff, E. B. and Kuijlaars, A. B., "Distributing many points on a sphere," Math. Intell. **19**(1), 5–11 (1997).
Schmutz, M., "The factorization method and ground state energy bounds," Phys. Lett. **108A**(4), 195–196 (1985).
Sigal, I. M., *Lectures on large Coulomb systems, mathematical quantum theory. II. Schödinger operators*, CRM Proceedings and Lecture Notes, Vol. 8 (Amer. Math. Soc., Providence, RI, 1995), pp. 73–107.
Thirring, W., *Quantum Mechanics of Atoms and Molecules*, A Course in mathematical physics, Vol. 3 (Springer-Verlag, New York, 1979).

II.5 Perspectives

Avec H. Giacomini et B. Boisseau du lmpt, nous essayons d'adapter la toute première idée qui consistait à tirer des informations sur les spectres à partir de conditions algébriques, pour tenter de remédier à l'un des défauts majeurs de la méthode différentielle, à savoir que la propriété de positivité nous empêche de pouvoir obtenir des informations sur les états excités et même sur le fondamental d'un système fermionique. Dans ce dernier cas l'enjeu est de taille car, à titre d'exemple, la nature fermionique est essentielle pour rendre compte des problèmes de stabilité de la matière (Lieb, 2005, et les références de (Mouchet, 2006b)) pour lesquels des minorations de l'énergie du fondamental sont réclamées.

Pour, tout de même, ne pas rester dans le flou, fût-il artistique, ébauchons juste l'idée de base d'H. Giacomini et puis montrons comment elle s'inscrit dans le même esprit que la méthode différentielle. Une équation de Schrödinger à une dimension pour une fonction d'onde stationnaire réelle φ d'énergie E décrivant une particule de masse m évoluant dans un potentiel $V(x)$ s'écrit

$$\varphi''(x) = v(x)\varphi(x) \tag{II.5–1}$$

en posant $v(x) \stackrel{\text{def}}{=} V(x) - E$ dans un système d'unités où $\hbar = 1$ et $m = 1/2$. Soient $\{g_n\}_{n\in\{0,\ldots,N\}}$ un ensemble de $N+1$ fonctions réelles à deux variables réelles au moins $\mathcal{C}^1$ à partir desquelles on construit un polynôme de degré N en φ' :

$$F_N(x) \stackrel{\text{def}}{=} \sum_{n=0}^{N} g_n\big(x, \varphi(x)\big)\,\big(\varphi'(x)\big)^n\,. \tag{II.5–2}$$

Le calcul de $F_N'(x)$ conduit, une fois fait usage de (II.5–1), à un polynôme $P(\varphi')$ de degré au plus $N+1$ en φ' dont les coefficients dépendent de v, des $\{g_n\}_{n\in\{0,\ldots,N\}}$ et de leurs dérivées premières. Si l'on cherche un jeu de fonctions $\{g_n\}_{n\in\{0,\ldots,N\}}$ de façon que P ne dépende pas, en définitive de φ', cela impose des contraintes sur le choix de celles-ci qui se résolvent facilement : si l'on prend $\forall k \in \{0,\ldots,N\}$, $g_{N-k}\big(x, \varphi(x)\big) = c_k(x)\varphi^k(x)$ alors la dérivée de ce qui est maintenant un polynôme homogène de degré N en (φ, φ'),

$$F_N(x) = \sum_{n=0}^{N} c_{N-n}(x)\big(\varphi(x)\big)^{N-n}\,\big(\varphi'(x)\big)^n\,, \tag{II.5–3}$$

se simplifie en

$$F_N'(x) = \Big(c_N'(x) + v(x)c_{N-1}(x)\Big)\,\varphi^N(x) \tag{II.5–4}$$

pourvu que les fonctions $\{c_n\}_{n\in\{1,\dots,N\}}$ vérifient une hiérarchie de relations qui permet de toutes les construire explicitement à partir de v et de c_0.

Si maintenant (a,b) désignent deux réels, en intégrant l'identité (II.5–4) on a

$$\int_a^b \Big(c_N'(x)+v(x)c_{N-1}(x)\Big)\,\varphi^N(x)\,\mathrm{d}x = F_N(b)-F_N(a)\,. \tag{II.5–5}$$

En choisissant a, b et c_0 de façon à annuler F_N, par exemple en les choisissant aux points où l'on est certain que φ ou φ' s'annule assez vite — en bord de domaine si l'on considère des conditions de Dirichlet ou de Neumann ou à l'infini pour un problème de Schrödinger défini sur un domaine non borné —, l'annulation de l'intégrale de (II.5–5) implique que, si l'on choisit dès le départ de travailler avec N pair on obtient des inégalités n'impliquant plus la fonction propre inconnue φ. On retrouve une certaine similarité avec l'argument central de la méthode différentielle mais sans avoir recours à l'hypothèse de positivité : La double condition qu'il doive exister des points pour lesquels $c_N'+vc_{N-1}\leqslant 0$ et $c_N'+vc_{N-1}\geqslant 0$ impose à priori des contraintes sur les énergies E, via v, pour toute fonction d'essai c_0. Par exemple, pour $N=2$, il est facile de vérifier que l'on a

$$c_2'+vc_1=\frac{1}{2}c_0'''-2vc_0'-v'c_0=\frac{1}{2}c_0'''-2(V-E)c_0'-V'c_0 \tag{II.5–6}$$

qui permet de tirer des inégalités sur E ; lesquelles sont immédiates si l'on choisit c_0' de signe constant (mais ce n'est pas un choix obligatoire) tout en annulant (II.5–5). En effet, en posant

$$E^{[c]}(x)\stackrel{\text{def}}{=}V(x)+\frac{1}{2c'(x)}\left(V'(x)c(x)-\frac{1}{2}c'''(x)\right)\,, \tag{II.5–7}$$

on a

$$\inf E^{[c_0]}\leqslant E\leqslant \sup E^{[c_0]}\,. \tag{II.5–8}$$

On peut également espérer, ce que tendent à montrer nos premiers essais, que l'on puisse obtenir par ce genre de méthode des informations spectrales du type : « Il n'existe pas d'énergies propres discrètes entre telle et telle valeur », ce qui, dans certains systèmes, peut être une information physique substantielle. Évidemment cela requiert un travail de généralisation qui n'est encore qu'à peine entamé.

Les problèmes de convergence d'algorithmes fondés sur la méthode différentielle sont on ne peut plus ouverts : il me semble que l'on ne pourra pas obtenir de résultats satisfaisants sans une stratégie pilotée sans doute dans le cadre de la théorie des bifurcations.

Il apparaît peu raisonnable, étant donné la marginalité extrême de la méthode différentielle d'envisager de proposer un sujet de thèse ou de M2 sur ce sujet si embryonnaire.

Un étudiant en physique n'aurait que très peu à y apprendre qui lui soit utile pour son avenir dans cette discipline et je n'aurais pas les capacités à apporter quoique ce soit à un étudiant mathématicien qu'il ne puisse trouver dans les traités de base.

Bibliographie

Arnold V.I. (1984): *Catastrophe Theory*. New York: Springer-Verlag, isbn 0-387-54811-4.

Auerbach A. & Kivelson S. (1985): "The path decomposition expansion and multidimmensional tunneling", *Nuclear Phys. B*, **257**, pp. 799–858.

Averbukh V., Moiseyev N., Mirbach B. & Korsh H.J. (1995): "Dynamical tunneling through a chaotic region", *Z. Phys. D*, **35**, pp. 247–256.

Averbukh V., Osovski S. & Moiseyev N. (2002): "Controlled tunneling of cold atoms : from full suppression to strong enhancement", *Phys. Rev. Lett.*, **89**(25), p. 253201.

Azbel M.Y. (1991): "Resonances and oscillations in tunneling in a time-dependent potential", *Phys. Rev. B*, **43**(8), pp. 6847–6850.

Balian R. & Bloch C. (1974): "Solution of the Schrödinger Equation in Terms of Classical Paths", *Ann. Physics*, **85**, pp. 514–545.

Balibar F. & Lévy-leblond J.M. (1984): *Quantique (rudiments)*. Paris: Editions du CNRS : Interéditions, isbn 2729600469, (in french).

Barnsley M.F. & Duffin R.J. (1980): "Bounds for the r th characteristic frequency of a beaded string or of an electrical filter", *Proc. Nat. Acad. Sci. USA.*, **77**(6), pp. 3120–3124.

Barta J. (1937): "Sur la vibration fondamentale d'une membrane", *C. R. Acad. Sci. Paris*, **204**(7), pp. 472–473, (in french).

Bazzani A. & Turchetti G. (1992): "Singularities of normal forms and topology of orbits in area-preserving maps", *J. Phys. A*, **25**(8), pp. L427–L432.

Benderskii V.A., Vetoshkin E.V., Kats E.I. & Trommsdorff H.P. (2003): "Competing tunneling trajectories in a two-dimensional potential with variable topology as a model for quantum bifurcations", *Phys. Rev. E*, **67**(2), p. 026102.

Berry M.V., Balazs N.L., Tabor M. & Voros A. (1979): "Quantum Maps", *Ann. Physics*, **122**, pp. 26–63.

Billi L., Turchetti G. & Xie R. (1993): "Natural boundaries for Hamiltonian maps and the genesis of the Siegel disk", *Phys. Rev. Lett.*, **71**(16), pp. 2513–2516.

Bogomolny E.B. & Rouben D. (1998): "Semiclassical description of resonant tunneling", *Europhys. Lett.*, **43**, pp. 111–116.

——— (1999): "Semiclassical description of resonant tunneling", *Eur. Phys. J. B*, **9**, pp. 695–718.

Bohigas O. (1989): "Random matrices and chaotic dynamics", in (Giannoni, Voros & Zinn-Justin, 1991), pp. 87–199, isbn 0-444-89277-X.

Bohigas O., Boosé D., Egydio de Carvalho R. & Marvulle V. (1993): "Quantum tunneling and chaotic dynamics", *Nuclear Phys. A*, **560**, pp. 197–210.

Bohigas O., Giannoni M. & Schmit C. (1983): "Characterization of Chaotic Quantum Spectra and Universality of Level Fluctuation Laws", *Phys. Rev. Lett.*, **52**, pp. 1–4, Reprinted in (Casati & Chirikov, 1995).

Bohigas O., Tomsovic S. & Ullmo D. (1993): "Manifestations of classical phase space structures in quantum mechanics", *Phys. Rep.*, **223**(2), pp. 43–133.

Bonci L., Farusi A., Grigolini P. & Roncaglia R. (1998): "Tunneling rate fluctuations induced by nonlinear resonances: A quantitative treatment based on semiclassical arguments", *Phys. Rev. E*, **58**(5), pp. 5689–5692.

Brillouin L. (1926): "La mécanique ondulatoire de Schrödinger; une méthode générale de résolution par approximations successives", *C. R. Acad. Sci. Paris*, **183**, pp. 24–26, (in french).

Brodier O., Schlagheck P. & Ullmo D. (2001): "Resonance-Assisted Tunneling in Near-Integrable Systems", *Phys. Rev. Lett.*, **87**, p. 064101.

——— (2002): "Resonance-Assisted Tunneling", *Ann. Physics*, **300**(1), pp. 88–136.

Buchleitner A., Delande D. & Zakrzewski J. (2002): "Non-dispersive wave packets in periodically driven quantum systems", *Phys. Rep.*, **368**, pp. 409–547.

Burgess C.P. (1991): "Quantum tunneling and imaginary-time paths", *Amer. J. Phys.*, **59**, pp. 994–998.

Büttiker M. & Landauer R. (1982): "Traversal Time for Tunneling", *Phys. Rev. Lett.*, **49**(23), pp. 1739–1742.

——— (1985): "Traversal Time for Tunneling", *Phys. Scripta*, **32**, pp. 429–434.

Caldeira A.O. & Leggett A.J. (1983): "Quantum Tunnelling in a Dissipative System", *Ann. Physics*, **149**(2), pp. 374–456, and (Caldeira & Leggett, 1984).

——— (1984): "Erratum", *Ann. Physics*, **153**, p. 445.

Casati G. & Chirikov B. (eds.) (1995): *Rendiconti della scuola internazionale di fisica Enrico Fermi — CXIX Corso: Quantum chaos; 1991*. Amsterdam: North-Holland.

Casati G., Graham R., Guarneri I. & Izrailev F.M. (1994): "Tunneling between localized states in classically chaotic systems", *Phys. Lett. A*, **190**, pp. 159–164.

Chirikov B. (1979): "A universal instability of many-dimensional oscillator systems", *Phys. Rep.*, **52**, pp. 263–379.

Coleman S. (1985): *Aspects of symmetry (selected Erice lectures)*. Cambridge: Cambridge University Press, isbn 0-521-26706-4.

Condon E.U. (1978): "Tunneling — How it started", *Amer. J. Phys.*, **46**(4), pp. 319–323.

Creagh S.C. (1994): "Tunnelling in multidimensional systems", *J. Phys. A*, **27**, pp. 4969–4993.

——— (1997): "Tunneling in two dimensions", in (Tomsovic, 1998), pp. 35–100, isbn 981-02-3446-5.

Creagh S.C. & Finn M.D. (2001): "Evanescent coupling between discs: a model for near-integrable tunnelling", *J. Phys. A*, **34**, pp. 3791–3801.

Creagh S.C. & Whelan N.D. (1996): "Complex Periodic Orbits and Tunnelling in Chaotic Potentials", *Phys. Rev. Lett.*, **77**(25), pp. 4975–4979.

Davies E.B. (1982): "The twisting trick for double well hamiltonians", *Comm. Math. Phys.*, **85**, pp. 471–479.

Davis M.J. & Heller E.J. (1981): "Quantum dynamical tunneling in bound states", *J. Chem. Phys.*, **75**, p. 246.

Delande D. & Zakrzewski J. (2003): "Experimentally attainable example of chaotic tunneling: The hydrogen atom in parallel static electric and magnetic fields", *Phys. Rev. A*, **68**, p. 062110.

Demazure M. (1989): *Bifurcations et catastrophes*. Paris: Éditions Ellipses Marketing, isbn 2729889469, (in french), Springer for the english edition.

Dembowski C., Gräf H.D., Heine A., Hofferbert R., Rehfeld H. & Richter A. (2000): "First Experimental Evidence for Chaos-Assisted Tunneling in a Microwave Annular Billiard", *Phys. Rev. Lett.*, **84**(5), pp. 867–870.

Dobrokhotov S.Y. & Kolokoltsov V.N. (1993): "Splitting amplitudes of the lowest energy levels of the Schrödinger operator with double-well potential", *Theoret. and Math. Phys.*, **94**(3), pp. 300–305, Translation from the original russian: *Teoret. Mat. Fiz.* 1993; **94**(3), pp 426–434.

Dobrokhotov S.Y., Kolokoltsov V.N. & Maslov V.P. (1991): "Splitting of the lowest energy levels of the Schrödinger equation and asymptotic behavior of the fundamental solution of the equation $h u_t = h^2 \Delta u/2 - V(x)u$", *Theoret. and Math. Phys.*, **87**(3), pp. 561–599, Translation from the original russian : *Teoret. Mat. Fiz.* 1991; **87**(3), pp. 323–375.

Doron E. & Frischat S.D. (1995): "Semiclassical Description of Tunneling in Mixed Systems: the Case of the Annular Billiard", *Phys. Rev. Lett.*, **75**(20), pp. 3661–3664.

Einstein A. (1917): "Zum Quantensatz von Sommerfeld und Epstein", *Verh. Deutsch. Phys. Ges.*, **19**, pp. 82–92, (in german) It is discussed and partially translated in (Percival, 1977). See also (Stone, 2005). For a complete translation (by A. Engel) see "On the Quantum Theorem of Sommerfeld and Epstein" in (Kox, Klein & Schulmann, 1997).

Eltschka C. & Schlagheck P. (2005): "Resonance- and Chaos-Assisted Tunneling in Mixed Regular-Chaotic Systems", *Phys. Rev. Lett.*, **94**, p. 014101.

Esaki L. (1974): "Long journey into tunneling", *Rev. Modern Phys.*, **46**(2), pp. 237–245.

Farrelly D. & Uzer T. (1986): "Semiclassical quantization of slightly nonresonant systems: Avoided crossings, dynamical tunneling, and molecular spectra", *J. Chem. Phys.*, **85**(1), pp. 308–318.

Fisher M.P.A. (1988): "Resonantly enhanced quantum decay: A time-dependent Wentzel-Kramers-Brillouin approach", *Phys. Rev. B*, **37**(1), pp. 75–82.

Fowler R. & Nordheim L. (1928): "Electron emission in intense electric fields", *Proc. Roy. Soc. London Ser. A*, **119**, pp. 173–181.

GAMOW G. (1928): "Zur Quantentheorie des Atomkernes", *Zts. f. Phys.*, **51**((3-4)), pp. 204–212, (in german).

GARG A. (2000): "Tunnel splittings for one-dimensional potential wells revisited", *Amer. J. Phys.*, **68**(5), p. 430.

GEORGE T.F. & MILLER W.H. (1972): "Classical S-matrix theory of reactive tunneling: Linear $H + H_2$ collisions", *J. Chem. Phys.*, **57**(6), pp. 2458–2467.

GIANNONI M., VOROS A. & ZINN-JUSTIN J. (eds.) (1991): *Chaos et Physique Quantique — Chaos and Quantum Physics*Amsterdam. Les Houches, école d'été de physique théorique 1989, session LII, North-Holland, ISBN 0-444-89277-X.

GOMEZ LLORENTE J.M. & PLATA J. (1994): "Analytical solutions for a resonantly driven two-doublet system", *Phys. Rev. A*, **49**(4), pp. 2759–2765.

GOSS LEVI B. (2001): "Atoms Hop between Islands of Regular Motion in a Sea of Chaos", *Physics Today*, **54**(8), p. 15.

GREENE J.M. & PERCIVAL I.C. (1981): "Hamiltonian maps in the complex plane", *Physica D*, **3**(3), pp. 530–548.

GROSSMANN F., DITTRICH T., JUNG P. & HÄNGGI P. (1991): "Coherent Destruction of Tunneling", *Phys. Rev. Lett.*, **67**(4), pp. 516–519.

GURNEY R.W. & CONDON E.U. (1928): "Wave mechanics and radioactive disintegration", *Nature*, **122**, p. 439.

HANDY C.R. (2006): "(Quasi)-convexification of Barta's (multi-extrema) bounding theorem: $\inf_x \frac{H\Phi(x)}{\Phi(x)} \leqslant E_{\mathrm{gr}} \leqslant \sup_x \frac{H\Phi(x)}{\Phi(x)}$", *J. Phys. A*, **39**, pp. 3425–3446.

HÄNGGI P. (1995): "Control of tunneling", in *Quantum Dynamics of Submicron Structures*, ed. by Cerdeira H.A. *et al.*, pp. 673–686. Kluwer.

HARRELL E.M. (1978): "On the rate of asymptotic eigenvalue degeneracy", *Comm. Math. Phys.*, **60**, pp. 73–95.

HELFFER B. & SJÖSTRAND J. (1984): "Multiple wells in the semi-classical limit. I.", *Commun. Partial Differ. Equations*, **9**, pp. 337–408.

——— (1985): "Effet tunnel pour l'opérateur de Schrödinger semi-classique", *Journées Équations aux dérivées partielles*, **2**, pp. 1–38, (in french) http://www.numdam.org/item?id=JEDP_1985___2_A2_0.

_____ (1986): "Résonances en limite semi-classique", *Mém. Soc. Math. France, 2^e Série*, **114**(24-25), pp. 1–228, (in french) http://www.numdam.org/item?id=MSMF_1986_2_24-25__1_0.

_____ (1987): "Effet tunnel pour l'équation de Schrödinger avec champ magnétique", *Ann. Scuola Norm. Sup. Pisa*, **14**, pp. 625–657, (in french).

Heller E.J. (2001): "Air juggling and other tricks", *Nature*, **412**(6842), pp. 33–34.

Heller E.J. & Davis M.J. (1981): "Quantum dynamical tunneling in large molecules. A plausible conjecture", *J. Phys. Chem.*, **85**(4), pp. 307–309.

Hensinger W.K., Häffner H., Browaeys A., Heckenberg N.R., Helmerson K., McKenzie C., Milburn G.J., Phillips W.D., Rolston S.L., Rubinsztein-Dunlop H. & Upcroft B. (2001): "Dynamical tunnelling of ultracold atoms", *Nature*, **412**(6842), pp. 52–55.

Hensinger W.K., Mouchet A., Julienne P.S., Delande D., Heckenberg N.R. & Rubinsztein-Dunlop H. (2004): "Analysis of dynamical tunneling experiments with a Bose-Einstein condensate", *Phys. Rev. A*, **70**, p. 013408.

Hofferbert R., Alt H., Dembowski C., Gräf H.D., Harney H.L., Heine A., Rehfeld H. & Richter A. (2005): "Experimental investigations of chaos-assisted tunneling in a microwave annular billiard", *Phys. Rev. E*, **71**, p. 046201.

Holthaus M. (1992): "Pulse-shape-controlled tunneling in a laser field", *Phys. Rev. Lett.*, **69**(10), pp. 1596–1599.

_____ (1995): "On the Classical-Quantum Correspondance for Periodically Time Dependent Systems", *Chaos, Solitons & Fractals*, **5**(7), pp. 1143–1167.

Hund F. (1927a): "Zur Deutung der Molekelspektren. I", *Zts. f. Phys.*, **40**(10), pp. 742–764, (in german).

_____ (1927b): "Zur Deutung der Molekelspektren. III.", *Zts. f. Phys.*, **43**(11-12), pp. 805–826, (in german).

Jauho A.P. (1990): "Numerical simulations of resonant tunneling in the presence of inelastic processes", *Phys. Rev. B*, **41**(17), pp. 12327–12329.

Jeffreys H. (1925): "On certain approximate solutions of linear differential equations of the second order", *Proc. London Math. Soc. (2nd ser.)*, **23**, pp. 428–436.

Keshavamurthy S. (2003): "Dynamical tunneling in molecules: Role of the classical resonances and chaos", *J. Chem. Phys.*, **119**(1), pp. 161–164.

_____ (2005): "On dynamical tunneling and classical resonances", *J. Chem. Phys.*, **122**, p. 114109.

Korsch H.J., Mirbach B. & Schellhaaß B. (1997): "Semiclassical analysis of tunnelling splittings in periodically driven quantum systems", *J. Phys. A*, **30**, pp. 1659–1677.

Kox A.J., Klein M. & Schulmann R. (1997): *The Collected Papers of Albert Einstein, Volume 6: The Berlin Years: Writings, 1914-1917*. Princeton, New-Jersey: Princeton U. Press, isbn 0691017344, p.434.

Kramers H.A. (1926): "Wellenmechanik und halbzahlige Quantisierung", *Zts. f. Phys.*, **39**, pp. 828–840, (in german).

Kuś M., Haake F. & Delande D. (1993): "Prebifurcation Periodic Ghost Orbits in Semiclassical Quantization", *Phys. Rev. Lett.*, **71**(14), pp. 2167–2171.

Kuvshinov V.I., Kuzmin A.V. & Shulyakovsky R.G. (2003): "Chaos assisted instanton tunneling in one dimensional perturbed periodic potential", *Phys. Rev. E*, **67**, p. 015201.

Landau L.D. & Lifshitz E.M. (1977): *Quantum Mechanics (non relativistic theory)*, vol. 3 of *Course of Theoretical Physics*. Oxford: Pergamon Press, 3rd edition.

Latka M., Grigolini P. & West B.J. (1994a): "Chaos and avoided level crossings", *Phys. Rev. E*, **50**(1), pp. 596–599.

_____ (1994b): "Chaos-induced avoided level crossing and tunneling", *Phys. Rev. A*, **50**(2), pp. 1071–1081.

Lawton R.T. & Child M.S. (1981): "Local and normal stretching vibrational states of H_2O. Classical and semiclassical considerations", *Molecular Phys.*, **44**(3), pp. 709–23.

Lebœuf P., Kurchan J., Feingold M. & Arovas D.P. (1990): "Phase Space Localization: Topological aspects of quantum chaos", *Phys. Rev. Lett.*, **65**(25), pp. 3076–3079.

Lebœuf P. & Mouchet A. (1994): "Tunneling and the Band Structure of Chaotic Systems", *Phys. Rev. Lett.*, **73**(10), pp. 1360–1363.

_____ (1999): "Normal forms and complex periodic orbits in semiclassical expansions of Hamiltonian systems", *Ann. Physics*, **275**, pp. 54–112.

Leggett A.J. (1997): "Some general aspects of quantum tunneling and coherence : application to the bec atomic gases", in (Tomsovic, 1998), pp. 1–34, isbn 981-02-3446-5.

Leyvraz F. & Ullmo D. (1996): "The level splitting distribution in chaos-assisted tunnelling", *J. Phys. A*, **29**, pp. 2529–2551.

Lichtenberg A.J. & Lieberman M.A. (1983): *Regular and Stochastic Motion*, vol. 38 of *Applied Mathematical Sciences*. New York: Springer-Verlag, isbn 0-387-90707-6.

Lieb E.H. (2005): *The stability of matter: from atoms to stars*. Berlin: Springer-Verlag, isbn 0-540-22212-X, (4th edition).

Lin W.A. & Ballentine L.E. (1990): "Quantum Tunneling and Chaos in a Driven Anharmonic Oscillator", *Phys. Rev. Lett.*, **65**, pp. 2927–2930, The dynamical symmetry underlying the model has been highlit by Peres (1991).

——— (1992): "Quantum tunneling and regular and irregular quantum dynamics of a driven double-well oscillator", *Phys. Rev. A*, **45**(6), pp. 3637–3645.

Maitra N.T. & Heller E.J. (1997): "Barrier tunneling and reflection in the time and energy domain : the battle of exponentials", *Phys. Rev. Lett.*, **78**(16), pp. 3035–3038.

Marcus R.A. (1971): "Theory of Semiclassical Transition Probabilities (S Matrix) for Inelastic and Reactive Collisions", *J. Chem. Phys.*, **54**, pp. 3965–3979.

Martinez A. (1987): "Estimations de l'effet tunnel pour le double puits. I", *J. Math. Pures Appl.*, **66**(9), pp. 195–215, (in french).

——— (1988): "Estimations de l'effet tunnel pour le double puits. II: états hautement excités.", *Bull. Soc. Math. France*, **116**(2), pp. 199–229, (in french).

Maslov V.P. (1985): "Global exponential asymptotic behavior of the solutions of tunnel-type equations and the problem of. large deviations", *Proc. Steklov Inst. Math.*, **4**, pp. 177–209, Translation from the original russian: *Trudy Mat. Inst. Steklov* 1984; **163**, pp 150–180.

Mclaughlin D.W. (1972): "Complex time, contour independent path integrals, and barrier penetration", *J. Math. Phys.*, **13**, pp. 1099–1108.

Merzbacher E. (2002): "The early history of quantum tunneling", *Phys. Today*, **55**(8), pp. 44–50.

Miller W.H. (1970): "The Classical S-matrix: A more detailed study of classically forbidden transitions in inelastic collisions", *Chem. Phys. Lett.*, **7**(4), pp. 431–435.

——— (1974): "Classical-limit quantum mechanics and the theory of molecular collisions", *Adv. Chem. Phys.*, **25**, pp. 69–177.

——— (1979): "Periodic Orbit Description of Tunneling in Symmetric and Asymmetric Double-Well Potentials", *J. Phys. Chem.*, **83**(8), pp. 960–963.

Monteiro T.S., Delande D., Fisher A.J. & Boebinger G.S. (1997): "Bifurcations and the transition to chaos in the resonant-tunneling diode", *Phys. Rev. B*, **56**(7), pp. 3913–3921.

Moore F.L., Robinson J.C., Bharucha C., Williams P.E. & Raizen M.G. (1994): "Observation of Dynamical Localisation in Atomic Momentum Transfer: A New Testing Ground for Quantum Chaos", *Phys. Rev. Lett.*, **73**(22), pp. 2974–2977.

Mouchet A. (1996): "Quelques applications des méthodes semiclassiques en chaos quantique", Ph.D. thesis, Université Pierre et Marie Curie, Paris.

_____ (1998): "Introduction aux méthodes semiclassiques en chaos quantique", http://hal.ccsd.cnrs.fr/ccsd-00003591 (in french).

_____ (2005): "A differential method for bounding the ground state energy", *J. Phys. A*, **38**, pp. 1039–1047.

_____ (2006a): "Bounding the ground-state energy of a many-body system with the differential method", *Nuclear Phys. A*, **765**, pp. 319–341.

_____ (2006b): "Upper and lower bounds for an eigenvalue associated with a positive eigenvector", *J. Math. Phys.*, **47**, p. 022109.

Mouchet A. & Delande D. (2003): "Signatures of chaotic tunneling", *Phys. Rev. E*, **67**, p. 046216.

Mouchet A., Eltschka C. & Schlagheck P. (2006): "Influence of classical resonances on chaotic tunneling", *Phys. Rev. E*, **74**, p. 026211.

Mouchet A., Miniatura C., Kaiser R., Grémaud B. & Delande D. (2001): "Chaos assisted tunneling with cold atoms", *Phys. Rev. E*, **64**, p. 016221.

Mouchet A. & Ullmo D. (2001): "Chaos gives quantum tunnelling a hand", *Physics World*, **14**(9), pp. 24–25.

Nöckel J.U. & Stone A.D. (1997): "Ray and wave chaos in asymmetric resonant optical cavities", *Nature*, **385**, pp. 45–47.

Nordheim L. (1927): "Zur Theorie der thermischen Emission und der Reflexion von Elektronen an Metallen", *Zts. f. Phys.*, **46**(11-12), p. 833, (in german).

Oppenheimer R. (1928): "Three notes on the quantum theory of aperiodic effects", *Phys. Rev.*, **31**, pp. 66–81.

Ozorio de Almeida A.M. (1984): "Tunnelling and the semiclassical spectrum for an isolated classical resonance", *J. Phys. Chem.*, **88**(25), pp. 6139–6146.

Pance K., Violaand L. & Sridhar S. (2000): "Tunneling proximity resonances: interplay between symmetry and dissipations", *Phys. Lett. A*, **268**, pp. 399–405.

Patrascioiu A. (1981): "Complex time and the Gaussian approximation", *Phys. Rev. D*, **24**, p. 496.

Percival I.C. (1977): "Semiclassical theory of bound states", *Adv. Chem. Phys.*, **36**, pp. 1–61.

——— (1982): "Chaotic boundary of a Hamiltonian map", *Physica D*, **6**(1), pp. 67–77.

Peres A. (1991): "Dynamical quasidegeneracies and quantum tunneling", *Phys. Rev. Lett.*, **67**(1), p. 158.

Plata J. & Gomez Llorente J.M. (1992): "Classical-quantum correspondence for barrier crossing in a driven bistable potential", *J. Phys. A*, **25**, pp. L303–L310.

Podolskiy V.A. & Narimanov E.E. (2003): "Semiclassical Description of Chaos-Assisted Tunneling", *Phys. Rev. Lett.*, **91**, p. 263601.

Polyakov A.M. (1977): "Quark confinement and topology of gauge theory", *Nuclear Phys. B*, **120**, pp. 429–458.

Roncaglia R., Bonci L., Izrailev F.M., West B.J. & Grigolini P. (1994): "Tunneling versus Chaos in the Kicked Harper Model", *Phys. Rev. Lett.*, **73**(6), pp. 802–805.

Scharf R. (1988): "The Campbell-Baker-Hausdorff expansion for classical and quantum kicked dynamics", *J. Phys. A*, **21**, pp. 2007–2021.

Scharf R. & Sundaram B. (1994): "Traces of ghost orbits in the quantum standard map", *Phys. Rev. E*, **49**(6), pp. R4767–R4770.

Schlagheck P., Eltschka C. & Ullmo D. (2006): "Resonance- and Chaos-Assisted Tunneling", in *Progress in Ultrafast Intense Laser Science I*, ed. by Yamanouchi K., Chin S.L., Agostini P. & Ferrante G., Springer Series in Chemical Physics, p. 107, Berlin. Springer, isbn 3540344217.

Schmid A. (1986): "Quasiclassical wave function in multidimensional quantum decay problems", *Ann. Physics*, **170**, pp. 333–369.

Schottky W. (1931): "Conduction and photoelectric effects in blocking layers", *Phys. Z.*, **32**, pp. 833–842.

Shudo A. & Ikeda K.S. (1995): "Complex Classical Trajectories and Chaotic Tunneling", *Phys. Rev. Lett.*, **74**(5), pp. 682–685.

_____ (1998): "Chaotic tunneling: A remarkable manifestation of complex classical dynamics in non-integrable quantum phenomena", *Physica D*, **115**, pp. 234–292.

Shudo A., Ishii Y. & Ikeda K.S. (2002): "Julia set describes quantum tunnelling in the presence of chaos", *J. Phys. A*, **35**(17), pp. L225–L231.

Simon B. (1983): "Instantons, double wells and large deviations", *Bull. Amer. Math. Soc. (N.S.)*, **8**(2), pp. 323–326.

_____ (1984): "Semiclassical analysis of low lying eigenvalues, II. Tunneling", *Ann. of Math.*, **120**, pp. 89–118.

Smith G.C. & Creagh S.C. (2006): "Tunnelling in near-integrable systems", *J. Phys. A*, **39**, pp. 8283–8306.

Sordoni V. (1997): "Instantons and splitting", *J. Math. Phys.*, **38**(2), pp. 770–795.

Stamp P.C.E. (1997): "Quantum environments : spins baths, oscillator bath, and applications to quantum magnetism", in (Tomsovic, 1998), pp. 101–197, isbn 981-02-3446-5.

Steck D.A., Windell H.O. & Raizen M.G. (2001): "Observation of Chaos-Assisted Tunneling between Islands of Stability", *Science*, **293**, pp. 274–278.

Stine J. & Marcus R.A. (1972): "Theory of semiclassical transition probabilities for inelastic and reactive collisions. IV. Classically-inaccessible transitions calculated by integration along complex-valued trajectories", *Chem. Phys. Lett.*, **15**(4), pp. 536–544.

Stone A.D. (2005): "Einstein's unknown insight and the problem of quantizing chaos", *Physics Today*, **58**(8), pp. 37–43.

Tabor M. (1989): *Chaos and integrability in nonlinear dynamics — An introduction*. New York: John Wiley and sons, Inc., isbn 0-471-82728-2.

Takada S. (1996): "Multidimensional tunneling in terms of complex classical mechanics: wave functions, energy splittings, and decay rates in nonintegrable systems", *J. Chem. Phys.*, **104**(10), pp. 3742–3759.

Takada S. & Nakamura H. (1994): "Wentzel-Kramers-Brillouin theory of multidimensional tunneling:General theory of energy splitting", *J. Chem. Phys.*, **100**(1), pp. 98–113.

Takada S., Walker P.N. & Wilkinson M. (1995): "Transfer-matrix approach to tunneling between Kolmogorov-Arnold-Moser tori", *Phys. Rev. A*, **52**(4), pp. 1–8.

Tomsovic S. (ed.) (1998): *Tunneling in complex systems*vol. 5 of *Proceedings from the Institute for Nuclear Theory*, Singapore. World Scientific Publishing, isbn 981-02-3446-5.

Tomsovic S. & Ullmo D. (1994): "Chaos-assisted tunneling", *Phys. Rev. E*, **50**(1), pp. 145–161.

Utermann R., Dittrich T. & Hänggi P. (1994): "Tunneling and the onset of chaos in a driven bistable system", *Phys. Rev. E*, **49**(1), pp. 273–280.

Uzer T., Noid D.W. & Marcus R.A. (1983): "Uniform semiclassical theory of avoided crossings", *J. Chem. Phys.*, **79**(9), pp. 4412–4425.

Voros A. (1983): "The return of the quartic oscillator. The complex WKB method.", *Ann. Inst. H. Poincaré. Phys. Théor.*, **39**(3), pp. 211–338.

Wentzel G. (1926): "Eine Verallgemeinerung der Quantenbedingungen für die Zwecke der Wellenmechanik", *Zts. f. Phys.*, **38**, pp. 518–529, (in german).

Wilkinson M. (1986): "Tunnelling between tori in phase space", *Physica D*, **21**, pp. 341–354.

——— (1987): "Narrowly avoided crossings", *J. Phys. A*, **20**, pp. 635–645.

Wilkinson M. & Hannay J.H. (1987): "Multidimensional tunnelling between excited states", *Physica D*, **27**, pp. 201–212.

Zakrzewski J., Delande D. & Buchleitner A. (1998): "Ionization via chaos assisted tunneling", *Phys. Rev. E*, **57**(2), pp. 1458–1474.

Zanardi E.M. & Gomez Llorente J.M. (1997): "Dynamical resonance and tunneling in a driven system wih periodic potential", *Chem. Phys.*, **217**, pp. 221–231.

Résumé du mémoire

Effet tunnel chaotique — Méthode différentielle

Amaury Mouchet

Ce mémoire d'habilitation à diriger des recherches présente de façon synthétique mon activité professionnelle s'étalant sur une période qui couvre mon activité de recherche au Laboratoire de Mathématiques et de Physique Théorique depuis le printemps 1997 en tant que maître de conférences de l'université François Rabelais de Tours.

Après une fiche signalétique qui décrit surtout mon activité d'enseignement, d'administration et d'animation au sein du département de physique et du laboratoire, ce mémoire s'articule autour de deux axes qui en constituent les deux chapitres et s'accompagne d'une bibliographie détaillée.

Le premier, intitulé « Effet tunnel chaotique » est consacré à l'étude de processus quantiques interdits à la physique classique réelle. Pourtant, paradoxalement, le caractère intégrable ou chaotique de la dynamique hamiltonienne influence considérablement l'effet tunnel, sur plusieurs ordres de grandeurs. Après un rappel du contexte historique dans lequel s'inscrit l'effet tunnel en général et l'effet tunnel chaotique en particulier, je reproduis cinq de mes articles publiés sur ce sujet et les accompagne tous d'une présentation en soulignant leurs contributions originales. Il s'agit d'un travail théorique qui s'appuie souvent sur des expériences numériques et qui, pour trois articles, est explicitement relié à des expériences sur des atomes froids. Ce chapitre se clôt sur un programme de recherche étayé par des arguments précis.

Le second chapitre intitulé « Méthode différentielle » porte sur un thème et des motivations complètement distincts du précédent. Il s'agit ici, de mettre en œuvre une stratégie qui vise à donner un encadrement de l'énergie fondamentale d'un système en s'appuyant sur une manœuvre radicalement différente des méthodes éprouvées comme l'approche perturbative ou l'approche variationnelle. Je reproduis les trois articles que j'ai publiés sur ce sujet, proche de la physique mathématique et, comme dans le chapitre précédent, ils sont accompagnés d'une présentation ainsi que d'un tableau des perspectives qu'ils suscitent.